THE DISINTEGRATION CHARACTERISTICS OF RESIDUAL GRANITE SOIL

BY

DANICA MONG

Thesis submitted in partial fulfilment of the requirements for the degree of Masters in the Faculty of Engineering (MEng) at the University of Stellenbosch

Supervisor: Dr N Fouché

April 2022

DECLARATION

By submitting this thesis electronically, I declare that the entirety of the work contained therein is my own, original work, that I am the sole author thereof (save to the extent explicitly otherwise stated), that reproduction and publication thereof by Stellenbosch University will not infringe any third party rights and that I have not previously in its entirety or in part submitted it for obtaining any qualification.

Date: April 2022

ABSTRACT

Plutons of the Cape Granite Suite are largely limited to the south-western Cape with exception of occurrences near George and in Namaqualand (Brink, 1981). The composition and texture of Cape granitoids are very complex and variable, depending on the location of the plutons. Problems associated with residual granite soil from the Cape Granite Suite include the presence of a collapsible grain structure. In partially saturated residual granite soils, quartz particles have colloidal coatings around individual grains, contributing to a seemingly high strength soil, and when saturated under load, the colloidal bridges become unstable, causing particles to pack into a denser state, leading to sudden settlement of the foundation.

This research contributes towards classifying and characterising decomposed granite soil, from the Cape Granite Suite, in terms of its physical properties and engineering behaviour. The soil was classified based on its grading properties, Atterberg limits, maximum dry density, and optimum moisture content, and characterised based on triaxial compression test results. The triaxial compression test results provided shear strength properties, volumetric behaviour during shearing, critical state properties, and stress paths. Focus was placed on the influence of water on the behaviour of decomposed granite soil during different stages of the triaxial compression test, and on individual grains and/or aggregated particles which resulted in particle breakage after triaxial shearing. The amount of particle breakage was determined from the relative breakage of particles after triaxial shearing.

Classification properties primarily depended on the degree of weathering for decomposed granite soil. The particle size distribution (PSD) shows that the decomposed granite soil ranges from gravel to clay size particles with the greatest amount of particles present in the medium-sand and fine-sand size ranges. Decomposed granite soil has a low plasticity with a typical fines content (<0.075mm) of around 15%. Descriptions for some of the soil properties are given below:

- The mineralogy consists of quartz, plagioclase, K-feldspar, mica, kaolinite, and calcite.
- SM “poorly graded silty sand” material (USCS), Class A-2-4 material (AASHTO system), and G8 quality “gravel soil” (TRH14 system).
- Maximum dry density of 2120.5 kg/m^3 by using modified AASHTO compaction effort, and an optimum moisture content of 8.5%.

The mechanical behaviour of decomposed granite soil is evaluated through an isotropic compression and swelling test, and triaxial compression tests on saturated, dry, partially saturated, flooded, and air-dried specimens. Saturated results show that the soil conforms to the critical state Modified Cam-Clay model with a friction parameter, M = 1.41, an isotropic normal compression line $\lambda = 0.073$ and N = 1.88, and an unload reload line $\kappa = 0.012$. Partially saturated specimens (S_r = 20% - 80%) had similar strength and stiffness results as the saturated specimens indicating relatively small pore water suctions, and flooded specimens had a decrease in strength. Air-dried specimens reflected the effects of seasonal wetting and drying. Interparticle bonds gave the soil a cohesive component of strength whereas saturation of the soil caused the collapsible grain structure to collapse and cause a significant decrease in strength.

Particle breakage of decomposed granite soil increased with increasing confining pressure and also with the presence of water. CT scans showed that larger particles primarily underwent particle degradation and that the process of particle breakage was mainly due to the separation of particle amalgams and breakage along pre-existing fissures.

OPSOMMING

Plutone van Kaapse graniet is grootliks beperk tot die suidwestelike Kaap met uitsondering op voorvalle naby George en Namakwaland (Brink, 1981). Die samestelling en tekstuur van Kaapse granitoïede is baie kompleks en veranderlik, afhangende van die ligging van die plutone. Probleme wat verband hou met residuele granietgrond van die Kaapse graniet sluit in die teenwoordigheid van 'n swigversakkende korrelstruktuur. Residuele graniet gronde wat gedeeltelik versadig is bevat kwarts partikels wat bedek is met kolloïdale materiaal. Hierdie dra by tot ‘n klaarblyklike hoë krag in die granietgrond en wanneer dit versadig word onder lading, word die kolloïdale brûe onstabiel en veroorsaak dat die partikels saam pak in ‘n digter toestand wat lei tot skielike versakking van die fondasie.

Hierdie navorsing dra by tot die klassifikasie en karakterisering van verweerde granietgrond van die Kaapse graniet in terme van die grond se fisiese eienskappe en ingenieurs gedrag. Die grond is geklassifiseer op grond van sy graderings eienskappe, Atterberg grense, maksimum droë digtheid en optimum voginhoud, en gekenmerk op grond van drieassige kompressietoets resultate. Die resultate van die drieassige kompressietoets het skuif sterkte eienskappe, volumetriese gedrag tydens skeer, eienskappe in kritieke toestande en spanning paaie. Fokus is geplaas op die invloed van water op die gedrag van verweerde granietgrond tydens verskillende stadiums van die drieassige kompressietoets, veral op individuele partikels en/of saamgestelde partikels wat gelei het tot partikel breking na drieassige skering. Die hoeveelheid partikel breking was bepaal deur die relatiewe breek van deeltjies na skeer te evalueer.

Klassifikasie eienskappe hang hoofsaaklik af van die graad van verwering van die verweerde granietgrond. Die partikelgrootteverdeling-kurwe toon aan dat die verweerde granietgrond wissel van gruis tot klei-grootte partikels met die meeste hoeveelheid partikels teenwoordig in die medium-sand en fyn-sand grootte reekse. Verweerde granietgrond het 'n lae plastisiteit met 'n tipiese fyn stof inhoud (<0,075 mm) van ongeveer 15%. Beskrywings vir sommige van die grondeienskappe word hieronder gegee:

- Die mineralogie bestaan uit kwarts, plagioklaas, K-veldspaat, mika, kaoliniet en kalsiet.
- SM-materiaal met 'swak gegradeerde siltagtige sand' (USCS), klas A-2-4 materiaal (AASHTO stelsel) en 'gruisgrond' van G8-kwaliteit (TRH14 stelsel).
- Maksimum droë digtheid van 2120,5 kg/m3 deur gebruik te maak van gewysigde AASHTO verdigtingspoging en 'n optimum voginhoud van 8.5%.

Die meganiese gedrag van verweerde granietgrond is geëvalueer deur middel van 'n isotropiese druk-en-swel toets, en drieassige kompressietoetse op versadigde, droë, gedeeltelik versadigde, oorstroomde en luggedroogde monsters uit te voer. Versadigde resultate het getoon dat die grond voldoen aan die kritieke toestand gewysigde Cam-klei model met 'n wrywings parameter, M = 1.41, 'n isotropiese normale kompressie lyn $\lambda = 0.073$ en N = 1.88, en 'n aflaai-herlaai lyn $\kappa = 0.012$. Gedeeltelik versadigde monsters (Sr = 20% - 80%) het soortgelyke sterkte- en styfheid resultate gehad as die versadigde monsters wat aandui dat gedeeltelik versadigde monsters relatief klein porie water suiging het. Monsters wat oorstroom is, het 'n afname in sterkte gehad Luggedroogde monsters weerspieël die gevolge van seisoenale benatting en droging. Interpartikelbindings het die grond 'n samehangende komponent van sterkte gegee, terwyl versadiging van die grond veroorsaak het dat die swigversakkende korrelstruktuur in duie gestort het en 'n aansienlike afname in sterkte veroorsaak het.

Partikel breuking van verweerde granietgrond het toegeneem met toenemende beperkte druk en ook met die teenwoordigheid van water. CT-skanderings het getoon dat groter deeltjies hoofsaaklik partikel breuking ondergaan het en dat die proses van partikel breuking hoofsaaklik te wyte was aan die skeiding van partikel-amalgame en breek langs bestaande splete.

ACKNOWLEDGEMENTS

Firstly, I would like to thank Dr Nanine Fouché for her supervision and willingness to assist whenever necessary. She provided guidance and encouragement to the very end of this thesis. Dr Nanine Fouché delivered valuable insight, especially after reading the draft of my thesis. Without the help of Mr Frank Coetzee of Steyn Wilson laboratories, this research would not have been completed. His knowledge and guidance with regards to triaxial testing are highly appreciated and it will not be forgotten. I extend my gratitude to Steyn Wilson laboratories for allowing me to use their equipment for triaxial testing. The assistance of Mr Elvin Johnson at the laboratory is also acknowledged. He helped with the preparation and disassembling of specimens which made for timeous testing.

My thanks are also due to the Pavement and Geotechnical Research Laboratory (PGRL) in Stellenbosch and its manager, Mr Guillaume Nel, and personnel Colin, and Gaven. Their assistance and guidance are truly valued. Thank you to the Central Analytical Facility in Stellenbosch for making their CT scanner available, and for Ms Muofhe Tshibalanganda, their junior assistant, for performing my scans and assisting me with the analysis process. Finally, I would like to give thanks to close family and friends for their considerable amount of encouragement. I admire their support and patience.

TABLE OF CONTENT

LIST OF FIGURES

LIST OF TABLES

LIST OF SYMBOLS AND ABBREVIATIONS

Symbols

ϕ	Friction angle (˚)
ϕ’	Effective friction angle (˚)
ϕ_{max}	Peak friction angle (˚)
ϕ_{cv}	Critical state friction angle (˚)
c	Cohesion (kPa)
c’	Effective cohesion (kPa)
Γ	Specific volume at p’ = 1 kPa of critical state line in ν: lnp’ space (-)
γ	Bulk unit weight (kN/m^3)
γ_{dmax}	Maximum dry density (kN/m^3)
γ_w	Unit weight of water (kN/m^3)
$\delta\varepsilon_p$	Total volumetric strain (%)
$\delta\varepsilon_p^e$	Elastic volumetric strain (%)
$\delta\varepsilon_p^p$	Plastic volumetric strain (%)
$\delta\varepsilon_q$	Total shear strain (%)
$\delta\varepsilon_q^e$	Elastic shear strain (%)
$\delta\varepsilon_q^p$	Plastic shear strain (%)
ε_a	Axial strain (%)
ε_p	Volumetric strain (%)
ε_q	Shear strain (%)
ε_r	Radial strain (%)
η	q/p’ (-)
κ	Slope of unload reload line (-)
λ	Slope of virgin isotropic compression line (-)
λ_{cs}	Slope of critical state line in ν: lnp’ space (-)
ν	Specific volume (-)
ν_κ	Specific volume of unload reload line at p’ = 1 kPa
ρ	Bulk density (kg/m^3)
ρ_d	Dry density (kg/m^3)
$\rho_{d,\,max}$	Maximum dry density (kg/m^3)
σ	Total normal stress (kPa)

σ'	Effective normal stress (kPa)
σ'_a	Effective axial stress (kPa)
σ'_r	Effective radial stress (kPa)
σ_1	Major principle stress (kPa)
σ_3	Minor principle stress (kPa)
B_p	Breakage potential (-)
B_r	Relative breakage (-)
B_t	Total breakage (-)
C_c	Compression index (-)
Ce	Expansion index (-)
C_u	Coefficient of uniformity (-)
C_{ze}	Coefficient of curvature (-)
c_v	Coefficient of consolidation (m^2/year)
D	Particle size (mm)
D_{10}	Effective size (mm)
D_{30}	Size such that 30% of particles are smaller than that size (mm)
D_{50}	Mean particle size (mm)
D_{60}	Size such that 60% of particles are smaller than that size (mm)
d	Dilatancy parameter (kPa)
E'_{oed}	Constrained modulus (MPa)
e/e_0	Void ratio (-)
G	Shear Modulus (MPa)
G_s	Specific gravity (-)
H	Height (mm)
k	Coefficient of permeability (m/s)
M	Frictional constant (-)
m_v	Coefficient of volume compressibility (m^2/MN)
N	Isotropic normal compression line at p' = 1 kPa
P_n	Percentage material retained on sieve with size n (%)
p'	Mean normal effective stress (kPa)
q'	Deviator stress (kPa)
Sf	Soil fines in total material (%)
S_r	Degree of saturation (%)

t_{100}	Shear speed (mm/min)
u	Pore water pressure (kPa)
Wfl	Flow limit function (-)
W_n	Mass of fraction passing sieve with size n (g)
w	Water content (%)

Abbreviations

A	Activity
AASHTO	American Association of State Highway and Transportation Officials
APC	Air pressure control
CAF	Central Analytical Facility
CD	Consolidated drained
CSL	Critical state line
CT	Computed tomography
CU	Consolidated Undrained
GM	Grading modulus
LI	Liquidity index
LL	Liquid limit
LS	Linear shrinkage
LVDT	Linear variable differential transducers
MCC	Modified Cam-Clay
MDD	Maximum dry density
Mod	Modified
NCL	Normal compression line
OMC	Optimum moisture content
PI	Plasticity index
PL	Plastic limit
PSD	Particle size distribution
SANS	South African National Standard
SEM	Scanning electron microscopy
TMH	Technical Methods for Highway
URL	Unload reload line
USCS	Unified Soil Classification System
UU	Unconsolidated Undrained

CHAPTER 1: INTRODUCTION

1.1 BACKGROUND INFORMATION

The earth's continental crust is rich in granite and geologist commonly find it to be an intrusive igneous rock. The term granitic rock is frequently used to describe a class of rock that is abundant in minerals of quartz and feldspar. Granitic rock can also be characterised as being felsic which is a term derived from feldspar and silica (quartz). Bowen's reaction series (Bowen, 1922) illustrates both the composition and weathering of granitic rock where the order of crystallisation is as follows: biotite, potassium feldspar, muscovite mica and quartz (Tarbuck, Lutgens & Tasa, 2014).

The broken fragments of decomposing granitic rock are called gruss. These fragments form after the weathering of plagioclase feldspar and before the weathering of orthoclase. The majority of orthoclase weathers to kaolinite after which the gruss deteriorates to a silty sand (Mitchell & Soga, 2005). It is not uncommon to find mica flakes within the silty sand. Quartz grains that were once interlocked in the feldspar are released during weathering. A significant property of quartz is its ability to resist chemical weathering causing it to remain unaltered during the decomposition of granite (Mitchell & Soga, 2005).

The bedrock profile of decomposed granite is remarkably irregular, and competent bedrock may be located at variable depths below the ground surface. Weathering of granitic rock can be a combination of residual debris and solid rock where the quantity of the latter decreases towards the surface. Profile depths of weathered granite can reach 30m or more however, the variability in depth to competent bedrock can be troublesome when considering construction on such an area. Other difficulties that may be encountered during construction on weathered granite include seemingly sound rock or gravel pieces breaking during excavation due to the presence of core stones, and a highly compressible soil due to the presence of mica.(Mitchell & Soga, 2005).

Decomposed granite soil, a frequently encountered residual soil, has undergone chemical weathering to create intensely leached soils. This forms a honeycomb-like fabric held together by bridging colloidal material (kaolinite) and suction, giving an apparent strength at low moisture content. When such soil is saturated under load, the bridging colloids lose their strength and stiffness, resulting in a densely packed fabric termed a collapsible soil structure (Fouché & Asante, 2019). The first discovery of soil illustrating a collapsible grain structure in South Africa was founded in 1955 during an investigation of a tilting water tower at White

River. At the time, collapsible soils were associated with aeolian soils, but the discovery found that this phenomenon also occurs in decomposed granite. Areas in Southern Africa underlain by granitic soil include Tzaneen, Mbabane, the northern suburbs of Johannesburg, and certain parts of the Cape Peninsula with the three main types of granite being the Old Granite, Cape Granite, and Bushveld Granite. The composition of the granite soils is generally quartz, feldspar, and mica with varying abundant accessory minerals (Brink & Kantey, 1961).

It is estimated that, on average, 67% of the country's total area is susceptible to potentially collapsible soils (Diop *et al*.,2011). These areas typically coincide with areas that receive an annual water surplus. Repeated seasonal wetting and drying of decomposed granite will generate strong interparticle bonds, but flooding will result in a less stable soil structure as bonds soften. Thus, a sudden increase in pore water pressure will cause large strains in the soil. This is partly responsible for large settlements and the loss of slope stability in these soils; when in its natural state and when used as construction material (Lee & Coop, 1995).

Weathering of mica, a mineral present in decomposed granite, is known to be subjected to expansion, causing microfractures through particles within the residual granite soil. Lee and Coop (1995) concluded that particle breakage is the most important function of plastic volumetric compression during isotropic loading and shearing, especially upon flooding of dry soil. Normal compression is thus a function of the particle breakage. Lee and Coop (1995) also mention that particle breakage is a factor of particle size distribution, particle angularity (shape), primary void ratio, and the stresses applied.

1.2 PROBLEM STATEMENT

As described in Section 1.1, decomposed granite soils are prone to the formation of a collapsible fabric. Collapse settlement associated with these soils has caused many houses in South Africa to experience cracking. It is important to understand the intrinsic properties of residual granite soil. Brink and Kantey (1961) mentioned that within the Cape Town area, decomposed granite may range from collapsible to expansive soils even at a particular site. It has been found that the areas underlain by decomposed granite in South Africa are confined to well-drained slopes which correspond to areas with a yearly water surplus. The White River occurrence in 1955 illustrated that the soil's compressibility decreases with depth, and further research has shown that the increase in annual rainfall increases the void ratio (Brink & Kantey, 1961).

Terblanche (1989) analysed the settlement of columns of an industrial development corporation that consisted of three-storeys. The construction site was situated on deeply weathered residual granite soil. Due to poor investigation of the problematic granite soil, a single column settled 300mm. Both the cases mentioned indicate that settlement can be large even if the foundation is lightly loaded, collapse can occur many years after the completion of construction, and how localised a problem can occur on-site. When used as engineering fill, residual granite soils have shown to be the cause of significant problems, such as large bulk volume decrease upon wetting. The influence of water is substantial in this research and a common factor in the stability of weathered granites during the rainy season. During dryer seasons the soil fabric has seemingly strong interparticle bonds due to suction being generated however, once saturated under load, the interparticle bonds weaken and the soil experiences large volume decrease.

Residual granite soils in South Africa, especially the Cape Granite Suite, are often overlooked as potential collapsible soils. In general, collapsible soils consist of silts and fine sands coated with colloidal matter, with high void ratio, and low dry density however, residual granite soils do not necessarily present these characteristics. Problems associated with residual granite soil are still occurring in South Africa since its behaviour is not fully understood yet. It is important to determine the effects of wetting/flooding on the behaviour of these soils, especially in their natural form and when used as compacted fill material. The presence of water has a large impact on the behaviour of collapsible soil fabric. During dryer seasons, water evaporates from the soil structure, causing suction between voids and particles, resulting in higher strength at low moisture content. When such a soil fabric is flooded, large volume changes occur due to the densification of the soil. Thus, it is significant to determine the intrinsic behaviour of residual granite soil in South Africa.

1.3 AIM AND OBJECTIVES OF RESEARCH STUDY

The research study aims to study the disintegration characteristics of residual granite soils from the Cape Granite Suite. Classification of the soil is based on mineralogy, grading properties, Atterberg limits, and maximum dry density and optimum water content. The characterisation is based on the geotechnical properties of the decomposed granite soil derived from triaxial compression tests. The properties include shear strength, volumetric behaviour during shearing, critical state properties, stress paths, and relative breakage of particles. The collapsing nature of decomposed granite soil is poorly understood, and therefore the current research will emphasise the influence of water on the properties of the soil. The presence of water also affects

the strength of individual and/or aggregated particles which may result in particle breakage of coarser particles. These aspects form the basis of the current research.

The following objectives will be focused on to achieve the abovementioned primary aim:

- Provide research on the behaviour of decomposed granite soil by simulating field conditions in a triaxial compression apparatus. This includes varying the initial density, confining pressure, and initial water content of the triaxial specimens, and air-drying specimens until they reach constant mass.
- Determine whether a potential collapse settlement fabric forms after being exposed to the abovementioned initial conditions by flooding the specimen and analysing the effects it will have on the shear strength of the soil.
- Qualify the influence of particle breakage during shearing and the sudden increase in pore water pressure on the stability of decomposed granite soil.
- Determine whether decomposed granite soil used in this research can be represented by critical state soil mechanics by using the Modified Cam-Clay model and the results obtained from numerous triaxial tests.
- Discuss results obtained and compare it with previous research and critical state models created for residual granite soils.

1.4 ASSUMPTIONS AND LIMITATIONS

Various tests will be carried out on the residual granite soil to determine its geotechnical properties. These include classification tests, triaxial compression tests, and CT scans. The moisture content of specimens is predetermined, however, evaporation and the addition of too much water due to possible scale error will cause different initial moisture conditions than anticipated. These limitations are accounted for during the calculation of initial moisture content for each specimen, during both classification tests and triaxial tests, by taking moisture content samples. During the preparation of triaxial test specimens, the moulded specimens are handled carefully but particles along the edge seem to be friable. This is also the case for specimens after they have been sheared and sent for CT scans. The loss of particles due to handling will result in different amounts of particles before and after shearing, influencing the sieve analysis results. Specimens will be oven dried in paper bags to prevent the loss of friable particle and they will also be transported in these bags for CT scans.

Limitations on the triaxial compression test include the use of side drains and the effects of membrane penetration. Both affect the deviator stress of each specimen. Fortunately, these

have been accounted for in the calculations by including membrane and side drain corrections. Specimens that are partially saturated are limited to displacement and load measurements since the volume change cannot be measured with the typical triaxial cell setup used in this research. Flooding, of partially saturated samples, is set to take place over 24 hours, however, there will be no measurement proving that the sample is truly saturated. The maximum confining pressure is limited to 1000 kPa, restricting the amount of particle breakage.

The parameters used for the critical state model were based on the triaxial tests performed in this research and the number of tests (drained/undrained) performed limits the precision of the parameters. The axial strain boundary, which is at 20%, causes the test programme to stop, even if it has not yet reached the critical state. Specimens sent for CT scans before shearing have formed interparticle bonds due to drying out before being sheared. This has been accounted for by fully saturating the specimens before shearing.

1.5 CHAPTER OVERVIEWS

This thesis corresponds to the typical structure of an experimental study, and it is divided into the following five chapters:

Chapter 1: Introduction. This chapter provides the background to the research study, the problem statement, the aims and objectives of the study, the assumptions, and limitations.

Chapter 2: Literature study. The literature study provides a foundation for the research study and focuses on findings from various literature sources. It highlights the prediction and evaluation of the behaviour of decomposed granite soils and what problems are associated with this soil. It describes the problems encountered within South Africa on residual granite soil, especially within the construction industry. This chapter also considers the intrinsic properties of decomposed granite soil that has been concluded by researchers and outlines the basic concepts of critical state soil mechanics, which will form the basis of the analysis of triaxial test data.

Chapter 3: Methodology. Chapter 3 describes the procedures followed to gather test data to reach the aims of this study. It gives reference to the specific standards that are correlated to each test.

Chapter 4: Results and Discussion. Classification and characterisation test data are presented in this chapter which includes triaxial compression test results. Results presented in this chapter will be discussed and compared to previous findings to determine the behaviour of the soil. It

will be modelled against the typical Modified Cam-Clay model to determine whether the soil can be presented by a critical state model. This chapter will also focus on the presence of water and the effects of varying degrees of saturation on the stress and strain of the soil. Particle breakage after triaxial compression tests will also be evaluated.

Chapter 5: Conclusions and recommendations. The last chapter will emphasise and highlight the findings of this research discussed in Chapters 4. Recommendations are also made to further the study if necessary. The recommendations will include improved methods and additional tests to perform on possible future research of decomposed granite soil.

CHAPTER 2: LITERATURE STUDY

2.1 INTRODUCTION

This chapter presents the general composition of decomposed granite soil distributed through South Africa. It briefly discusses the various methods of weathering to the soil, followed by a detailed description of the formation of residual granite soil. Understanding these processes help define the characteristics of the soil. Section 2.5 discusses the problems associated with decomposed granite soil and Section 2.6 the problems encountered when constructing on such a soil. Subsequently, the mechanical engineering properties of decomposed granite soils are presented in Section 2.7 with specific emphasis on permeability, compaction, compressibility, strength, and stress-strain behaviour. Decomposed granite strengthens over time due to suction between interparticle voids caused by seasonal wetting and drying (Lee & Coop, 1995). It exists in a partially saturated state and may collapse when flooded. This behaviour, along with the concepts of particle breakage and unsaturated soil mechanics will be accounted for in Sections 2.8 and 2.9. Lastly, the critical state model for Modified Cam-Clay and the application thereof will be explained in Section 2.10.

2.2 DEVELOPMENT OF WEATHERED SOIL

Weathering is a very important process that involves the decomposition and disintegration of rocks. It can contribute to the formation of astounding sceneries, but also bring about the deterioration in structures built. Weathering gradually deteriorates paint, chemical weathering causes oxidation which is responsible for rust, plant roots can break through concrete, and the freeze-thaw cycles coupled with salty water contributes to pavement destruction. Mechanical and chemical weathering are the two fundamental types of weathering where the former is carried out through physical forces breaking rock down into smaller pieces, and the latter by changing the rock's mineral composition. These two processes go hand in hand and weathering seldomly occurs due to only one process (Tarbuck *et al.*, 2014).

2.2.1 Mechanical weathering

When a rock is being broken down into smaller pieces through physical processes, its surface area increases making it more susceptible to chemical weathering. Mitchell and Soga (2005) and Tarbuck et al. (2014) listed five processes that lead to the fragmentation of rock:

- **Unloading.** Deep below the earth's surface igneous rock can be found surrounded by great confining pressures. When the overlying bedrock erodes, the confining pressure reduces,

and the igneous mass expands and separates from the rock below. This process causes cracks to form at great depths, and joints to form parallel to the surface. Continuous weathering of the exposed rock causes the rock to peel or spall, creating an exfoliation dome. If confining pressures are reduced too quickly, the rock can explode as a result of stress release. This is termed popping rock.

- **Thermal expansion and contraction.** Thermal expansion and contraction target the weakened planes already present in the rock until it fractures. Rapidly increasing temperatures from fires also cause weathering of rocks.
- **Crystal growth, including frost action.** It is known that when water freezes, it has the property of expanding up to 9%. Thus, when water fills the cracks within rocks and freezes, it gradually weakens the rock. The frozen wedge accumulates more and more films of water from unfrozen areas and eventually the rock fractures. This process is called frost wedging. When salt from sea spray gets caught in rock crevices along with the evaporation of water, salt crystals start to form and gradually grow larger. Surrounding grains are pushed apart, and the rock weakens over time.
- **Colloid plucking.** The shrinkage of colloidal materials, especially those with high plasticity, exert tensile stresses on surfaces they are in contact with when drying.
- **Organic activity.** Plant roots in search of water and nutrients wedge through existing fractures. Burrowing animals, such as worms and rodents, remove fresh material from the fractures and relocate it at the surface where it is more prone to chemical weathering. Human activities, such as rock blasting for road construction or in search of minerals, have a noticeable effect on the weathering of rock.

2.2.2 Chemical weathering

As previously mentioned, mechanical weathering increases the surface area available for chemical weathering. Then again, chemical weathering weakens the outer portion of some rocks making physical breakdown easier (Tarbuck *et al.*, 2014). The internal structure of minerals is broken down and completely transformed into another. Some minerals are released into its surrounding environment or completely dissolved. Water is the main element as it is a good solvent that increases the chemical activity for weathering processes. Mitchell and Soga (2005) and Tarbuck et al. (2014) listed some of the major processes of chemical weathering:

- **Hydrolysis.** The silicate group minerals are primarily decomposed through a reaction between the mineral and water ions (H^+ and OH). It is the hydrogen ion that eradicates the original arrangement of the mineral and causes it to decompose. Some clay minerals form

as a result of weathering of silicate minerals. An example of this is the weathering of feldspar:

Orthoclase feldspar

$$K\ silicate + H^+OH^- \rightarrow H\ silicate + K^+OH^-\ (alkaline)$$

Anorthite

$$Ca\ silicate + 2H^+OH^- \rightarrow H\ silicate + Ca(OH)_2\ (basic)$$

Continuous introduction of hydrogen ions together with the removal of soluble materials allows the reactions to progress to the right. Soluble materials are removed through leaching, precipitation, complexing, and adsorption.

- **Chelation.** This process chemically removes metallic ions from minerals when organic acids are dissolved in water. Organic acids can be derived from decomposing plants in soil known as humus. The dissolution of muscovite is enhanced by a chelating agent, oxalic acid, releasing oxalate and forming a soluble complex with an aluminium cation.
- **Cation exchange.** It has an important role in the process of chemical weathering in the following ways:
  - It can reduce the colloids' ability to carry hydrogen onto unweathered surfaces by replacing the hydrogen on hydrogen bearing colloids.
  - The types of clay minerals formed through weathering are influenced by ions held by Al_2O_3 and SiO_2.
  - The adsorbed ion concentration may influence the physical properties of the system, for example, permeability.
- **Oxidation.** Iron-rich minerals undergo a chemical reaction, called oxidation when electrons are lost to oxygen. Oxygen combines with iron and the oxidation is as follows:

$$4Fe + 3O_2 \rightarrow 2Fe_2O_3$$

Reddish-brown iron oxide called hematite is the product of decomposing ferromagnesium minerals like pyroxene, olivine, biotite, and hornblende. Hematite has an important role in the colouring and cementing of sedimentary rocks. In dry areas oxidation takes place very slowly, but water speeds up the reaction due to the presence of dissolved oxygen. The decomposition of pyrite poses an environmental hazard, especially within the coal mining industry. When pyrite oxidises, it yields sulfuric acid and iron oxide which makes its way into aquatic habitats, executing living organisms. Reduction is a reaction in which electrons are gained and these reactions store energy that can be used in later periods of weathering.

- **Carbonation.** Carbonic acid forms when carbon dioxide from the atmosphere dissolves in raindrops. When the earth's materials are exposed to these carbonate or bicarbonate ions they start to weather. Calcite can be found in limestone and marble buildings, and it is highly susceptible to even a weak acidic solution. Calcium carbonate transforms into soluble products when reacting with water containing carbon dioxide, and the reaction is as follows:

$$CaCO_3 + (H^+ + HCO_3^-) \rightarrow Ca^{2+} + 2HCO_3^-$$

An example in nature is the limestone caverns formed by the transportation of dissolved limestone. Soluble ions can manifest in underground water supply, termed hard water, and generally, water softener needs to be added to make the water useful.

2.2.3 Rates of weathering and soil formation

The effects of climate, rock characteristics, topography, plants and animals, and time are all factors that influence the rate of rock weathering and the type of soil forming. Mitchell and Soga (2005) and Tarbuck et al. (2014) described these factors as follows:

- **Climate.** Factors of climate include temperature, water, and character of vegetative cover. Chemical weathering thrives in areas with abundant moisture and warm temperatures. If temperatures are too high, such as in arid areas, insufficient moisture will halt the process of chemical weathering. The same goes for polar regions where moisture is locked up as ice. Another climate factor is the intensity of rainfall: long lasting light-intensity rainfall promotes leaching, whereas short intense rainfall causes erosion and runoff. Climate conditions also control the type of animal and plant life present in an area which plays a vital role in the formation of soil.
- **Rock characteristics.** The parent material is a very important factor in the early stages of weathering. According to Bowen's reaction series (Bowen, 1922), quartz crystallises last, and it has sufficient chemical durability to withstand great periods of weathering. An example of the importance of parent material is the construction of structures made from marble and granite. Granite structures are more resistant to weathering due to its silicate mineralogy, whereas marble consists of calcite which dissolves even in weak acidic solutions.

  Weathered soil developed from bedrock as a parent material is called residual soil, whereas weathered soil developed from unconsolidated deposits as a parent material is called transported soil. The term transported soil refers to the parent material (unconsolidated deposits) that has been carried from elsewhere through water, wind, gravity, or ice, while

the weathered soil is formed in place on the parent material. Weathering will take place more rapidly on unconsolidated deposits since they are already partly weathered.

- **Topography.** The terrain determines the rate of erosion based on the steepness and lengths of slopes. Steep slopes accelerate the process of erosion to such an extent that soils are thin or even non-existing. The steepness causes water to run off and not sufficiently saturate the soil for plant growth. These down-slope movements generally form talus slopes.

  Soils that are poorly drained usually contain large quantities of organic matter due to saturated conditions obstructing the decay of vegetation. They are typically dark of colour and have thick soils. The best topography for soil development is a flat to wavy surface with good drainage and adequate infiltration of water into the soil.
- **Plants and animals.** The fertility of soil depends on the amount of organic matter present. Plants, animals, and microorganisms are primary contributors to the addition of organic matter into the soil. When plants and animals decay, certain nutrients and organic acids are released, aiding the weathering process. Organic material also has the ability to retain water in the soil. Burrowing animals create intrusions for waterflow, and they aid in the mixing of soil and organic matter.
- **Time.** Generally, the longer a soil has been allowed to weather, the less it resembles its parent material. In the early stages of weathering, the parent material determines the rate of weathering. After some time has passed, the climate becomes the primary factor of weathering. Each soil formation takes place under its own circumstances in its own amount of time. The length of time strongly influences the nature of the soil.

2.3 DEVELOPMENT OF RESIDUAL GRANITE SOIL

Igneous rocks are formed when magma cools down and solidifies. Magma rises from the earth's core and presents itself as lava on the earth's surface. Lava can either violently erupt from volcanoes, producing ash and steam or it can quietly flow without any major disruptions (Tarbuck *et al.*, 2014). Generally, magmas consist of three main components: solid, liquid, and gas. If any solid components are present in magma, they are in the form of crystals of silicate minerals. When magma cools down these crystals increase and forms a cluster of crystals (Tarbuck *et al.*, 2014).

The liquid component of magma is termed melt, and it consists of the following most common elements found in the crust of the earth: silicon, oxygen, potassium, sodium, magnesium, and aluminium (Tarbuck *et al.*, 2014). Volatiles are the gaseous components of magmas, and they

either vaporise at the surface due to pressure or they migrate through surrounding rocks through water-rich fluids (Tarbuck *et al.*, 2014). Igneous rocks form when magma crystalizes deep below the earth's surface or when it solidifies on the earth's surface. The former is called intrusive igneous rock, and the latter is extrusive igneous rock. When intrusive igneous rocks are exposed, it is mainly due to erosion and uplift of the overlying rocks (Tarbuck *et al.*, 2014).

Granite compositions are considered to be light silicates. They typically consist of minerals like quartz, potassium feldspar, and muscovite mica and are abundant in the earth's crust. The quartz grains found in granite appear to be somewhat rounded mainly due to spheroidal weathering (Tarbuck *et al.*, 2014). Bowen's reaction series shows how magma cools and how minerals crystalise when certain temperatures are reached (see Figure 2.1). The systematic order of this series also represents the weathering of granitic rock.

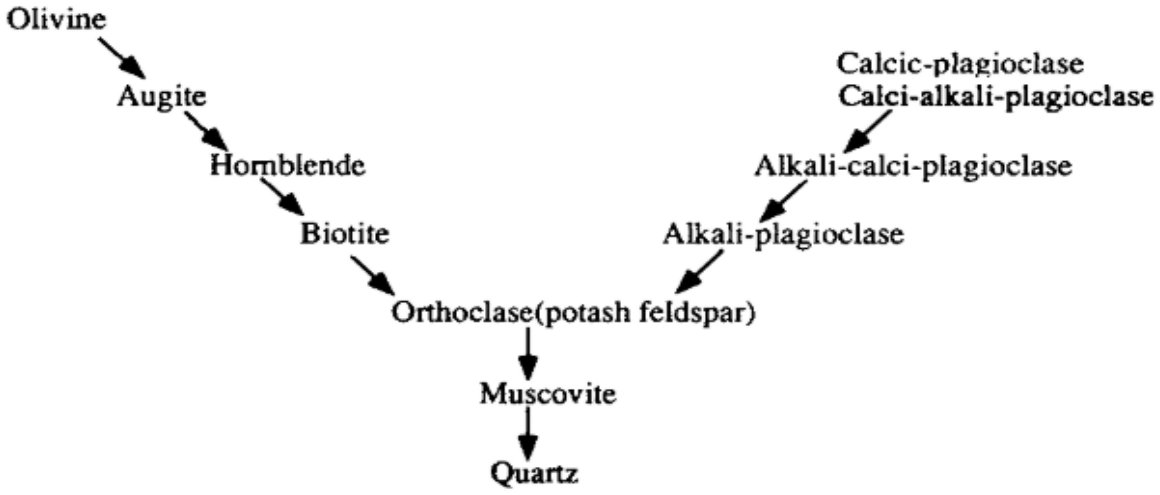

Figure 2.1 Bowen's reaction series (Mitchell & Soga, 2005)

The decomposition of granitic rock is as follows: biotite, plagioclase feldspar, orthoclase, and finally kaolinite. Quartz particles remain unchanged and mica particles are obtained from gruss formations during the breakdown of orthoclase. As seen with the decomposition of granite, clay minerals are the end product of weathering and can either be kaolinite, smectite, or other clay minerals (Mitchell & Soga, 2005). Feldspar becomes altered by a process called hydrolysis, producing clay minerals along with other ions in solution. This process involves a chemical reaction where water loosens the chemical bonds within a mineral. The following reaction shows the chemical weathering of potassium feldspar to one of the most abundant minerals, kaolinite, along with quartz and ions (Earle, 2014):

$$2KAlSi_3O_8 + 3H_2O \rightarrow Al_2Si_2O_5(OH)_4 + 2K^+ + 2OH^- + 4SiO_2$$

Physical weathering of decomposed granite soil includes the disintegration and disaggregation of the material and is dependent on the applied force. The applied forces may range from those listed in Section 2.2.1. A combination of physical and chemical weathering of granitic rock contributes to the formation of residual granite soil. Different zones of a matured granitic profile can be viewed in Figure 2.2. The top clayey sand layer composes mostly of variably sized particles and no structured mass. Progressing down the granitic profile, the amount of gruss decreases and the angularity of the core stones increases. At the deepest profile, angular granitic blocks can be found with very little debris (Mitchell & Soga, 2005). Galer, Sasaki, and Nakamura (1998) concluded in their field investigation of decomposed granite that weathering decreases with depth.

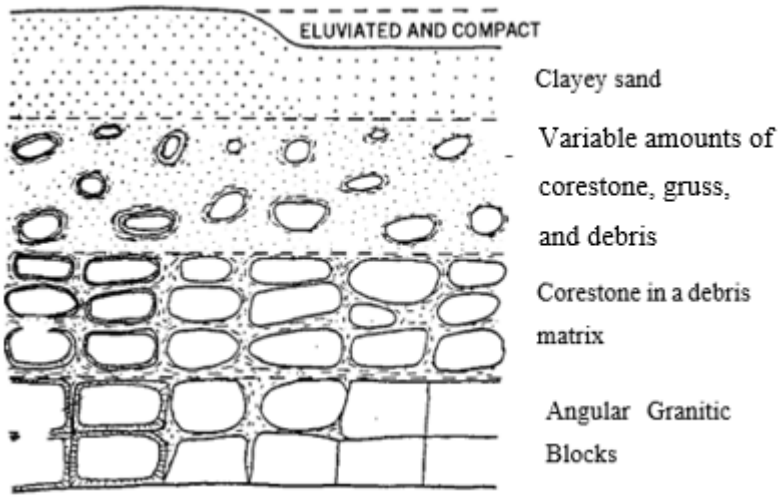

Figure 2.2: Decomposed granite profile (Mitchell & Soga, 2005)

2.4 DISTRIBUTION OF RESIDUAL GRANITE SOILS IN SOUTH AFRICA

2.4.1 Basement Complex: granite

The underlying Basement Complex of southern Africa consists of four cratons surrounded by mobile belts. Two cratons located in the eastern section of South Africa are older than 2500 million years and are called the Zimbabwean- and Kaapvaal cratons (Brink, 1979). In the western section, the Angolan- and Richtersveld cratons are situated, and they are younger than the two forementioned cratons (Brink, 1979). The composition of the cratons is crystalline rock, primarily granites and gneisses, and they are considered stable masses. However, the surrounding mobile belts are less stable than the cratons and are mostly elongated zones of crustal rock. They have undergone considerable deformation related to metamorphism and

igneous activity. Younger volcanic and sedimentary rocks overlie these cratons and mobile belts either partially or completely (Brink, 1979).

Granites of the Basement Complex in the eastern parts of South Africa are distinct from those in the western parts due to the varying climates. In the eastern parts where the subcontinent is predominantly humid, residual granite soils reach great depths as a result of granite decomposition. The soil is composed of unaltered quartz sand grains, mica particles, and feldspar that has been completely kaolinized. The chemical reaction between felspar and water charged with carbon dioxide is as follows:

$$\underset{\text{Orthoclase}}{4KAlSi_3O_8} + 4H_2O + 2CO_2 = \underset{\text{Kaolinite}}{(OH)_8Al_4Si_4O_{10}} + \underset{\text{Colloidal silica}}{8SiO_2} + \underset{\text{Solute}}{2K_2CO_3}$$

In areas of high rainfall, the colloidal kaolinite particles are mostly removed in suspension through circulating ground waters. This process leaves behind a spongy residuum of micaceous silty sand which exhibits high collapse potential (Brink, 1979). In the western parts of South Africa in regions with arid to semi-arid climates, granites are weathered mainly by mechanical disintegration. Residual soils are shallower in these regions compared to the humid regions previously mentioned. The underlying granites present no problems in foundation engineering and any problems that may arise are likely associated with deep transported soils (Brink, 1979).

2.4.2 Cape Granite Suite

Plutons of the Cape Granite Suite are largely limited to the south-western Cape with the exception of occurrences near George and in Namaqualand (Brink, 1981). The composition and texture of Cape granitoids are very complex and variable, depending on the location of the plutons. In South Africa, problems associated with collapsible soils have occurred on Cape Granite. This phenomenon was not previously associated with residual granite soils, but rather with aeolian sands. Fortunately, it was established that the intense leaching of decomposing rock resulted in a grain structure similar to that of weathered aeolian sands (Brink & Kantey, 1961). The presence of water thus has a very large influence on the behaviour of such soil.

The lithology of the Cape Granite Suite may vary considerably depending on its locality. The rocks' compositions can range from fine-grained quartz porphyries to coarse-grained porphyritic biotite granites, and even include some syenites (Rooiberg near Namaqualand) and quartz diorites (Malmesbury and Ysterfontein). Figure 2.3 shows the localities of the plutons of the Cape Granite Suite which includes Swellendam, Robertson, Greyton, Onrus, Wellington,

Paarl, Paardeberg, Saldanha-Langebaan, Stellenbosch, Kuils River-Helderberg, Avoca, Dassen Island, Darling, Haelkraal and the Cape Peninsula in the southwestern pluton, Bavianskloof, Woodville, and George in the eastern pluton, and Kuboos and Swartbank in the northern pluton. In plutons such as Paardeberg and Malmesbury, where little denudation has occurred, the finer-grained suite tends to predominate. Coarser varieties are mainly present where deeper erosion has taken place, such as the Cape Peninsula.

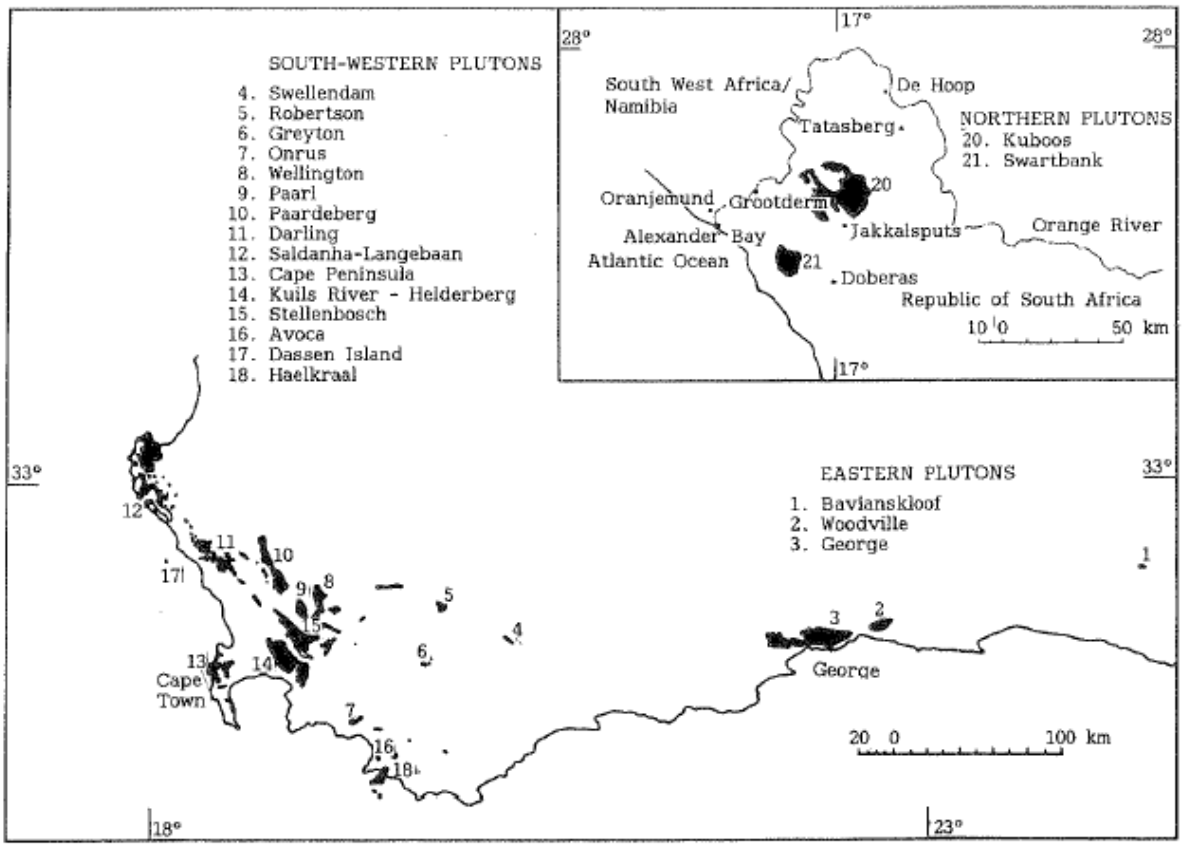

Figure 2.3 Localities of plutons of Cape Granite Suite (Brink, 1981)

The map in Figure 2.4 illustrates the micro-climatic regions of South Africa adapted from Weinert's map (Weinert, 1980), and Weinert's N-values are as follows:

- N<2: wet climatic region
- 2<N<5: moderate climatic region
- N>5: dry climatic region

According to Weinert (1980), weathering characteristics are influenced by the climate. For regions with N>5, physical weathering is the main mode of weathering with almost no secondary minerals, whereas regions with N<5 are more susceptible to chemical weathering. From Figure 2.4 it is evident that the southwestern Cape has a moderate climatic region with

an N-value of 2 – 5, suggesting that the Cape Granite Suite in this area is primarily weathered through decomposition (chemical weathering). Similarly, George has a wet climatic region with an N-value of less than 2. In Section 2.2.2 the weathering characteristics of chemical weathering is discussed in detail.

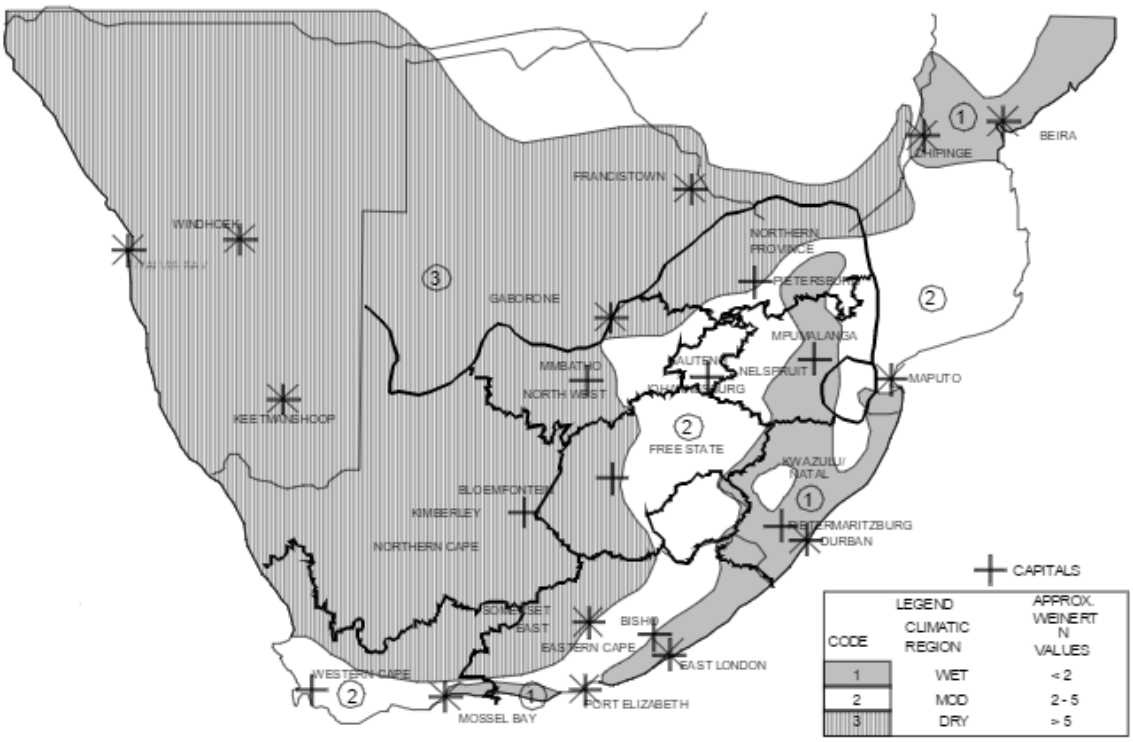

Figure 2.4 Macro-climatic regions of South Africa (Adapted from Weinert, 1980)

Residual granite found in humid zones are often rich in mica and contain coarse sand-sized quartz particles, with an appearance of intact clayey silt (Brink, 1981). Engineering problems associated with residual granite soil from the Cape Granite Suite in humid areas are largely due to the leaching of clays and the formation of collapsible soil fabric. In areas of annual water surplus (Figure 2.5), such as the southwestern Cape and George, residual soils are deep and the kaolinization of feldspar is far advanced. When soluble and colloidal matter leach out from decomposing granite, the void ratio increases and quartz, mica plates, and feldspar grains form an unstable arrangement (Brink & Kantey, 1961). The development of residual granite soil is discussed in Section 2.3.

In contrast, more arid areas, such as Namaqualand and between St Helena and Saldanha, have thinly developed residual soils with a coarse sandy texture (Brink, 1981). Weathered granites in these areas rarely cause engineering problems and this also contributes to the lack of test

data available for weathered granite soils in the wetter climate zones. Frequent engineering problems encountered with residual granite soil from the Cape Granite Suite in wet areas include the formation of a collapsible soil fabric, slope instability when saturated, dispersiveness (physical and chemical) of clay particles contributing to a collapsible soil fabric, and core-stones within the residual granite soil. These problems will be discussed in more detail in Section 2.5.

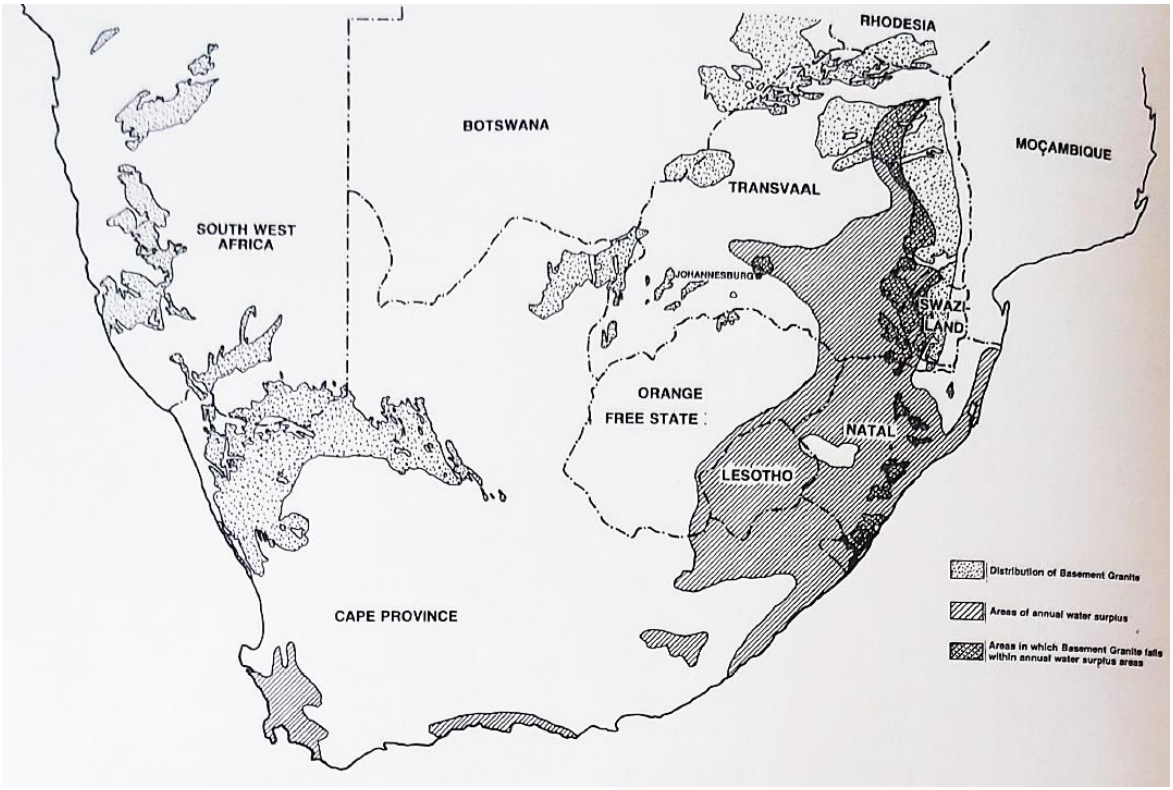

Figure 2.5 Areas of an annual water surplus in South Africa (Brink, 1979)

2.5 PROBLEMS ASSOCIATED WITH RESIDUAL GRANITE SOIL

2.5.1 Collapsible grain structure (instability upon saturation)

When a soil experiences sudden, large settlements upon saturation, it is called a collapsible soil. Soils with a collapsible grain structure usually have a high void ratio accompanied by strength from the colloidal bridges between particles at low moisture content. In these conditions, a collapsible soil can typically withstand relatively large, imposed loads with limited settlement occurring (Figure 2.6). However, when the soil is saturated with no change in load, immediate settlement will occur, resulting in large volume changes (Schwartz, 1985)(Figure 2.6). Since water has such a great influence on the behaviour of collapsible soils, it is apparent that no collapse will occur below the water table. Another factor that can lead to the collapse of a soil structure is the application of dynamic loads, like earthquakes. In such

instances, no additional water is necessary to cause collapse since colloidal bridges are subjected to shear failure (Schwartz, 1985).

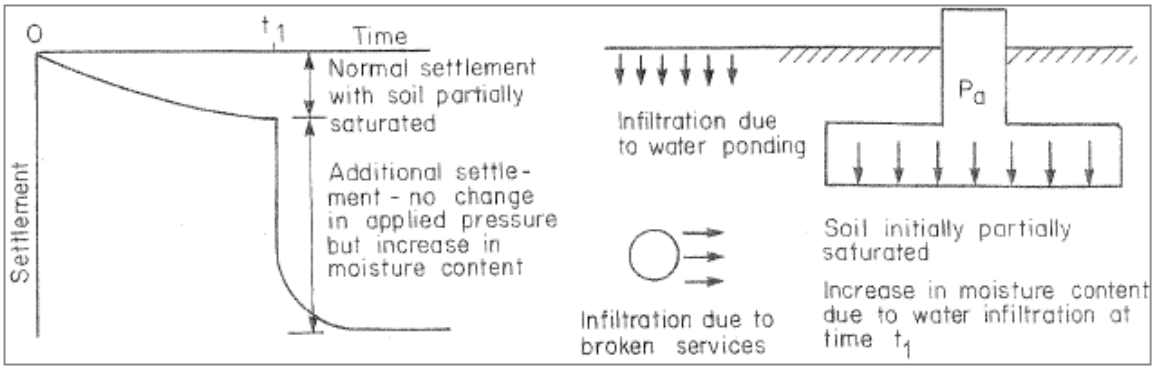

Figure 2.6 Basic concept of additional settlement due to collapse of soil fabric (Schwartz, 1985)

Residual granite soil, in both its natural and compacted states, have the tendency to become unstable when saturated (Lee & Coop, 1995), conforming to the conditions of a collapsible soil. For residual granite soils, quartz particles have colloidal coatings around individual grains, contributing to a seemingly high strength soil. When saturated under load, the colloidal bridges soften causing particles to pack into a denser state leading to sudden settlement of the foundation. Lee and Coop (1995) attribute the plastic volumetric compression of residual granite soils to particle degradation (breakage) in addition to the softening of interparticle bonds. Aggregated particles in weathered granite soils separate when saturated due to the loss of interparticle bonds. Particles weakened by weathering typically have pre-existing fissures held together by electrostatic forces, particle interlocking, or pore suction inside the micro-fractures. The presence of water can weaken these forces and cause the collapse of the soil fabric (Lee & Coop, 1995). Collapse of weathered granite soil researched by Lee and Coop (1995) was associated with the weakening of intraparticle bonds rather than interparticle bonds. However, as previously mentioned, the soluble and colloidal bridges between particles (interparticle bonds) constitute the structure of a collapsible soil fabric, and that the breakdown of these bridges due to saturation causes collapse. Lee and Coop (1995) attributed the separation of aggregations to the presence of swelling minerals since their residual granite contained smectite, an active clay known for being expansive.

Problems associated with collapsible soils usually occur many years after construction. The collapse of structures is primarily due to ponding of rainfall in poor drainage areas or leaking of a nearby pipeline (Schwartz, 1985). Settlement will particularly occur on the saturated area,

resulting in localised collapse, and causing severe cracking of structures. As previously mentioned, when collapsible soils are exposed to dynamic loads, with no addition of water, it can lead to collapse. This is largely the cause of collapse in roads, railways, and airfields where dynamic forces are continuously occurring (Schwartz, 1985). When using collapsible fabric as a fill material, it is necessary to account for volume reduction after excavation and compaction. During both excavation and compaction, the collapsible structure is destroyed, and particles are densely arranged. This is also applicable during the construction of earth dams/reservoirs. Failing to account for the shortage of material will result in an unbalanced cut-to-fill ratio. When the presence of collapsible soils are completely disregarded, severe circumstances of collapse settlement may lead to overtopping of the embankment (Schwartz, 1985).

In most cases, residual granite soil does not conform to the typical characteristics associated with collapsible soils, yet it still possesses a collapse potential (Fouché & Asante, 2019). According to Fouché and Asante (2019), residual Cape granites from Stellenbosch, Paarl, and Darling showed collapse potentials ranging from non-collapsible to collapsible (see Table 2.1). In the Stellenbosch area, residual granites can have a collapse potential value between 1.7% - 10% with a maximum potential of 18.4%, whereas Paarl had collapse potential values of 0% - 1% and 5.7%, and Darling 0% - 1% and 3% (Fouché & Asante, 2019). Fouché and Asante (2019), established that scanning electron microscopy (SEM) and computed tomography (CT-scanning) can aid in the identification of collapsible soils with atypical properties.

Table 2.1 Guiding values of collapse potential (Jennings & Knight, 1975)

Collapse Potential	Severity of problem
0% - 1%	No problem
1% - 5%	Moderate problem
5% - 10%	Trouble
10% - 20%	Severe trouble
>20%	Very severe trouble

2.5.2 Dispersive behaviour

When feldspar-rich granite-gneisses go through chemical weathering, residual sediments like kaolinite, smectite, and illite clays develop (Haldar & Tišljar, 2014). Up until now, only kaolinite has been discussed as a secondary mineral of decomposing granite. Kaolinite clay is a 1:1 clay mineral consisting of layers formed by one tetrahedral sheet combined with one octahedral (gibbsite) sheet. Interlayer swelling of kaolinite clay is restricted by van der Waals

forces and hydrogen interlayer bonding, resulting in a stable clay with very little isomorphous substitution (Mitchell & Soga, 2005). Dispersibility and high exchangeable sodium percentage values are rarely associated with kaolinite clays, but resonate largely with smectites (montmorillonite) (Elges, 1985) and other 2:1 clays, like hydromicas (illite and vermiculite) and micas (Harmse, 1980). Unlike kaolinite, the van der Waals forces for dispersive clays are less than the repulsive forces, and when the clay mass is in contact with water, clay particles detach from the surface and go into suspension (Elges, 1985). Suspended particles are carried away by flowing water and this leads to erosion of the soil.

Weathered granites of South Africa are known for their dispersive nature and Elges (1985) expressed that decomposing granite soils are prone to the development of high exchangeable sodium percentage values. Dispersive soils are primarily found in regions located between Weinert's climatic N-values of 2 and 10 (Elges, 1985). Many dams in South Africa have failed due to damages caused by dispersive soils. Visible signs of internal erosion include piping and jugging, often leading to slope failure. Cracking and/or settlement of dispersive soils located in embankment dams can occur during either of the following instances: during the first fill, at contacts between soil and solid material (e.g. conduits), when filling a reservoir after it has been empty for an extended period, or as reservoir levels rise (Mitchell & Soga, 2005). Figure 2.7 illustrates the known dispersive soil occurrences in South Africa according to Elges (1985), and it can be seen that the Cape Granite Suite includes dispersive encounters.

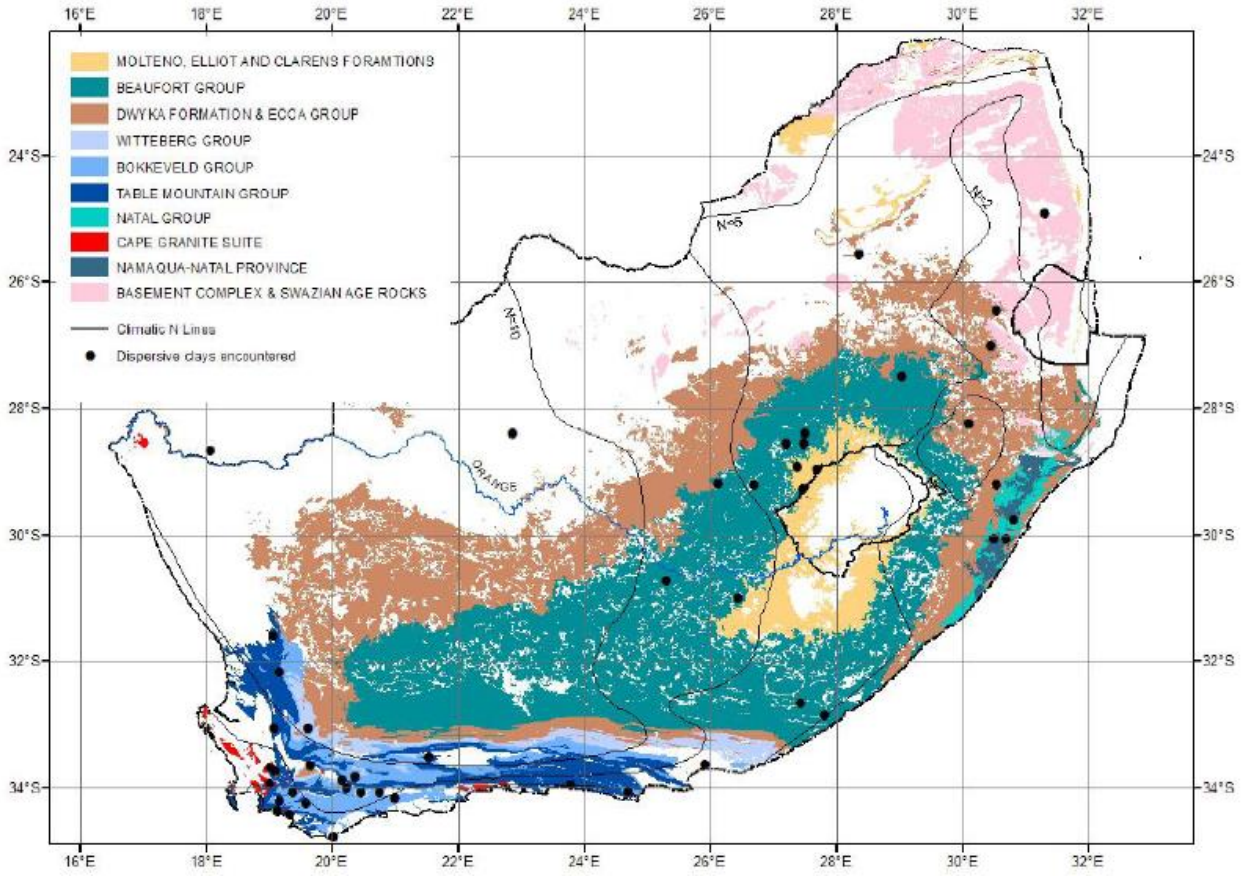

Figure 2.7 Identified dispersive clay occurrences (Elges, 1985)

2.5.3 Heaving behaviour

Heaving behaviour of soil is associated with expansive clays having a 2:1 lattice structure like smectites (montmorillonite). Figure 2.8 shows how clay platelets are spaced when dry and when allowed access to water (Day, 2021). Heaving clays expand when water molecules move into the clay platelets, and they can experience considerable volume change due to the fluctuation of interlayer water (Mitchell & Soga, 2005). Specific area is one of the most important factors influencing the effects that mechanical and physicochemical factors have on swelling and consolidation (Mitchell & Soga, 2005). It is defined as the total area of all grains in a unit mass of soil (m^2/g), and clays with very high specific surface area have very small particles. Table 2.2 lists the specific surface area of different clays and clean sand. Here it is evident that montmorillonite, which is a highly active clay mineral, has a very high specific surface area.

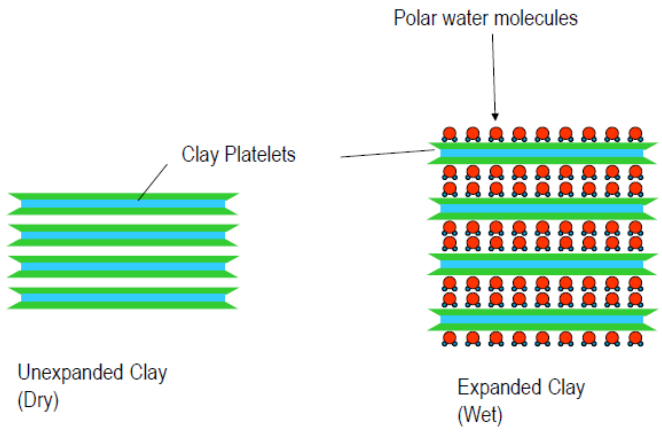

Figure 2.8 Clay platelets in unexpanded and expanded state (Day, 2021)

Table 2.2 Specific surface area of soils (Mitchell & Soga, 2005)

Soil grain	Specific surface area (m^2/g)
Montmorillonite	Up to 840
Illite	65 – 200
Kaolinite	10 – 20
Clean sand	$2x10^{-4}$

Expansive clays are presumably the most extensive of problem soils in South Africa (Williams, Pidgeon & Day, 1985) The formation of expansive clays is primarily influenced by the parent material and topography, and secondarily by time, living organisms, and climate which are all relatively constant. Residual soils developed from igneous rock and known for their expansive behaviour are as follows: dolerite of the Karoo Sequence, norite of the Bushveld Complex, lavas of the Ventersdorp Supergroup, or andesite or diabase in the Pretoria Group (Williams, Pidgeon & Day, 1985). Figure 2.9 shows the distribution of expansive clays and collapsing sand as proposed by Williams, Pidgeon, and Day (1985). In arid or semi-arid areas, the most apparent change in the clay structure is due to wetting of the soil, causing heave. Whereas in more humid regions, drying will most likely cause shrinkage of the active minerals.

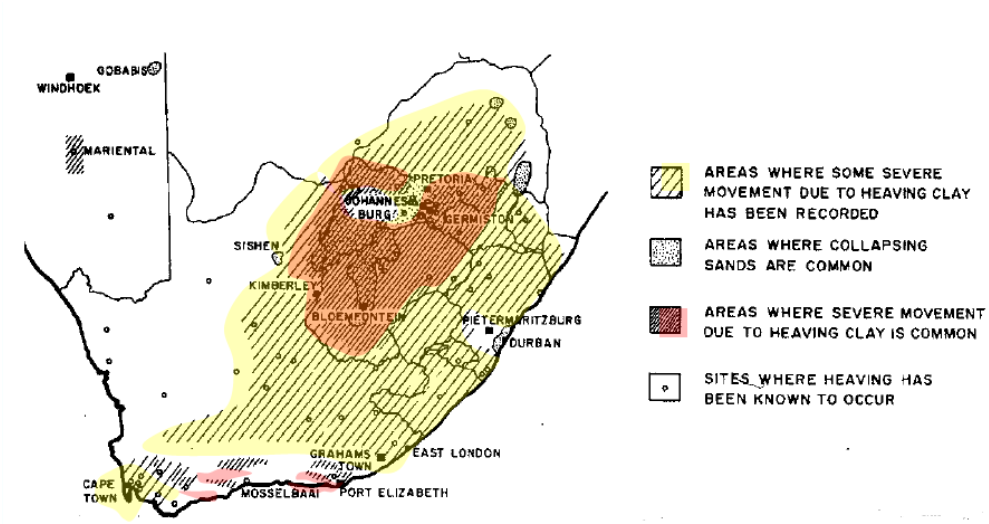

Figure 2.9 Distribution of expansive clays and collapsible soils in South Africa (Williams, Pidgeon & Day, 1985)

Problems associated with heaving soils can cause costly damages to structures and roads. Generally, single-storey buildings or structures with low external pressures are more likely to be affected by heave. Houses typically show signs of heave within a few years of construction. Damages include cracks running up towards the corners of the roof, doming formations in the floors, and jamming of doors and windows. Seasonal wetting and drying of heaving soils can cause the edges of roads to move up and down and form longitudinal cracks. When vegetation is located near roads, roots can extract moisture from the soil and cause undulation (Day, 2021). The development of expansive clays is not usually associated with residual granite soils and is considered to be non-expansive. Brink (1981) expressed that in certain areas, like the flatter northern slopes of Wynberg Hill, slightly expansive soils do occur in residual granite soils.

2.5.4 Problems associated with mica in residual granite soils.

Quartz, K-feldspar, plagioclase, and mica are the main constituents of granite (Haldar & Tišljar, 2014). For granites, mica is usually in the form of either biotite or muscovite, and when these minerals are subjected to weathering, they result in hydrous micas vermiculite and illite, respectively (Dumbleton & West, 1966). Muscovite is more resistant to weathering than biotite, and it is characterised by a gibbsite sheet amidst tetrahedral sheets with interlayer potassium cations (Mitchell & Soga, 2005). Illite is characterised by the same structure as muscovite but with fewer potassium cations (Figure 2.10(a)). Interlayer swelling of muscovite and illite is prevented by the potassium cations that are tightly fitted between layers, resulting in a low cation exchange capacity (Mitchell & Soga, 2005). The potassium cations in illite are replaced

with hydroxides and it is therefore also referred to as hydro-muscovite (Haldar & Tišljar, 2014). Muscovite does not contain iron and for that reason, it is a colourless mica (Pellant, 2000).

Biotite is rarely found fresh in clastic sedimentary rocks since it is relatively less resistant to chemical weathering than muscovite (Haldar & Tišljar, 2014). When biotite weathers to vermiculite, its colour changes from black to bronze, brown. Vermiculite has a brucite sheet between two tetrahedral sheets, and its interlayer space is occupied by calcium (Ca^{2+}), magnesium (Mg^{2+}), and two layers of water molecules (Mitchell & Soga, 2005) (Figure 2.10(b)). This mineral can easily and quickly be transformed when calcium and magnesium are exchanged by other cations, or when it is heated, resulting in the loss of the adsorbed water in the interlayer (Haldar & Tišljar, 2014). The properties of vermiculite closely resemble that of smectite when the exchangeable cations are not calcium and magnesium (Mitchell & Soga, 2005). As previously mentioned, smectite has weak interlayer bonding which attracts water and causes swelling. Mitchell and Soga (2005) expressed that vermiculite and smectite have sufficient specific area causing unsatisfied water adsorption forces at low water contents.

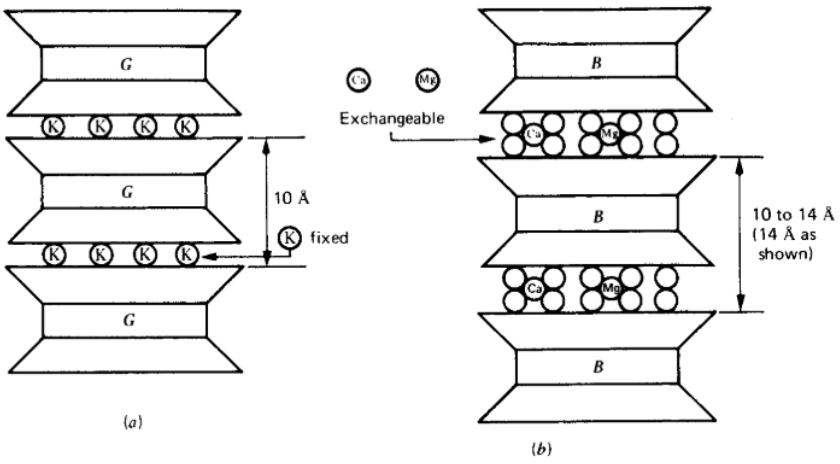

Figure 2.10: Schematic diagram of (a) muscovite and illite, and (b) vermiculite (Mitchell & Soga, 2005)

McCarthy (1962) researched the influence of coarse and fine mica (muscovite) on the compression characteristics of compacted micaceous soil. He established that the increase of both coarse and fine (<0.1 mm) mica lowered the dry density, increased the optimum moisture content and the compression of the soil. However, the presence of fine mica had a greater effect on the compression of the soil than coarse mica (McCarthy, 1962). Muscovite is not considered an expansive soil, but it does possess flexible, elastic laminae, resulting in a springy action during compaction (Pellant, 2000). Mshali and Visser (2014) also reported that the increase of mica (muscovite) content results in a decrease in compacted density, and an increase in water

absorption. If the platy crystals of muscovite get bent, it will likely recover to its original shape. During compaction, the elastic laminae will bend around the quartz particles after which they will likely recover, causing bridging between particles, and reducing the initial density of the soil (Weinert, 1980).

Since biotite decomposes more readily than muscovite, it is unlikely to be present in weathered soil in significant quantities. Therefore, limited problems associated with biotite have been reported (Weinert, 1980). Weathered biotite, vermiculite, closely resemble smectite and tends to swell when saturated. Section 2.5.3 discusses the behaviour of expansive and shrinking soils.

2.5.5 Pseudokarst phenomena

A pseudokarstic terrain is a granular landscape with landforms very much like karst terrains however, they are formed by water flowing within the material. This phenomenon is the result of suffusion of granite soils. Mechanical and chemical actions of underground waters induce the undermining of residual soils where granite soils are predominantly susceptible to mechanical suffusion. Mechanical suffusion is when fine particles are washed out from between coarser particles, specifically deflocculated kaolinitic colloids in granitic soils. An increased hydraulic gradient accelerates the process of suffusion and subsequently may lead to the formation of sinkholes and other pseudokarstic features. In South Africa, areas such as the northern Transvaal and Swaziland provide great examples of the pseudokarst phenomena (Brink, 1979).

2.5.6 Core-stones within residual granite

The presence of core-stone of hard granitic rock within residual granite causes distinctive problems in foundation engineering. Core-stone accompanied by a residual soil with a collapsible grain structure generates a severe problem, and piling becomes practically impossible if the core-stone cannot be removed by hand (Brink, 1979). The Atlantic coastline and the area between Table Mountain and Lion’s Head are significantly affected by the presence of core-stone. Areas along the Atlantic coastline such as Camps Bay, Clifton, and Fresnaye encounter more severe problems than the eastern side of Table Mountain. For the construction of houses along this area, it is necessary to cut into steep slopes to place platforms for stable founding conditions. However, if core-stones are encountered it may cause unpredictable founding conditions that are highly unstable. Remedial measures to support this problem include the installation of anchors, drains, mesh, gunite application, or modification of a design to render the removal thereof (Brink, 1981).

2.6 PROBLEMS ASSOCIATED WITH CONSTRUCTION ON RESIDUAL GRANITE SOIL: CASE STUDIES

2.6.1 Collapsible soils

The first reported case of collapse settlement was in 1957 when a water tower near White River was subjected to differential settlement. It occurred on residual granite soil of the Basement Complex, four years after construction. The significant settlement of two of the four columns, NE (northeast) and SE (southeast) base, were caused by the water tank overflowing, and a feed-pipe bursting as a result of the settlement, respectively (Brink, 1979)(Figure 2.11). Brink (1979) expressed that a trial hole dug near the NE base revealed a thoroughly leached residual granite soil profile. This soil was researched at the University of Witwatersrand where Knight (1961) developed a theory explaining the mechanism of collapse.

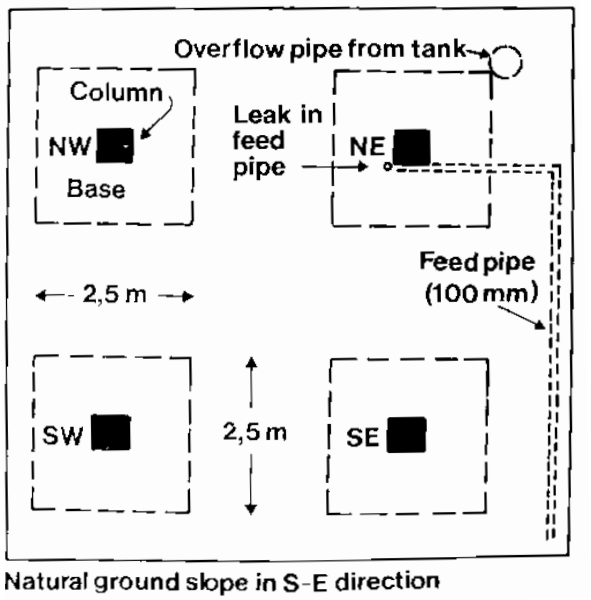

Figure 2.11 Foundation plan of White River water tower (Brink, 1979)

Terblanche (1989) attributed the collapse settlement of a three-storey industrial development corporation to the following factors: inadequate site investigation, inflexible underfloor and inappropriate foundation design, and poor site characterisation. Similarly, to the water tower in White River, the three-storey building was found on residual granite soil. Both case histories by Terblanche (1989) and Brink (1979) highlighted how very localised the problem can be at a particular site. For the three-storey building, significant settlement occurred in one of the three sections at a column founded too shallow in collapsible soil (Terblanche, 1989). This building required four phases of remediation entailing the following: compaction and grouting

around columns and to internal walls, underpinning of certain internal columns, additional geotechnical site and laboratory investigation, and repairs to cracked slabs (Terblanche, 1989).

Two major tunnelling projects, the Du Toitskloof Pilot Bore and the Franschhoek Tunnel, encountered slope stability problems in residual granite soil. When the residual granite soils were dry, they were generally stable although when saturated, resulted in slope instability (Brink, 1981). Both projects adopted different measures to counter the stability problems. The Franschhoek tunnel used a shield with an extensive programme of consolidation grouting, and the Du Toitskloof Pilot Bore used the technique of ground freezing (Brink, 1981). Construction of the latter tunnel resulted in a substantial amount of data gathered regarding the deformation and strength characteristics of the Cape Granites.

2.6.2 Dispersive soils

The Westphalia Leidam was constructed in residual granite soil and completed in November 1960. The design was very simplistic: it consisted of excavating residual granite soil and compacting material on three sides forming the earth embankment (Figure 2.12). At the time of construction, residual granite was not characterised as a collapsible soil, and therefore it was not accounted for during the calculation of quantities (Brink, 1979). Dispersive soils have also not been recognised as a problem soil in South Africa at this time. As discussed in Section 2.5.1, when excavating collapsible material, the volume will decrease as the soil's structure is destroyed. Once the dam was filled with water, problems associated with collapse settlement and dispersiveness proceeded to emerge. Change in electrolytes caused the clay aggregates to deflocculate into colloidal particles (Brink, 1979). Seeping water then carried the colloidal particles through interparticle voids resulting in piping developed along the flow path. Unfortunately, initial remediation proved to be ineffective, and further remediation was seen as uneconomical, and the dam was abandoned.

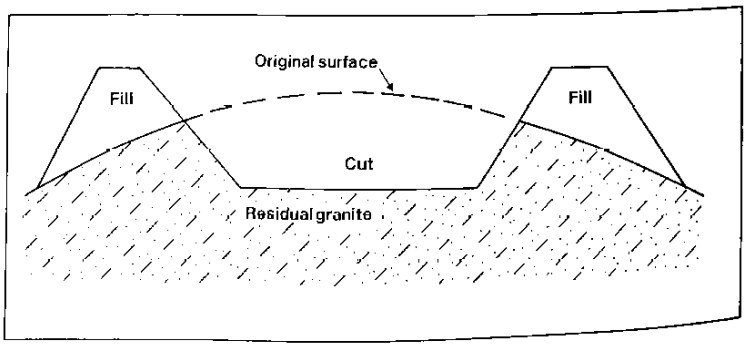

Figure 2.12 Diagrammatic cross-section through the Westphalia Leidam (Brink, 1979)

Similar to the Westphalia Leidam a small earth dam was constructed into residual granite soil on Stellenrust farm near Stellenbosch. The two dams experienced comparable problems which consisted of sinkholes caused by the selective washing out of deflocculated kaolinite (Brink, 1981). A visual inspection of the soil on the Stellenrust farm dam revealed a honeycombed structure with erosion piping lined with soft, wet clay throughout the residual soil (Brink, 1981). Fortunately, previous research on the stabilisation of dispersive soils by soil conservation workers from the United States of America allowed for effective remedial measures to be executed, along with increasing the dam's capacity.

2.7 PROPERTIES OF RESIDUAL GRANITE SOIL

The formation of decomposed granite is influenced by the method of weathering, whether it is chemical or mechanical weathering. Other factors influencing the variation in weathering products include the mineral composition and initial grain size of the parent rock, and varying drainage conditions. It is important to understand the formation of the residual granite soil as this influences the engineering properties. Such properties include permeability, shear strength, and compressibility.

2.7.1 Grading, mineralogy, and Atterberg limits

The size and shape of soil particles vary considerably from one another. Sand and silt-sized particles are more rotund whereas clay particles have a thin plate-like appearance. Figure 2.13 shows various grading curves, as per the labels, on the particle distribution chart (Atkinson & Bransby, 1978). Sand-sized and coarser particles can typically be seen with the naked eye, while silt-sized particles are visible through an optical microscope and clay-sized particles with an electron microscope. The size boundaries not only give the particles a classification but also correspond well with significant changes in engineering properties.

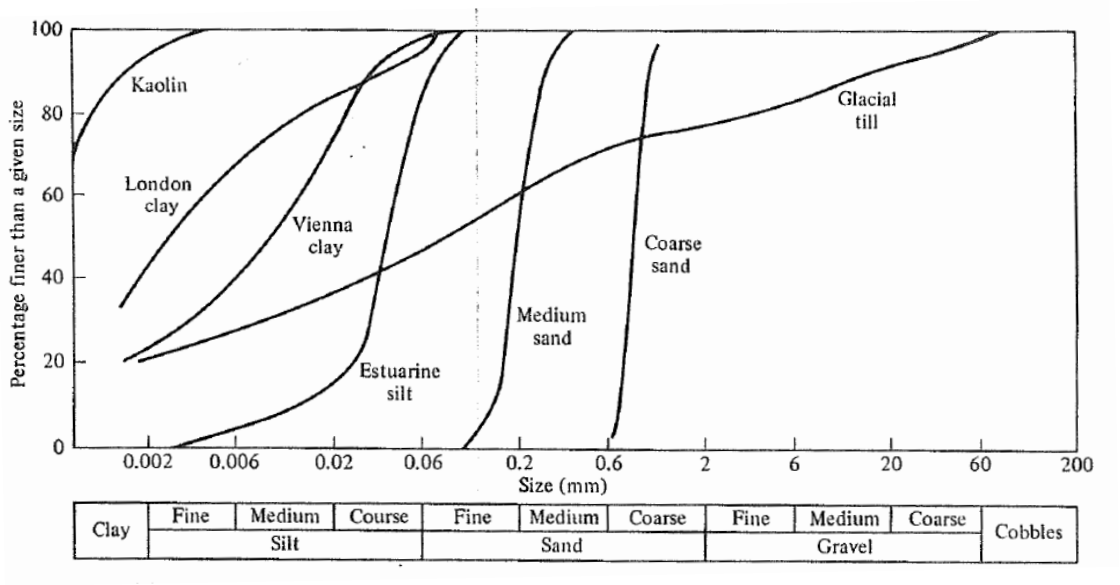

Figure 2.13 Particle size distribution chart of various grading curves (Atkinson & Bransby, 1978)

Lumb (1962) researched the properties of decomposed granite soil found in Hong Kong. The region forms part of a large batholith and many researchers have dealt with the material. Lumb (1962) tested 72 samples of decomposed granite soil found in this area to understand the nature of this material. The grading curves in Figure 2.14 show the extreme limits of the soil grading together with the average fine and coarse grading curves which include two-thirds of all samples, and the mean curve (Lumb, 1962). During the alteration of residual granite, leaching of silica and potash in colloidal form increases the porosity. Finer grains of felspar and mica are modified more rapidly compared to the coarser quartz grains, resulting in a soil with little clay and mostly coarse sand. From Figure 2.14 it is evident that the type and degree of weathering influences the particle size distribution of the soil. A sample with more coarse particles is potentially illustrative of intense leaching compared to a sample with more silt and clay size particles. A grading curve with more fines show that the soil has not yet undergone intense leaching and that the weathering is primarily due to mechanical

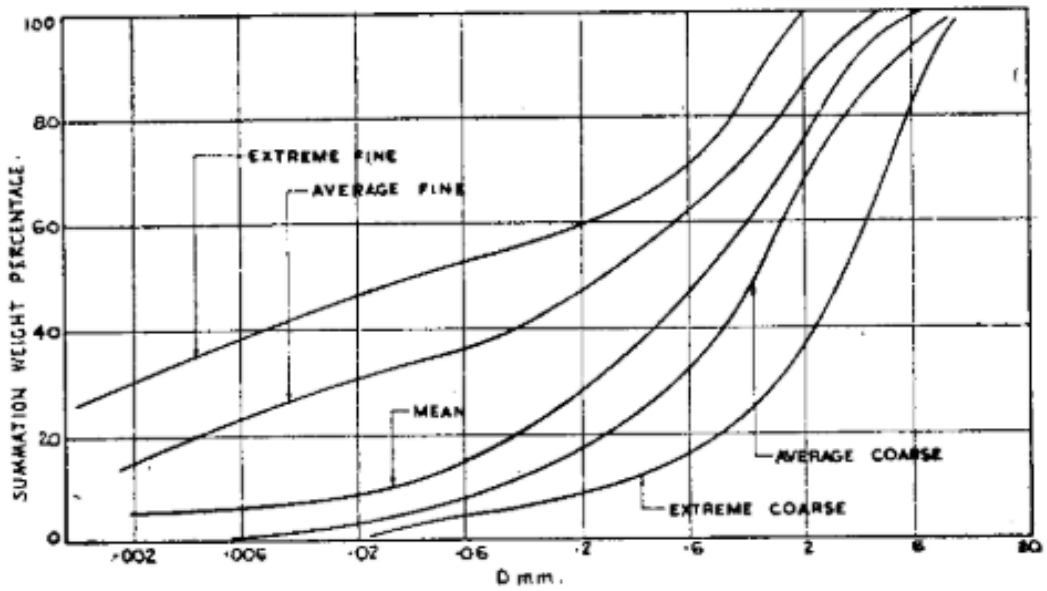

Figure 2.14 Limited average grading curves of 72 samples of decomposed granite soil from Hong Kong (Lumb, 1962)

Lumb (1962) used grading parameters to interpret the lateral and vertical variation of residual granite soil and found that the variation observed in 0.71 m^3 was not considerably less than for the entire area. Similarly, Galer, Sasaki and Nakamura (1998) also found that the properties of decomposed granite soils are diverse for zones of different weathering, even for zones 15 – 20m apart.

As mentioned in Section 2.3 the common composition of weathered granite is quartz, potassium feldspar, muscovite mica, and some clay minerals like illite, vermiculite, and smectite (montmorillonite). The parent rock determines the mineralogical composition, and it is changed by weathering. Weathering causes intraparticle voids and microcracks to develop, weakening particles with time (Lee, 1991). Matsuo and Nishida (1968) measured the strength of feldspar grains by compressing 1.6 mm orthoclase particles with a 3 mm diameter steel rod to obtain the compressive strength. They determined a relationship between the compressive strength and the specific gravity of the grains which also relates to the degree of weathering. Their research established that the reduction of specific gravity, which takes place during weathering, is related to rapidly decreasing compressive strengths of the grains.

When a soil has a considerable amount of clay, it is necessary to perform the Atterberg limits to determine its plasticity properties. Clay soil reacts differently at various percentages of water content. When the water content is raised, the strength decreases, and when an extensive amount of water is added it will cause the soil to flow like a liquid. On the other hand, if the water content is reduced, the soil strengthens, but lowering the water content too extensively

will cause the soil to be brittle and crumble at failure (Atkinson & Bransby, 1978). The water content at the exact point where the soil becomes liquid-like is termed the liquid limit (LL), whereas the water content at the point where the soil becomes brittle, is termed the plastic limit (PL). The range over which the soil remains plastic is termed the plasticity index (PI) and it is the difference between the PL and the LL (Atkinson & Bransby, 1978). The plasticity indices of soils with low clay content will approach zero, whereas pure clays such as montmorillonite clay may exceed 500%.

The liquidity index of a soil describes the current state in terms of its Atterberg limits and is defined by $LI = (w\% - PL)/PI$. Soils that have heavily overconsolidated clays will have liquidity indices near zero, while normally consolidated clays near 1.0. Certain clays can have liquidity indices greater than 1.0 under special circumstances such as 'quick' clays (Atkinson & Bransby, 1978). Another value that can be determined is the activity (A). This value is related to the mineralogy of the clay grains and the chemistry of the pore water. The activity of a soil indicates the plasticity of the pure clay fraction and it is determined with the following formula: $A = PI/\%\ clay\ by\ weight$ (Schofield & Wroth, 1968).

Atterberg limits investigated by Lumb (1962) on the fine fractions of decomposed granite soil resulted in plots on or near the A-line on the plasticity index chart. In an effort to identify the clay fractions, additional Atterberg limits were performed on three clay samples. Evidently, it was identified as kaolinite. White (1949) presented the liquid limit and plastic index values of various clay minerals such as illite, montmorillonite, and kaolinite. White's research indicated that the plastic limit of kaolinite would most likely range from less than 25% to 40%; the liquid limit from 30% to 75%; and the plastic index from 0% to 35%. According to Lumb (1962), plasticity index values higher than those of kaolinite were assumed to be due to the mica content present in the silt fraction (Lumb, 1962).

Matsuo, Fukuta and Nishida (1970) proposed a new method for determining the consistency of decomposed granite soil. Generally, the engineering properties of a soil is related to its consistency determined by the Atterberg limits. However, some decomposed granite soils that have been subjected to intense leaching mainly consist of coarse grains with a small fines portion. They performed slump tests on the decomposed granite; a test mostly used for concrete. The slump test results revealed that not only should the grain size be considered, but also the properties of the grains. Matsuo, Fukuta and Nishida (1970) used a flow limit function (instead of liquid limit) to express the factors affecting the grain properties:

$$Wfl = f(specific\ gravity\ of\ grains, grain\ size\ distribution, grain\ shape, kind\ of\ mineral\ grains, surface\ properties\ of\ grain)$$

They concluded that more weathered soils give a higher *Wfl* value due to the sum of the intergranular and intragranular water contents. Generally, slightly weathered soils have poor intragranular voids, whereas the highly weathered particles have more voids that water can penetrate (Matsuo, Fukuta & Nishida, 1970). A high value of *Wfl* is also related to soils with an abundance of flake-shaped coloured minerals. Figure 2.15 shows the relationship of *Wfl* and the degree of weathered grains as well as to coloured minerals, and here the numerous voids within the particles of the heavily weathered grains can be seen.

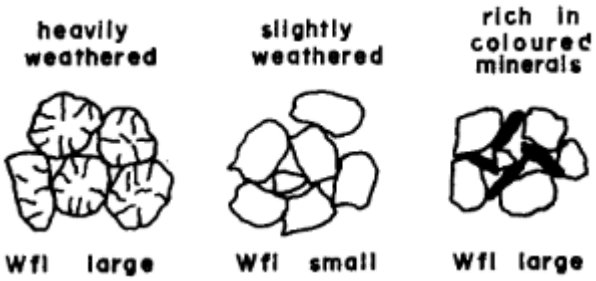

Figure 2.15 Schematic expression of soil grains (Matsuo, Fukuta & Nishida, 1970)

2.7.2 Permeability

Usually, soil particles are in physical contact with its neighbouring particles and this repetitious skeleton forms a cellular framework. When the volume occupied by this particle framework changes, the water in the voids will flow through the soil as a response to change in the soil structure. The quantity used to measure the ease of water flowing through voids is called permeability (*k*), and it is dependent on the void ratio (density), particle size, and structure of the soil. For clay particles of micron size, the permeability will have a low value as a result of surface area to particle volume ratio increasing, whereas a soil consisting of larger particles will likely have a greater permeability (Wood, 1994). Permeability is of great significance in soil mechanics as it shows the difference between clay and sand soils' mechanical behaviours (Schofield & Wroth, 1968).

Decomposed granite soil is generally considered a permeable soil. However, depending on the clay content, this may differ. Lumb (1962) researched the permeabilities of fine, medium and coarse grained decomposed granite soils which were either carved, driven, or remoulded. Figure 2.16 illustrates the results obtained by Lumb (1962) and here it is evident that the permeability of medium and fine grained soils are significantly influenced by the change in void ratio, compared to coarse grained soils. Generally, the permeability of decomposed granite

ranges from 10^{-5} to 10^{-7} m/s, but if the soil is compacted, particle crushing will occur, and its density will increase thus decreasing the permeability to well below 10^{-7} m/s (Kwon & Oh, 2011). A permeability test performed by Hoffmann (2019) on weathered granite soil from the Cape Granite Suite resulted in a permeability of 7.8×10^{-6} m/s which classified the soil as a poor drainage material according to Terzaghi, Peck and Mesri (1996) (Hoffman, 2019).

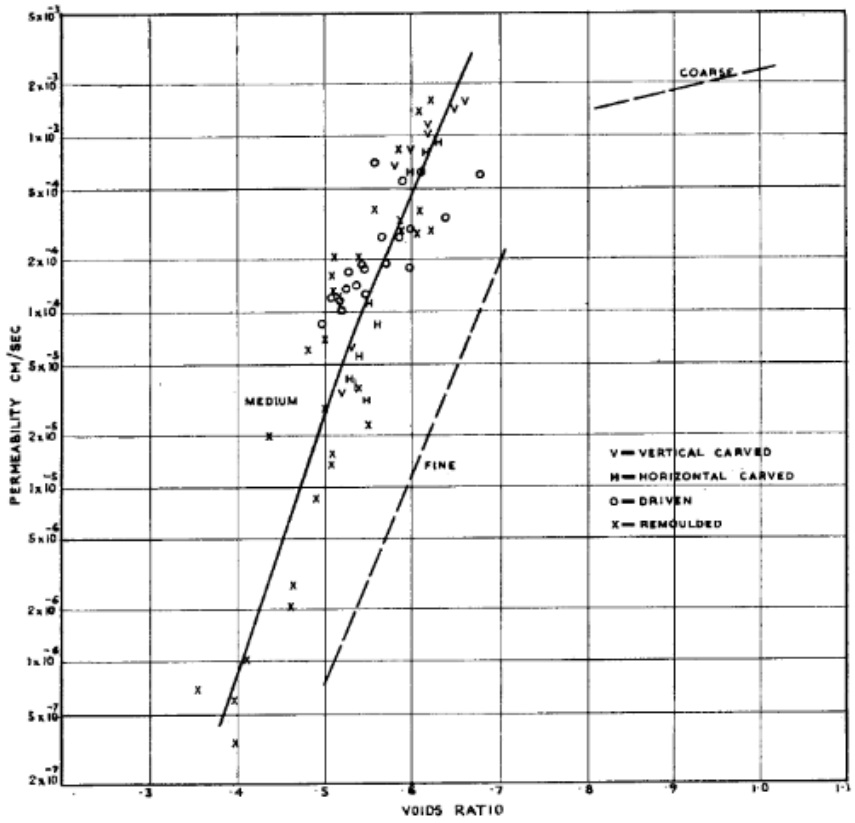

Figure 2.16 Variation of permeability with voids ratio of decomposed granite soil from Hong Kong (Lumb, 1962)

When weathering of residual granite soil progresses, intragranular voids increase (Figure 2.15). Intragranular voids have small capillaries through which water cannot permeate, however, these voids do affect the specific gravity of the soil. When intragranular voids increase, specific gravity decreases, and in turn permeability decreases (Matsuo & Nishida, 1970). Mechanical weathering may decrease the area through which water can permeate, lowering the coefficient of permeability, whereas chemical weathering causes leaching, resulting in more voids, and increasing the soil's permeability. Thus, the degree of weathering, formation of intragranular voids, and particle crushing through compaction have a pronounced influence on the permeability of decomposed granite soil.

2.7.3 Compressibility

The stress history of a soil has a great influence on the compressibility of that soil. Typically, an overconsolidated soil will be much less compressible compared to a normally consolidated soil. When a normally consolidated soil is compressed, it follows the almost linear path in e-logσ' space termed the virgin compression line (see Figure 2.17) where changes are irreversible. Whereas the compression of an overconsolidated soil can be represented by a plot on the expansion or recompression parts (see Figure 2.17). Along this part of the curve, the changes in the soil structure are almost fully recoverable where the soil may revert to its original structure during expansion (Knappett & Craig, 2012). Ultimately, the recompression line re-joins the virgin compression line after which compression will continue along this line. The following coefficients can be used to quantify a soil's compressibility:

1. **The coefficient of volume compressibility (m_v):**

$$m_v = \frac{1}{1+e_0}\left(\frac{e_0 - e_1}{\sigma_1' - \sigma_0'}\right) \quad \text{Equation 2.1}$$

$$m_v = \frac{1}{H_0}\left(\frac{H_0 - H_1}{\sigma_1' - \sigma_0'}\right) \quad \text{Equation 2.2}$$

Where m_v is the coefficient of volume compressibility (m^2/MN), e_1 is the decreased void ratio from e_0, and σ_1' is the effective stress increased from σ_0'(kPa). Similarly, H_1 is the decreased height from H_0.

2. **The constrained modulus ($E`_{oed}$):**

$$E'_{oed} = \frac{1}{m_v} \quad \text{Equation 2.3}$$

Where E'_{oed} is the constrained modulus, with units measured in (MPa).

3. **The compression index (C_c):**

$$C_c = \frac{e_0 - e_1}{\log(\sigma_1'/\sigma_0')} \quad \text{Equation 2.4}$$

Where C_c is the compression index and is dimensionless. Similarly, the expansion index, C_e, can also be approximated by a straight line but is usually many times less than C_c.

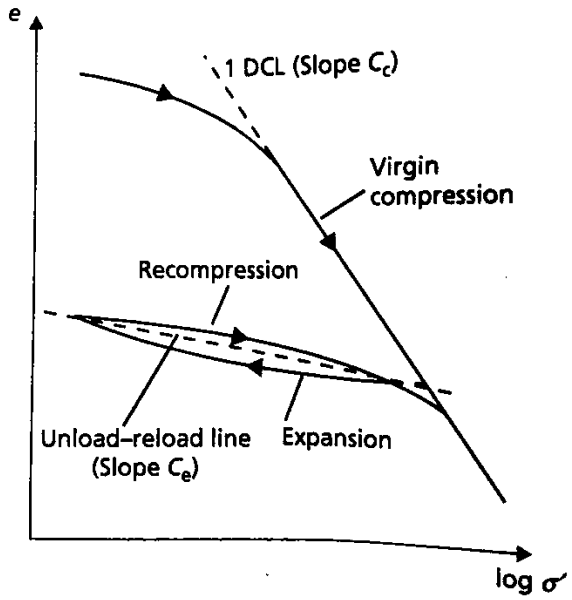

Figure 2.17 Void ratio and effective stress relationship (Knappett & Craig, 2012)

When a rapid load is applied to a fully saturated soil with low permeability, it results in an immediate undrained settlement. The soil will continue to shear beneath the constant loaded area until the excess pore water has dissipated, and volume will start to decrease. Further strains will occur as the effective stresses increase in the soil (Wood, 1994). This process is called consolidation and it does not only occur when a load is applied but also when the pore water pressure is reduced as a result of groundwater pumping (Knappett & Craig, 2012). For the theory of consolidation to be applied in practice, it is necessary to determine the coefficient of consolidation (c_v) which will aid in the determination of the rate of volume change. The coefficient of consolidation with units (m^2/year) can be calculated with the following formula:

$$c_v = \frac{k}{m_v y_w} \qquad \text{Equation 2.5}$$

Where k is the permeability (m/year), m_v is the coefficient of volume compressibility (m^2/kN), and y_w is the unit weight of water (kN/m^3). Since k and m_v are assumed to be constant, c_v is constant during consolidation (Knappett & Craig, 2012).

Yan and Li (2012) found that completely decomposed granite soil from Hong Kong is highly compressive during virgin isotropic compression. They researched the mechanical properties of medium-fine-grained decomposed granite and found that the slope of the virgin compression line, ξ (λ in this research) = 0.091 (Figure 2.18). Similarly, Lee and Coop (1995) researched the intrinsic behaviour of decomposed granite soil and obtained a compression slope λ = 0.087. Yan and Li (2012) attributed the high compressive behaviour to the soil's well-graded and fine-grained nature.

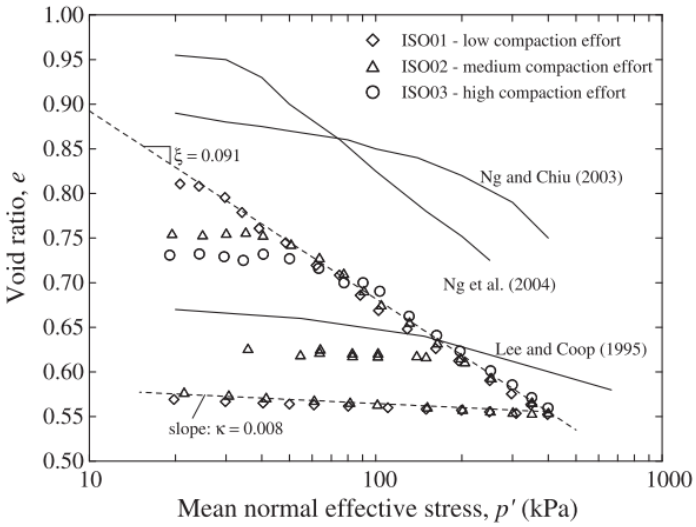

Figure 2.18 Isotropic compression and unloading curves of completely decomposed granite soil from Hong Kong (Yan & Li, 2012)

Galer, Sasaki and Nakamura (1998) studied two different zones, A and B, within one site where zone B had more weathered granite compared to zone A. Results from their plate loading tests showed that the more weathered zone B was more compressible than zone A. Thus, the soil becomes more compressive as weathering increases. The presence of mica also influences the compressibility of decomposed granite soil. Seethalakshmi and Sashan (2018) researched the influence of mica content on the compressibility of sand and found that a 30% mica content tended to rebound when subjected to compressive loading. Similarly, McCarthy (1962) found that the increase of mica content above 30% for fine mica, and 50% for coarse mica, increased the compressibility of the soil.

2.7.4 Shear strength

In the field, a soil element is exposed to vertical (z-direction), and horizontal (x-direction) normal stresses caused by the self-weight of the soil and applied external loadings. The elastic-perfectly plastic model is an idealised relationship of stress-strain which is represented by the dotted line in Figure 2.19. Between points O and Y', linear elastic behaviour (Hooke's law) is assumed and from Y' to P unrestricted plastic strain at constant stress. Failure will occur at a point where the shear stress equals the shear strength of the soil provided that the limiting strength is frictional (Knappett & Craig, 2012). When particles are loosely packed, they experience friction alone, however, if they are densely packed additional interlocking forces between the particles increase the frictional resistance. If the normal forces acting perpendicular to the slip plane is significant, the interlocking forces decrease as particle

breakage occurs, causing the material's behaviour to become purely frictional again (Knappett & Craig, 2012).

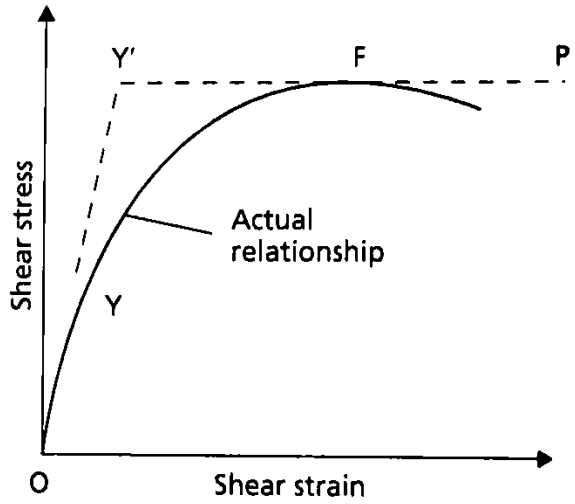

Figure 2.19 Stress-strain relationship of soil with the elastic-perfectly plastic model (Knappett & Craig, 2012)

Shear strength of soil is affected by its drainage condition (drained or undrained). When an applied total stress is applied to an undrained soil (e.g., silt and clay) the excess pore pressures produced, change the effective stresses. Whereas with drained conditions (e.g., sand and gravel) consolidation is immediate and thus there is no build-up of excess pore pressures. Generally, fine-grained soils with low permeabilities experience undrained loading in the short term and drained loading in the long term. In coarser grained soils, consolidation takes place rapidly due to the higher permeability of the soil. This also allows the soil to undergo drained loading in both the short and long term (Knappett & Craig, 2012).

Lumb (1962) performed a series of drained triaxial compression tests on both saturated and unsaturated samples. The variation of internal friction with change in void ratio and grading was studied during the saturated tests, and since the soil has no cohesion when fully saturated, the variation in cohesion with the degree of saturation was studied during the unsaturated tests. Results from the saturated tests showed that the mean internal friction angle for coarse and medium soils varied between 36˚ to 38˚ (Figure 2.20 (a) and (b)) and these high values were attributed to the angularity of the particles. The fine soil showed a greater change in internal friction angle, with values ranging from 21˚ to 40˚ (Figure 2.20 (a)) and this was attributed to the bi-modal grading of the soil.

Kwon and Oh (2011) found that the internal friction of effective stress path for decomposed granite under CU condition was 46.17˚ with no cohesion present in the Mohr circles. They also

established that the internal friction angle under CD condition was 33.12˚ with no cohesion. A micaceous residual granite soil was researched by Hoffman (2019) and a series of direct shear box tests resulted in an unsaturated internal friction angle of 37˚, and an apparent cohesion of 36 kPa. From the data presented in Hoffman's thesis, it was approximated that the micaceous residual granite soil had a void ratio of 0.412. Hoffman's friction angle and void ratio values correlate well with the medium soil presented in Lumb (1962) (Figure 2.20 (b)). Rahman *et al.* (2018) also researched the shear strength of granitic residual soils (grade V – completely weathered) in both the saturated and unsaturated states. Saturated tests were conducted under consolidated drained conditions and undrained tests were performed in a triaxial double-walled cell. Their results showed an internal friction angle of 31˚ for the saturated tests without apparent cohesion, whereas the unsaturated tests showed the same internal friction angle as the saturated test with a maximum apparent cohesion of 200 kPa. The apparent cohesion was attributable to the suction in the soil and it decreased with increasing saturation until it diminished (Rahman *et al.*, 2018).

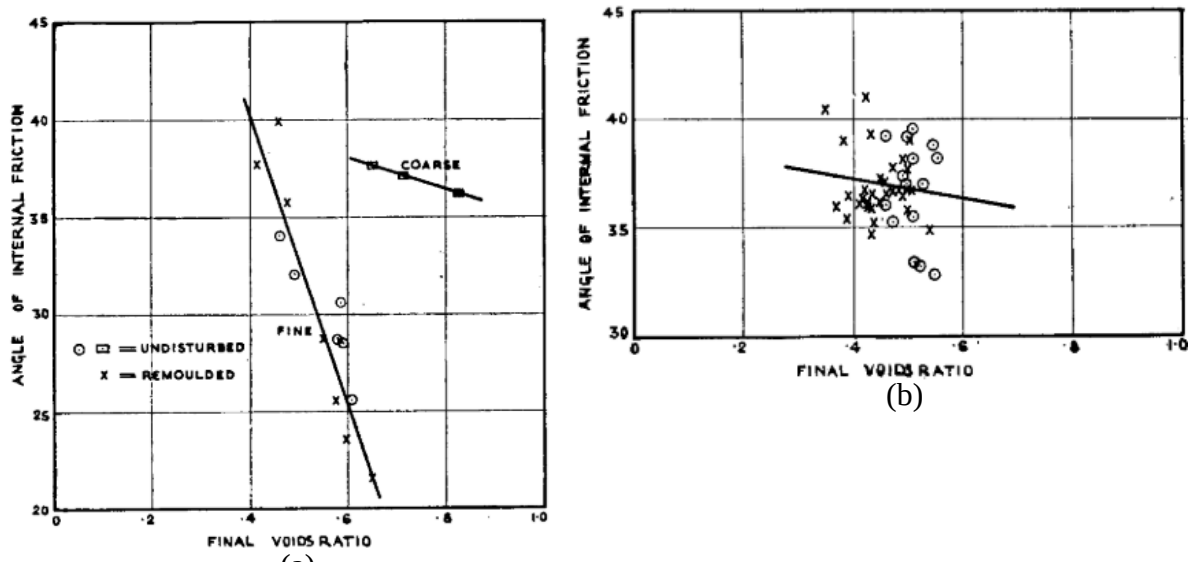

Figure 2.20 Variation of the angle of internal friction with voids ratio at failure of decomposed granite soil from Hong Kong (a) Fine and coarse soil; (b) Medium soil (Lumb, 1962)

The apparent cohesion of decomposed granite soil depends greatly on the saturation and grading of the soil. Coarse, medium and fine grained soils were studied by Lumb (1962), and each grading delivered a different response to the degree of saturation. Lumb (1962) found that fine-grained soils were the most sensitive to change in saturation (Figure 2.21 (a)). At low values of saturation, fine soils had apparent cohesion values greater than 196 kPa, alike Rahman *et al.* (2018). When saturation was increased from 0.4 to 0.95, the apparent cohesion

dropped from 226 kPa to 0 kPa. Medium-grained soils showed a rapid decrease in apparent cohesion until about 0.3 saturation, whereafter it roughly linearly decreased until there was no apparent cohesion at a saturation of 0.9 (Figure 2.21 (b)). The apparent cohesions for coarse-grained soils were very low, however, Lumb (1962) noted that at a saturation of 0.5, the apparent cohesion of 10 kPa is sufficient to account for an unsupported vertical cut of approximately 6 m (Figure 2.21 (a)). As previously mentioned, Hoffman (2019) established an apparent cohesion of 36 kPa for micaceous residual granite soil. From Hoffman's data, it was approximated that the saturation of the soil was around 55%, and these values fall well within the scattered plot of the medium soil presented in Lumb (1962) (Figure 2.21 (b)).

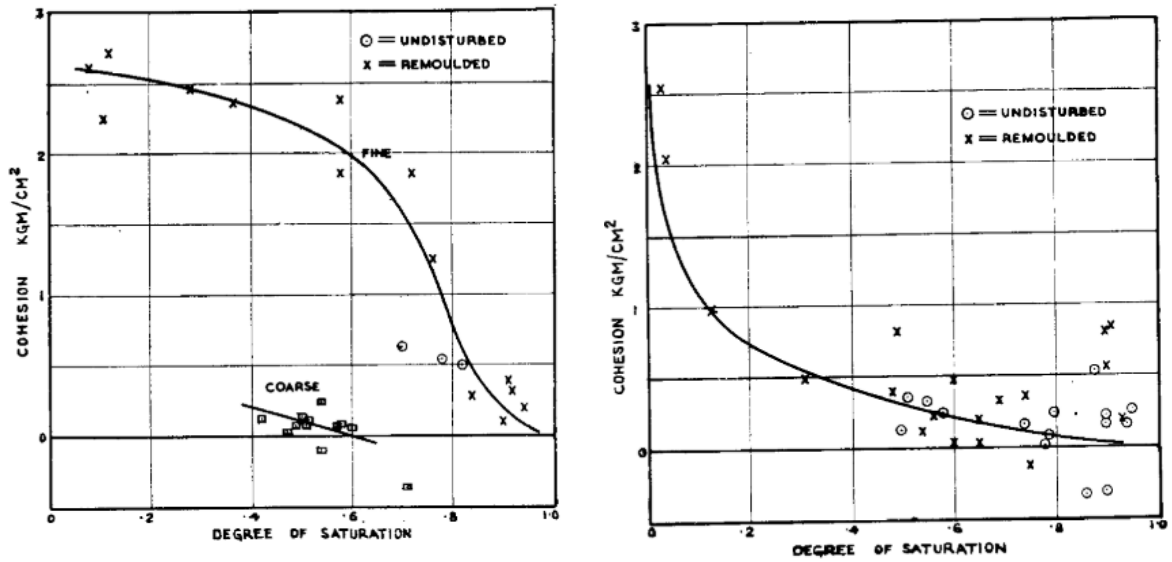

(a) (b)

Figure 2.21 Variation of apparent cohesion with saturation of decomposed granite soil from Hong Kong (a) Fine and coarse soil; (b) Medium soil (Lumb, 1962)

2.8 PARTICLE BREAKAGE

A crushable soil like decomposed granite generally has a weak particle structure consisting of breakable mineral components (e.g., feldspar, biotite, etc.) and microcracks (Niu *et al.*, 2018). On a particle scale, particle breakage can influence the particle size distribution, interparticle contact conditions, and particle shape, causing local stresses to redistribute(Zhao *et al.*, 2019). The particle size distribution of decomposed granite is considerably important as this characteristic influences the permeability, compressibility, strength, and stress-strain behaviour of the soil (Niu *et al.*, 2018). As the size of particles increases, the normal contact forces in a soil element increase which causes the amount of particle crushing to increase. Particle crushing is influenced by the presence of pore water and it progresses with particle angularity,

increasing shear stresses (Lee, 1991). Silt sized particles require much larger stresses to be crushed compared to particles greater than 74µm (Lee, 1991).

Miura and O-hara (1979) carried out a series of triaxial compression tests on decomposed granite soil under drained conditions to determine the influence of particle crushing on the shear stresses of the soil. Their research was based on correlative work done by Miura and Yamanouchi (1977) on quartz-rich sand under high pressure, and they found that the particle crushing phenomenon of decomposed granite under low pressure (10 kPa – 294 kPa) is substantially the same as the aforementioned soil. A particle-crushing rate was established to determine the degree of particle crushing at failure and this was related to both dilatancy rate (Figure 2.22 (a)), and maximum principal stress ratio (Figure 2.22 (b)). The figures below also indicate the respective confining pressures on the relation curves.

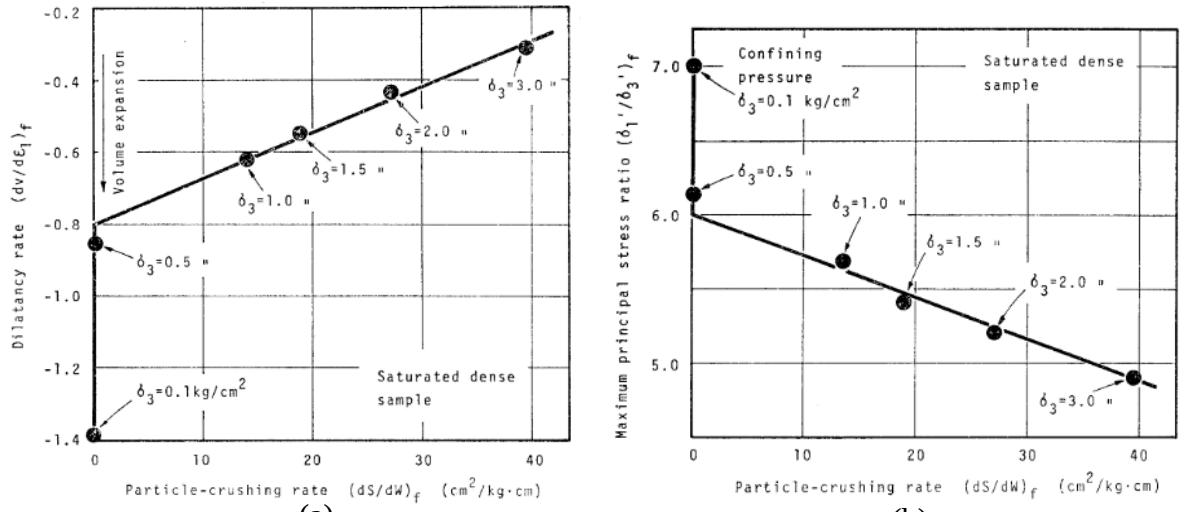

Figure 2.22 Relationship between particle-crushing rate and (a) dilatancy rate, and (b) maximum principal stress ratio in drained triaxial compression test of decomposed granite soil (Miura & O-hara, 1979)

From both Figure 2.22 (a) and (b) it is evident that at a confining pressure lower than 64 kPa the particle-crushing rate is substantially zero, meaning no particles are crushed under these conditions of the confining pressures. When the confining pressure is higher than 64 kPa, both the particle-crushing rate and rate of dilation increase as the confining pressure increases. Correspondingly the maximum principal stress ratio decreases as particle-crushing rate and confining pressure increase. Miura and O-hara (1979) also noted that the decrease in shear strength was not due to particle crushing, but rather the rate of particle-crushing at the time of failure.

The degradation of decomposed granite particles mainly result from the separation of particle amalgams and breakage along pre-existing fissures (Lee & Coop, 1995). Particle breakage for decomposed granite soil after shearing of consolidated drained and consolidated undrained triaxial tests was researched by Lee and Coop (1995). Isotropic compression values ranged from 50 – 400 kPa in the Bishop and Wesley triaxial cell (drained tests), whereas values ranged from 1800 – 8000 kPa in the high-pressure triaxial cell (undrained tests). For saturated soils, Lee and Coop (1995) established that particle breakage is the predominant mechanism of plastic volumetric compression during both isotropic loading and shearing. They also compared their results to correlative work done by Coop and Lee (1993) on carbonate and silica sands and found similar observations between the aforementioned soils and decomposed granite soil even though the nature of breakage was different. Carbonate and silica sands typically experience breakage of individual particles, whereas decomposed granite soil, as previously mentioned, experiences separation of amalgams of particles (Lee & Coop, 1995). The unique relationship between relative breakage B_r (discussed below) and effective stress p' at critical state can be seen in Figure 2.23. Lee and Coop (1995) established that the relationship is independent of the stress path taken and that the normal compression is a function of the breakage.

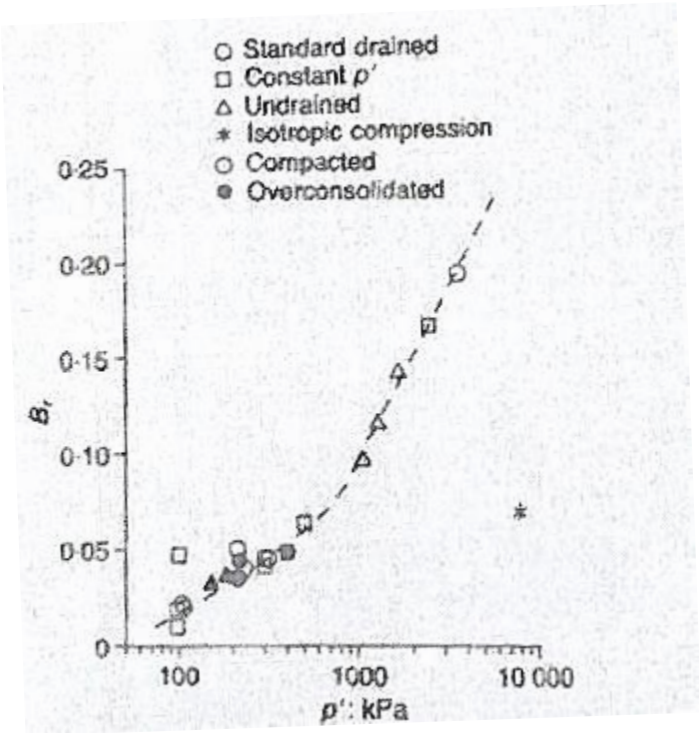

Figure 2.23 Relationship between relative breakage B_r and effective stress p' of saturated decomposed granite soil (Lee & Coop, 1995)

For unsaturated tests, Lee and Coop (1995) determined that partially saturated samples experienced similar particle breakage as saturated samples, whereas unbonded dry samples experienced significantly less particle breakage than the saturated samples. They also noted that the reduced particle breakage caused an increase in peak strength and greater dilation for unbonded dry soils.

Particle breakage can be measured with various methods such as those proposed by Marsal (1967), Miura and O-Hara (1979), Hardin (1985), and Lee and Farhoomad (1967). The concept of breakage potential, relative breakage, and total breakage proposed by Hardin (1985) is scientific and easy to measure and will also be the main method for determining particle breakage in this research. The breakage potential, B_p, is a condition where all the coarse particles are crushed to finer particles. It is equal to the area hatched between the line passing through 74μm and the original size distribution curve for particles greater than 74μm (Figure 2.24).

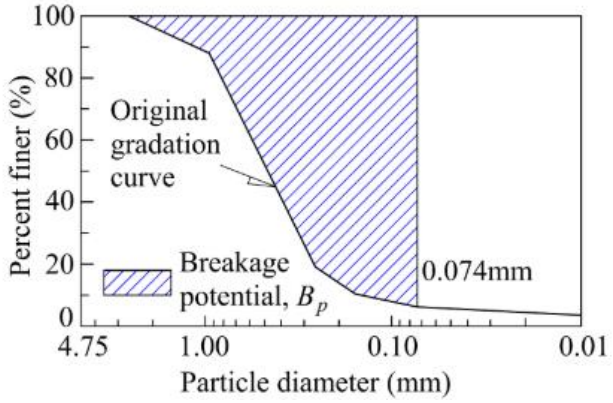

Figure 2.24 Definition of Hardin's breakage potential

Breakage potential is given by the following equation:

$$B_p = \int_0^1 b_p df \qquad \text{Equation 2.6}$$

Where $b_p = \log_{10}\left[\frac{D\ in\ mm}{0.074\ mm}\right] for\ D \geq 0.074mm$ and $b_p = 0\ for\ D < 0.074\ mm$, where D is a given particle size in mm, and df is a differential of the percentage of particles passing divided by 100. This area can be measured by either using a planimeter or by numerical integration, where the latter will also be the primary method used in this research. For particle sizes greater than 74μm, the area enclosed by the grading curve before and after being subjected to a state of stress is termed the total breakage, B_t (Figure 2.25).

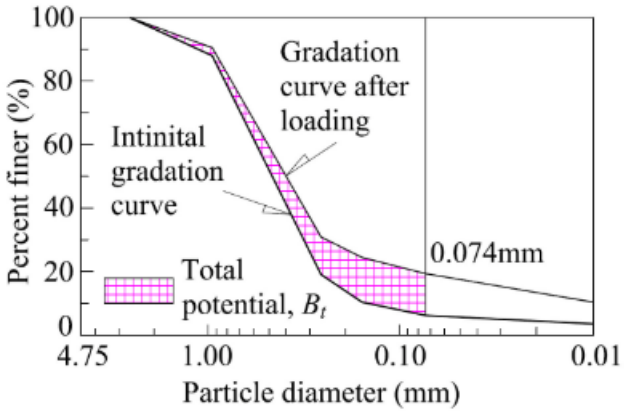

Figure 2.25 Definition of Hardin's total breakage

Total breakage is given by the following equation:

$$B_t = \int_0^1 (b_{po} - b_{pl})df \qquad \text{Equation 2.7}$$

Where b_{po} is the original value of b_p and b_{pl} is the values of b_p after loading. The definition of relative breakage B_r was derived from B_t being approximately proportional to B_p for a soil with similar particle shape and material, along a specified effective stress path to the same effective stress, at a given void ratio. Thus:

$$B_r = \frac{B_t}{B_p} \qquad \text{Equation 2.8}$$

Hardin (1985) concluded that when particle size distribution is the only variable, B_t is proportional to B_p. Relative breakage is approximately independent of particle size distribution when particle size distribution is the only variable (Hardin, 1985). Research done by Lee and Farhoomand (1967) supported this conclusion in their study of compressibility and crushing of crushed granitic gravel. Figure 2.26 (a) illustrates the original particle size distribution curve and the distribution curve after an isotropic compression of 7845 kPa. Data from Figure 2.26 (a) was used to plot Figure 2.26 (b) which shows an approximately linear relationship between B_t and B_p, suggesting that B_r is approximately independent of particle size distribution (Hardin, 1985).

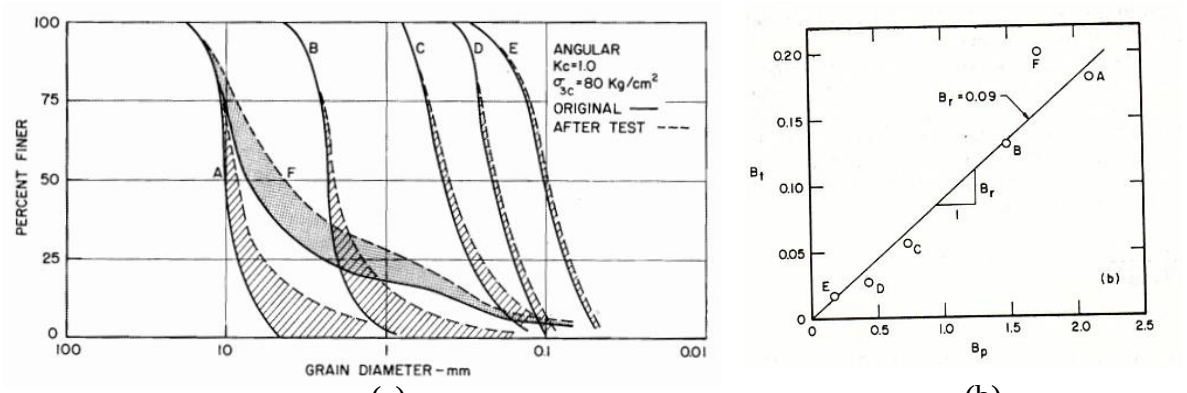

(a) (b)

Figure 2.26 (a) Particle size distribution curves for crushed granite measured by Lee and Farhoomand (1967); (b) Relationship between total breakage and breakage potential (Hardin, 1985)

2.9 PARTIALLY SATURATED SOILS

Partially saturated soils generally exist in either of the following two stages: at low saturation or at high saturation where $S_r<1$. Both water and air are present in the pores of a partially saturated soil, however, the degree of saturation influences the behaviour of the soil as well as the effective stresses. When the degree of saturation is low, both air and water pressure influence the soil's behaviour, but if the saturation is high, air pressure has little influence on the soil. The capillary menisci ensure that the water pressure is always less than the air pressure. In dry seasons, the area occupied by the menisci decreases due to water evaporation and the soil suction increases. This gives an additional component of effective stress.

Strength resulting from negative pore water pressure (suction) is not true strength. The apparent cohesion and resulting soil stiffness will diminish as the water content increases and will disappear when it is saturated. Saturation will result in loss of strength (cohesive strength). Soils with a collapsible fabric will undergo large bulk volume decrease (collapse settlement) upon saturation as interparticle bond strength is lost. Thus, the behaviour of partially saturated soils is dependent on the effect of suction on the shear strength, and also on effective stresses.

2.10 CRITICAL STATE SOIL MECHANICS

The purpose of this section is to summarise critical state soil mechanics which will be used to analyse results presented in Chapter 4. Mainly fully saturated triaxial tests are considered, however, the behaviour of partially saturated soil is briefly discussed in Section 2.9. A full description of critical state soil mechanics can be found in Atkinson & Bransby (1978), Wood (1994), and Schofield & Wroth (1968).

A few basic stress-strain parameters associated with a sample during triaxial testing are given below.

Table 2.3 Stress-strain parameters associated with a triaxial compression test

Parameter	Formula	Unit	Equation
Mean normal effective stress	$p' = \frac{\sigma'_a + 2\sigma'_r}{3}$	kPa	Equation 2.9
Deviator stress	$q' = \sigma'_a - \sigma'_r$	kPa	Equation 2.10
Specific volume	$v = 1 + e$	-	Equation 2.11
Volumetric strain	$\varepsilon_p = \varepsilon_a + 2\varepsilon_r$	%	Equation 2.12
Shear strain	$\varepsilon_q = \frac{2}{3}(\varepsilon_a - \varepsilon_r)$	%	Equation 2.13

Where σ'_a (kPa) is the effective axial stress ($\sigma_a - u$), σ'_r (kPa) is the effective radial stress ($\sigma_r - u$), e is the void ratio, ε_a and ε_r are the axial and radial strains respectively. When a soil is under isotropic compression, the normal compression line (NCL) can be idealised in a v: lnp' plane as a straight line. Repetitious unloading and reloading can also be presented by a straight line [unload reload line (URL)] in the v: lnp' plane as shown in Figure 2.27. Equations for these lines are as follows.

Table 2.4 Normal compression line and unload reload line parameters associated with an isotropic compression test

Parameter	Formula	Equation
NCL	$v = N - \lambda * \ln(p')$	Equation 2.14
URL	$v = v_\kappa - \kappa * \ln(p')$	Equation 2.15

Where N is a soil constant specifying the position of the isotropic normal compression of the soil and v_κ the specific volume of overconsolidated soil, both at p' = 1 kPa, and κ and λ are the slopes of the NCL and URL, respectively. Strains along the NCL are assumed to be elastoplastic, and elastic along the URL (Lee, 1991).

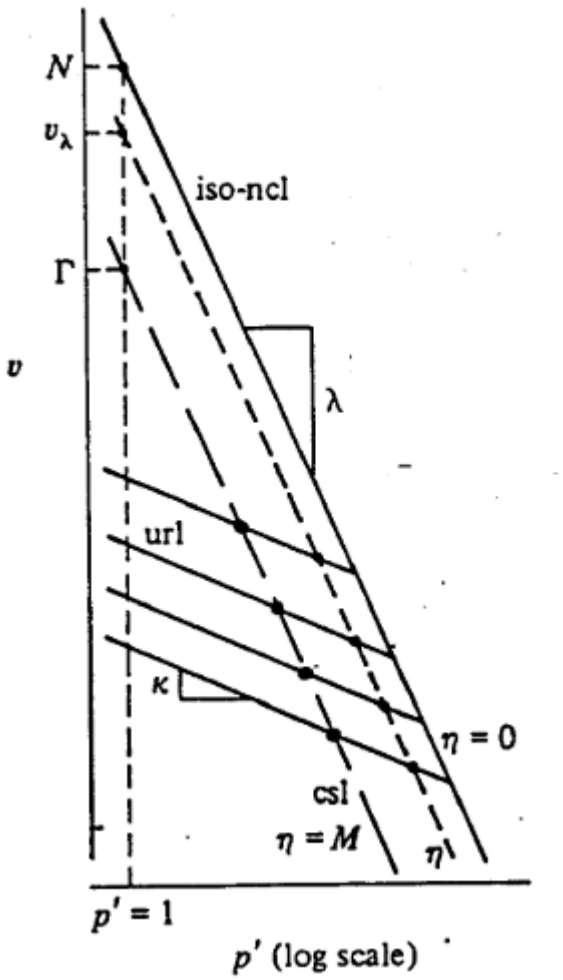

Figure 2.27 NCL and URL from Wood (1994)

When soil is sheared under drained conditions, dense soils show dilative behaviour, and loose soils show contractive behaviour. The increase in volume during dilation of a dense soil causes the sample to exhibit a peak strength, which thereafter lowers to reach the ultimate state, while for a loose sample the peak strength gradually increases until it reaches the ultimate state without reaching a peak strength (see Figure 2.28).

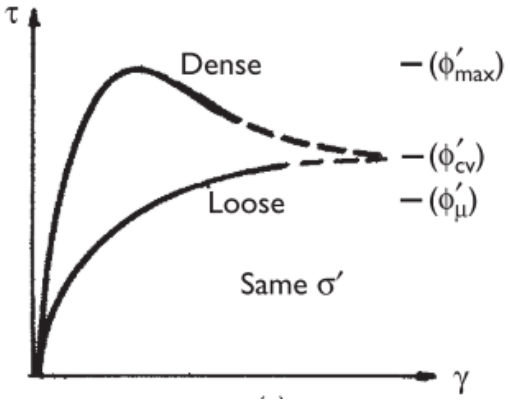

Figure 2.28 Stress-strain behaviour of soil (Knappett & Craig, 2012)

The critical state is reached when a soil undergoes deformations without change in stresses or specific volume. Figure 2.29 (a) shows the critical state line (CSL) defined in the p': q stress plane, as the line connecting the tops of the yield loci. In this plane, the critical state line can be described by $q' = Mp'$, where M is the frictional constant for a particular soil. Figure 2.29 (b) and (c) illustrates the critical state line in the compression plane (ν:p' and ν:lnp'), and it can be described by $\nu_{cs} = \Gamma - \lambda_{cs} ln(p'_{cs})$, where λ_{cs} is the slope of the critical state line in ν:lnp' space which should be approximately parallel to the NCL, and Γ is the specific volume at p' = 1 kPa (Wood, 1994), also $\Gamma = N - (\lambda - \kappa)\ln 2$. At ultimate failure, the critical state line limits all possible states, and it provides a reference for the soil's behaviour.

In the q': p': ν plane, the state boundary is assumed to be the yield surface that separates inelastic from elastic behaviour. Figure 2.30 illustrates the boundary surfaces for an isotropically compressed soil (Atkinson & Bransby, 1978). The critical state line limits all possible states for ultimate failure, and the Hvorslev surface between the critical state line and the 1:3 tension cut off represents the states of yielding for heavily overconsolidated soils. The normal compression line confines all states during isotropic normal compression, and the Roscoe surface joining the normal compression line and the critical state line limits the states of yielding for normally or lightly overconsolidated soils (Lee, 1991).

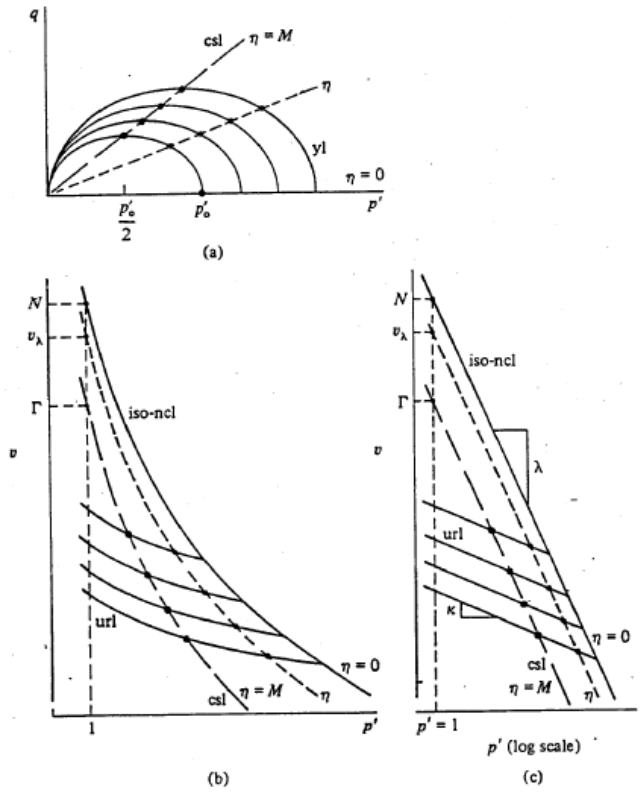

Figure 2.29 Critical state line in (a) q:p' space, (b) v:p' space, and (c) v:lnp' space (Wood, 1994)

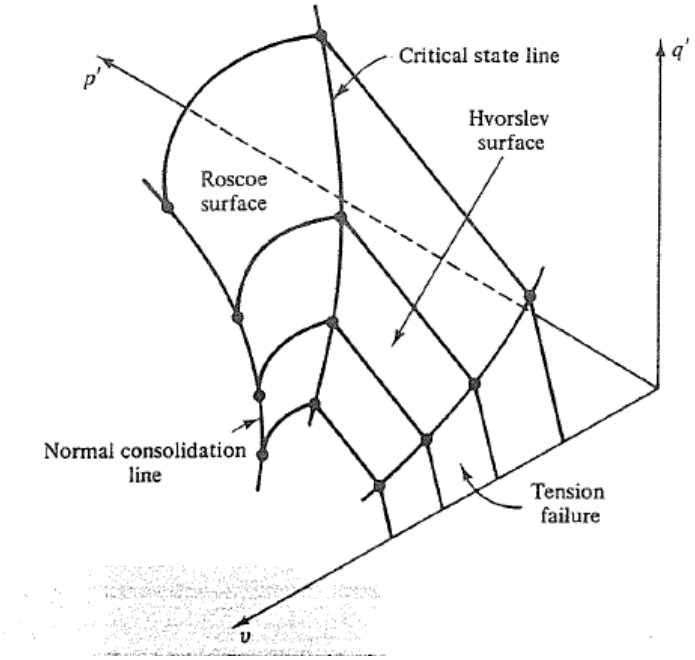

Figure 2.30 The complete state boundary surface in q':p':ν space (Atkinson & Bransby, 1978)

Originally, the Cam-clay model was proposed by Roscoe, Schofield, and Thurairajah (1963), whereafter Roscoe and Burland (1968) modified the original Cam-Clay model and generalised it to three dimensions. The following table shows the stress-strain relationships for the Modified Cam-Clay model namely: elastic and plastic volumetric strain increment, and elastic and plastic shear strain increment.

Table 2.5 Equations for calculating the Modified Cam-Clay parameters

Calculations for Modified Cam-Clay		
	Elastic (^{e})	**Plastic (^{p})**
Volumetric ($_p$)	$\delta\varepsilon_p^e = \frac{\kappa * \delta p'}{v * p'}$	$\delta\varepsilon_p^p = (\lambda - \kappa)\frac{\delta p_0'}{v * p_0'}$
Shear ($_q$)	$\delta\varepsilon_q^e = \frac{\delta q}{3G}$	$\delta\varepsilon_q^p = \frac{2\eta(\lambda - \kappa)\delta p_0'}{(M^2 - \eta^2) * v * p_0'}$

Where η = q/p'.

The necessary soil parameters for the stress-strain relationships listed above include the following:

- Elastic properties: Shear modulus G, Slope of the unload reload line κ,
- Shape of the yield locus: M,
- Volumetric strains during yielding: N and λ given by the isotropic normal compression line.

If the soil's state remains below the state boundary surface, it is assumed that the soil only undergoes elastic strains. When a soil moves closer to the boundary surface, the soil yields and undergoes plastic strains. Total strains can be quantified by the sum of the soil's elastic and plastic components i.e., $\delta\varepsilon_q = \delta\varepsilon_q^e + \delta\varepsilon_q^p$, and $\delta\varepsilon_p = \delta\varepsilon_p^e + \delta\varepsilon_p^p$.

Critical state values of decomposed granite soil have been researched by Lee (1991), Kwon and Oh (2011), Yan and Li (2012), and Liu, Zhou and Liu (2015) and their results are listed in the table below along with a description of the soil. The critical state values include the frictional constant (M), parameters of the critical state line in ν: lnp' space (λ_{cs} and Γ), the NCL slope and intercept at p' = 1 kPa (λ and N), and the slope of the URL (κ).

Table 2.6 Critical state values for decomposed granite soils

Author	Soil description	Critical state line			NCL and URL		
		M	λ_{cs}	Γ	λ	N	κ
Lee (1991)	Completely weathered granite soil (grade V)	1.59	0.087	2.04	0.09	2.10	0.005
Kwon and Oh (2011)	Decomposed granite soil sampled in Cheongju (mostly sandy soil)	1.74	-	-	0.026	1.63	0.007
Yan and Li (2012)	Completely decompose granite soil, medium-fine-grained with clays and silts	1.40	0.069	1.89	0.091	1.93	0.008
P. Liu, Zhao and W. Liu (2015)	Completely decompose granite soil, medium-grained with clays and silts	1.35			0.071	2.00	0.018

2.11 SYNTHESIS

The literature study shows that the degree of weathering of decomposed granite soils has a significant influence on the behaviour of the soil. Properties affected by this characteristic include the following: grading, permeability, compressibility, shear strength and stiffness. The primary problem associated with decomposed granite soils is the formation of a collapsible grain structure. This formation is promoted by seasonal wetting and drying and chemical weathering, causing soluble and colloidal matter to leach out. Other problems associated with residual granite soils include dispersive and heaving behaviour, however, this research will place more emphasis on the collapsible nature of decomposed granite soils.

Whilst investigating existing literature concerning the occurrences of decomposed granite soil in South Africa, limited research, including those by Knight (1961), Brink and Kantey (1961), Terblanche (1989), and Fouché and Asante (2019) were obtained. Section 2.5 and 2.6 summarise their research findings as well as the problems that occurred on these soils. Minimal research was found on the engineering properties of decomposed granite soils in South Africa, whereas most literature on engineering properties was gathered from research performed on decomposed granite soils sourced from Hong Kong, Korea, and Japan. The investigative work carried out by Fouché and Asante (2019) provided a foundation for the collapse potential of residual granite soils, whereas research done by Lumb (1962), Matsuo and Nishida (1970), and Galer, Sasaki and Nakamura (1998), provided literature on the properties of decomposed granite soils. A research paper by Hoffman (2019) contributed to the literature on the properties of decomposed granite soils from the Cape Granite Suite.

As a result of the limited engineering properties and poor familiarity with the collapse phenomenon in previous research, the behaviour of decomposed granite soils in South Africa is still misinterpreted. The current research will provide a basis for the engineering properties and produce a predictive model to evaluate and predict the behaviour of decomposed granite soils. The importance of investigating decomposed granite soils and the need for this research is supported by extensive past research done on such soils internationally.

CHAPTER 3: METHODOLOGY

3.1 INTRODUCTION

In this chapter, the methods used to achieve the objectives set out in Section 1.3 of Chapter 1 are presented. The mechanical properties of residual granite soil were investigated through basic classification testing and triaxial compression tests. Disturbed samples from Elsana quarry (located along the R315 towards Darling in the Western Cape) were transported to the laboratory for visual examination and testing. Classification tests were carried out to determine the particle size distribution, Atterberg limits, maximum dry density, and optimum moisture content of the soil. The test procedures are described in Section 3.4. In Section 3.5.2 the preparation of samples for triaxial testing is discussed along with the triaxial test schedule and procedures. Particle breakage of specimens was examined through CT scans and the procedure and basic specifications are discussed in Section 3.6.

3.2 METHOD OVERVIEW

The research methodology flow chart is given in Figure 3.1.

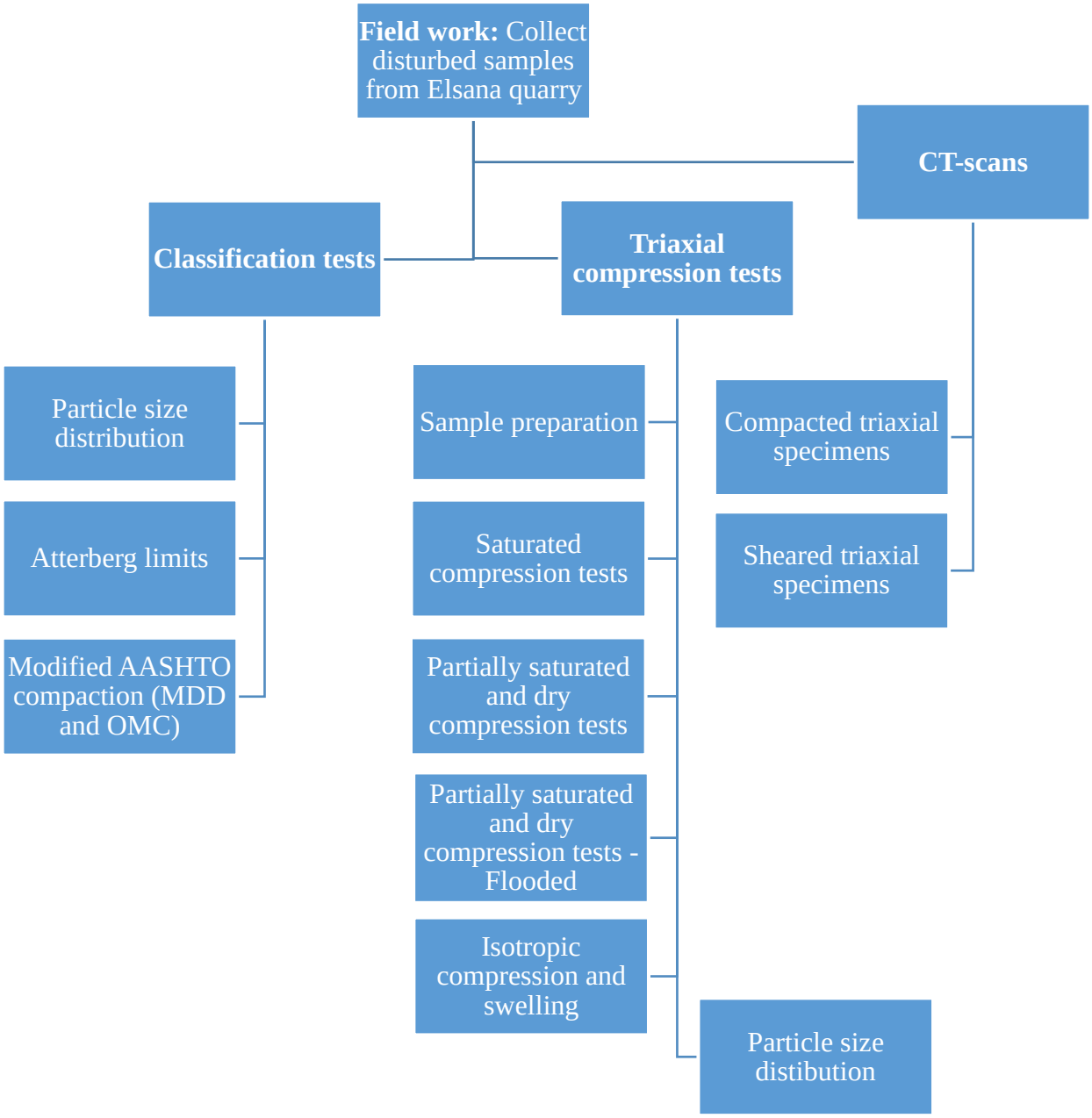

Figure 3.1 Flow chart of the methodology

3.3 FIELD WORK

Residual granite soil from the Cape Granite Suite was obtained from Elsana Aggregate Quarry, located 10km west of Malmesbury on the R315 in the direction of Darling, Western Cape (Figure 3.2). This quarry is a granite deposit with an estimated 30-year life of mine, and it produces various sizes of shaped and unshaped aggregates for building, road, and rail

industries. Elsana Aggregate Quarry has the following coordinates: -33.44185, 18.59960. Figure 3.3 shows a satellite view of the quarry with a red square indicating the residual granite soil sampling pit. The material was sampled through shovelling hence, the material was disturbed. In total, twenty vinyl bags were filled with approximately 20-30 kg residual granite soil and transported to the Pavement and Geotechnical Research Laboratory, Stellenbosch University, Western Cape.

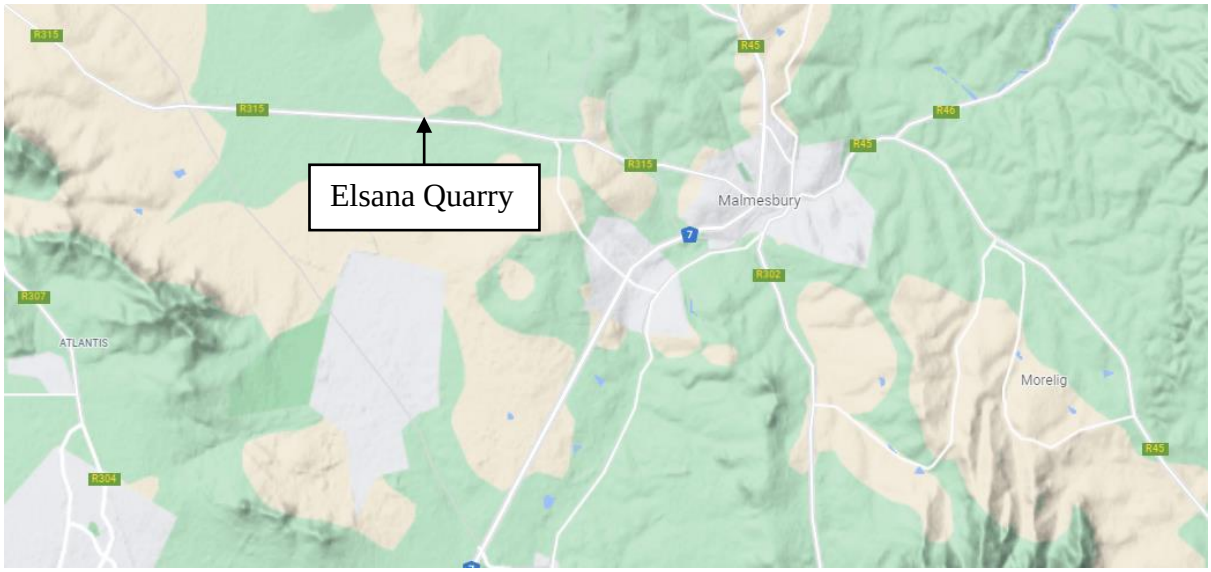

Figure 3.2 Map of Elsana Aggregate Quarry (Google Maps, 2021)

Figure 3.3 Satellite view of Elsana Aggregate Quarry (Google Maps, 2021)

Figure 3.4 illustrates the residual granite sampling pit at Elsana Aggregate Quarry. The residual granite was significantly weathered and the material in the figures below could easily be broken by hand and/or loosened from the seemingly intact structure. Residual granite soil from the vinyl bags dried out throughout sampling and time of use. Figure 3.5 (a) shows the material collected from the vinyl bags, (b) is the same material wetted with water, and (c) is a close-up photo of aggregated particles (approximately 35mm in diameter). It can be seen that the dried material is covered in fines which can easily be washed away once wetted.

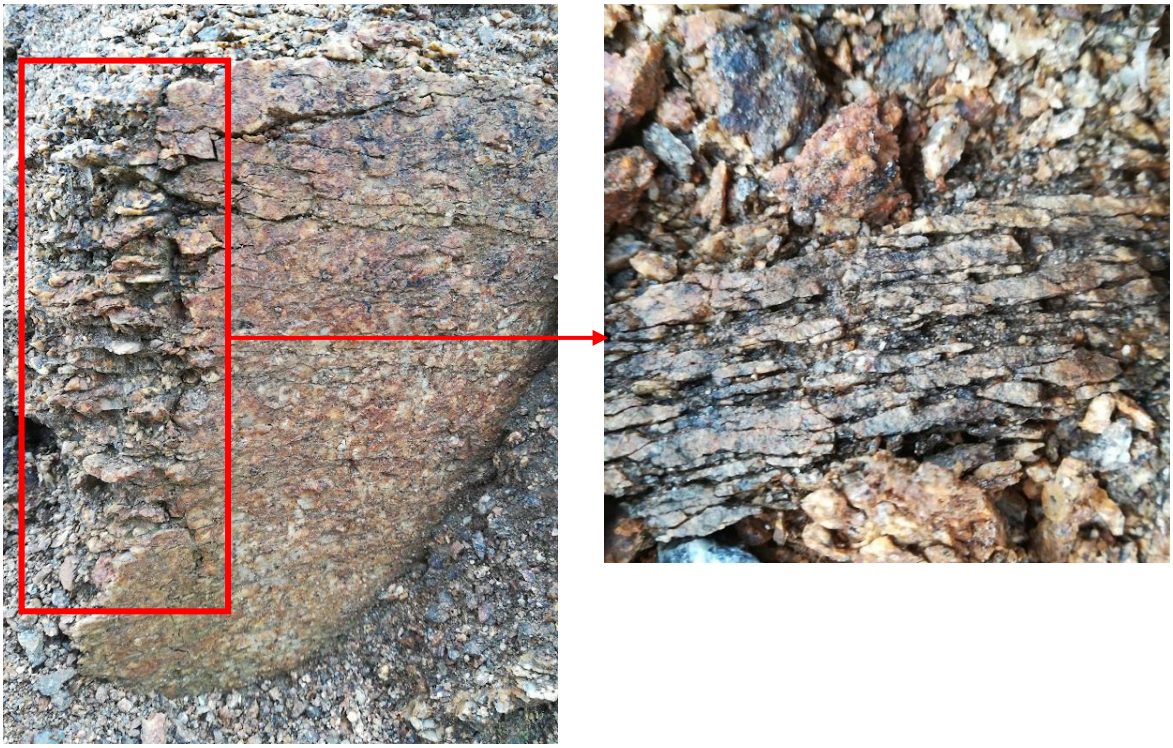

Figure 3.4 Residual granite sampling pit, Elsana Aggregate Quarry

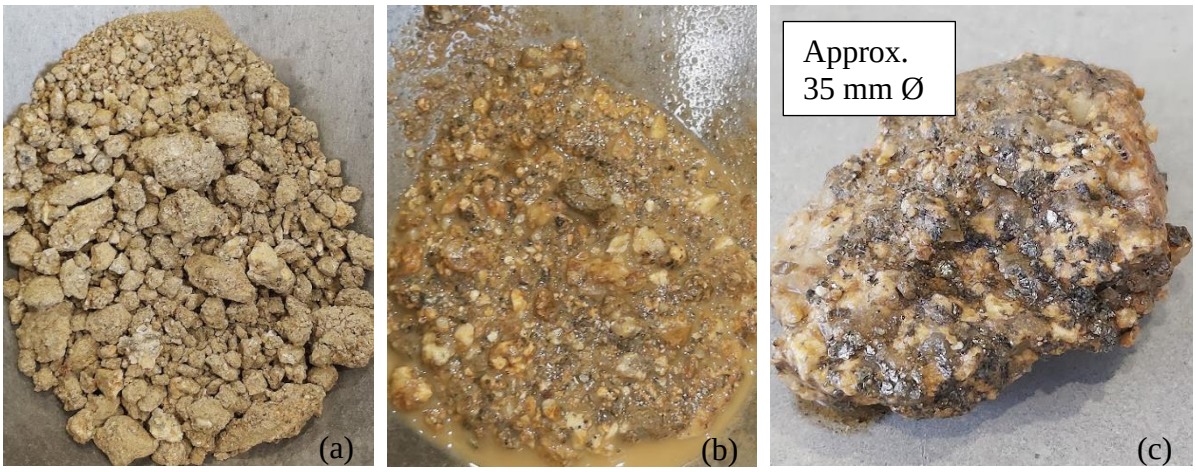

Figure 3.5 Residual granite soil in the laboratory: (a) dried soil from the vinyl bag, (b) washed material, and (c) aggregation of particles

3.4 CLASSIFICATION TESTING

3.4.1 Particle Size Distribution

A grading analysis was performed to determine the particle size distribution of the residual granite soil. The particle size distribution is necessary to determine the uniformity of the soil since this will be an important characteristic when preparing triaxial compression test specimens. This will also be discussed in Section 3.5.2 where more details are given on the preparation of triaxial specimens. Grading is certainly influenced by particle breakage, and it was also used as the primary method to determine particle breakage after shearing. This provided details on the behaviour of the soil and how it is affected by particle breakage.

The particle size distribution of residual granite soil was determined through sieve and hydrometer analyses. The analyses were undertaken in the Pavement and Geotechnical Research Laboratory at Stellenbosch University, using the methods given in SANS 3001-GR1:2013 and SANS 3001-GR3:2014. The methodology for particle size analysis described in SANS 3001-GR:2013 does not prescribe a minimum or maximum time limit for the mechanical sieve shaker. The mechanical sieve shaker was used for a maximum time of 10 minutes, as proposed by Lee & Coop (1995), to minimise the change in grading due to prolonged sieving. Soil masses retained on each sieve were weighed with an electronic balance scale to the nearest 0.1 g and converted to a percentage passing the respective sieve. The percentage passing values were plotted on a semilogarithmic graph against the sieve sizes to obtain a particle size distribution curve.

The hydrometer test allowed for the measurement of percentage passing the 0.05 mm and 0.005 mm sieve which were also added to the above-mentioned data. From the particle size distribution curve, the values of 10%, 30%, and 60% passing particle diameters were estimated to determine the coefficient of curvature (C_{ze}) and coefficient of uniformity (C_u). These shape coefficients distinguish a well-graded soil from a poorly graded soil. A value between 1 and 3 for the coefficient of curvature, and a value greater than 6 for the coefficient of uniformity indicates a well-graded soil. The grading modulus (GM) of the soil was also determined. Percentages retained on the nominal aperture size sieves 2.00 mm, 0.425 mm and 0.075 mm were used to calculate the cumulative fraction of the material.

3.4.2 Atterberg Limits

The Atterberg limits are essential parameters that characterise the soil's engineering properties based on its water content. These limits have been determined in accordance with SANS 3001-

GR10:2013. The liquid limit test was performed using a calibrated Casagrande cup by mixing and remixing material (with water) until an acceptable number of taps closes the groove created in the material. Generally, 22 to 28 taps are considered acceptable, whereas 25 is seen as the optimal amount of taps. The following equation was used to calculate the liquid limit for taps unequal to 25:

$$LL = w_N * h \quad \text{Equation 3.1}$$

Where:

w_N = moisture content expressed as a percentage

$h = \left(\frac{N}{25}\right)^{0.12}$, where N is the number of taps to close the grove.

Material remaining after the liquid limit test was used to fill a shrinkage trough, lined with paraffin wax, to determine the shrinkage limit. The shrinkage gap was recorded, and the following equation was used to determine the linear shrinkage:

$$LS = f * S \quad \text{Equation 3.2}$$

Where:

$f = \frac{0.5333}{1-0.008N}$, where N is the number of taps to close the grove, and

S = shrinkage measured in millimetres (mm).

To determine the plastic limit, stiff material left over in the mixing bowl was used to create a moulded ball. It was rolled in the palms of the hands until small cracks appeared in the surface due to the heat of the hands. Once this occurred, a fraction was taken and moulded into a continuous thread by rolling it between the palm of one hand and the finger of the other. This was repeated until the material could no longer create a thread of approximately 3mm and started crumbling. The liquid limit and plasticity index (LL – PL) values were used to plot the soil on the plasticity chart to describe the soil according to the Unified Soil Classification System (SAPEM, 2014)

3.4.3 Compaction properties: Maximum dry density and optimum moisture content

Compaction of soil reduces the air voids and increases the density without changing the volume of water. Laboratory tests were performed on the residual granite soil to determine the maximum dry density (MDD) and optimum moisture content (OMC) using Modified AASHTO compaction effort (SANS 3001-GR30:2015). These values were used to prepare the triaxial compression test specimens since the density of a soil will influence its behaviour. The compaction data affects the amount of soil and water required to compact a triaxial specimen

to a certain density. In total, five Modified AASHTO compaction effort tests were performed to obtain the compaction data.

A mould of known weight and volume was assembled and used to compact all five specimens. The mould was placed on the Modified AASHTO machine, filled to one-fifth of the mould height, and tamped 55 times. This was repeated for the remaining four layers. The moisture contents and respective dry densities of each specimen were plotted on a graph to produce a concave function where the vertex is equal to the MDD and OMC.

The Modified AASHTO compaction test resulted in a compaction curve as seen in Figure 3.6, along with the zero air voids line. The maximum dry density, $\rho_{d\ max}$, is 2102.5 kg/m^3 and the corresponding optimum water content, OMC, is 8.5%. Typical maximum dry density values for decomposed granite soils usually range from 1550 to 1800 kg/m^3 under ordinary proctor compaction tests and may exceed 2000 kg/m^3 under modified proctor tests (Lee, 1991). Using a heavy compaction effort of 2670 kNm/m^3, Niu et al. (2018) achieved maximum dry densities of 2130 – 2250 kg/m^3 for weathered granite soil. The Modified AASHTO compactor used on the decomposed granite soil applied an energy of 2430 kNm/m^3 to a specimen, justifying the maximum dry density obtained for this material. Material used in the compaction test was immediately discarded to avoid further use of this material. This was done to avoid unnecessary grading changes when determining the particle breakage potential of the material. Figure 3.7 shows the changes in grading after compaction for a specimen compacted at optimum moisture content. The dotted line represents the original distribution curve, and the solid line represents the grading after the Modified AASHTO compaction test. It can be seen that the coarse particles decreased slightly, and the fines fraction increased by approximately 8%.

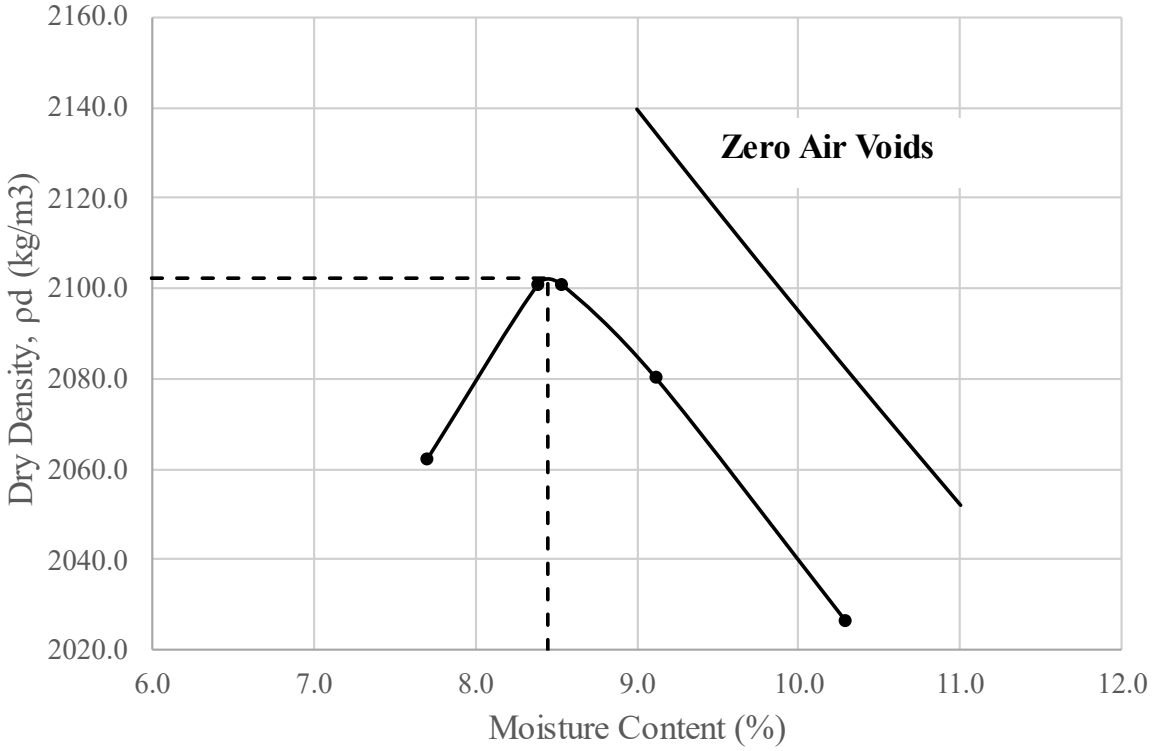

Figure 3.6 Modified AASHTO compaction curve of decomposed granite soil

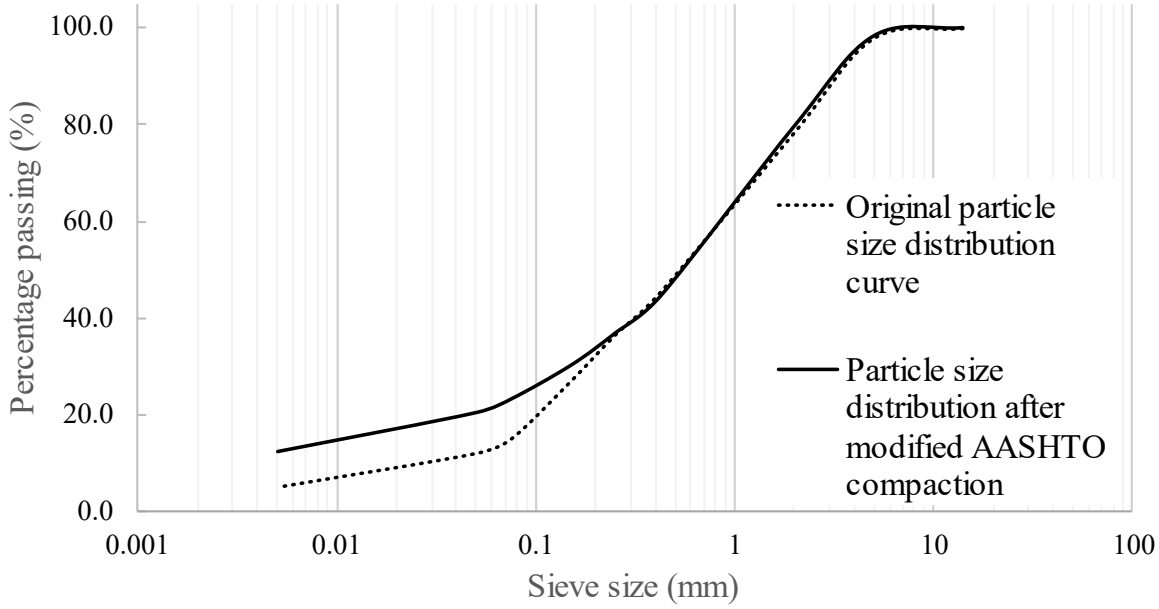

Figure 3.7 Particle size distribution after Modified AASHTO compaction of decomposed granite soil

3.5 TRIAXIAL COMPRESSION TESTING

Triaxial compression tests determine the shear strengths of a soil while replicating in-situ stresses. The triaxial data is significantly important in determining the behaviour of the soil under varying conditions. It forms an integral part in constructing the Modified Cam-Clay

model and determining the critical state of the residual granite soil. The versatility of the triaxial test allows the user to have various initial conditions and execute tests under various drainage conditions. Triaxial compression tests are primarily performed on saturated samples however, some adjustments were made to test unsaturated samples. The adjustments will be mentioned in the following sections where necessary. The triaxial compression tests were carried out at Steyn-Wilson Laboratories in Blackheath in accordance with BS 1377-8:1990.

3.5.1 VJ Tech: TriSCAN Pro Triaxial System

The triaxial apparatus manufactured by VJ Tech is equipped with a multi-purpose load frame, a dual automatic pressure controller (APC) (Figure 3.8), an automatic solenoid valve, a de-airing block connected to a pressure transducer, and the necessary linear variable differential transformers (LVDTs). Data is exported via the APC to the PC and can be viewed live while the system is operating. It can also be exported to Excel and manipulated to fit the required report. The triaxial load frames are capable of running fully automated consolidated undrained (CU), consolidated drained (CD), unconsolidated undrained (UU), and stress path tests. The Clisp Studio software is used to control, monitor, and analyse the triaxial data. It allows the user to configure the saturation, consolidation, and shearing stage to their specific needs with capabilities to monitor the status as the test proceeds.

Figure 3.8 TriSCAN PRO Load Frame (with cell and transducer) and a dual automatic pressure controller (VJ Tech Limited, 2021)

3.5.2 Sample Preparation

Preparation of triaxial test specimens requires the following equipment shown in Figure 3.9: two moulds (one for dry and the other for wet compaction), mould base, hammer, rammer, and mould extender. After compaction, the specimens require the following to be placed into the triaxial cell: porous disks, filter paper (optional), membrane and membrane stretcher, O-rings, and O-ring stretcher, triaxial cell, and its respective screws (Figure 3.9).

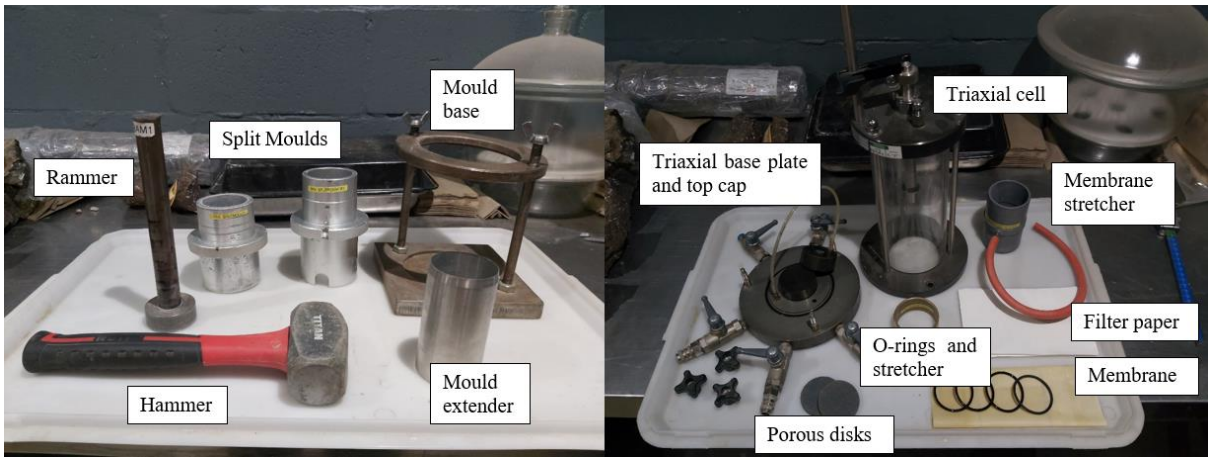

Figure 3.9 Triaxial test specimen preparation equipment

Residual granite soil air-dried for at least 3 – 4 days was separated and stored in seven batches according to particle size, i.e., 5 – 3.35 mm, 3.35 – 2 mm, 2 - 1.18 mm, 1.18 – 0.6 mm, 0.6 – 0.3 mm, 0.3 – 0.150 mm, and below 0.150 mm. Particles greater than 5mm were discarded, and particles smaller than 0.150 mm included all possible particles (clay and silt) in this particular batch. Figure 3.10 shows a simulated representative curve of the particle size distribution for triaxial test specimens. The curve was adjusted to obtain a coefficient of uniformity, $C_u \leq 2$, representing a uniformly graded soil. Typically, more homogenous soils conform to the application of the Modified Cam-Clay model and by keeping the coefficient of uniformity below 2, this can also be achieved for residual granite soil. The percentage material passing listed in Table 3.1 was used to create triaxial test specimens.

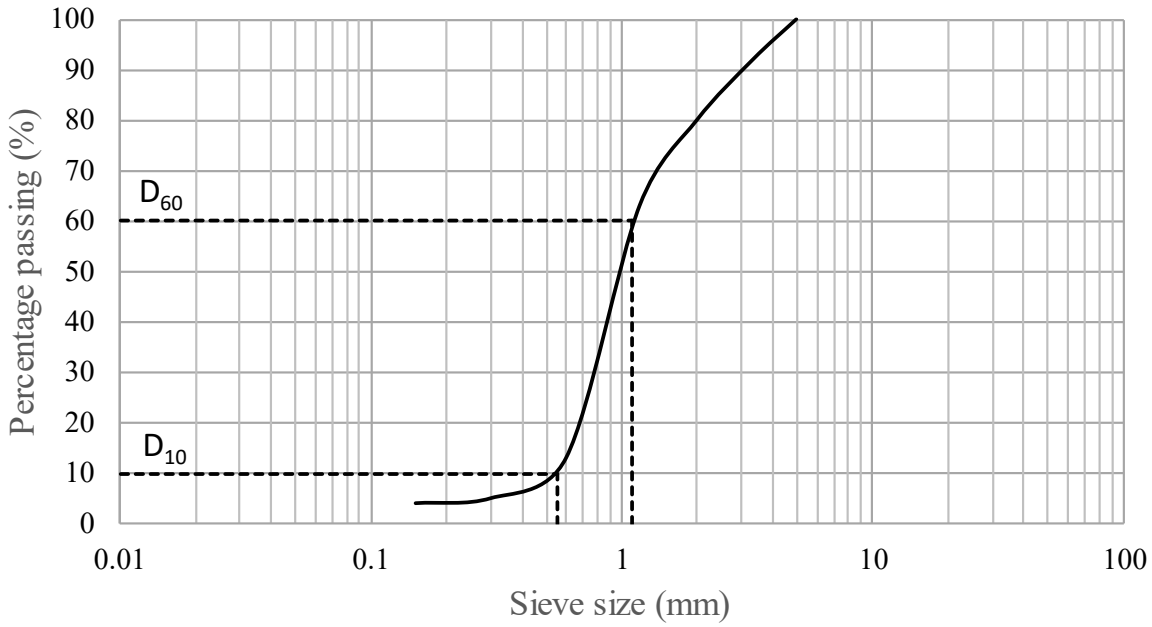

Figure 3.10 Particle size distribution curve for triaxial samples preparation

Table 3.1 Particle size distribution for triaxial samples preparation

Particle size (mm)	Percentage passing
5.00	100
3.35	92
2.00	80
1.18	63
0.60	13
0.30	5
0.150	4

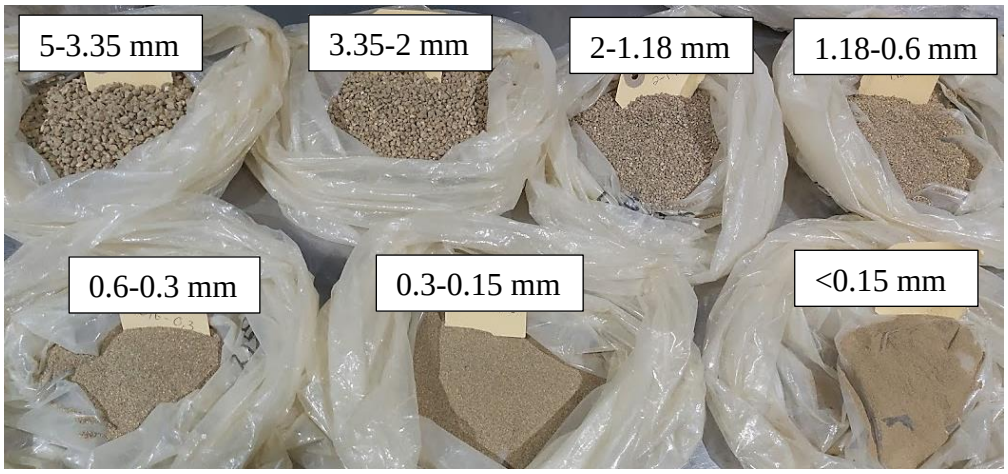

Figure 3.11 Seven batches for triaxial specimen preparation

The required weight of dry material was calculated for each sample and air-dried material was collected from the batches in the correct proportions listed in Table 3.1 and shown in Figure 3.11. The amount of moisture was determined from either the required density or saturation, depending on the predetermined property. The preparation of each specimen and its properties can be viewed in Table A. 1 in Appendix A (summary of specimen preparation properties is listed in Table 3.2). The saturation and void ratio values are for the specimens before testing and will change once saturated or flooded before or after the consolidation stage, and also during shearing. The test details in Table A. 1 are divided as follows: specimens 1 – 7 are saturated specimens (saturated before consolidation), specimen 8 is completely dry (tested without being saturated), 9 – 13 are partially saturated (varying saturations and tested without being saturated), specimen 16 is completely dry but flooded after consolidation, 17 – 20 are partially saturated (varying saturations) but flooded after consolidation, 14 and 15 are air-dried specimens where specimen 14 was tested without being saturated and 15 was flooded after consolidation, and finally CT 1 – 3 are specimens that were sent for CT scans.

The latter three specimens (CT 1 – 3) were prepared at 95% of MDD (1997 kg/m^3) and sent to the Central Analytical Facility (CAF) at Stellenbosch University to have the samples scanned through computed topography (CT). After the initial scans were completed, the same specimens underwent saturated consolidation undrained triaxial testing at confining pressures of 100 kPa, 500 kPa, and 1000 kPa (Table 3.3). Thereafter, CT scans were done on the sheared specimens to examine particle breakage.

The results achieved for specimens 1 – 7 will be used to determine the necessary parameters for the Modified Cam-Clay model, and to evaluate the standard behaviour of decomposed granite soil. Specimens 8 – 13 resembles the different initial moisture conditions the compacted soil might have, and the triaxial compression results will indicate the unflooded strength of the soil. Thus, specimens 16 – 20, which will be flooded after compaction, will be compared to the triaxial compression test results of specimens 8 – 13 to determine the difference in strength. Specimens 14 (unflooded) and 15 (flooded) are air-dried samples and their results will demonstrate the difference in strength in the dry versus wet season.

Table 3.2 Specimen preparation properties

Specimen No.	Compaction effort (% of MDD)	Dry density (kg/m^3)	Moisture (%)	Bulk density (kg/m^3)	Mass of soil (g)	Mass of water (g)	Total mass (g)	Mass per layer (5 layers in total)	Saturation (%)	Remarks
1	86	1808	8.45	1961	355.0	30.0	385.0	77.2	48.1	Saturated specimens
2	89	1871	8.45	2029	367.3	31.0	398.4	79.7	53.8	
3	92	1934	8.45	2098	379.7	32.1	411.8	82.4	60.5	
4	95	1997	8.45	2166	392.1	33.1	425.2	85.0	68.5	
5	95	1997	8.45	2166	392.1	33.1	425.2	85.0	68.5	
6	95	1997	8.45	2166	392.1	33.1	425.2	85.0	68.5	
7	95	1997	8.45	2166	392.1	33.1	425.2	85.0	68.5	
8	86	1808	0.0	1808	354.9	0.0	354.9	71.0	0.0	Dry specimen
9	86	1808	3.5	1872	354.9	12.5	367.4	73.5	20	Partially saturated specimens
10	86	1808	7.0	1935	354.9	24.9	379.9	76.0	40	
11	86	1808	10.5	1999	354.9	37.4	392.4	78.5	60	
12	86	1808	14.1	2062	354.9	49.9	404.8	81.0	80	
13	86	1808	17.6	2126	354.9	62.4	417.3	83.5	100	
14	95	1997	8.45	2166	392.1	33.1	425.2	85.0	68.5	Air-dried
15	95	1997	8.45	2166	392.1	33.1	425.2	85.0	68.5	Air-dried flooded
16	86	1808	0.0	1808	354.9	0.0	354.9	71.0	0	Dry specimen - flooded
17	86	1808	3.5	1872	354.9	12.5	367.4	73.5	20	Partially saturated specimens - flooded
18	86	1808	7.0	1935	354.9	24.9	379.9	76.0	40	
19	86	1808	10.5	1999	354.9	37.4	392.4	78.5	60	
20	86	1808	14.1	2062	354.9	49.9	404.8	81.0	80	
CT 1	95	1997	8.45	2166	392.1	33.1	425.2	85.0	68.5	Specimens sent for CT-scanning
CT 2	95	1997	8.45	2166	392.1	33.1	425.2	85.0	68.5	
CT 3	95	1997	8.45	2166	392.1	33.1	425.2	85.0	68.5	

Table 3.3 Summary of specimens' test schedule

Specimen No.	Confining pressure (kPa)	Drainage type
1 – 4	100	CU
5	200	CU
6	100	CD
7	200	CD
8 – 20	100	CD
CT 1	100	CU
CT 2	500	CU
CT 3	1000	CU

Once the material was weighed out in the correct proportions, it was thoroughly mixed with water ensuring even saturation throughout the soil (Figure 3.12 (a) – (b)). Afterwards, the material was divided into five equal layers and placed into sealed containers to avoid loss of moisture (Figure 3.12 (c)). A split mould, 50 mm in diameter and 100 mm in height, was used to compact a sample (Figure 3.12 (d)). After placing a layer into the mould, the surface was levelled with a spatula and compacted to a predetermined height (Figure 3.12 (e)). The compacted surface was scarified using the edge of a spatula to prevent stratification. This was repeated until the last layer was in place. Specimens were removed from the split mould after the final compacted layer and weighed to later determine the correct water content (Figure 3.12 (f)).

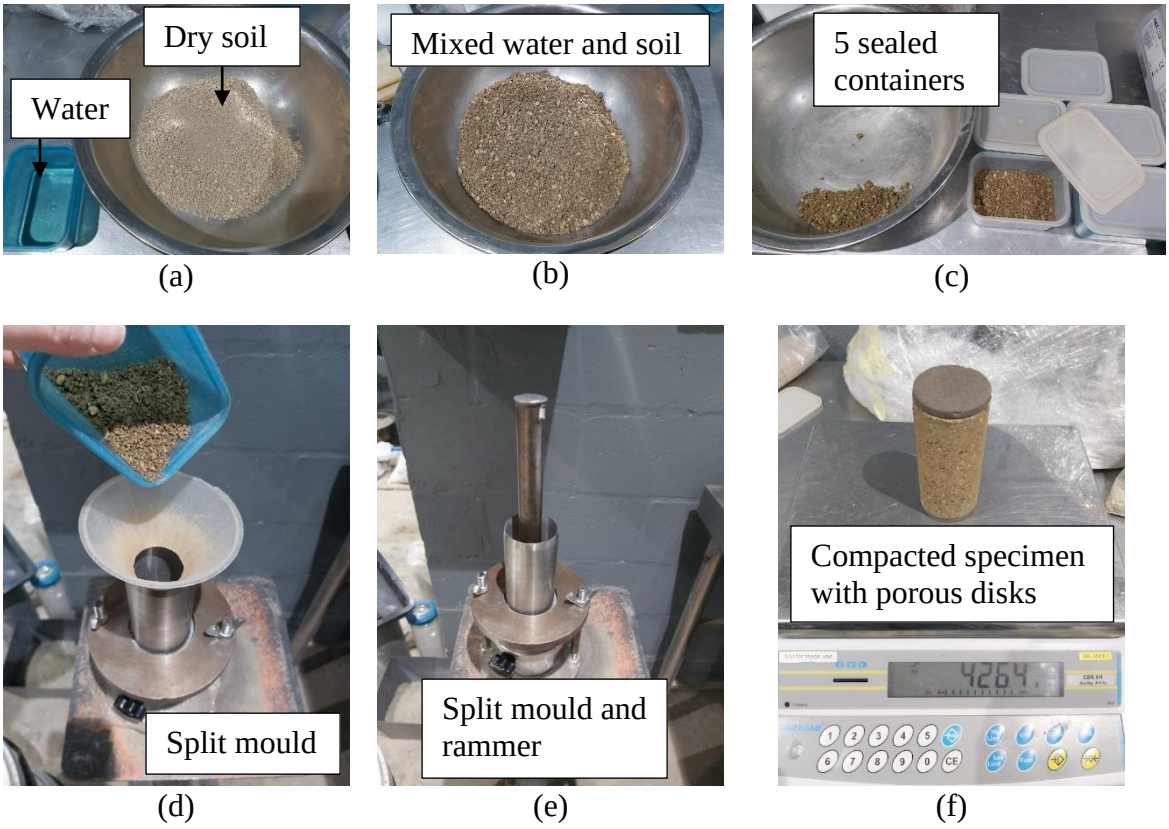

Figure 3.12 Triaxial test specimen preparation: (a) weighed out water and dry soil, (b) thoroughly mixed water and soil, (c) damp soil divided into 5 layers and sealed in containers, (d) split mould, (e) split mould and rammer, and (f) compacted specimen with two porous disks being weighed.

After taking the specimen's weight, it was transferred onto the triaxial cell base where porous disks, a membrane, and O-rings were used to secure and isolate the specimen (Figure 3.13). Loose samples were prepared on the triaxial base plate within a membrane to avoid collapse. This method was applied to samples with saturations of 0% and 20%. Most samples had filter paper strips running up and down the sides of the specimen to act as side drains during saturation and shearing. Specimens 8 – 13 did not have side drains since they did not undergo saturation (flooding).

(a) (b) (c)

Figure 3.13 Triaxial test specimen preparation: (a) side drains placement, (b) membrane and O-rings placement, and (c) securing the triaxial cell.

Testing schedule

Saturation:

From Table A. 1 it is evident that ten tests were saturated before isotropic compression (specimens 1 – 7 and CT 1 – 3). Saturation of samples is necessary to produce accurate measurements of volume change in drained tests and pore pressure response in undrained tests. Before saturating a sample, the cell was flushed with de-aired water to remove any entrapped air. The back pressure method was used to flush the system at a pressure of 20kPa. Using the Assistant in Clisp Studio, the initial conditions were set to varying back pressure increments (see Figure 3.14(a)) used in the B-step analysis, and the effective pressure was kept at 10 kPa. During each back pressure condition, a B-check was done to measure the degree of saturation (the B-value), which is calculated with the following equation:

$$B = \frac{\delta u}{\delta \sigma_3} \qquad \text{Equation 3.3}$$

Where: δu is the change in pore pressure, and $\delta\sigma_3$ is a suitable increment of cell pressure. Generally, a specimen with a B-check value of 0.95 or higher is considered adequately saturated, however, if this value is not achieved, the system automatically moves to the next B-step. Data was logged every 10 seconds for the calculation of the B-check value (Figure 3.14(b)). The B-step and B-check were complete when the pore pressure changes by less than 1 kPa/h, and the B value was equal to or above 0.95 (Figure 3.14(c)). At this stage, not all of the samples were saturated. Some samples were kept dry or at a specific saturation throughout the test and others were saturated (flooded) after isotropic compression. In Table A. 1 it is evident that the former is true for specimens 8 – 14 and the latter for specimens 15 – 20.

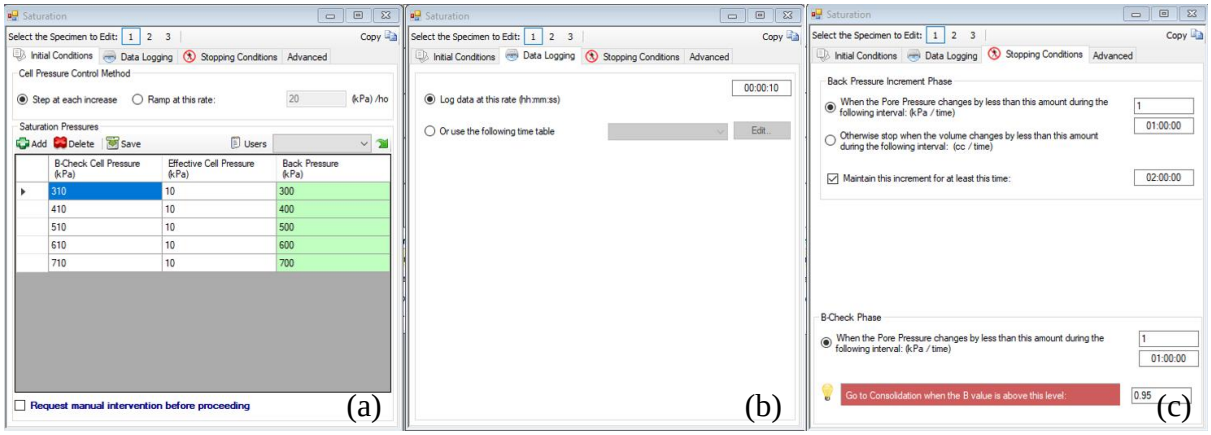

Figure 3.14 Clisp Studio Assistant saturation (a) initial conditions, (b) data logging, (c) stopping conditions

Isotropic Compression and Shearing:

After the B-check value was reached, the last back pressure value was rounded up to the nearest 10 kPa with 300 kPa as the minimum. The confining pressures used for different samples included 100, 200, 500, and 1000 kPa, and the consolidation only started once the pore water pressure stabilised (Figure 3.15 (a)). Drainage conditions were either drained or undrained, depending on the specimen being tested (see Table A. 1). When side drains were used, drainage could occur from the radial boundary and one end, whereas no side drains limited the drainage to one end only. The data were logged on a logarithmic graph which was used to determine t_{100} (Figure 3.15 (b)). Consolidation was stopped once the volume change was less than 0.01 cc over 30 minutes (Figure 3.15 (c)). For the partially samples the back pressure was set to zero to prevent water from entering the specimen, and the cell pressure was increased to the respective effective pressures.

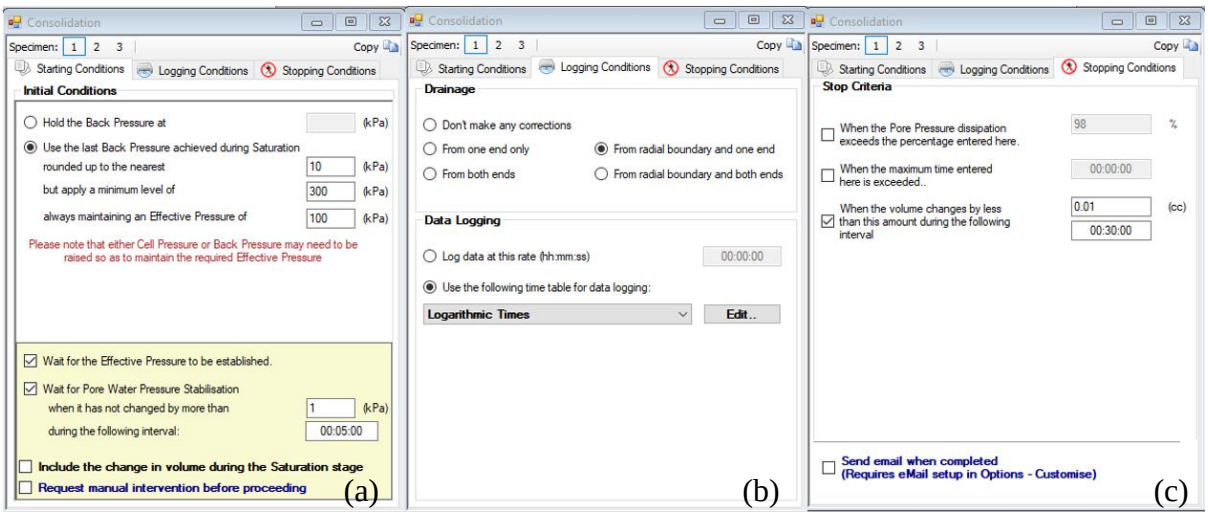

Figure 3.15 Clisp Studio Assistant consolidation (a) start conditions, (b) logging conditions, (c) stopping conditions

Once the consolidation stage ended, the shear speed based on t_{100} was calculated, and a minimum shear speed of 0.022 mm/min was chosen. The cell pressure was kept at the level from the consolidation stage (Figure 3.16 (a)). The top cap was aligned using the engage speed values in Figure 3.16 (b), and the data was logged when the axial strain changed by 0.1%. During the conventional drained test, the back pressure was open, and the volume change was measured, whereas with the undrained test, the back pressure was closed, and pore pressure was measured. For the unsaturated specimens, the drainage valves were left open to the atmosphere. Thus, no volume change or pore pressure was measured for these specimens, only displacement and axial load.

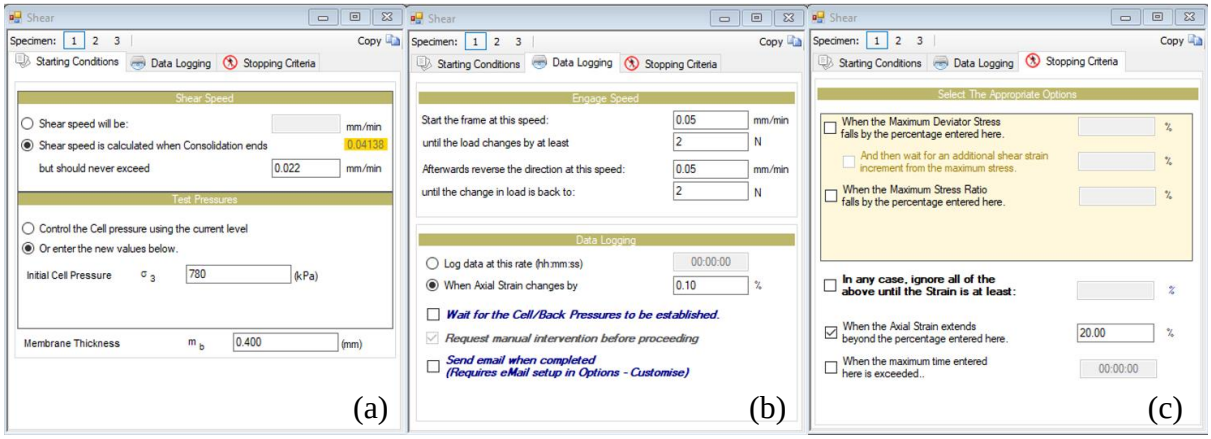

Figure 3.16 Clisp Studio Assistant shear (a) starting conditions, (b) data logging, (c) stopping criteria

An isotropic compression and swelling test was performed on a loose specimen and the programme can be viewed in Appendix A, Table A. 2. The specimen was compacted at 78% of MDD, resulting in a void ratio of 0.62. The gradients of the NCL and URL are significantly important in the calculation of the critical state values of a soil. This was discussed in detail in Section 2.10 and the relevant equations are Equation 2.14 and Equation 2.15.

Post-test procedures:

After the final shearing stage, samples were carefully removed from the cell and oven-dried so that the initial water content could be determined. Sieve analyses were carried out on each specimen to measure the change in the particle size distribution after the triaxial compression test. In order to separate the particles of the highly densified specimen, samples were soaked overnight to break the strong bonds between particles (Figure 3.17 (a) and (b)). Fines were washed out on a 0.150 mm sieve, and the passing material was captured in large pans ready to be oven-dried and weighed. Material collected on the 0.150 mm sieve was oven-dried overnight

and placed in the mechanical sieve shaker for 10 minutes, after which the retained material was weighed and plotted on a semi-logarithmic graph. In order to quantify the particle breakage, Equation 2.6, Equation 2.7, and Equation 2.8 from Section 2.8 were used to determine the breakage potential, total breakage, and relative breakage, respectively.

(a) (b)

Figure 3.17 Triaxial specimen after shearing: (a) dense specimen, and (b) specimen being soaked

3.6 CT SCANNING

3.6.1 CT-scanning unit

CT scans were performed by the Central Analytical Facility at Stellenbosch University to assess the particle breakage on the failure plane of certain specimens. The micro-CT scanner was manufactured by General Electric Sensing and Inspection Technologies/Phoenix X-ray (Wunstorff, Germany), and it is a General Electric VTomex L240 model (Figure 3.18). Two X-ray tubes are located within the micro-CT scanner. One with a transmission target (max. 180 kV), and the other with a reflection-type target (max. 240 kV). CT-scanning mainly involves obtaining projected images taken from 360° around an object and constructing it into a 3D volume by using computer algorithms. Some features of the micro-CT scanner are tabulated in Table 3.4. The facility makes use of Volume Graphics VGStudioMax 3.5 (Volume Graphics, Heidelberg, Germany) software to analyse the tasks. They provided a completed data set along with full volume data which was analysed on a free viewer program, myVGL (Volume Graphics, Heidelberg, Germany)(DuPlessis, Le Roux & Guelpa, 2016).

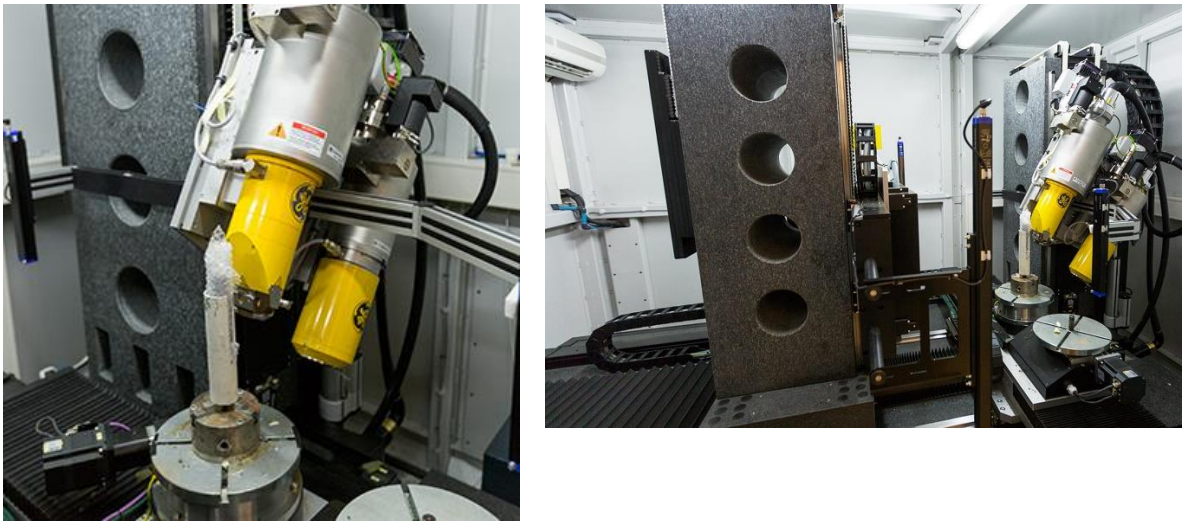

Figure 3.18 Micro-CT scanner at the Central Analytical Facility, Stellenbosch

Table 3.4 Basic specifications for micro-CT scanner at Stellenbosch University (du Plessis, le Roux & Guelpa, 2016)

Micro-CT Scanner	
Voltage (kV)	10-240
Current (µA)	5-3000
Typical best voxel size (µm)	5
Beam angle (°)	Approx. 30
Sample limits for single scan volume	
Weight (kg)	50
Height (mm)	320
Width (mm)	300
Typical maximum wall thickness per material type (mm)	
Steel	10
Rock	40
Plastic	100
Wood	200

3.6.2 CT-scanning procedure

As seen in Table A. 1, three specimens were sent for CT scans (CT 1 – 3). The specimens were scanned after compaction, and once more after they were sheared, resulting in a total of six CT scans. CT 1, 2, and 3 were subjected to 100 kPa, 500 kPa, and 1000 kPa confining pressure during the consolidation stage, respectively, and the CT scans illustrated the effects of the pressures on particle breakage of the specimens. The compacted specimens were 50 mm in

diameter and 100 mm in height, whereas the sheared specimens were deformed after shearing (Figure 3.19 (a) and (b)). CT-scans of CT 1 can be seen in Figure 3.19 (c) and (d) where the former figure represents the specimen after compaction and the specimen after shearing, and the latter shows a section through the sheared specimen.

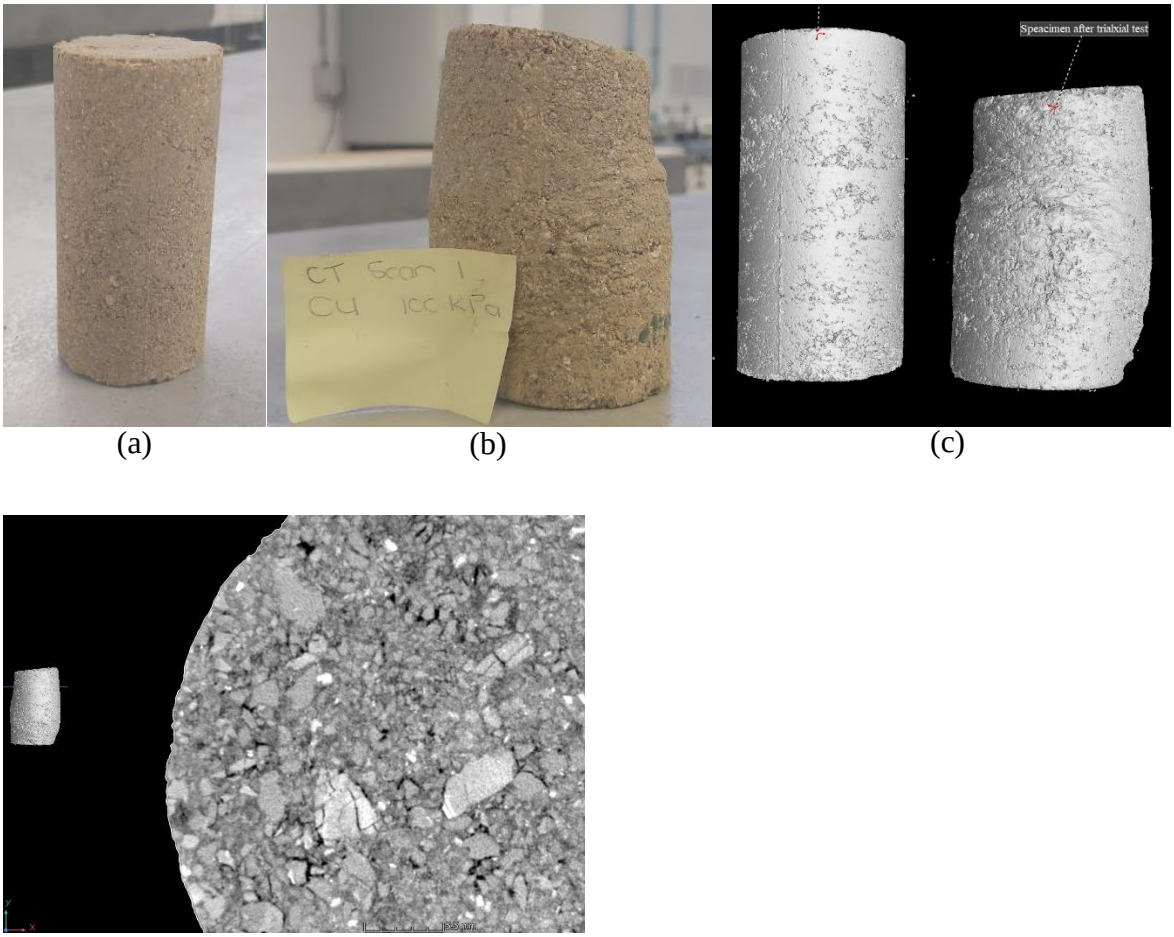

(a) (b) (c)

(d)

Figure 3.19 CT 1 scan procedure: (a) compacted specimen, (b) sheared specimen, (c) scanned specimens after compaction and after shearing, and (d) section through the sheared specimen

Particle tracking could not be achieved with the CT scans due to the deformation of the specimen. From the figures above it can be seen that the sheared specimen does not have the same structure as the compacted specimen. Sieve analyses were performed to determine the degree of particle breakage, whereas the CT scans visually represented the broken particles.

CHAPTER 4: RESULTS AND DISCUSSION

4.1 INTRODUCTION

This chapter presents the data from the laboratory tests conducted, along with a discussion of the results. Section 4.2 considers the results of classification tests such as mineral composition, particle size analyses, Atterberg limits, and the overall classification of the material. Preparation of the specimens and details of the triaxial testing programme were given in Section 3.5 (summary given in Table 4.1). The triaxial tests were conducted to study the intrinsic behaviour of the residual granite soil and to assess the effects of varying densities, saturations (initial water content), and confining pressures on the behaviour of the soil. Data collected from the triaxial compression tests will be discussed in Section 4.3 and it is subdivided into principal points of discussion namely: critical state modelling, shearing and ultimate states (saturated tests), shearing behaviour of dry and partially saturated samples, and the behaviour of flooded specimens.

Table 4.1 Summary of test schedule

Specimen No.	Compaction effort (% of MDD)	Confining Pressure	Drainage	Remarks
1	86	100	CU	Saturated specimens
2	89	100	CU	
3	92	100	CU	
4	95	100	CU	
5	95	200	CU	
6	95	100	CD	
7	95	200	CD	
8 – 13	86	100	CD	Dry/partially saturated specimens
16 – 20	86	100	CD	Dry/partially saturated specimens - flooded
14	95	100	CD	Air-dried sample
15	95	100	CD	Air-dried sample - flooded
CT 1	95	100	CU	Samples sent for CT scans
CT 2	95	500	CU	
CT 3	95	1000	CU	

The critical state line analysis is based on the theoretical foundation of critical state soil mechanics outlined in Section 2.10. The data will be analysed to determine whether the behaviour of the material can be described within a critical state framework. In this regard, the Modified Cam-Clay model was used. The data presented in Section 4.3.3 for the dry and partially saturated samples focus on the presence of water from initial compaction on the behaviour of decomposed granite soil. Volume changes and pore water pressure readings were not measured for these specimens due to the method used for testing such samples (Section 3.5). Only displacement and loading results are presented and compared to saturated samples. Section 4.3.4 discusses the possible effects of flooding after the specimens have been confined to a certain pressure, and two air-dried specimens were tested to determine the soil's behaviour relative to the development of interparticle bonds. The last section presents the data for particle breakage of both saturated and unsaturated tests, and how the breakage was influenced by the variation of properties.

4.2 CLASSIFICATION TEST RESULTS

4.2.1 Mineral Composition

The material was visually examined, and the colour was described according to the procedure given in Jennings, Brink, and Williams (1973). The colour of the material is light brown in its dry state, and upon wetting, the fines coating the coarse particles wash away, revealing whitish-grey quartz, pinkish feldspar, and black mica flakes. An X-ray diffraction analysis was performed by the Department of Geology at the University of the Free State, using a PANalytical Empyrical with a Cu-anode X-ray tub. The mineralogy obtained from the analysis for the whole sample is as follows: quartz (25%), mica (26%), kaolinite (20%), plagioclase (13%), K-feldspar (12%), and calcite (4%). The high score interpretation of the material's diffraction waves can be viewed in Figure 4.1. Sample 1 illustrates the wave of the in-situ material, whereas the wave of sample 2 shows the mineralogy after an attempt was made to remove most of the mica flakes. Sample 2 is not relevant in this research paper, only sample 1. Table 4.2 lists the specific gravities of the individual minerals derived from Pellant (2000). By averaging these values based on their proportions in the soil, the specific gravity of this material, $G_s = 2.65$.

The feldspar group, comprising of plagioclase and potassium feldspar, have a combined representation of 25%. Comparing the amount of feldspar with kaolinite indicates that feldspar has considerably broken down to finer particles resulting in almost equal amounts of feldspar and kaolinite. Coarse grains are typically associated with quartz and feldspar producing a

combined representation of 50% coarse particles, leaving 50% fine particles consisting of kaolinite, mica, and calcite. The particle size distribution will be discussed in more detail in the following section.

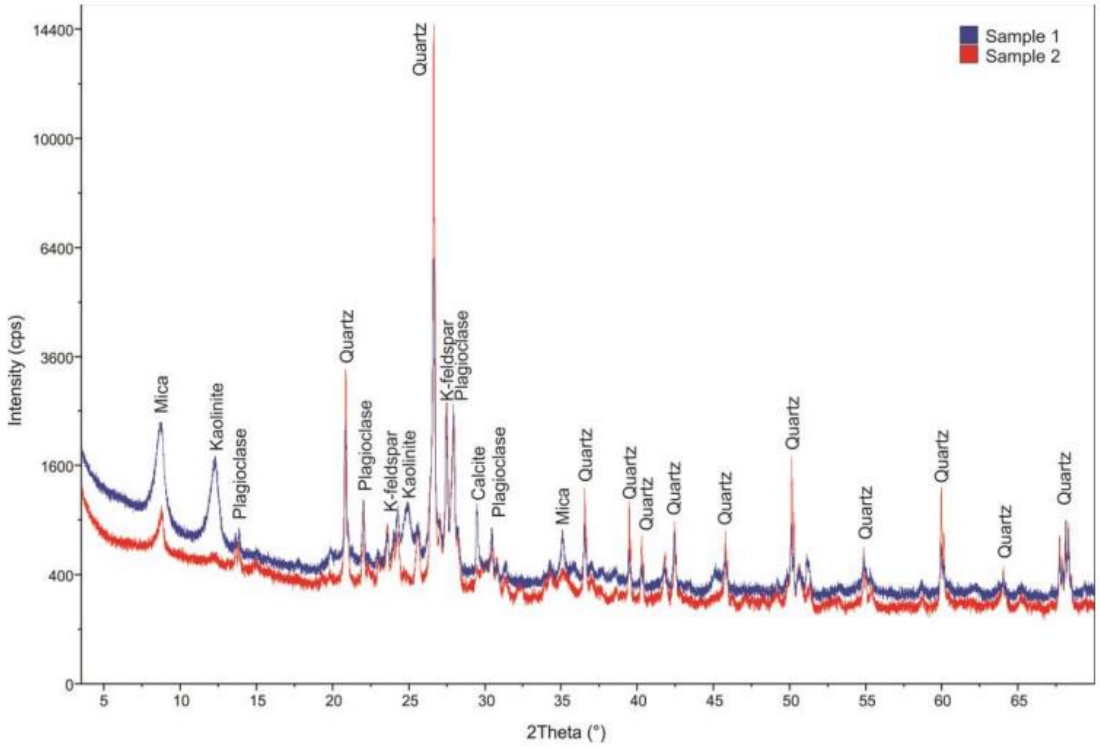

Figure 4.1 X-ray diffraction waves (Sample 1: Blue wave) of decomposed granite soil

Table 4.2 Specific gravities of minerals found in decomposed granite soil

Mineral	Quartz	Mica	Kaolinite	Plagioclase	K-feldspar	Calcite
Specific gravity	2.65	2.88	2.35	2.65	2.35	2.7

4.2.2 Particle size analysis and Atterberg limits

The sampled material comprises of coarse-grained particles coated with fines. Clumps of material have an average size of 40 mm but can easily be broken by hand. These aggregations appear to be formed by both bonding between particles and pore water suction. The wet sieve method allowed these aggregations to be broken down by loosening the fines adhering to it. The grading curve presented in Figure 4.2 (with ASTM classification size ranges) reveals a wide particle size distribution ranging from gravel size to clay size with the most particles present in the medium-sand and fine-sand size ranges. Values of D_{60}, D_{30}, and D_{10} are interpreted from the semi-logarithmic curve as 0.85 mm, 0.18 mm, and 0.05 mm, respectively. The coefficient of uniformity (C_u) has a value of 17, and the coefficient of curvature (C_{ze}), is 0.76. This soil adequately correlates to the mean grading curve of decomposed granite

determined by Lumb (1962) in Section 2.7.1. The mean particle size of the material D_{50} = 0.54 mm, and the grading modulus, GM = 0.64.

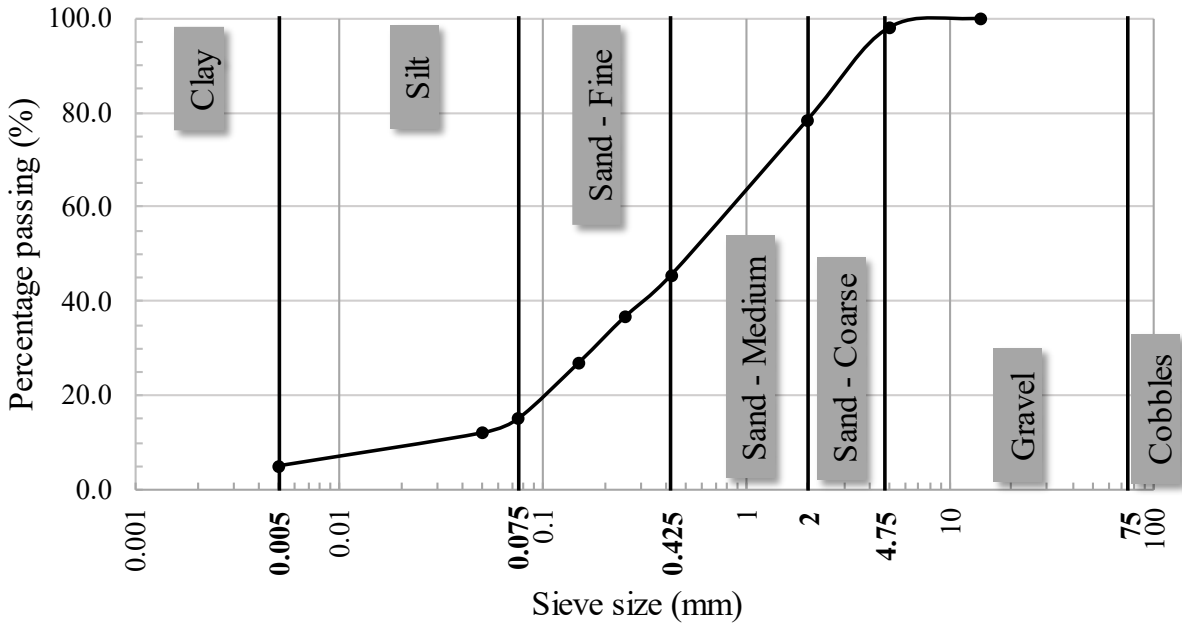

Figure 4.2 Particle size distribution curve for decomposed granite soil

The amount of fines for the decomposed granite soil corresponds well with the mineralogy of the material. The liquid limit and plasticity index (33.3% and 6.5%, respectively) were plotted on the Unified plasticity chart (see Figure 4.3, the black square), falling below the A-line. According to the Unified Soil Classification System (SAPEM, 2014) the decomposed granite soil is classified as a "poorly graded silty sand" with the symbol SM. Values determined for the plastic limit and shrinkage limit were 26.8% and 2%, respectively.

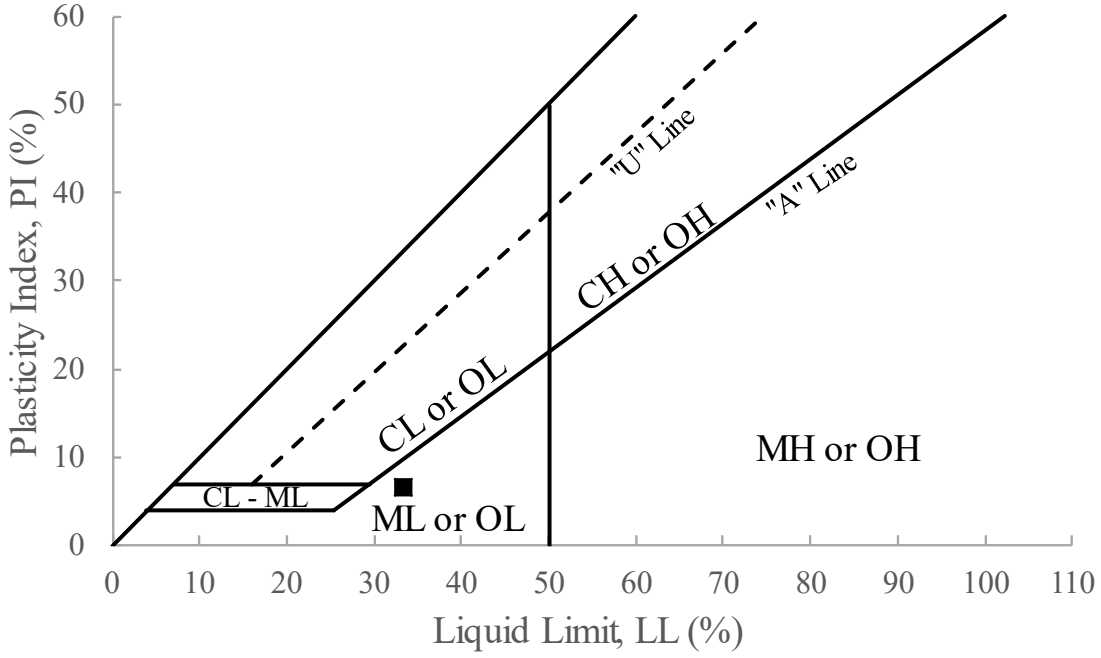

Figure 4.3 Atterberg limits of decomposed granite soil plotted on the Unified plasticity chart

According to AASHTO (SAPEM, 2014), the decomposed granite soil is classified as an A-2-4 material with a subgrade rating of good-excellent. The constituent material is considered to be silty or clayey gravel and sand. The TRH14 (SAPEM, 2014) classification system categorises this soil as a G8 quality "gravel soil".

4.2.3 Summary of classification test results

The index properties of residual granite soil primarily depend on the degree of weathering of the material, and this can vary across the same site. For this material, the mineralogy comprised of the following: quartz, mica, kaolinite, plagioclase, K-feldspar, and calcite. From the mineralogy, the coarse and fines quantities were assumed to be around 50% each. According to the Unified Soil Classification System (SAPEM, 2014), this material is classified as a 'poorly graded silty sand' with the symbol SM. Values for the coefficient of uniformity and curvature were 17 and 0.76 respectively, revealing a poorly graded soil. The AASHTO (SAPEM, 2014) soil classification system characterises the decomposed granite soil as an A-2-4 material whereas, the TRH14 (SAPEM, 2014) classification system categorises it as a G8 material. Past research by Hoffman (2019) shows that the decomposed granite soil tested in this research has a permeability of $7.8x10^{-6}$ m/s and that its permeability is classified as 'poor drainage comprised of sand silt and clay blends' according to Terzaghi, Mesri, and Peck (1996). The basic properties for this material fall within the range of expected properties for other decomposed granite soils, however, it is not identical. It demonstrates that no two residual granite soils are alike. If this material had undergone more weathering, the properties will be different. Mechanical weathering will cause an increase of fine particles, whereas chemical weathering will result in a gap-graded soil due to washing out of the colloidal material. The former will primarily stem from the feldspar particles degrading to kaolinite and quartz particles remaining unaltered. However, if water flows through the soil, colloidal material will exit the soil structure (chemical weathering), resulting in a coarse sandy soil.

4.3 TRIAXIAL TEST RESULTS

4.3.1 Critical state line

As defined in Section 2.10, the critical state is where deformations occur without any further changes in volume or stresses. There are however specimen boundary conditions and limitations associated with the measurement system that should be considered in practice. For this research, criteria have been set to identify the critical state. Lee (1991) suggested that a

specimen reached the critical state when changes were less than 0.1% volumetric strain (ε_p), 0.03 stress ratio (q'/p'), and 5 kPa pore pressure in the last 3% of axial strain for well-graded decomposed granite soil, however, these values were slightly adjusted to fit the results of the soil used in this research. It was assumed that when changes in volumetric strain (ε_p) and the stress ratio (q'/p') were less than 0.2% and 0.05 respectively (during the last 3% of axial strain), the specimen had reached the critical state. For undrained tests, a change in pore pressure of less than 5 kPa was used instead of the volumetric strain criterion.

Table 4.3 shows the critical/end state stresses for specimens 1 – 7, CT 1 – 3, and a summary of each specimen's testing properties. Specimens CT 1 – 3 were sent for CT scans before and after shearing. A detailed description of the specimens' testing programme can be viewed in Appendix A, Table A. 1. The end state refers to specimens that do not fall within the criteria thus, they have not yet reached the critical state within 20% axial strain. These specimens are not plotted on the critical state graphs since they do not contribute to the determination of the gradients, however, their values are listed in the tables marked with an asterisk. When plotting the stresses at critical states in q': p' space, the critical state line is defined by the straight line in Figure 4.4. The critical state friction parameter, M, can be determined from the slope of the linear line characterised by the equation q' = Mp'. The gradient gives an M value of 1.41. This value is higher than the 1.35 value determined by Liu, Zhou, and Liu (2015) for completely decomposed granite soil, and lower than the 1.59 value determined by Lee (1991).

Table 4.3 Critical/end states of decomposed granite soil saturated triaxial compression test samples
***End state**

Test No.	Critical State/*End state				Test properties		
	q' (kPa)	p' (kPa)	q'/p'	v	Dry density (kg/m^3)	Confining pressure (kPa)	Type
1	183	134	1.37	1.425	1808	100	CU
2	289	205	1.41	1.377	1871	100	CU
3	404	282	1.43	1.344	1934	100	CU
4	515	369	1.40	1.293	1997	100	CU
5	706	493	1.43	1.302	1997	200	CU
6	298	200	1.49	1.329	1997	100	CD
7	599	400	1.50	1.297	1997	200	CD
CT 1	556	430	1.29	1.375	1997	100	CU
CT 2*	955	632	1.51	1.344	1997	500	CU
CT 3*	1314	889	1.48	1.331	1997	1000	CU

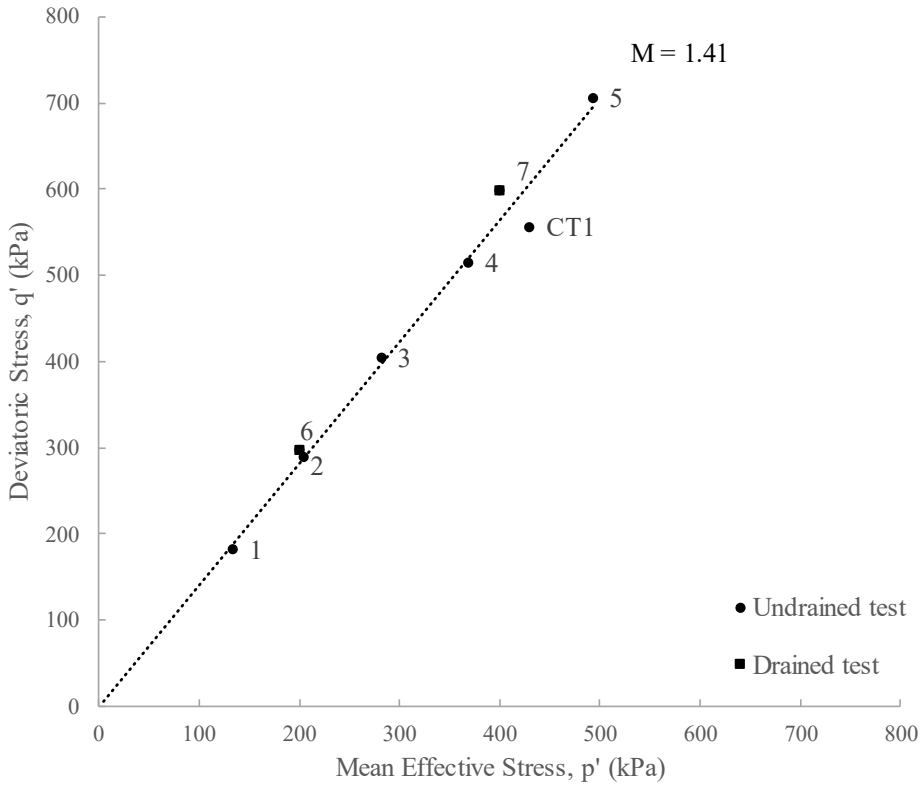

Figure 4.4 Critical state in q': p' space of decomposed granite soil

Parameters from the normal compression line form the basis of critical state soil models. Isotropic compression and swelling tests were performed on a loose sample with an initial specific volume of 1.616. The specimen was compressed under all-around pressure ranging from 25 → 50 → 100 → 200 → 400 → 800 kPa and unloaded to 200 and 25 kPa. The results are listed in Table 4.4 and plotted in ν: lnp' space in Figure 4.5. A straight line for the normal compression line (NCL) and unload reload line (URL) can be seen in the figure. Values of λ, N, and κ were determined from these straight lines as 0.073, 1.88, and 0.012, respectively. These parameters are comparable to those determined by Liu, Zhou, and Liu (2015) where λ = 0.071, N = 2.00, and κ = 0.018. The Modified Cam-Clay model requires these three parameters along with the friction parameter (M), and shear modulus (G) of the soil to be carried out (Table 4.5). The shear modulus was determined from the deviatoric stress versus deviatoric strain plot from the gradient of the curve before failure (3G). This resulted in G = 70 MPa for decomposed granite soil.

Table 4.4 Isotropic compression and swelling test results for decomposed granite soil

Stage	v_i	Pressure (kPa)	v_f
Compression	0.616	25	0.606
Compression	0.606	50	0.580
Compression	0.580	100	0.540
Compression	0.540	200	0.490
Compression	0.490	400	0.438
Compression	0.438	800	0.388
Unloading	0.388	200	0.399
Unloading	0.399	25	0.427

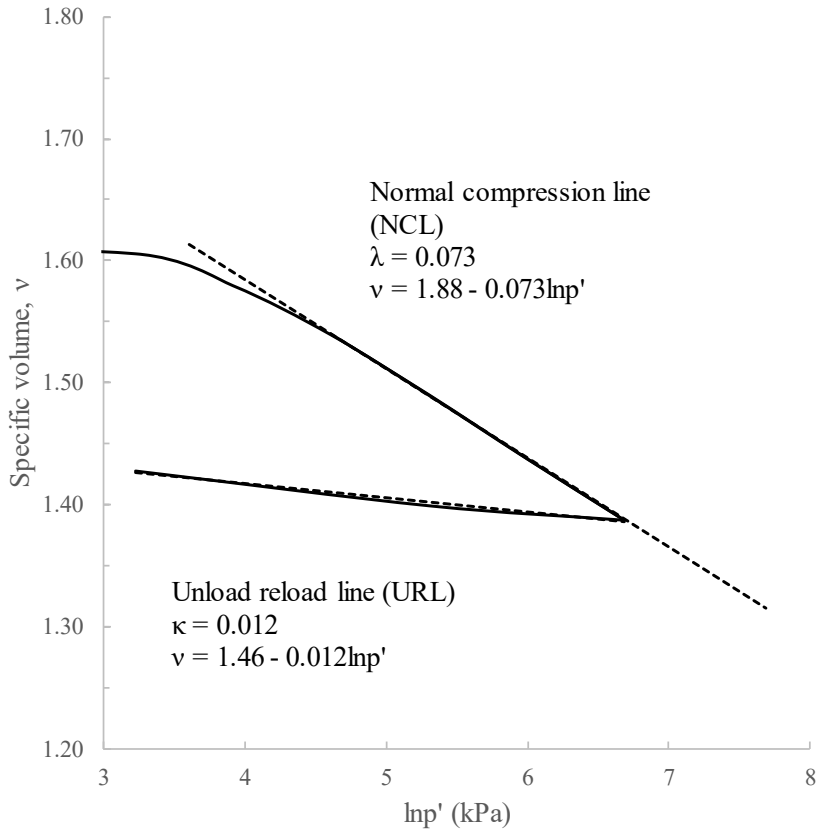

Figure 4.5 Isotropic compression and swelling lines of decomposed granite soil

Table 4.5 Modified Cam-Clay model parameters

Parameter (unit)	Modified Cam-Clay requirements (Wood, 1994)	Values for decomposed granite soil
M (-)	0.8 – 1.5	1.41
λ (-)	0.05 – 0.35	0.073
N (-)	1.6 – 3.0	1.88
κ (-)	0.1 – 0.5 of λ	0.012
G (MPa)	5 – 100	70

Figure 4.6 shows the critical states in ν: lnp’ space along with the best fit critical state line. From the figure, it is evident that the critical state parameters λ and Γ are 0.090 and 1.824, respectively. The critical state line is found to be almost parallel with the normal compression line, indicating that the soil conforms to the basic assumption of the critical state soil model.

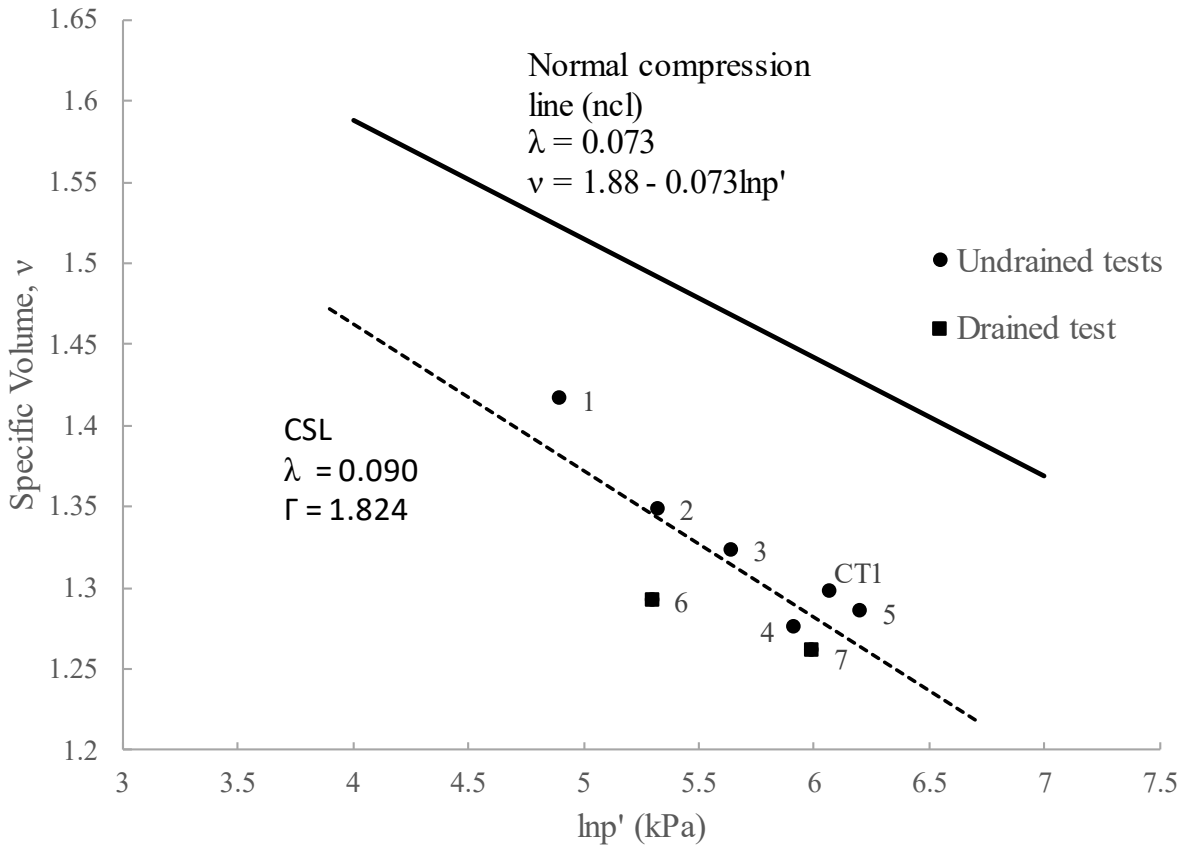

Figure 4.6 Critical state in ν: lnp' space

A Modified Cam-Clay model for decomposed granite soil was created in MS Excel to simulate various drained scenarios. The model uses the five soil parameters previously identified to simulate conditions like normally consolidated, lightly overconsolidated, and heavily overconsolidated soils. This simulation allows the user to predict the deviator stress (q'), effective stress (p') and specific volume (ν) at critical state under different isotropic pressures. When these critical state values are plotted in q': p' space and ν: lnp' space, they line up to form gradients with values of M and λ, respectively. If the model is created correctly and the soil conforms to the Modified Cam-Clay model, the predicted values will be consistent with the input parameters. The equation of the critical state line in the compression plane is expressed by $\upsilon_{cs} = \Gamma - \lambda_{cs} ln p'_{cs}$, where $\Gamma = N - (\lambda - \kappa) ln 2$. From the compression plane, Γ is equal to the y-intercept (p' = 1 kPa), thus Γ can be calculated for the input parameters as well as for the predicted outcomes.

The model was initially tested at six different isotropic pressures under normally consolidated conditions. In Appendix B, Table B. 1 and Table B. 2 lists the input parameters and predicted results for a normally consolidated simulation at 100 kPa isotropic pressure, respectively. Figure B. 1 and Figure B. 2 illustrates the predicted values graphed in q': ε_q and ν: ε_q space,

respectively. This simulation was repeated for other values of isotropic compression to determine the critical state parameters. The predicted values for the simulations are listed in Table 4.6 and their respective graphs can be viewed in Appendix B (Figure B. 3 - Figure B. 12). Figure 4.7 and Figure 4.8 shows the predicted critical state results plotted in q': p' space and v: lnp' space, respectively. From Figure 4.7 it is evident that the gradient, M = 1.41, and from Figure 4.8 that the gradient, $\lambda = 0.073$. For the input parameters Γ is calculated as 1.728 and in Figure 4.8 the y-intercept, $\Gamma = 1.727$. From these simulations, it is evident that the soil parameters determined for this material conform to the Modified Cam-Clay model. This will also be discussed in later sections where appropriate.

Table 4.6 Predicted values for drained decomposed granite soil simulations modelled after the Modified Cam-Clay model

Simulation No.	Isotropic pressure (kPa)	Deviator stress, p'_{cs} (kPa)	Effective stress, q'_{cs} (kPa)	Specific volume, v_{cs} (-)
1	100	189	266	1.345
2	300	566	798	1.265
3	500	943	1330	1.228
4	700	1321	1862	1.203
5	900	1698	2394	1.185
6	1100	2076	2926	1.170

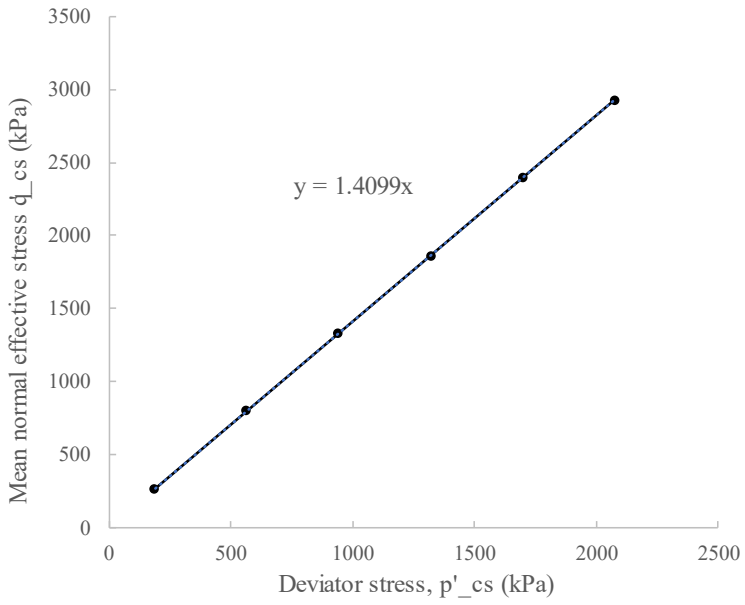

Figure 4.7 Predicted critical state results in q': p' space for decomposed granite soil

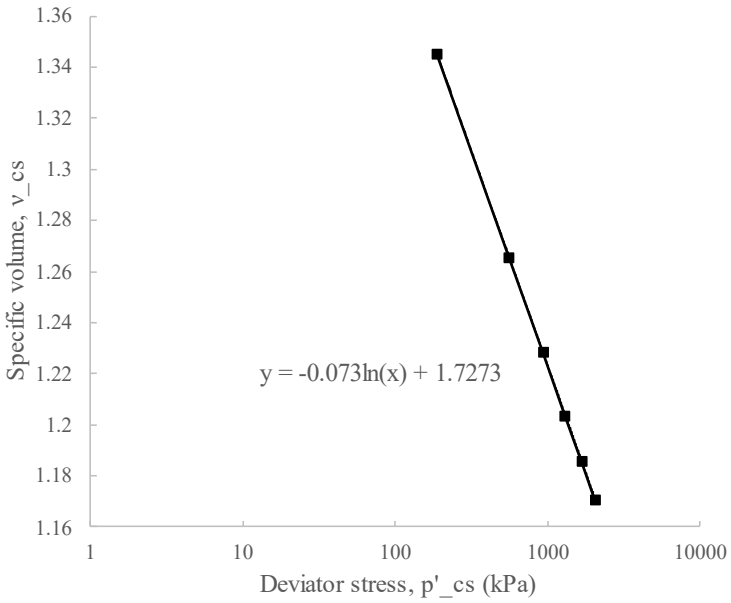

Figure 4.8 Predicted critical state results in v: lnp' space for decomposed granite soil

In Appendix B, Figure B. 13 - Figure B. 16, the predicted graphs for lightly overconsolidated and heavily overconsolidated simulations are shown. The purpose of this model is to predict a qualitative match between predicted and experimental results. For the normally consolidated tests, it is evident that the deviator stress monotonically increases with no distinctive peaks, and that specific volume decreases monotonically as shear progresses. For heavily overconsolidated tests, it shows that the deviator stress reaches a peak before exhibiting a reduction, and that specific volume initially decreases before it increases.

4.3.2 Shearing and ultimate states of saturated tests (specimens 1 – 7)

The samples considered in this section were compacted in a partially saturated state near optimum moisture content and saturated before isotropic compression. These tests were completely saturated before isotropic compression and will be referred to as the saturated tests/samples. In this section, topics of interest include the following: general trends of shearing data, identification of the ultimate state, the critical state line concerning saturated specimens, dilation and peak states, and stress paths. For the saturated tests, the initial density, effective confining pressure, and drainage condition of the specimens were varied to determine the effects of these conditions on the behaviour of the soil. Initial densities ranged from 86% to 95% of Modified AASHTO maximum dry density, and the effective all-around pressures were varied from 100 kPa to 1000 kPa. The two drainage conditions were consolidated undrained (CU) and consolidated drained (CD) tests.

In total, 10 specimens were prepared and tested in this state to determine the effects of the varying conditions, and the preparation of these specimens are summarised in Table A. 1. Four undrained specimens were investigated to determine the effects of different initial densities (constant confining pressure), and another four samples (prepared at the same density) to determine the effects of varying confining pressures. A total of eight specimens were therefore tested under undrained conditions, and two specimens, prepared at the same density, were tested under drained conditions (varying confining pressure). Specimens that were partially saturated or completely dry will be considered in Section 4.3.3, and the results will be compared to the information discussed in this section. Results in addition to those discussed will be presented in Appendix C.

The stress-strain plot of a given soil has two ‘failure’ points. One at the maximum value of stress known as the peak state, and the other at the critical state. For a loose soil, these two points are not determined separately since the peak state coincides with the critical state. Stress-strain plots can either be in the form of maximum deviatoric stress or maximum stress ratio and for the purpose of comparing data from different types of tests, the maximum stress ratio is used for the selection of peak states. For a drained test the maximum stress ratio and the maximum deviatoric stress can occur at the same state, but this may be different for an undrained test. Dense samples mainly show greater peak strength and stiffness than looser samples, however, all samples have the same strength at critical state.

Table 4.7 summarises the peak states, and friction angles, of the saturated series at maximum stress ratio and Figure 4.9 shows the peak states plotted in q’: p’ space. Note that these values are not the peaks at maximum deviatoric stress. The stress ratio at peak ranges from 1.51 to 1.87 and all the peak states lie above the critical state previously determined (Figure 4.9). Unlike the critical stress ratio, there is no definitive relationship between the peak states. The peak stress ratio of a soil is dependent on the initial density and confining pressure, whereas the critical stress ratio is a property of a soil, independent of these characteristics.

Table 4.7 Peak states at maximum stress ratio and peak friction angle of saturated specimens
***Peak secant friction angle**

Test No.	Peak state at maximum stress ratio			Peak friction angle ϕ_p (deg)	Test properties		
	q' (kPa)	p' (kPa)	q'/p'		Dry Density (kg/m^3)	Confining pressure (kPa)	Type
1	183	115	1.59	38*	1808	100	CU
2	225	136	1.65	40*	1871	100	CU
3	303	179	1.69	38*	1934	100	CU
4	371	210	1.77	37	1997	100	CU
5	578	337	1.72	37	1997	200	CU
6	407	238	1.71	42*	1997	100	CD
7	686	428	1.60	40*	1997	200	CD
CT 1	338	181	1.87	37	1997	100	CU
CT 2	923	595	1.55	37	1997	500	CU
CT 3	1325	879	1.51	37	1997	1000	CU

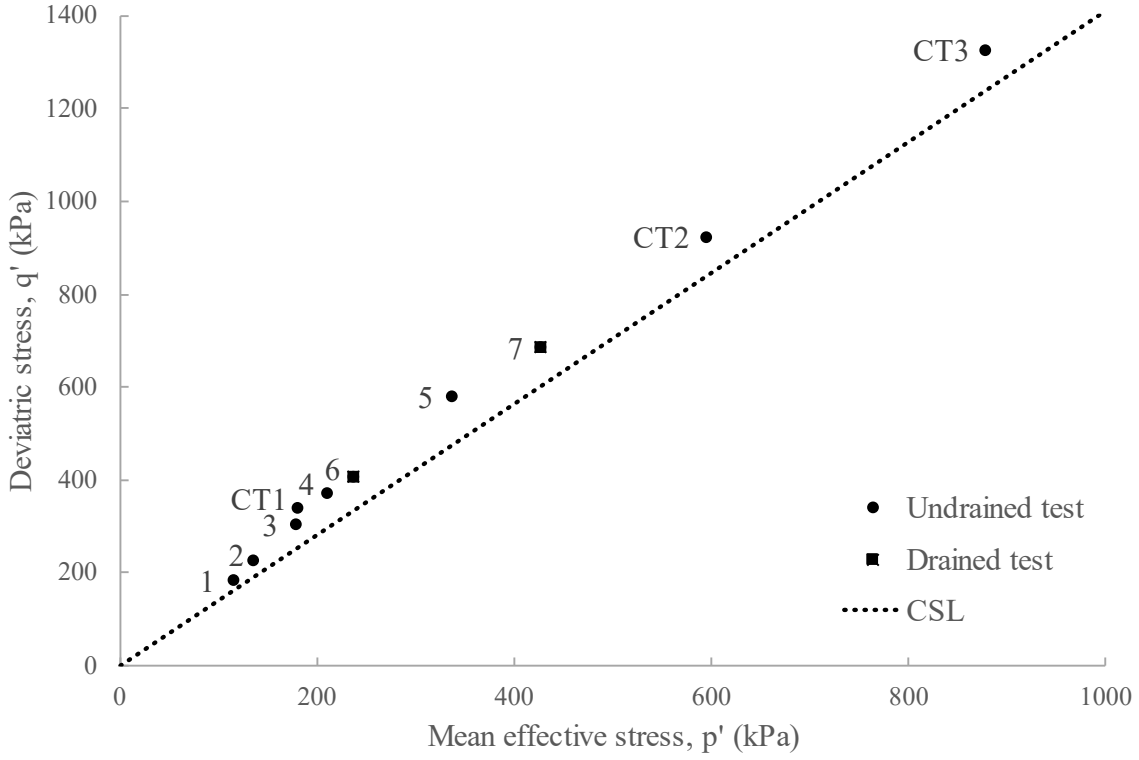

Figure 4.9 Peak states of saturated triaxial test specimens at maximum stress ratio in q': p' space with the critical state line

The dry densities of four undrained specimens were varied from 86% to 95% of Modified AASHTO MDD and the deviator stress and change in pore pressure results can be seen in Figure 4.10. Other properties like the confining stresses and drainage conditions were kept constant i.e., 100 kPa and consolidated undrained tests. The selected densities were 86%, 89%, 92%, and 95% (1808, 1871, 1934 and 1997 kg/m^3) of Modified AASHTO MDD, increasing from specimen 1 – 4. From the figure below it can be seen that the denser samples, 3 and 4, have greater strengths than the looser samples, 1 and 2. Even though there are no distinctive peaks in any of the deviatoric stress curves, it is evident that the initial density governs the behaviour of the patterns by increasing the peak strength with increasing density. The change-in-pore-pressure curves indicate that looser samples have a higher pore pressure which is also equivalent to compressive volume changes for a drained test. For the denser samples, the change in pore pressure is lower, and they associate with dilative volume changes for a drained test.

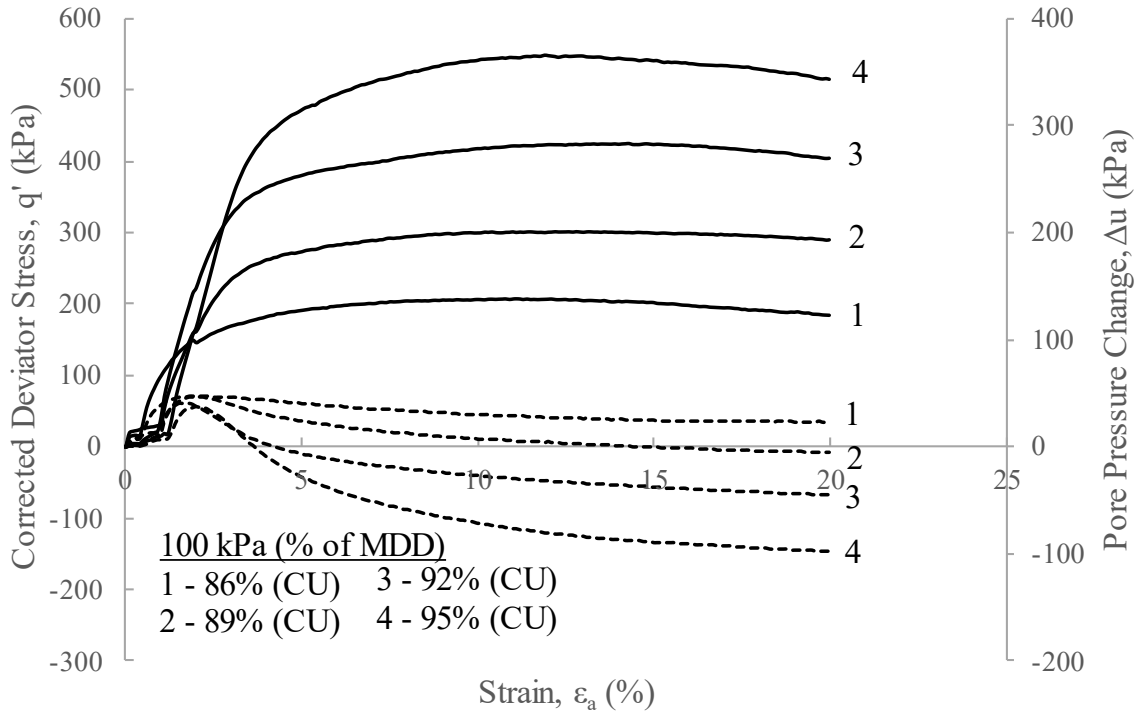

Figure 4.10 Behaviour of decomposed granite soil under varying initial densities and the same confining pressure in q': ε_a: Δu space (undrained)

Figure 4.11 illustrates the peaks of the denser samples considerably better than Figure 4.10 due to the relationship of the individual graphs. As previously mentioned, the maximum deviatoric stress and maximum stress ratio for an undrained specimen do not necessarily occur at the same state. Thus, from Figure 4.11 it is evident that the dense samples show peaks, whereas loose samples show slight peaks, and that all samples are approaching the ultimate state at the end of

the test (point C). This also shows that the ultimate state (critical state) does not depend on the initial density of the soil, unlike the peak state.

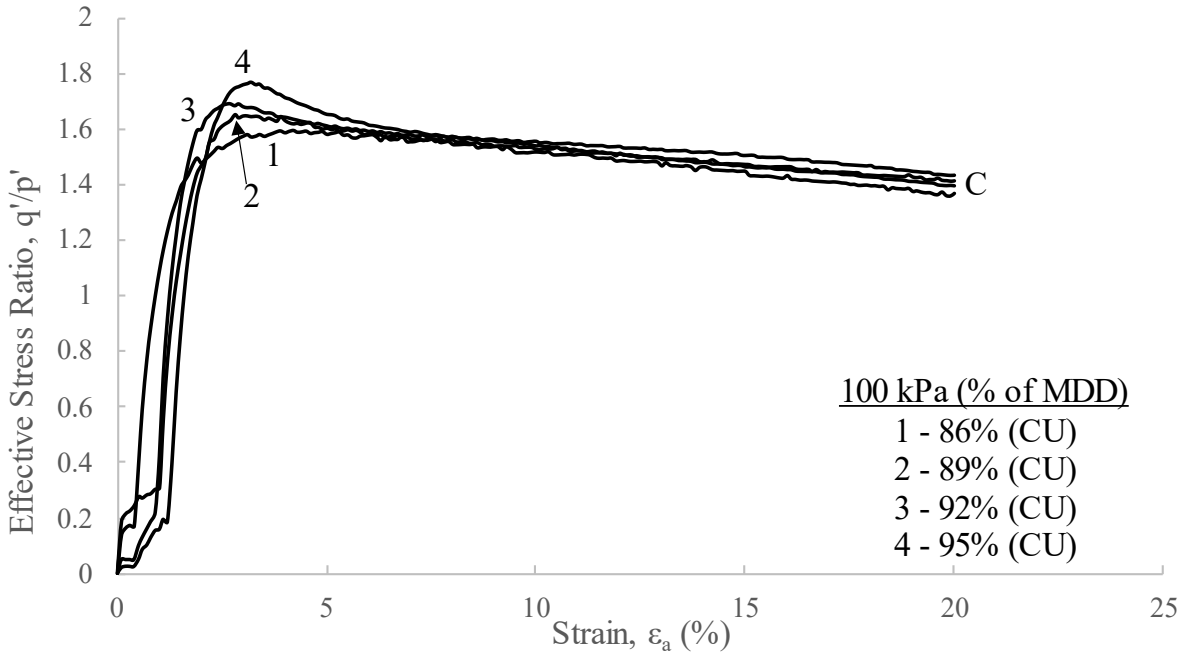

Figure 4.11 Behaviour of decomposed granite soil under varying initial densities and the same confining pressure in q'/p': ε_a (undrained)

Figure 4.12 and Figure 4.13 shows how the behaviour of the soil is affected by varying confining pressures under undrained conditions. All the specimens had an initial density of 95% of Modified AASHTO MDD corresponding to an initial specific volume of 1.327. At low confining stresses, pore water pressure decreases to negative values, whereas specimens confined to higher stresses display an increase in pore water pressure (see Figure 4.12). As previously specified, these changes in pore pressure correspond to dilative and contractive volume changes for a drained test, respectively.

In Figure 4.13 it is apparent that all specimens reach the ultimate state regardless of the confining stress. Here it can also be seen that at lower confining stresses the specimens have distinctive peaks and at high confining stresses, the specimens barely have peaks. The peak stress ratio approaches the critical stress ratio as the confining stress increases. This characteristic is also present in loose specimens, showing that at high confining stresses, specimens will behave like a loose soil. The change in peak values indicates that the stress ratio at the peak depends on the initial state i.e., confining stress, of the sample.

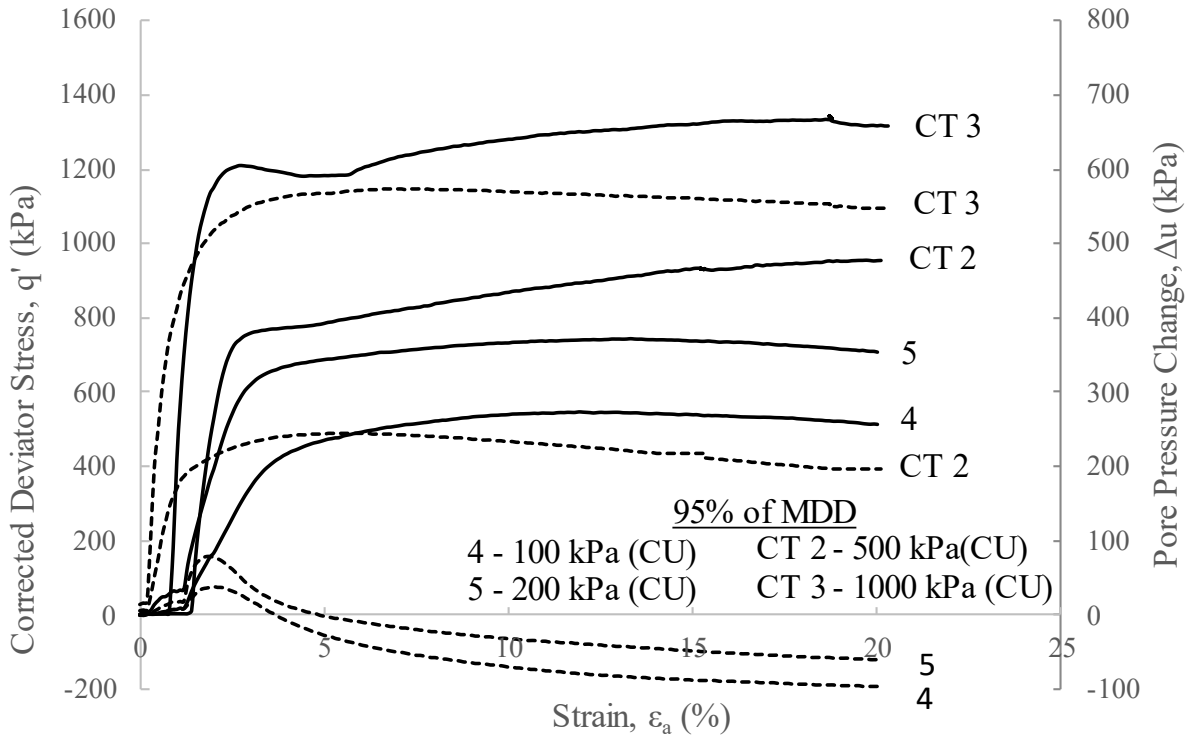

Figure 4.12 Behaviour of decomposed granite soil under varying confining pressures and the same initial density q': ε_a: Δu space (undrained)

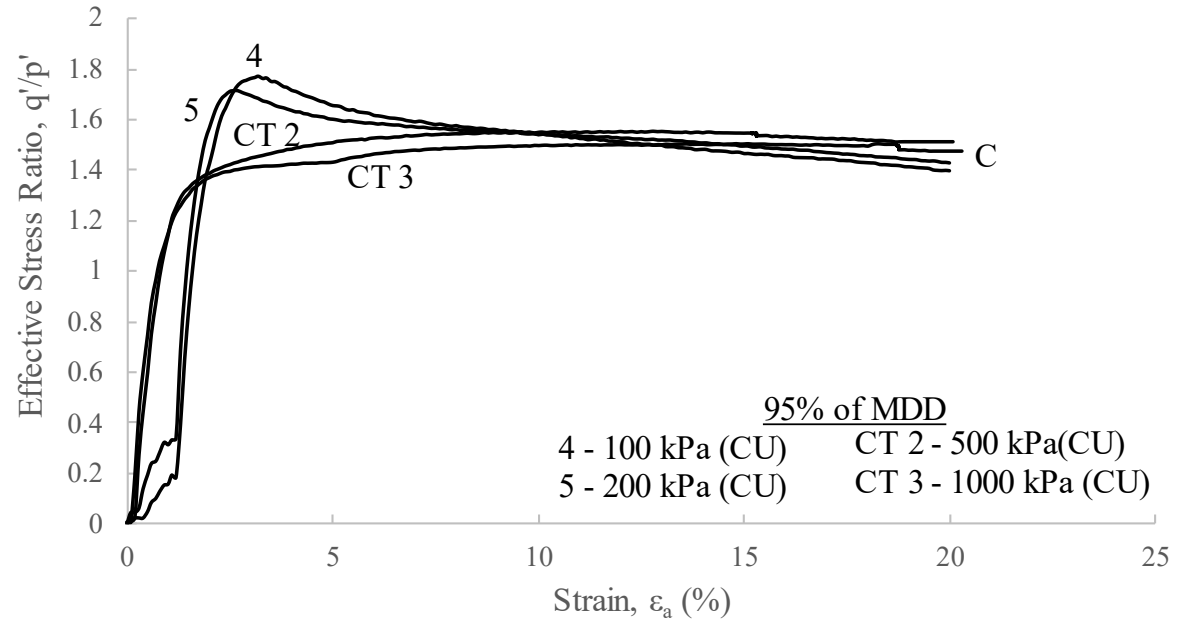

Figure 4.13 Behaviour of decomposed granite soil under varying confining pressures and the same initial density in q'/p': ε_a space (undrained)

Two drained specimens were prepared at an initial density of 95% of Modified AASHTO MDD and confined to pressures of 100 kPa and 200 kPa. Specimens 6 and 7 have similar behavioural characteristics as specimens 4 and 5, where the higher confined specimen has a lower peak

with respect to the critical state, and both tests show dilative behaviour (see Figure 4.14). A dilatancy parameter, *d*, has been identified as the distance between the peak and critical state in the deviator stress plot, and from Figure 4.14 it is evident that this parameter decreases with increasing confining stress. This attribute is also remarkably noticeable in Figure 4.13 test CT 2 and CT 3, showing that the tendency of a specimen to dilate decreases and the soil's behaviour moves towards contractive volume changes. Specimens 6 and 7 have peaks in both Figure 4.14 and Figure 4.15, however, they only reach the same ultimate state in the stress ratio space (Figure 4.15), again showing that the ultimate state does not depend on the confining stress.

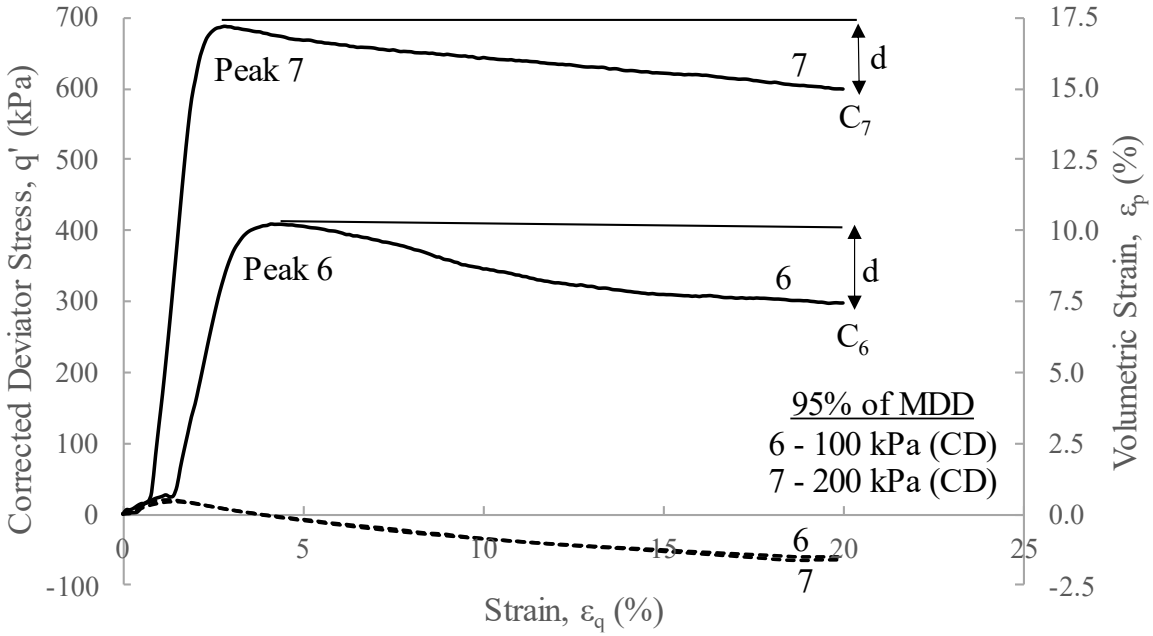

Figure 4.14 Behaviour of decomposed granite soil under varying confining pressures and the same initial density in q': ε_q: ε_p space (drained)

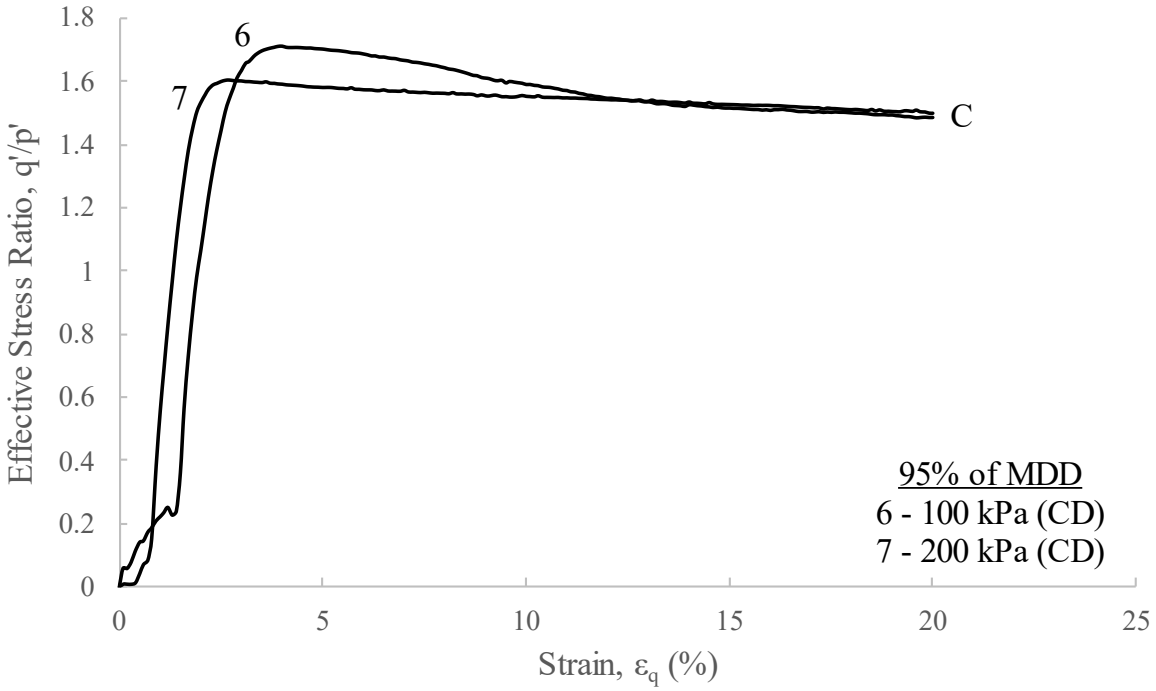

Figure 4.15 Behaviour of decomposed granite soil under varying confining pressures and the same initial density in q'/p': ε_q space (drained)

Peak states, and any stress ratio greater than the ultimate, in the stress ratio space, is primarily due to a certain degree of dilation. In the subsequent discussion on stress paths, for both drained and undrained tests, it will become apparent that the stress ratio depends on the friction parameter, M. The Mohr-Coulomb envelopes of samples 6, 7, and the critical state are presented in Figure 4.16 with their respective Mohr circles. It illustrates that higher confining pressures have lower peak secant friction angles and that if the confining pressure was considerably higher, the peak secant friction angle will approach the critical state friction angle so that $\phi_p = \phi_c$. Similarly, the peak stress ratio approaches the critical stress ratio as the confining pressure is increased. In Figure 4.14, C_6 and C_7 correspond to the different critical state Mohr circles of specimens 6 and 7, respectively. From the figure below it is recognised that although these specimens have different critical state Mohr circles, they share the same critical state failure envelope with a friction angle ϕ_c, corresponding to point C in the stress ratio space (Figure 4.15). Therefore, the critical state stress ratio, $(q'/p')_c$, and friction angle, ϕ_c, are unique values for this material.

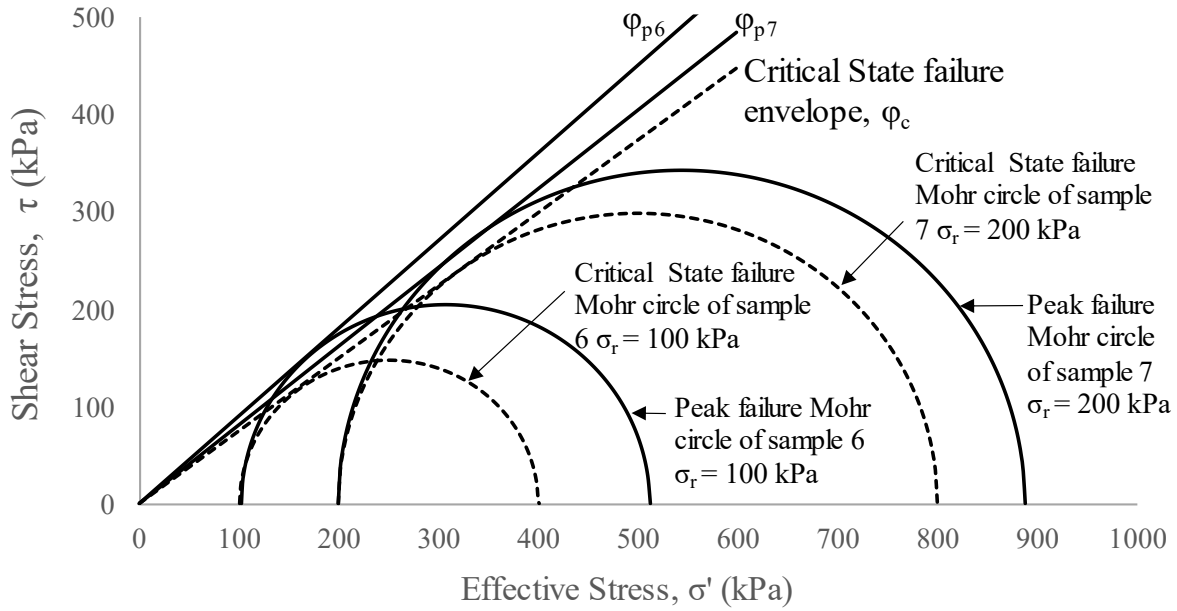

Figure 4.16 Mohr-Coulomb peak and critical state conditions for decomposed granite soil under varying confining pressures and the same initial density (drained)

Figure 4.17 and Figure 4.18 illustrate the stress paths for undrained and drained tests, respectively. It can be seen that a loose sample, such as specimen 1, had an increase in excess pore pressure as the shear stress increased. The decrease in pore pressures due to the effects of dilatancy causes the denser paths to move to the right. Other soils seldomly have peaks for each undrained test, however for this material all the undrained tests showed peaks. After the soil has reached its peak stress the deviator stress decreased to a stress ratio similar to the critical state.

The drained tests intersect the x-axis at p' = σ_3 and form a straight line with a constant slope of 3. This is a result of dp' = $\frac{1}{3}$dσ_1' and dq' = dσ_1'in the shearing stage of a consolidated undrained test so that dq'/dp' = 3. As expected, the dense samples reached their peaks first and retraced their paths to arrive at the ultimate state. From the stress path graphs below, it is evident that both drained and undrained tests under the varying conditions mentioned, approach (more or less) the same critical state value, $(q'/p')_c$. This shows that irrespective of the density and confining stress, this material reaches a critical state with a unique and constant friction angle, ϕ_c. Unlike the critical state friction angle, the peak friction angle is a state property and depends on the initial density, stress state, and frictional characteristics of the soil.

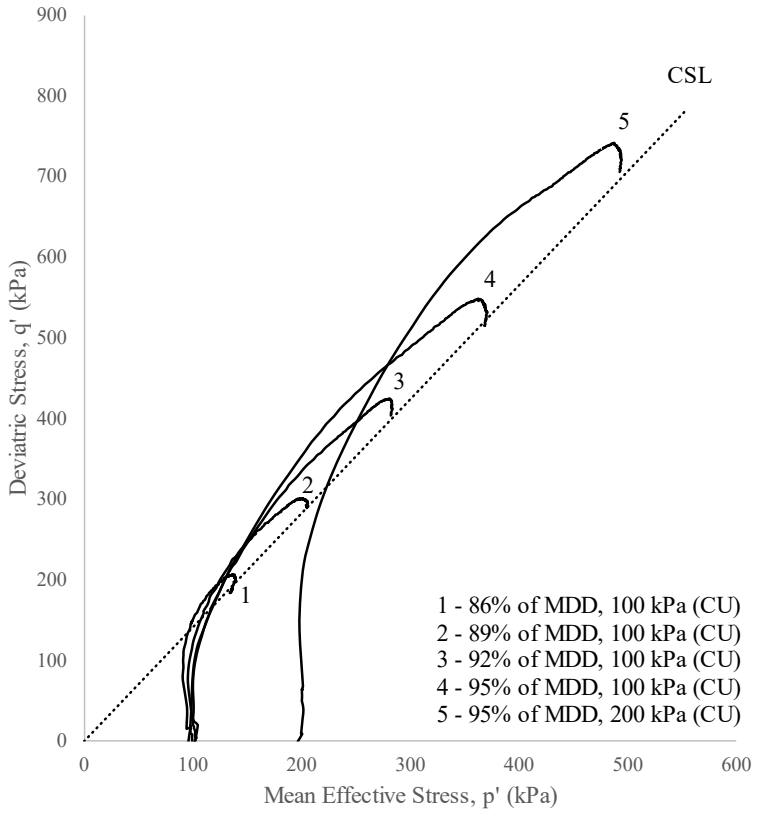

Figure 4.17 Stress paths for undrained triaxial tests on decomposed granite soil

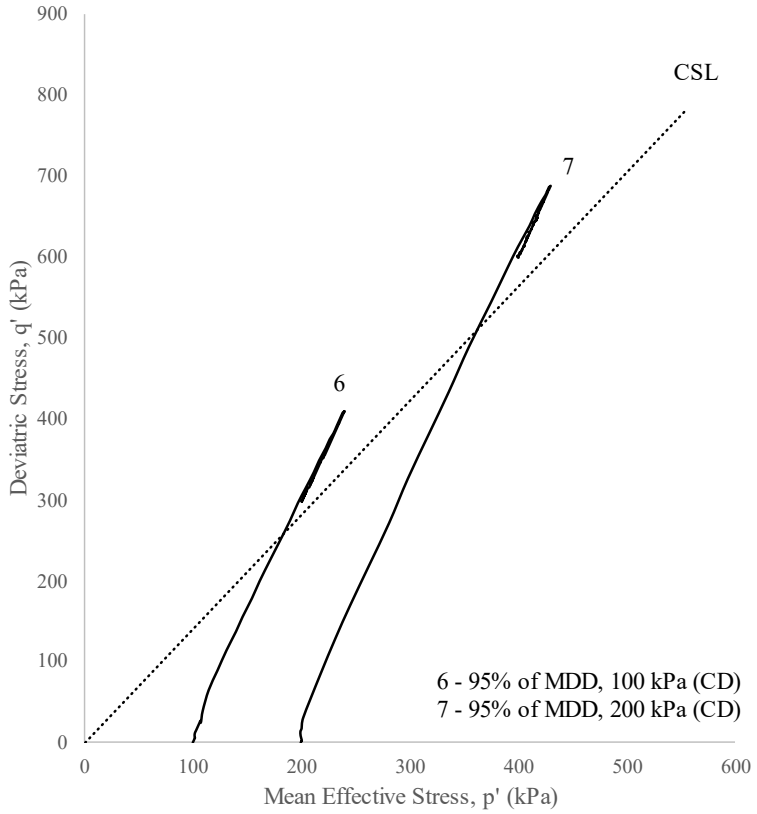

Figure 4.18 Stress paths for drained triaxial tests on decomposed granite soil

Figure 4.19 and Figure 4.20 shows the stress ratio and rate of dilation ($\delta\varepsilon_p/\delta\varepsilon_q$) of specimen 6 and 7, respectively. The horizontal axis indicates the rate of dilation where a negative sign indicates volume dilation, and a positive sign, volume contraction. From the figures below it is evident that both specimens are initially compressive and that they start to dilate as they are approaching the ultimate stress ratio of 1.41. This value was also previously identified as the soil's friction parameter, M. The maximum stress ratio appears to coincide with the maximum rate of dilation, which was 1.71 for test 6 and 1.60 for test 7. The stress-dilatancy paths approach the ultimate state again towards the end of the tests. A relationship between the stress ratio and rate of dilation could unfortunately not be derived from the figures below. More data on the volume change is required, hence, more drained tests with varying parameters are necessary.

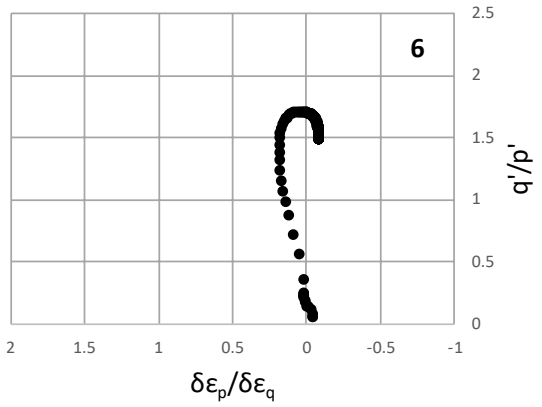

Figure 4.19 Stress-dilatancy relationship of specimen 6

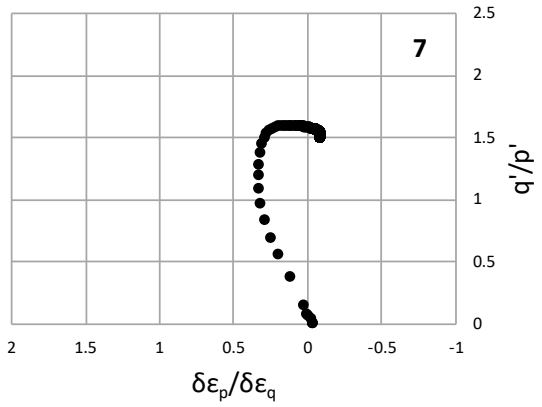

Figure 4.20 Stress-dilatancy relationship of specimen 7

4.3.3 Shearing behaviour of dry and partially saturated samples

In this section, the results of samples tested in a dry or partially saturated state are presented. The results gathered for this series of tests will be compared to those of the saturated samples previously discussed. The initial densities of specimens 8 – 13 and 16 – 20 were 86% of Modified AASHTO MDD, however, specimens 16 – 20 will not be discussed in this section since these specimens were flooded. Specimens 14 and 15 were compacted to 95% of Modified AASHTO MDD and were allowed to air-dry until constant mass. These two specimens will also be considered in the following section and not discussed in this section. Specimens 8 – 13 had varying moisture conditions during compaction, and these moisture conditions were kept constant through the entire triaxial compression test. Thus, these specimens were not saturated before isotropic compression. In total, seven specimens fall under the dry and partially saturated series (8 – 14) of which six will be discussed in this section. Specimen 13 which was

100% saturated during preparation is also included in this series since it was not saturated (flushed) before isotropic compression. Triaxial preparation of these specimens can be viewed in Appendix A, Table A. 1.

All triaxial tests in this series were conducted in a drained condition. The back pressure was kept at zero while increasing the cell pressure to 100 kPa, and the drainage tube was open to the atmosphere. Volume changes were not measured for these samples since they were not fully saturated before isotropic compression, resulting in compressible air trapped inside of the specimens. However, displacement and loading were measured. The following discussions assume that the effective stresses of the dry and partially saturated samples are equal to the total stresses.

Figure 4.21 shows the stress-strain curves for partially saturated sample 11 compared to those of saturated samples (1, 4, and 6) previously discussed. The samples were all tested at a confining pressure of 100 kPa and a summary of the triaxial testing programme is shown in Table 4.8. From the figure, it is evident that even though certain properties are similar, there is no distinctive correlation between these curves due to the varying initial conditions such as the initial dry densities and the moisture conditions throughout the triaxial compression test. Thus, the stress ratio versus axial strain plot is considered, rather than the deviatoric stress plot. Figure 4.22 shows that sample 11, with a specific volume of 1.466, corresponds well with sample 1 with a specific volume of 1.466. The initial stiffness of specimen 11 appears to be about the same as the saturated ones and has a slightly greater peak than specimen 1. It seems that the test prepared at 60% degree of saturation (sample 11) exhibits similar behaviour to the saturated tests at comparable density (sample 1). The somewhat higher stress path of specimen 11, compared to specimen 1, is assumed to be caused by the densification of specimen 11 during isotropic compression since the specimen is not fully saturated during this stage. As shown for the saturated tests, a denser specimen follows a higher stress path.

Table 4.8 Triaxial compression test properties of partially saturated specimens and comparable saturated specimens

Specimen No.	% Of MDD	Dry density (kg/m^3)	Saturation (%)	Void ratio	v	Drainage type	Confining pressure (kPa)
1	86	1808	48.1	0.466	1.466	CU	100
4	95	1997	68.5	0.327	1.327	CU	100
6	95	1997	68.5	0.327	1.327	CD	100
11	86	1808	60	0.466	1.466	CD	100

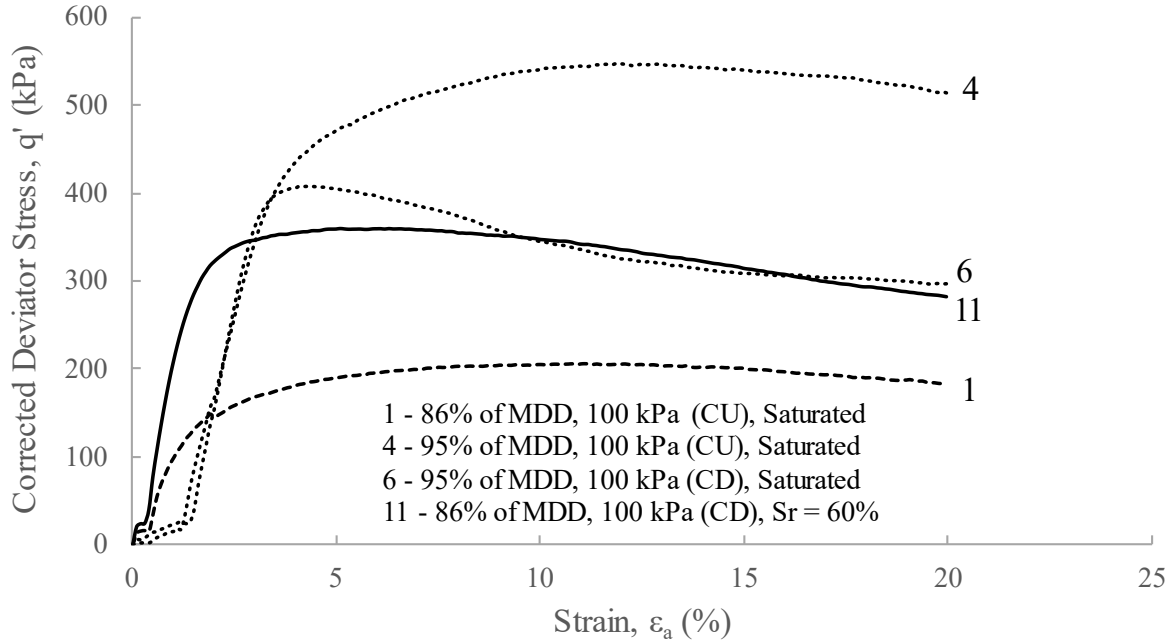

Figure 4.21 Behaviour of partially saturated compared to saturated decomposed granite soil in q': ε_a space

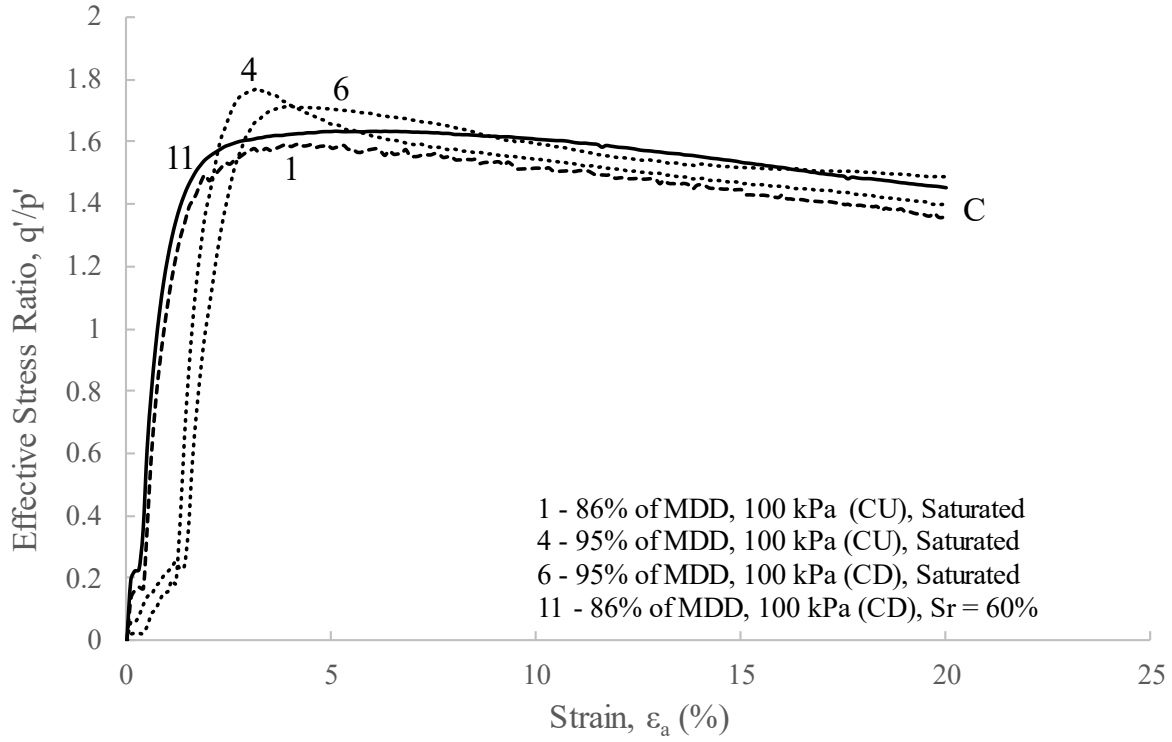

Figure 4.22 Behaviour of partially saturated soil compared to saturated decomposed granite soil in q'/p': ε_a space

Figure 4.23 and Figure 4.24 show the stress-strain plots for dry (sample 8) and partially saturated samples (10 and 13) with varying saturations, and Figure 4.25 shows dry specimen 8 compared to saturated specimens from the previous section (1 – 4, 6 and 7). Specimen 10 was prepared at 40% degree of saturation, and specimen 13, 100% degree of saturation. Even though specimen 13 was prepared at 100% degree of saturation, it still falls under the partially saturated series since it was not saturated (flushed) before isotropic compression. From the figures it can be seen that the dry sample 8, with 0% saturation, shows much greater peak strength than both the partially saturated specimens and the saturated specimens previously discussed, indicating that the dry sample has a greater tendency to dilate. The initial stiffnesses of these specimens correlate well with that of the saturated samples (Section 4.3.2) except for sample 13 having a much lower initial stiffness. This may be due to sample preparation which had to be done promptly for the 100% saturated test (sample 13) and also the extensive amount of water present in the specimen. The specimen had trouble holding its own weight after compaction and was extremely mouldable, even when placed in the membrane. Normally, specimens are hand-compacted to create a dense soil structure before it undergoes isotropic compression however, specimen 13 barely had a soil structure due to the excess water in the soil mixture. It can be seen that specimen 13 barely peaks before reaching the ultimate state (Figure 4.24). Similar behaviour of partially saturated samples with respect to specimens from

the saturated series (discussed in the previous section) (Figure 4.25) indicates that the pore water suctions may be very small relative to the total stresses for these specimens. If this were not true, the partially saturated specimens would have had higher strengths than the saturated specimens.

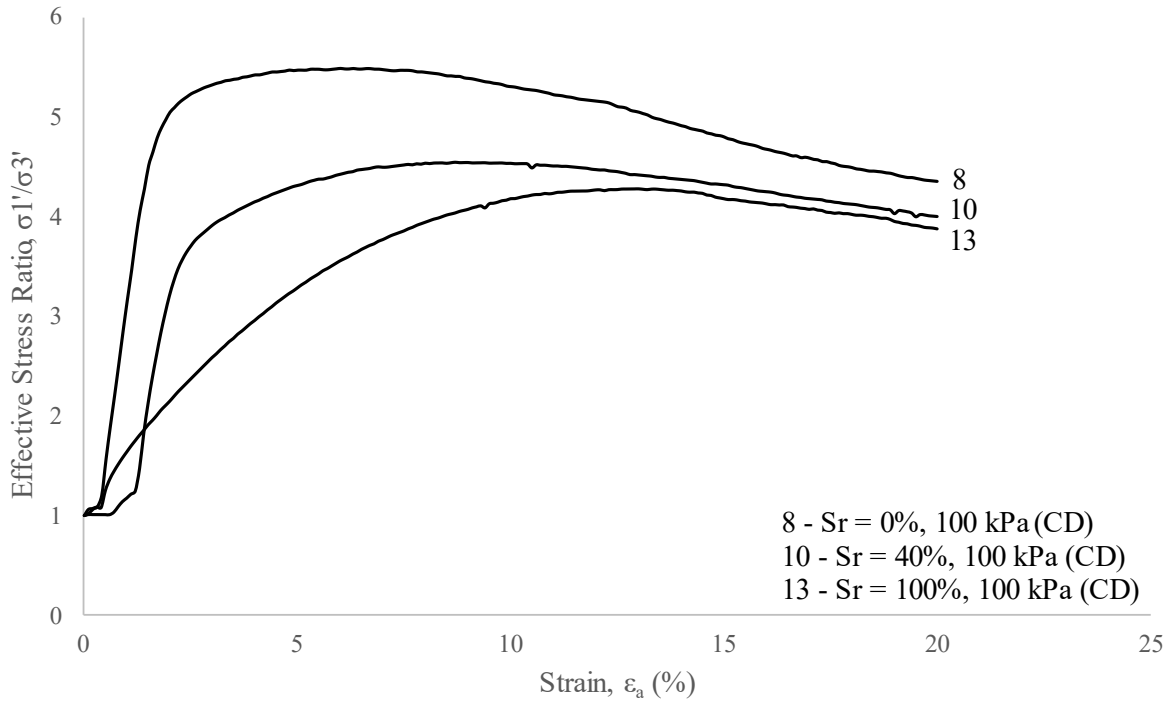

Figure 4.23 Behaviour of dry and partially saturated decomposed granite soil in q': ε_a space

In Figure 4.24 the ultimate state of the dry and partially saturated samples approaches the same stress ratio as that of the saturated samples (discussed in the previous section). Dry sample 8 does not quite reach the ultimate state at the end of the test however, it is assumed that it is approaching the ultimate state. Unfortunately, the tests were terminated prematurely since the axial strain was limited to 20% for the triaxial compression tests. The stress ratio peak of the dry sample exceeds the maximum stress ratios of the saturated drained and undrained tests, whereas the partially saturated specimens (with S_r between 40% and 80%) were comparable to the saturated samples.

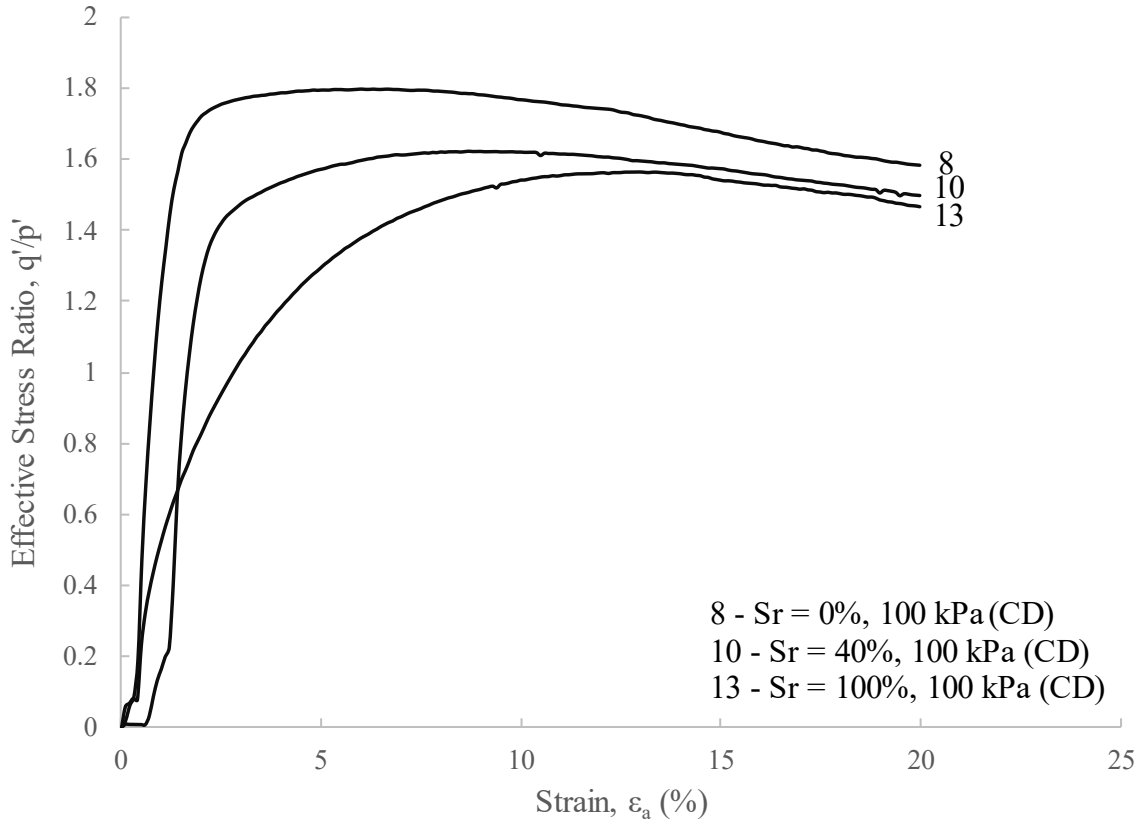

Figure 4.24 Behaviour of dry and partially saturated decomposed granite soil in q'/p': ε_a space

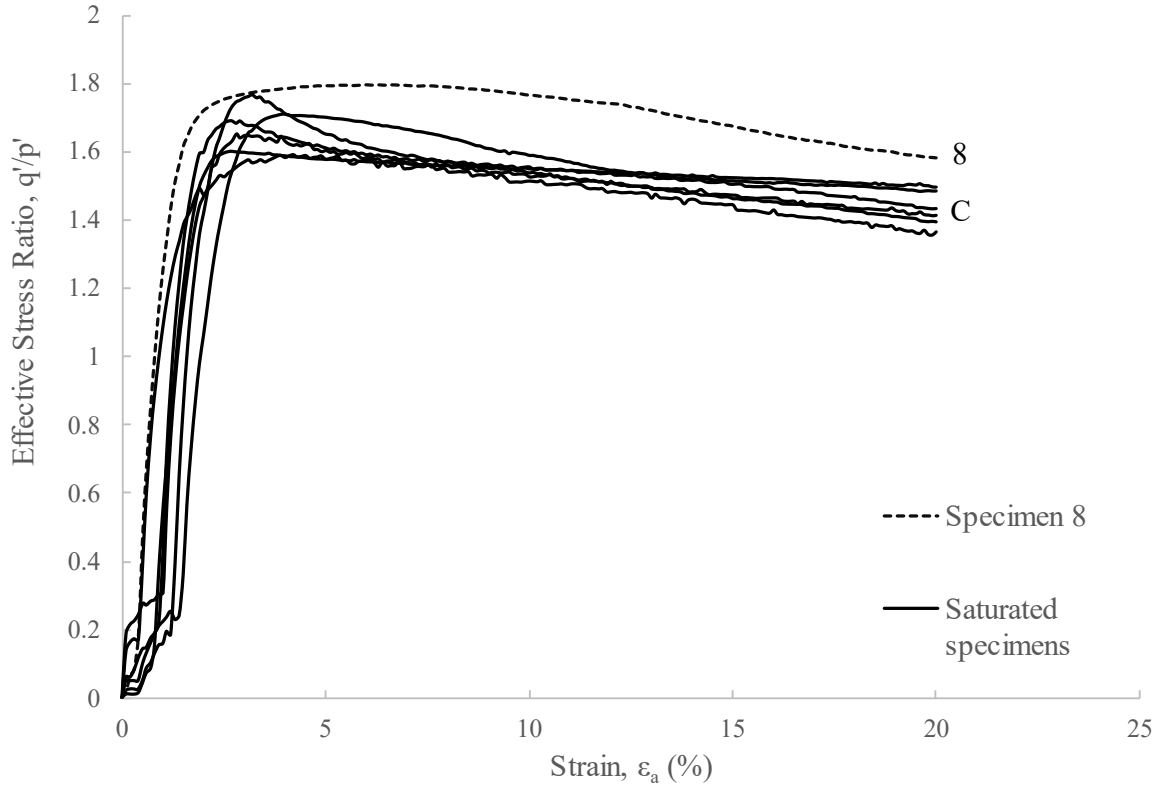

Figure 4.25 Behaviour of dry decomposed granite soil compared to saturated decomposed granite soil in q'/p': ε_a

Table 4.9 lists the critical/end states of the dry and partially saturated samples and here it can also be seen that dry sample 8, 20% saturated sample 9, and 80% saturated sample 12 does not entirely reach critical state at 20% axial strain. In Figure 4.26 the critical/end state values are plotted in q': p' space along with the critical state line obtained from the saturated samples (Figure 4.4). The values appear to lie on the critical state line, except for samples 8, 9, and 12 which have not yet reached critical state, indicating that the critical state friction parameter, M, does not depend on the sample moisture conditions during compaction and shearing. Thus far the critical state friction parameter, M, has proven to be independent of the initial density, confining pressure, and the saturation of the material, emphasising the importance of the ultimate strength as a material property. It is presumed that the difference in strength of dry (0% saturation) and partially saturated (>20% saturation) or saturated samples are due to the influence of water weakening the soil grains since it is not caused by the change of friction parameter, M.

Table 4.9 Critical/end state of dry and partially saturated samples
***End state**

Test No	Critical state/End state			Test Properties			
	q' (kPa)	p' (kPa)	q'/p'	Dry Density (kg/m^3)	Confining pressure (kPa)	Type	S_r (%)
8*	336	212	1.58	1808	100	CD	0
9*	349	216	1.62	1808	100	CD	20
10	300	200	1.50	1808	100	CD	40
11	283	194	1.46	1808	100	CD	60
12	324	208	1.56	1808	100	CD	80
13	288	196	1.47	1808	100	CD	100

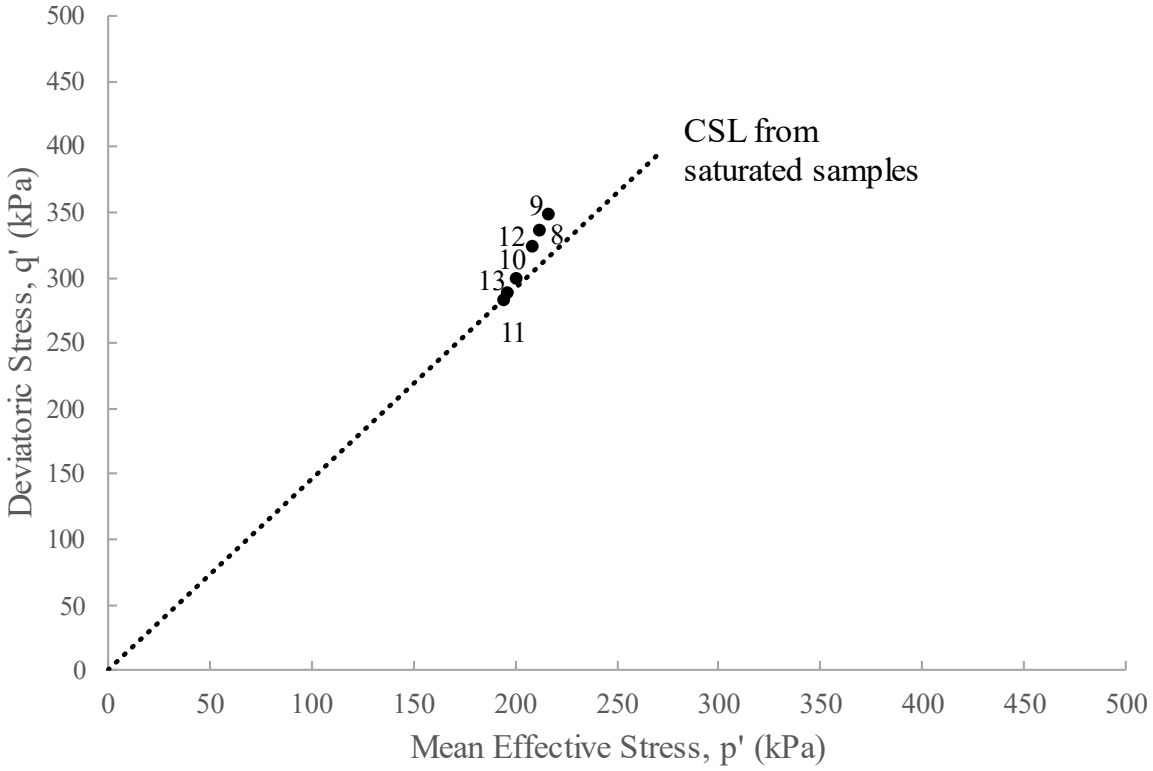

Figure 4.26 Critical state in q': p' space of partially saturated decomposed granite soil specimens

4.3.4 Flooded tests

Both dry and partially saturated samples were flooded after isotropic compression to evaluate the effects of flooding on the behaviour of the decomposed granite soil. Samples were flooded for 24 hours and sheared thereafter. The sample preparation was the same as for the non-flooded samples discussed in Section 4.3.3 (same initial degree of saturation, confining pressure, and drainage condition) and can be viewed in Appendix A, Table A. 1 (specimen 15 – 20). A total of 6 tests were flooded, and samples 16 – 20 were compacted to 86% of Modified AASHTO MDD, consolidated drained tests, and confined to a pressure of 100 kPa. Sample 15 (compacted to 95% of Modified AASHTO MDD) was air-dried for a week, similar to sample 14, and flooded before shearing.

Figure 4.27 shows the behaviour of three specimens with about the same initial specific volume (1.466). Specimen 1 is a saturated sample from Section 4.3.2, whereas specimens 11 and 19 are partially saturated at S_r = 60%, however, specimen 19 was flooded before shearing. By comparing specimens 1 and 19 to one another, it can be seen that the peak strength and stiffness of specimen 1 is greater than that of specimen 19. This indicates that the moisture increase (flooding) after the specimen has been confined, influences the behaviour of the soil since specimen 1 was saturated before isotropic compression.

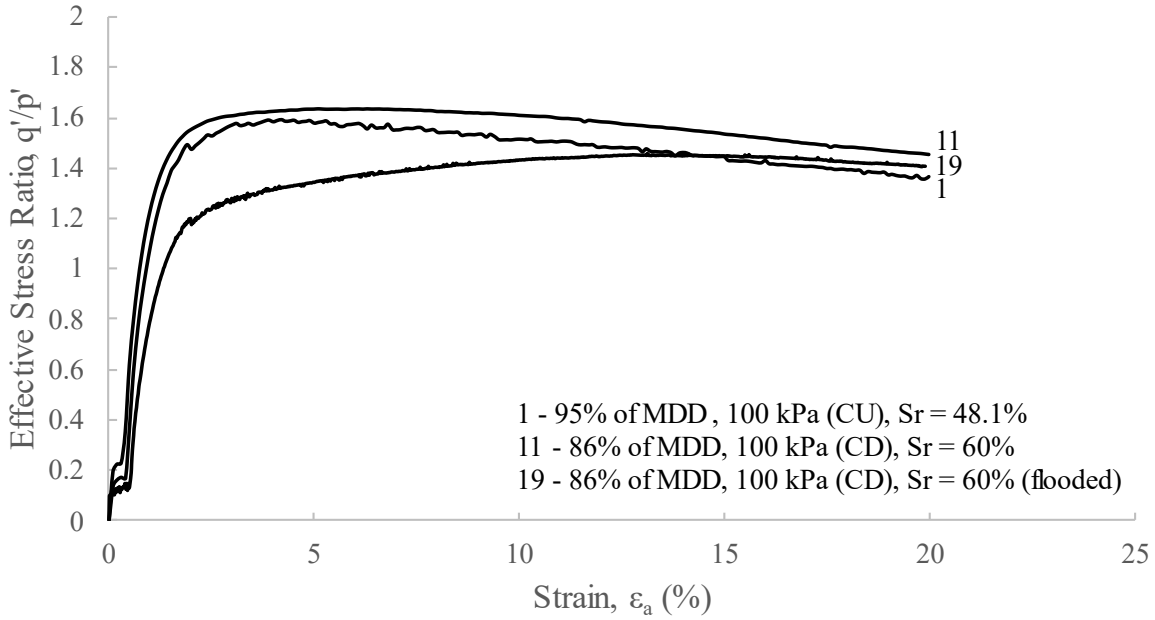

Figure 4.27 Behaviour of flooded partially saturated decomposed granite soil in q'/p': ε_a space

The effects of flooding can be analysed by comparing specimens 11 and 19. As expected, the strength and stiffness of specimen 19 were lower than that of specimen 11. This is also a common characteristic of collapsible soils when they are saturated. However, it should be noted that the specimens were mechanically compacted and that the structure of a collapsible soil is typically not formed in this manner. The possible collapsing nature shown for specimen 19 is caused by further densification of the material while aggregations are being broken down by the presence of water, and not by the loss of suction or bonding between particles. This aspect will be further investigated in Section 4.4. Intra-particle bonding might cause non-flooded specimens to show higher strengths, and when flooded, cause the particles to become weaker and likely experience crushing. Refer to Appendix C for similar results for dry specimen 8 and flooded specimen 16. In general, dry samples are more prone to collapse when flooded. The specific volume and confining stress influence the magnitude of collapse. An increase in specific volume signifies a looser sample, which is more prone to collapse. Similarly, a specimen with a higher confining pressure will have a greater amount of collapse, and as previously discussed; a higher confined specimen behaves like a loose soil. The three curves in the figure above suggest that the presence of water after isotropic compression decreases the strength and stiffness of the soil.

Specimens 14 and 15 were compacted to an initial density of 95% of Modified AASHTO MDD and allowed to air dry for a week, also achieving constant mass. Only specimen 15 was flooded.

Figure 4.28 and Figure 4.29 shows the results for these samples where specimen 14 (not flooded) illustrates very high strength and stiffness in comparison to the flooded specimen. The brittle failure demonstrated by specimen 14 indicates that the soil might be very stable and exceptionally strong in the dryer seasons. It appears that the high strength and stiffness primarily originates from the bonding and suction between the particles during the evaporation of water. Flooding of the air-dried sample supports this statement as seen in the figures below. The extensive difference between peaks illustrates the effects of water on the behaviour of soil after being air-dried. In both Figure 4.28 and Figure 4.29 specimens, 14 and 15 do not reach critical state at 20% axial strain, however, it is assumed that they would have reached critical state upon further shearing, beyond the limited strain boundary. Table 4.10 lists the end and peak state conditions for the air-dried samples, and here it is evident that these specimens do not reach critical state at 20% axial strain. The results shown for the saturated samples indicate that critical state is reached when q'/p' approaches 1.41, whereas tests 14 and 15 reach 1.9 and 1.7, respectively.

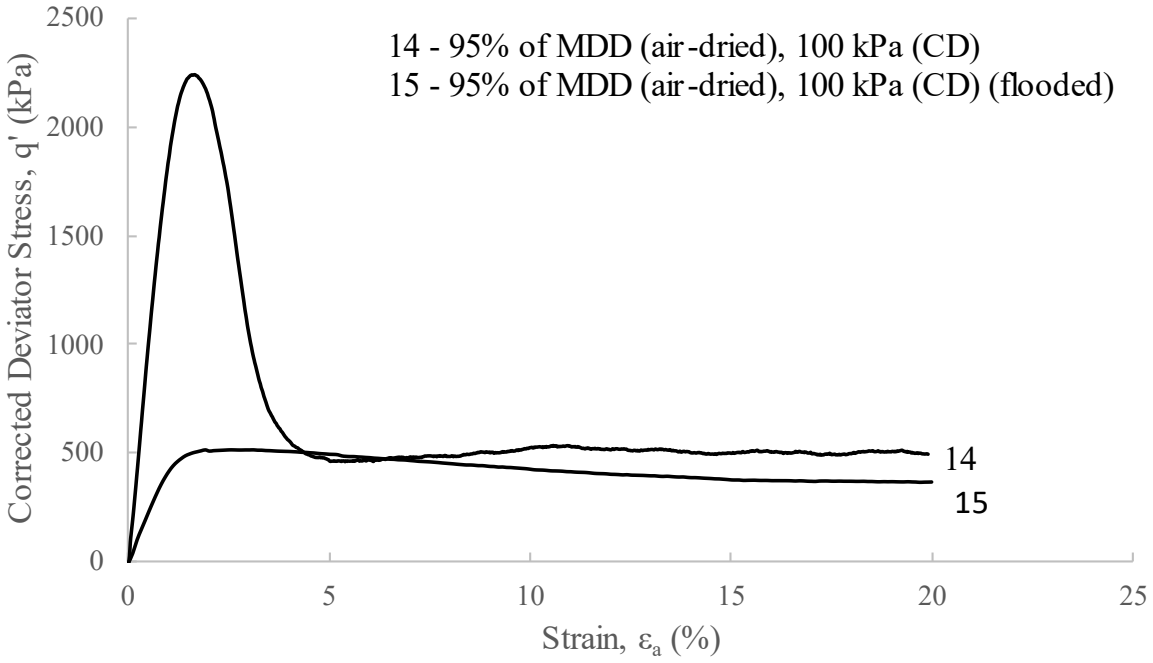

Figure 4.28 Behaviour of air-dried decomposed granite soil samples in q': ε_a space

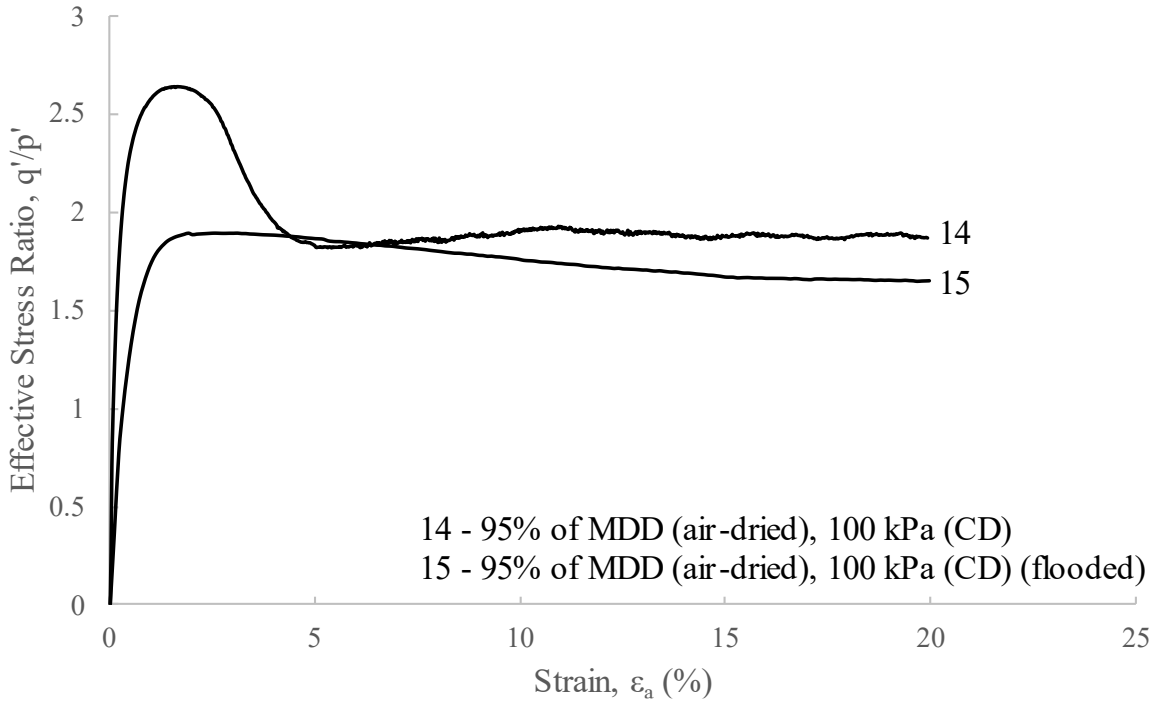

Figure 4.29 Behaviour of air-dried decomposed granite soil samples in q'/p': ε_a space

Table 4.10 Critical state of air-dried decomposed granite soil samples
*** End state**

Test No	Critical/*End state			Peak state			Test Properties		
	q' (kPa)	p' (kPa)	q'/p'	q' (kPa)	p' (kPa)	q'/p'	Dry Density (kg/m^3)	Confining pressure (kPa)	Remarks
14*	497	267	1.9	2242	848	2.6	1997	100	Air-dried Not flooded
15*	369	223	1.7	517	272	1.9	1997	100	Air-dried Flooded

4.4 PARTICLE BREAKAGE

Particle crushing occurs throughout the preparation, isotropic compression, and shearing of a specimen. For decomposed granite soil, particle crushing not only occurs as breakage of individual particles but also as a result of segregation of aggregated particles. This section considers the crushing of particles, evaluated after shearing has taken place. CT scanning was thus employed to study the fabric of the prepared specimens before and after triaxial testing. No attempt was made to measure particle crushing after mechanical compaction or after isotropic compression. The particle size distributions of all specimens were known, and post

triaxial test, the specimens were mechanically sieved to determine the new particle size distribution curves. Section 4.4.1 discusses the particle breakage after shearing of saturated specimens, whereas Section 4.4.2 considers the particle breakage of dry, partially saturated, and flooded specimens.

4.4.1 Analysis of saturated samples

After the first grading analysis of a sheared specimen, it was observed that the difference in grading curves (before and after shearing) were significantly large. This was caused by not initially washing the particles to allow fines to be separated from the coarser particles. Thus, the simulated predetermined grading curve (presented in Section 3.5.2, Figure 3.10) was altered, and a mock specimen was prepared to determine the actual grading curve before compaction of a specimen. Figure 4.30 illustrates the actual grading curve compared to the simulated predetermined grading curve (with fines coating the coarse particles and aggregations). It can be seen that the amount of fines is considerably more than before, and the coarser particles, somewhat less. It is assumed that this was caused by aggregation of smaller particles creating a larger particle. From here on the actual grading curve will be used for calculations, comparison, and discussions.

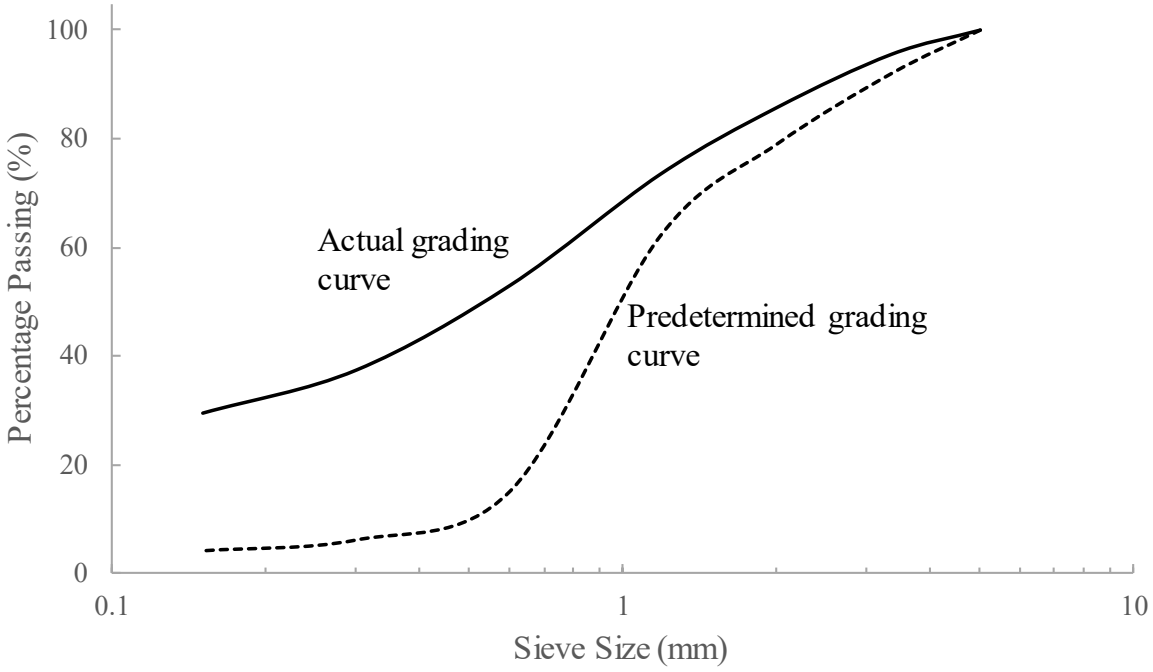

Figure 4.30 Actual grading curve before mechanical compaction compared to simulated predetermined grading curve from Figure 3.9

Parameters identified by Hardin (1985), as discussed in Section 2.8, will be used to analyse particle crushing. This includes the following parameters: breakage potential, total breakage, and relative breakage. These parameters were defined for particle sizes greater than 0.074 mm,

however, the smallest sieve aperture used in this research was 0.150 mm. Thus, for convenience, the parameters were adapted to 0.150 mm. The breakage potential, B_p, of the soil before triaxial testing was determined to be 0.766.

Figure 4.31 shows the grading changes after triaxial testing for specimens 1 – 5. It can be seen that for all specimens there is a difference in the grading curve before shearing versus after being sheared. Specimens 1 – 4 were tested at a confining pressure of 100 kPa whereas specimen 5 was confined to 200 kPa. From the grading curves, it is evident that specimens 1 – 4 had no noticeable grading difference from one another, and that a higher confined specimen (sample 5) had more particle breakage. Total breakage is defined as the area enclosed by the curve before and after testing for sizes greater than 0.150 mm, and in Table 4.11 the breakage parameters for specimens 1 – 7 are listed. The total breakage of each specimen was scaled down using the breakage potential to yield a normalised parameter, relative breakage, B_r. All the undrained specimens tested at 100 kPa (samples 1 – 4) showed similar relative breakage values between 0.139 - 0.146, whereas specimen 5, with a confining pressure of 200 kPa, had a higher value of 0.172. This was also observed for the drained specimens where test 6 (100 kPa) had $B_r = 0.085$ and test 7 (200 kPa) $B_r = 0.141$.

The relative breakage for saturated drained specimens (6 and 7) was considerably lower in comparison to saturated undrained specimens, with similar initial densities and confining pressures. Undrained tests 4 and 5 had a relative breakage of 0.150 and 0.172, whereas tests 6 and 7 had a relative breakage of 0.085 and 0.141, respectively. This variability was caused by the decrease in pore pressure for the undrained tests (see Figure 4.12). When the pore pressure decreases, the effective pressure increases, causing more particle breakage to occur in the undrained specimens.

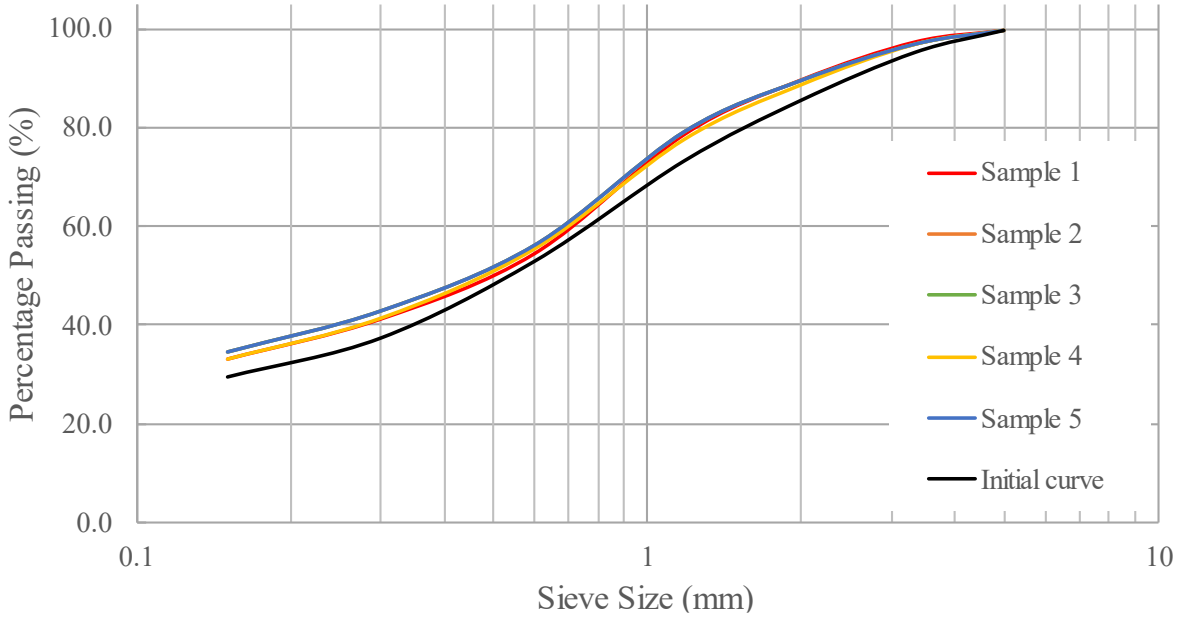

Figure 4.31 Grading changes of decomposed granite soil during triaxial compression test at varying densities and two confining stresses

Table 4.11 Particle crushing during triaxial compression test of saturated decomposed granite soil samples

Test No.	B_p	B_t	B_r	Test Properties		
				Dry Density (kg/m^3)	Confining pressure (kPa)	Type
1	0.766	0.106	0.139	1808	100	CU
2	0.766	0.109	0.143	1871	100	CU
3	0.766	0.112	0.146	1934	100	CU
4	0.766	0.115	0.150	1997	100	CU
5	0.766	0.132	0.172	1997	200	CU
6	0.766	0.065	0.085	1997	100	CD
7	0.766	0.108	0.141	1997	200	CD

From Figure 4.32 it can be seen that more grading changes occur under higher confining pressures. The curves shown have confining stresses of 100 kPa, 500 kPa, and 1000 kPa, and their breakage parameters are listed in Table 4.12. Here it can be seen that the grading curve of the specimen tested at 100 kPa is distinguishable from the specimen tested at 500 kPa and 1000 kPa, experiencing less particle breakage than both these tests. Both grading changes in Figure 4.31 and Figure 4.32 typically indicate a decrease in coarse particles and an increase in finer particles. Since all specimens reach/approach the ultimate state as previously discussed, it is

apparent that the friction parameter, M, is independent of particle breakage. It is logical to assume that the larger particles will experience the most particle breakage, whereas most finer particles will go through the test procedure unchanged.

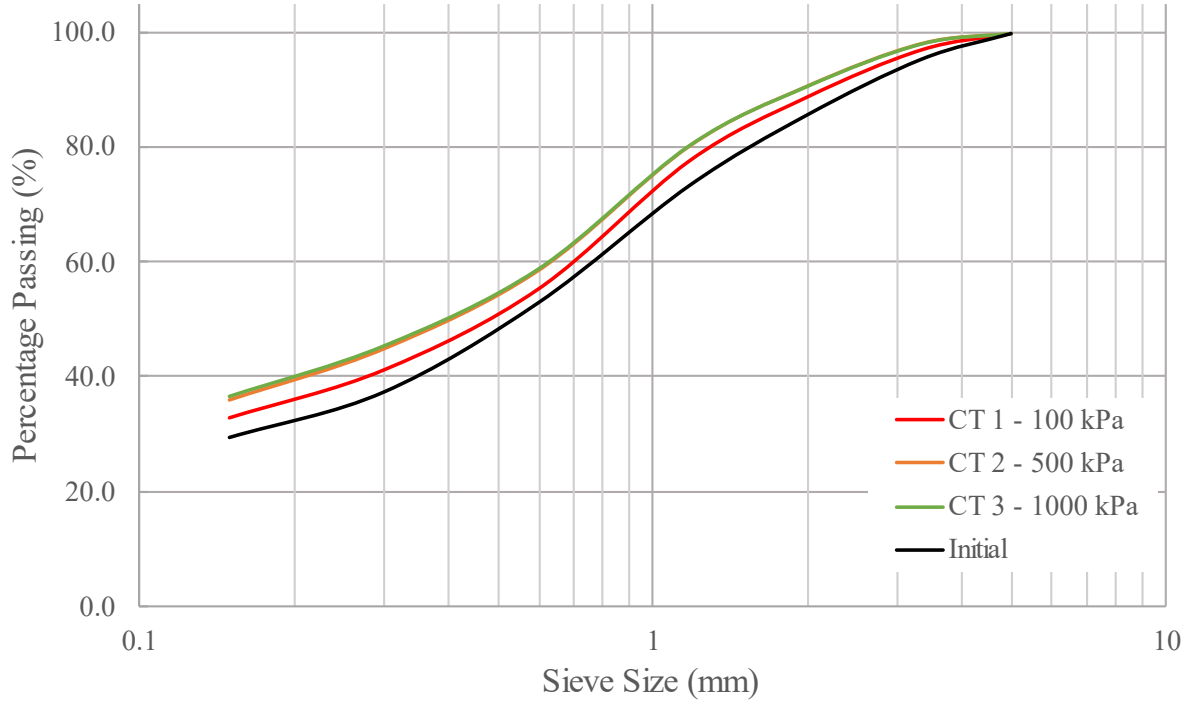

Figure 4.32 Grading changes during triaxial compression test at varying confining pressures

Table 4.12 Particle crushing during triaxial compression test of saturated samples CT 1 - 3

Test No.	B_p	B_t	B_r	Test Properties			
				Dry Density (kg/m^3)	Confining pressure (kPa)	Type	Remarks
CT 1	0.766	0.107	0.139	1997	100	CU	Specimens sent for CT-scanning
CT 2	0.766	0.189	0.246	1997	500	CU	
CT 3	0.766	0.188	0.246	1997	1000	CU	

Another rational assumption made is that the amount of particle crushing behaves proportionally to the pressure applied to the specimen. Figure 4.33 and Figure 4.34 shows the relationship between the maximum pressure p' and q' and the amount of particle breakage expressed as relative breakage. From the figure, it is evident that the relative breakage increases as the stresses increase. The increase trends from the grouped 100 kPa confined specimens, to test number 5 (200 kPa), to CT 2 (500 kPa). There is however no difference in relative breakage

for tests CT 2 and CT 3, confined at a pressure of 500 kPa and 1000 kPa, respectively. It is presumed that the maximum amount of breakage has occurred after confining a specimen to 500 kPa or higher. However, no additional tests at higher confining pressures were tested to confirm this. Figure 4.35 shows the relationship of relative breakage to the square root of q'max, with a potential trend line, indicating that particle crushing depends on the shear stress experienced.

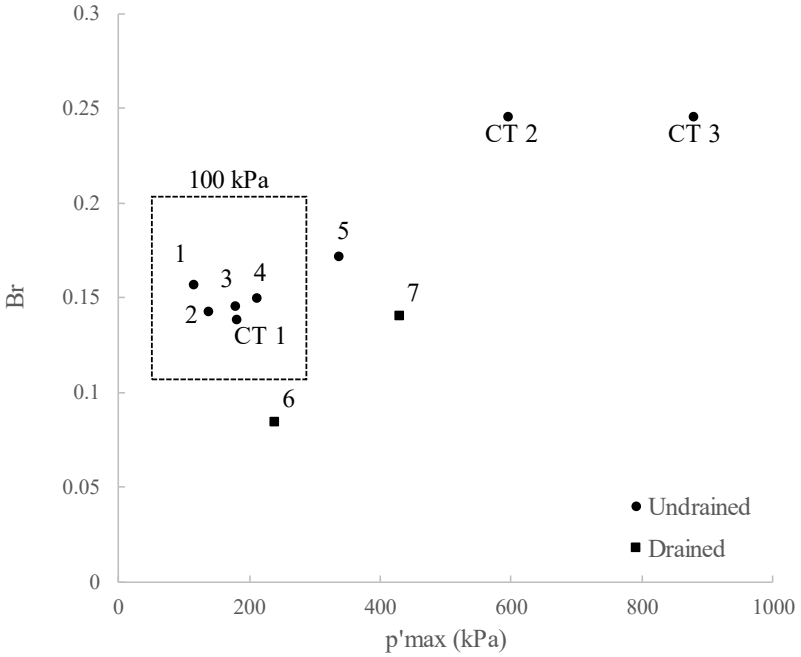

Figure 4.33 Relationship between decomposed granite soil saturated specimens' particle crushing and pressure: B_r: p'max

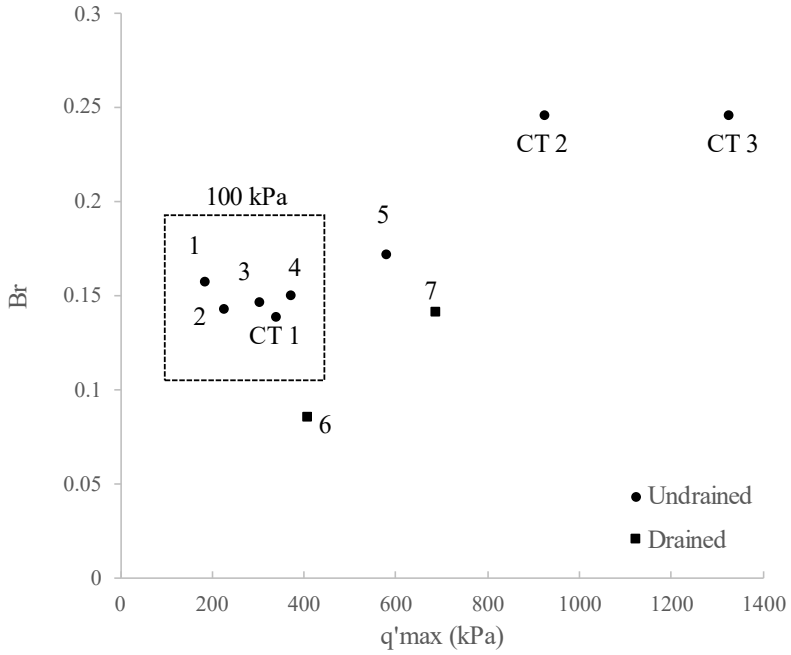

Figure 4.34 Relationship between decomposed granite soil saturated specimens' particle crushing and pressure: B_r: q'max

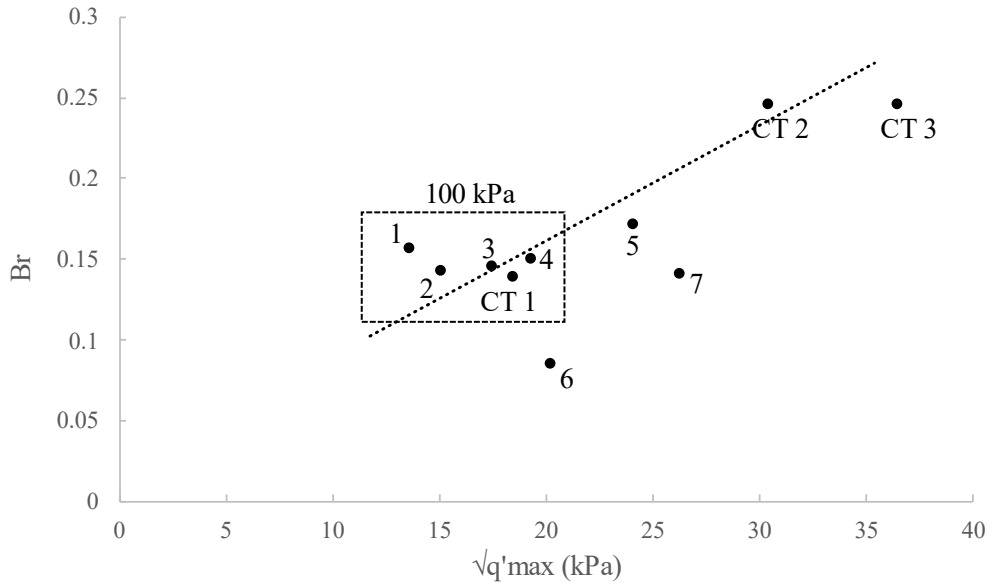

Figure 4.35 Relationship between decomposed granite soil saturated specimens' particle crushing and pressure B_r: √q'max

CT scans were performed on specimens CT 1, CT 2, and CT 3 to evaluate the particle crushing experienced by each sample. The scans of CT 1 will be discussed in this section whereas the results of CT 2 and CT 3 can be viewed in Appendix D. The scans of each specimen include the following: a comparison of the before-and-after-specimen side by side and an image showing the specimen scanned after triaxial testing overlying the original specimen (Figure 4.36), and three top slices per specimen indicating broken particles and their original particle sizes (Figure 4.37 - Figure 4.39). The scans revealed limited particle breakage for the mechanically compacted samples (pre-test specimens), with most of the breakage occurring in the larger particles (3.35mm – 5mm).

From the post triaxial test scans, it is evident that the specimens underwent quite an amount of particle breakage during shearing. The broken particles could easily be identified when scrolling through the height of the specimen, and it was observed that these particles were not as visible from the side views. Figure 4.37 - Figure 4.39 shows the broken particles of specimen CT 1 and the text in the figures indicate the original size range of the particle before it was broken, as well as the size ranges of the broken particles and the diameter of the broken particle in brackets. The size ranges are those mentioned in Section 3.5.2 for the preparation of the triaxial specimens (5 – 3.35, 3.35 – 2, 2- 1.18, 1.18 – 0.6, 0.6 – 0.3, and <0.15 mm). The scans showed that mainly coarser particles experience particle breakage during shearing.

Due to the deformation of the specimens after shearing, tracking individual particles was impossible. It is presumed that the broken particles from the CT scans were caused by shearing,

which is also confirmed by the grading curves post triaxial shearing (see Figure 4.31 and Figure 4.32).

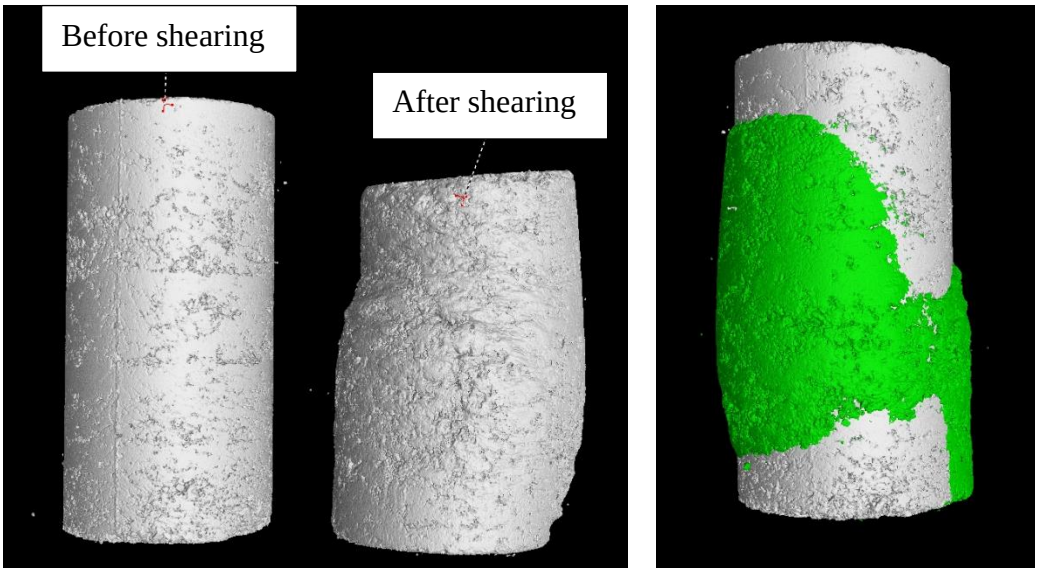

Figure 4.36 CT-scan front view of CT 1 before and after shearing, and overlaying one another

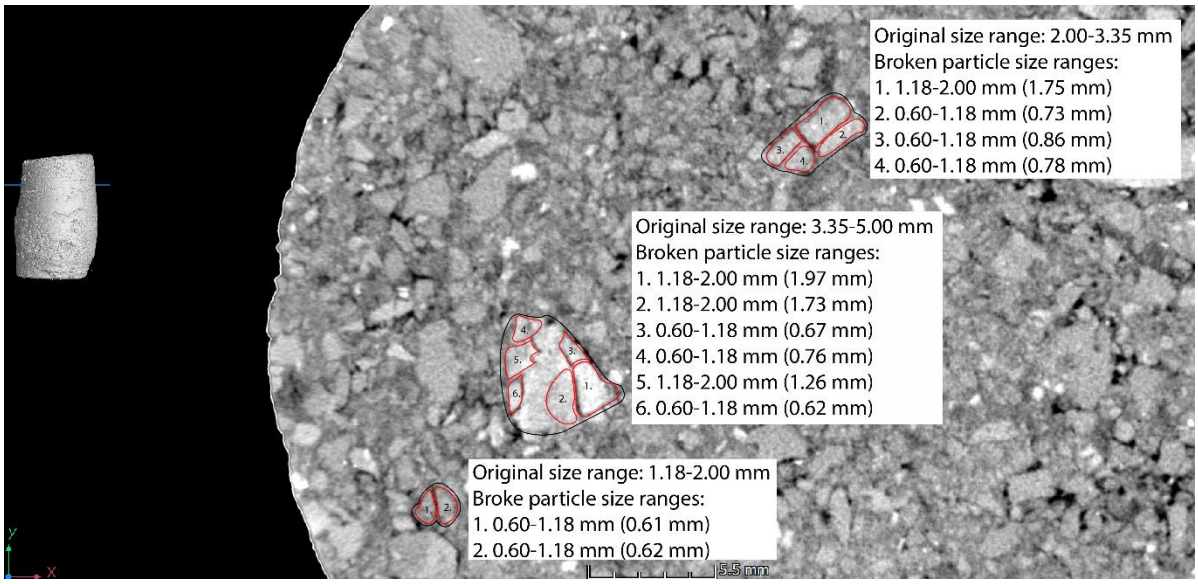

Figure 4.37 CT-scan top view of specimen CT 1 and its particle breakage – 1

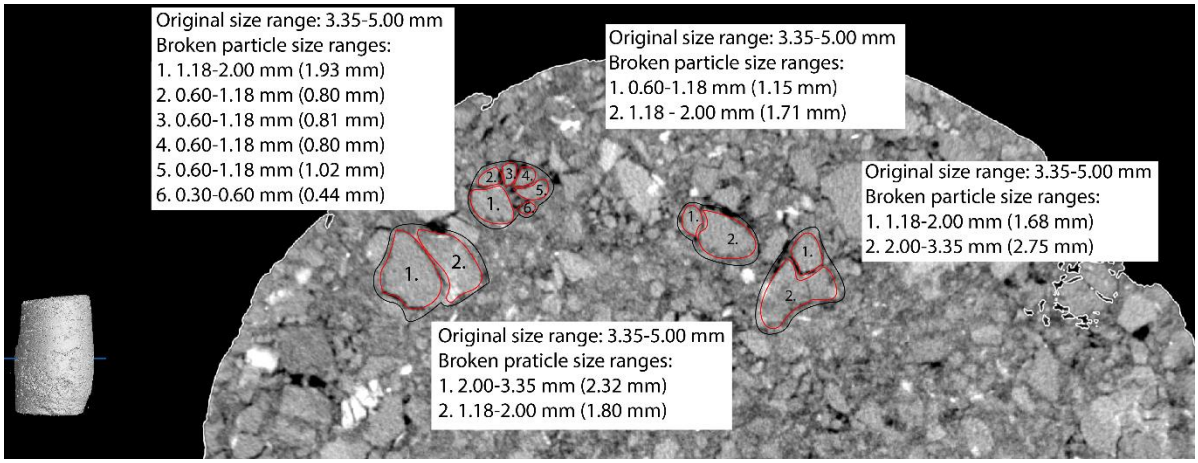

Figure 4.38 CT-scan top view of specimen CT 1 and its particle breakage – 2

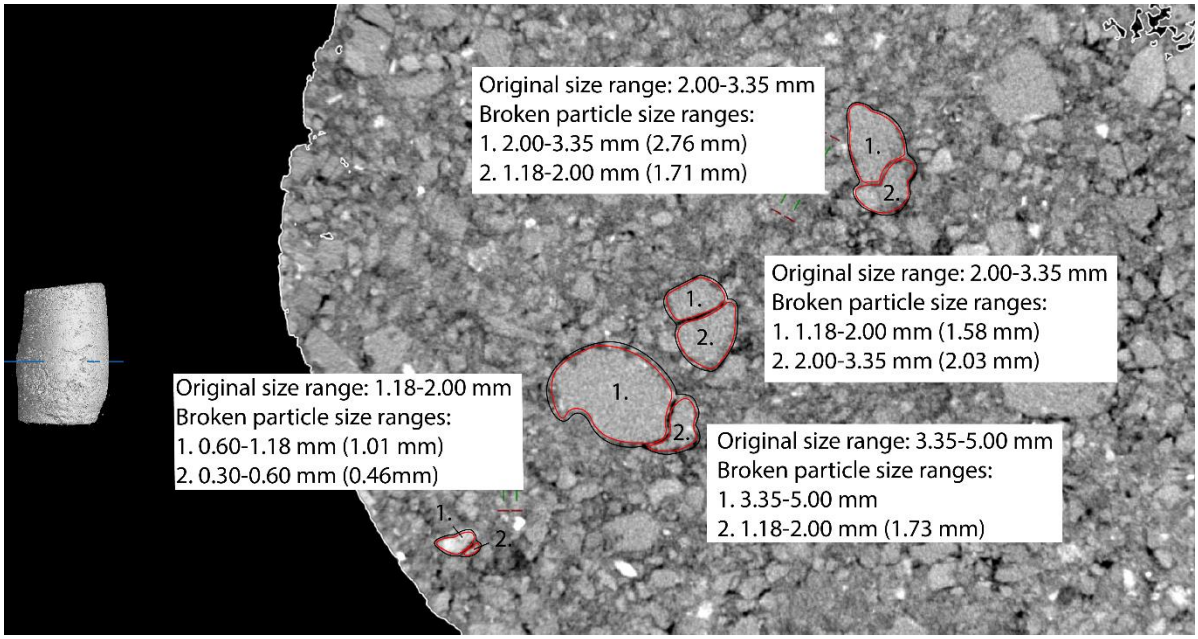

Figure 4.39 CT-scan top view of specimen CT 1 and its particle breakage – 3

4.4.2 Analysis of dry, partially saturated and flooded tests

The amount of particle crushing for the dry, partially saturated, and flooded tests have been summarised in Table 4.13. Figure 4.40 shows the correlation between relative breakage and maximum shear stress of both saturated and partially saturated (flooded and non-flooded) specimens. The results for the partially saturated (flooded and non-flooded) specimens are very scattered and no unique relationship can be seen. However, the variability in the amount of particle breakage seems to be derived from the different moisture contents, since all specimens were confined to a pressure of 100 kPa.

Table 4.13 Particle crushing during the triaxial test of dry and partially saturated samples of decomposed granite soil

Test No.	B_p	B_t	B_r	Test Properties				
				Dry Density (kg/m^3)	Confining pressure (kPa)	Type	S_r (%)	Remarks
8	0.766	0.048	0.063	1808	100	CD	0	Not flooded
9	0.766	-	-	1808	100	CD	20	Not flooded
10	0.766	0.055	0.072	1808	100	CD	40	Not flooded
11	0.766	0.088	0.115	1808	100	CD	60	Not flooded
12	0.766	0.083	0.108	1808	100	CD	80	Not flooded
13	0.766	0.087	0.115	1808	100	CD	100	Not flooded
14	0.766	0.149	0.195	1997	100	CD	68.5	Air-dried, Not flooded
15	0.766	0.118	0.155	1997	100	CD	68.5	Air-dried, flooded
16	0.766	-	-	1808	100	CD	0	Flooded
17	0.766	-	-	1808	100	CD	20	Flooded
18	0.766	0.164	0.215	1808	100	CD	40	Flooded
19	0.766	0.082	0.107	1808	100	CD	60	Flooded
20	0.766	0.107	0.140	1808	100	CD	80	Flooded

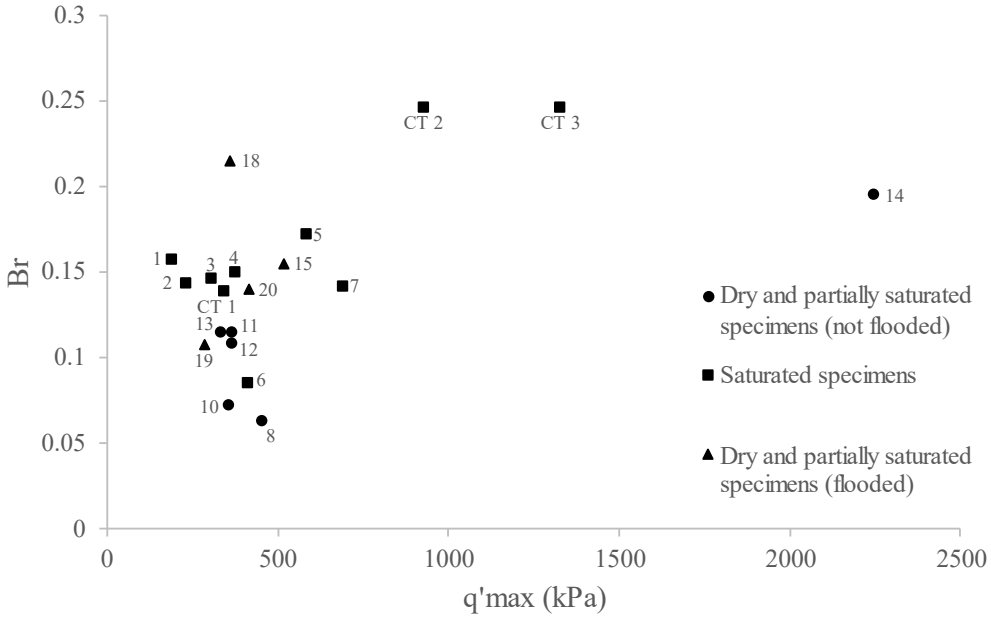

Figure 4.40 Particle crushing of dry and partially saturated samples compared to saturated samples of decomposed granite soil

In Figure 4.40 it can be seen that from the dry and partially saturated series, dry specimen 8 (S_r = 0%, unflooded) experienced the least particle breakage and specimen 18 (S_r = 40%, flooded) the most (tested at the same confining pressure of 100 kPa). Here the particle crushing increases with the presence of water where specimen 10 (S_r = 40%, unflooded) has a B_r = 0.072, specimen 13 (S_r = 100%) B_r = 0.115, and test 18 (S_r = 40%, flooded) has B_r = 0.215. Specimen CT 2 (500 kPa) and CT 3 (1000 kPa) experienced the most particle breakage with respect to the applied confining pressure. From Figure 4.40 it is evident that these two specimens have a higher relative breakage of 0.246. The results for the partially saturated specimens at 100 kPa are scattered between those of the saturated tests at 100 kPa. For partially saturated tests it is assumed that the intra-particle bonding of particles was broken down and that suction was lost, promoting the crushing of particles with the presence of water. Dry samples, on the other hand, had no suction, since the material was completely dry and flowed freely during preparation. When water breaks the suction or bonds in partially saturated specimens, the particles are weakened, and accordingly, more particles experience crushing. Figure 4.41 shows the different grading curves for dry specimen 8 (S_r = 0%, unflooded) and flooded specimen 18 (S_r = 40%), and here it can also be seen that the former experiences less particle breakage than the latter.

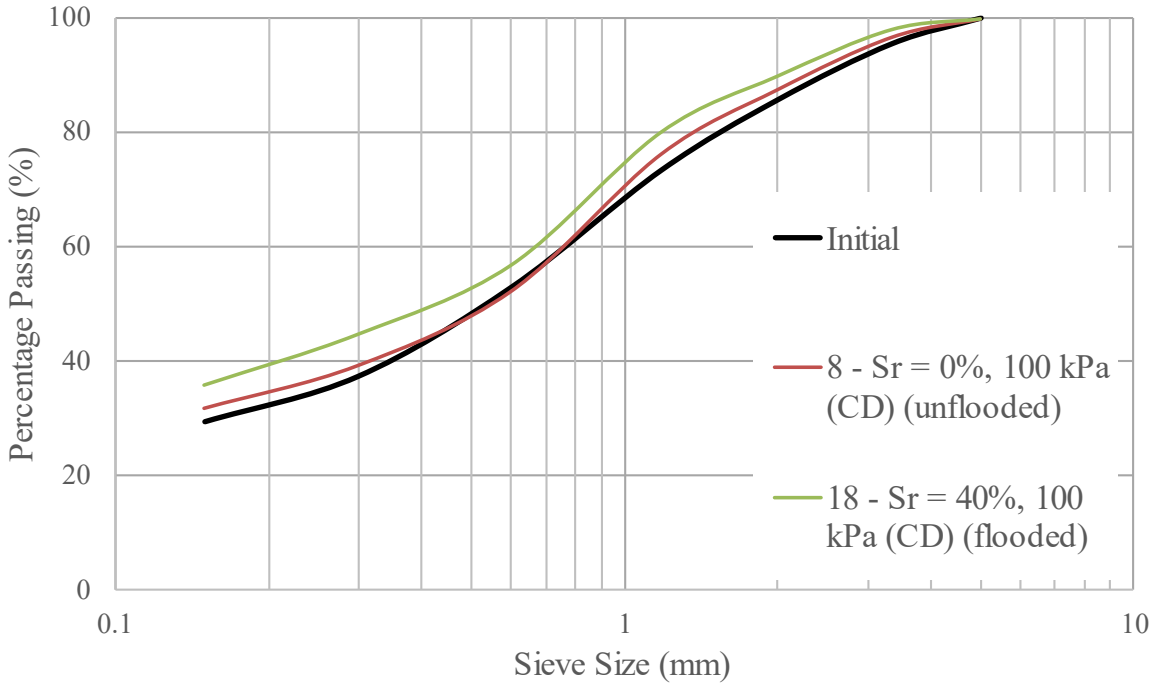

Figure 4.41 Grading changes during the triaxial test for partially saturated and dry specimens of decomposed granite soil

CHAPTER 5: CONCLUSION AND RECOMMENDATIONS

5.1 INTRODUCTION

As stated in the introduction and literature chapters, there are very few publications on the geotechnical properties of decomposed granite soils from the Cape Granite Suite. The geotechnical data is limited and the behaviour of decomposed granite soils in South Africa are still misinterpreted. Decomposed granite soil can cause significant problems when identified incorrectly, or when its behaviour is not fully understood. Residual granite is prone to the formation of a collapsible fabric and can cause the volume to decrease when saturated. Water has a substantial influence on the stability of decomposed granite soil and was an important factor in this research. This research aimed to study the influence of water and particle breakage on the intrinsic behaviour of decomposed granite soil and determine whether its critical state and the stress-strain response can be represented by the Modified Cam-Clay model.

5.2 CONCLUSIONS

5.2.1 Soil classification properties

Based on the results of this study, the following conclusions concerning the classification properties of the decomposed granite soil can be drawn.

- The mineralogy of the decomposed granite soil consisted of quartz (25%), mica (26%), kaolinite (20%), plagioclase (13%), K-feldspar (12%), and calcite (4%). During the visual examination of the in-situ material, quartz, felspar, and mica particles could easily be identified.
- The particle size distribution (PSD) ranged from gravel size to clay size with a fines (silt and clay) content of around 12%. The wide grading of the decomposed granite soil is reflected in the soil's gradation coefficients, showing a poorly graded material, which does not satisfy the criteria for well-graded soil (C_u>6 and 1<C_{ze}<3).
- The decomposed granite soil was classified as a 'poorly graded silty sand' with symbol SM (USCS (SAPEM, 2014)), type A-2-4 material with a subgrade rating of good-excellent ('silty or clayey gravel sand') (AASHTO (SAPEM, 2014)), and a G8 material (TRH14 (SAPEM, 2014)).
- The fines content allowed for a measurable plasticity index (PI) of 6.5% which is associated with a soil with slight plasticity. This is most likely due to the clay mineral type which is kaolinite and calcite for decomposed granite soil. Kaolinites are typically stable clays with very little isomorphous substitution, and calcite is easily dissolved in weak acidic solutions.

- A compacted dry density of 2120.5 kg/m^3 and optimum moisture content of 8.5% was achieved using Modified AASHTO compaction effort. The wide PSD may be associated with the high density of this material.

5.2.2 Triaxial compression tests

Based on the results of this study, the following conclusions concerning the triaxial compression test on decomposed granite soil can be drawn.

- The critical state of decomposed granite soil was determined, and the Modified Cam-Clay model was used to create a predictive model for this material. The important soil parameters required for this model were obtained from various triaxial compression tests and the parameters are as follows: the slope of unload reload line (κ), shear modulus (G), friction parameter (M), the slope of the normal compression line (λ) and the normal compression line at p' = 1 kPa (N).
- The behaviour of the reconstituted saturated decomposed granite soil can be described within the general framework (i.e., yield surface and the presence of both plastic and elastic deformations) of critical state soil mechanics.
- Eight saturated consolidated undrained tests, two consolidated drained tests, and an isotropic compression and swelling test were performed to determine the critical state soil parameters. The results concluded κ = 0.012, G = 70 MPa, M = 1.14, λ = 0.079, and N = 1.77.
- A predictive Modified Cam-Clay model was created with these soil parameters, and numerous simulations showed that the decomposed granite soil can be predicted with this model. The simulations were only tested in the consolidated drained state and can predict the results of normally consolidated, lightly overconsolidated, and heavily overconsolidated decomposed granite soils. This model provides a qualitative match between predicted and experimental results.
- Denser saturated specimens had greater strengths than the looser saturated specimens, and they also showed lower changes in pore water pressure whereas the looser specimens showed higher changes in pore water pressure. Irrespective of the initial dry density, all specimens reached critical state after 20% axial strain. This showed that the critical state did not depend on the initial dry density of the decomposed granite soil.
- Specimens confined to a higher confining pressure had an increase in pore water pressure and higher peak stresses than specimens confined to lower confining pressure. The latter

specimens also had lower pore water pressures which decreased to negative values. Similarly, the confining pressure does not influence the critical state of the soil and ultimately all specimens reached/approached the critical state.

- One dry and five partially saturated specimens (not saturated during triaxial compression) underwent triaxial compression. The partially saturated specimens (40% - 80% degree of saturation) showed similar behaviour to the saturated specimens, indicating that the pore water suctions were small relative to the total stresses. The dry specimen had a very high peak strength, and the 100% saturated specimen (not saturated during the triaxial test) had a lower stiffness than all the saturated specimens. These tests emphasised that the strengths of the partially saturated specimens are weakened by the presence of water.
- Partially saturated specimens reached/approached critical state after 20% axial strain, indicating that the friction parameter M does not depend on the initial moisture condition of decomposed granite soil.
- Partially saturated specimens were saturated after isotropic compression to resemble the impact of flooding. Flooded specimens had a lower strength and stiffness than both saturated (saturated before isotropic compression) and partially saturated (non-flooded) specimens. It is presumed that partially saturated (non-flooded) specimens have higher strengths than flooded specimens due to intra-particle bonding and once flooded, particles become weaker and likely experience particle crushing.
- Seasonal wetting and drying of decomposed granite soil influence the strength of the soil. Air-dried specimens represented the soil in dryer seasons, whereas flooding an air-dried specimen represented wetting of the soil after a dry season. Allowing moisture to evaporate from a compacted specimen caused interparticle bonds and suction to form, strengthening the soil structure. However, flooding significantly decreased its high strengths causing the soil structure to collapse. The flooded specimen showed lower peak strength and stiffness than the unflooded specimens.
- It has been found that the interparticle bonds between air-dried samples give the soil a cohesive component of strength and this is instantly lost when water breaks down these bonds. This may lead to loss of stability of the soil structure and contribute to the increased settlement of decomposed granite soil in rainy seasons.

5.2.3 Construction implication

Based on the results of this study, the following conclusions concerning construction implications with decomposed granite soil can be made.

- An air-dried decomposed granite sample compacted to 95% of MDD and not saturated before/after isotropic compression resulted in the soil having seemingly high strengths. At the specimen's peak state, the deviator stress, q' = 2242 kPa, and the stress ratio, q'/p' = 2.6. The assumption was made that during the drying time, the moisture evaporated from the pores and caused suction between the particle, creating strong interparticle bonds. These circumstances may also cause implications during construction with decomposed granite soil as these high strengths are reached in the dryer seasons, however, lost during the wetter seasons.
- Another air-dried sample compacted to 95% off MDD and saturated after isotropic compression resembled the influence of flooding on such a soil. The strengths were significantly lower than those achieved for a dry sample, indicating that the soil may experience collapse during the wetter seasons. The flooded specimen had a deviator stress of 517 kPa and a stress ratio of 1.9 at its peak state.
- The results obtained for both flooded and unflooded air-dried samples showed that the soil's structure is potentially collapsible and that it can cause complications to construction activities. It is important to understand the soil's behaviour in both its natural form and after being compacted for fill material. The air-dried specimens demonstrated that even though the material was compacted to 95% of MDD, the effects of drying out gave the soil a seemingly high strength, and flooding caused the interparticle bonds to break, weakening the soil's structure.
- When used as engineered fill, residual granite soils have shown to be the cause of significant problems, such as large bulk volume decrease upon wetting. The results of such an occurrence are emphasised by the behaviour of air-dried samples before and after flooding. This shows that water causes instability of weathered granites during rainy seasons.
- Specimens that were partially saturated and flooded after isotropic compression also showed a decrease in strength compared to their counterparts that were not flooded. However, it was assumed that these results were attributable to the breaking of aggregations as the specimens were being saturated. These specimens do not have collapsible structures in the states they were tested in i.e., interparticle bonds created by drying out, but rather weakened intra-particle bonds causing the soil to likely experience crushing.

5.2.4 Particle breakage

Based on the results of this study, the following conclusions can be drawn concerning particle breakage of decomposed granite soil after triaxial compression.

- As expected, higher confined specimens experienced more particle breakage than lower confined specimens. The relative breakage increased for specimens tested at a confining pressure of 100 kPa (B_r = 0.139 – 0.150) to 500 kPa (B_r = 0.246) and stayed constant for specimens tested at 500kPa to 1000kPa. CT scans showed that larger particles primarily experienced particle crushing whereas smaller particles remained unchanged.
- For decomposed granite soil it was found that the particle breakage process is probably due to breakage along existing fissures, and separation of particle amalgams.
- The friction parameter, M, was not influenced by the increase in particle breakage since all specimens reached/approached the critical state regardless of their relative breakage. This indicated that the critical state was independent of particle breakage after triaxial compression testing.
- Partially saturated (non-flooded) specimens showed increasing particle breakage with increasing initial moisture content (i.e., moisture content at the preparation of specimens).
- Flooded specimens experienced more particle breakage compared to unflooded specimens which showed that the presence of moisture after a specimen has been confined to a certain pressure, increased the amount of particle breakage.

5.3 RECOMMENDATIONS

After completing the research, the following recommendations can be made for future research:

- Triaxial compression tests are typically performed on fully saturated specimens to avoid volume changes created by compressible air. This research also focussed on unsaturated which do require some advanced methods. Unsaturated triaxial tests require modified triaxial cells to measure the change in volume since all the voids are not entirely occupied by water. The recommended triaxial cells are the Double-Wall and Twin-Cell types which are equipped with High Air Entry value disks. These cells can measure the change in volume of unsaturated soils much more accurately.
- Volume changes of unsaturated specimens can also be measured with on-sample transducers. These transducers typically measure the change in height and change in diameter and can deliver accurate results when used correctly.
- Particle breakage was limited to a maximum applied confining pressure of 1000 kPa which resulted in a similar relative breakage value as a specimen confined to 500 kPa. Triaxial compression tests at higher confining pressures are required to determine whether the maximum amount of particle breakage has occurred at a confining pressure of 500 kPa or whether it will continue.
- This research study had only two saturated drained tests which limited the dilatancy results. It is recommended that more drained triaxial compression tests be executed to determine a relationship between the stress ratio and the rate of dilation which should ultimately show the uniqueness of the critical stress ratio.
- Perform triaxial compression past 20% axial strain to determine whether specimens reach the critical state.
- Flood partially saturated specimens for longer than 24 hours to ensure full saturation of the specimen or run a B-step, B-check saturation programme before shearing.

CHAPTER 6: REFERENCES

Atkinson, J.H. & Bransby, P.L. 1978. *The Mechanics of soil*. Maidenhead: McGraw-Hill Book Company (UK) Limited.

Bowen, N.L. 1922. The Reaction Principle in Petrogenesis. *The Journal of Geology*. 30(3):177–198.

Brink, A.B.A. 1979. *Engineering Geology of Southern Africa: The first 2000 million years of geological time*. Silverton: Building Publications.

Brink, A.B.A. 1981. *Engineering Geology of Southern Africa: Rocks of 2000 to 300 million years in age.* Silverton: Building Publications.

Brink, A.B.A. & Kantey, B.A. 1961. Collapsible Grain Structure in Residual Granite Soils in Southern Africa. In Paris *5th International Conference on Soil Mechanics and Foundation Engineering*. 611–614.

BS 1377-8. 1990. *Methods of test for soils for civil engineering purposes. Part 8: Shear strength tests (effective stress) (Withdrawn)*. London: British Standards Institution.

Coop, M.R. & Lee, I.K. 1993. The behaviour of granular soils at elevated stresses. In *Predictive soil mechanics*. 186–198.

Day, P. 2021. *Lecture 5: A practical perspective on heaving, dispersivity and collapsing behaviour in South Africa*. Unpublished lecture notes, Soil Behaviour 841, Stellenbosch University.

Diop, S., Stapelberg, F., Tegegn, K., Ngubelanga, S. & Heath, L. 2011. *A review on Problem Soils in South Africa*. Bellville.

Dumbleton, M.J. & West, G. 1966. Some factors affecting the relation between the clay minerals in soils and their plasticity. *Clay Minerals*. 6:179–193.

DuPlessis, A., Le Roux, S.G. & Guelpa, A. 2016. The CT Scanner Facility at Stellenbosch University: An open access X-ray computed tomography laboratory. *Nuclear Instruments and Methods in Physics Research, Section B: Beam Interactions with Materials and Atoms*. 384:42–49.

Earle, S. 2014. *Physical Geology*. Saskatoon.

Elges, H.F.W.K. 1985. Dispersive Soils. *The Civil engineer in South Africa*. 27(7):347–349, 351.

Fouché, N. & Asante, S.Y. 2019. The collapsible nature of residual granite soils of the Cape Granite Suite. *Journal of the South African Institution of Civil Engineering*. 61(2):57–63.

Galer, M.M., Sasaki, Y. & Nakamura, Y. 1998. Field investigation of a decomposed granite site. In Rotterdam *Symposium on Engineering Problems of Crushable Soils*. 453–456.

Google Maps. 2021. *Elsana Aggregate Quarry*. [Online], Available: www.google.com/maps [2021, February 16].

Haldar, S.K. & Tišljar, J. 2014. *Introduction to Mineralogy and Petrology*. First ed. Waltham: Elsevier.

Hardin, B.O. 1985. Crushing of soil particles. *Journal of Geotechnical Engineering*. 111(10):1177–1192.

Harmse, H.J. 1980. Dispersive Soils: Their Origin, Identification and Stabilisation. *Ground Profile*. (22):10–31.

Hoffman, K. 2019. Determination of pullout resistance of galvanized-steel strips within select South African soils based on their free draining potential in mechanically stabilized earth wall backfill conditions. Stellenbosch University.

Jennings, J.E. & Knight, K. 1975. A guide to construction on or with material exhibiting additional settlement due to collapse of grain structure. In Durban *Sixth Regional Conference for Africa on Soil Mechanics & Foundation Engineering*. 99–105.

Jennings, J.E., Brink, A.B.A. & Williams, A.A.B. 1973. Revised Guide To Soil Profiling for Civil Engineering Purposes in Southern Africa. *Transactions of the South African Institution of Civil Engineers*. 15(1):3–13.

Knappett, J.A. & Craig, R.F. 2012. *Craig's Soil Mechanics*. Eighth ed. London: Spon Press.

Knight, K. 1961. The collapse of structure of sandy sub-soils on wetting. University of Witwatersrand.

Kwon, Y. & Oh, S. 2011. Physical and mechanical properties of decomposed granite soils sampled in Cheongju, Korea. *International Journal of Physical Sciences*. 6(24):5777–5794.

Lee, I.K. 1991. Mechanical Behaviour of Compacted Decomposed Granite Soil. City University.

Lee, I.K. & Coop, M.R. 1995. The intrinsic behaviour of a decomposed granite soil. *Geotechnique*. 45(1):117–130.

Lee, K.L. & Farhoomand, I. 1967. Compressibility and Crushing of Granular Soil in Anisotropic Triaxial Compression. *Canadian Geotechnical Journal*. 4(1).

Liu, P., Zhou, X. & Liu, W. 2015. Numerical Simulation of Triaxial Test for Remoulded Completely Decomposed Granite. *Journal of Information and Computational Science*. 12(15):5667–5678.

Lumb, P. 1962. The Properties of Decomposed Granite. *Geotechnique*. 12(3):226–243.

Marsal, R.J. 1967. Large scale testing of rockfill materials. *Soil Mechanics and Foundation Division*. 93(2):27–43.

Matsuo, S.I. & Nishida, K. 1968. Physical and Chemical Properties of Decomposed Granite Soil Grains. *Soils and Foundations*. 8(4):10–20.

Matsuo, S.I. & Nishida, K. 1970. The Properties of Decomposed Granite Soils and their Influence on Permeability. *Soils and Foundations*. 10(1):93–105.

Matsuo, S.I., Fukuta, M. & Nishida, K. 1970. Consistency of Decomposed Granite Soils and its Relation to Engineering Properties. *Soils and Foundations*. 10(4):1–9.

McCarthy, D.F.J. 1962. Compression charatceristics of compacted micaceous soils. Lehigh University.

Mitchell, J.K. & Soga, K. 2005. *Fundamentals of Soil Behavior*. Third ed. Hoboken: John Wiley & Sons.

Miura, N. & O-hara, S. 1979. Particle-crushing of a decomposed granite soil under shear stresses. *Soils and Foundations*. 19(3):1–14.

Miura, N. & Yamanouchi, T. 1977. Effect of particle-crushing on the shear characteristics of a sand. *Proceedings of the Japan Society of Civil Engineers*. (260):109–118.

Mshali, M.R. & Visser, A.T. 2014. Influence of mica on compactability and moisture content of cement-treated weathered granite gravel. In Pretoria *33rd Southern African Transport Conference*. 546–555.

Niu, X., Yao, Y., Sun, Y. & Luo, Z. 2018. Weathering process of in situ granite and particle breakage characteristics of compacted weathered granite. *Applied Sciences*. 8(1108):1–22.

Pellant, C. 2000. *Rocks and Minerals*. London: Dorling Kindersley Limited.

Rahman, A.S.A., Noor, M.J.M., Jais, I.B.M., Sidek, N. & Ahmad, J. 2018. Shear strength of granitic residual soil in saturated and unsaturated conditions. In *AIP Conference Proceedings*.

Roscoe, K.H. & Burland, J. 1968. On the Generalized Stress-Strain Behavior of Wet Clays.

Roscoe, K.H., Schofield, A.N. & Thurairajah, A. 1963. Yielding of Clays in States Wetter than Critical. *Géotechnique*. 13(3):211–240.

Schofield, A.N. & Wroth, C.P. 1968. *Critical State Soil Mechanics*. Maidenhead: McGraw-Hill Publishing.

Schwartz, K. 1985. Collapsible Soils. *The Civil Engineer in South Africa*. 27(7):379–393.

Seethalakshmi, P. & Sachan, A. 2018. Effect of mica content on pore pressure and stress-strain response of micaceous sand using energy dissipation and different failure mechanisms. *International Journal of Geotechnical Engineering*.

South African National Standard. 2013a. *Civil engineering test methods Part GR1: Wet preparation and particle size analysis*. (SANS 3001-GR1:2013). Pretoria: SABS.

South African National Standard. 2013b. *Civil engineering test methods. Part GR10. Determination of the one-point liquid limit, plastic limit, plasticity index and linear shrinkage*. (SANS 3001-GR10:2013) Pretoria: SABS.

South African National Standard. 2014. *Civil engineering test methods Part GR3: Particle size analysis of material smaller than 2 mm (hydrometer method)*. (SANS 3001-GR3:2014) Pretoria: SABS.

South African National Standard. 2015. *Civil engineering test methods Part GR30: Determination of the maximum dry density and optimum moisture content*. (SANS 3001-GR30:2015) Pretoria: SABS.

South African Pavement Engineering Manual (SAPEM). 2014. *Chapter 4: Standards*. Second ed. South African National Road Agency Ltd.

Tarbuck, E.J., Lutgens, F.K. & Tasa, D.G. 2014. *Earth: An Introduction to Physical Geology*. Eleventh ed. Harlow: Ashford Colour Press Ltd.

Terblanche, E.H. 1989. *Settlement and underpinning of a building founded on residual granite: a case history*.

Terzaghi, K., Peck, R.B. & Mesri, G. 1996. *Soil Mechanics in Engineering Practice*. New York: John Wiley & Sons.

VJ Tech Limited. 2021. *VJ Tech*. [Online], Available: www.vjtech.co.uk [2021, May 10].

Weinert, H.H. 1980. *The Natural Road Construction Materials of Southern Africa*. Pretoria: H & R Academia.

White, W.A. 1949. *Atterberg plastic limits of clay minerals*. Urbana.

Williams, A.A.B., Pidgeon, J.T. & Day, P.W. 1985. Expansive soils. *The Civil Engineer in South Africa*. (7):367–378.

Wood, D.M. 1994. *Soil behaviour and critical state soil mechanics*. Cambridge: Cambridge University Press.

Yan, W.M. & Li, X.S. 2012. Mechanical response of a medium-fine-grained decomposed granite in Hong Kong. *Engineering Geology*. 129–130:1–8.

Zhao, B., Wang, J., Andò, E., Viggiani, G. & Coop, M.R. 2019. Investigation of particle breakage under one-dimensional compression of sand using x-ray microtomography. *Canadian Geotechnical Journal*. 57(5):754–762.

APPENDIX A – PREPARATION OF TRIAXIAL SPECIMENS

Table A. 1 Preparation of decomposed granite soil triaxial compression test specimens

Specimen No.	Compaction effort (% of MDD)	Dry density (kg/m^3)	Moisture (%)	Bulk density (kg/m^3)	Mass of soil (g)	Mass of water (g)	Total mass (g)	Mass per layer (5 layers in total)	Confining pressure (kPa)	Drainage type	Saturation (%)	Initial void ratio	Remarks
1	86	1808	8.45	1961	355.0	30.0	385.0	77.2	100	CU	48.1	0.46	Saturated specimens
2	89	1871	8.45	2029	367.3	31.0	398.4	79.7	100	CU	53.8	0.42	
3	92	1934	8.45	2098	379.7	32.1	411.8	82.4	100	CU	60.5	0.37	
4	95	1997	8.45	2166	392.1	33.1	425.2	85.0	100	CU	68.5	0.33	
5	95	1997	8.45	2166	392.1	33.1	425.2	85.0	200	CU	68.5	0.33	
6	95	1997	8.45	2166	392.1	33.1	425.2	85.0	100	CD	68.5	0.33	
7	95	1997	8.45	2166	392.1	33.1	425.2	85.0	200	CD	68.5	0.33	
8	86	1808	0.0	1808	354.9	0.0	354.9	71.0	100	CD	0.0	0.47	Dry specimen
9	86	1808	3.5	1872	354.9	12.5	367.4	73.5	100	CD	20	0.47	Partially saturated specimens
10	86	1808	7.0	1935	354.9	24.9	379.9	76.0	100	CD	40	0.47	
11	86	1808	10.5	1999	354.9	37.4	392.4	78.5	100	CD	60	0.47	
12	86	1808	14.1	2062	354.9	49.9	404.8	81.0	100	CD	80	0.47	
13	86	1808	17.6	2126	354.9	62.4	417.3	83.5	100	CD	100	0.47	
14	95	1997	8.45	2166	392.1	33.1	425.2	85.0	100	CD	68.5	0.33	Air-dried
15	95	1997	8.45	2166	392.1	33.1	425.2	85.0	100	CD	68.5	0.33	Air-dried flooded

16	86	1808	0.0	1808	354.9	0.0	354.9	71.0	100	CD	0	0.47	Dry specimen flooded
17	86	1808	3.5	1872	354.9	12.5	367.4	73.5	100	CD	20	0.47	Partially saturated specimens flooded
18	86	1808	7.0	1935	354.9	24.9	379.9	76.0	100	CD	40	0.47	
19	86	1808	10.5	1999	354.9	37.4	392.4	78.5	100	CD	60	0.47	
20	86	1808	14.1	2062	354.9	49.9	404.8	81.0	100	CD	80	0.47	
CT 1	95	1997	8.45	2166	392.1	33.1	425.2	85.0	100	CU	68.5	0.33	Specimens sent for CT-scanning
CT 2	95	1997	8.45	2166	392.1	33.1	425.2	85.0	500	CU	68.5	0.33	
CT 3	95	1997	8.45	2166	392.1	33.1	425.2	85.0	1000	CU	68.5	0.33	

Table A. 2 Isotropic compression and swelling programme of decomposed granite soil

Specimen No.	**Compaction effort (% of MDD)**	**Moisture (%)**	**Dry density (kg/m^3)**	**Bulk density (kg/m^3)**	**Mass of soil (g)**	**Mass of water (g)**	**Total mass (g)**	**Mass per layer (5 layers in total)**	**Confining pressure - start (kPa)**	**Confining pressure - end (kPa)**	**Saturation (%)**	**Initial void ratio**	**Remarks**
ISO	78	8.45	1640	1779	321.9	27.2	349.1	69.8	- 25 50 100 200 400 800 200	25 50 100 200 400 800 200 25	36.4	0.62	Saturated specimen isotropic compression and swelling

APPENDIX B – CRITICAL STATE MODEL

Table B. 1 Input parameters for drained decomposed granite soil under normal consolidation at 100 kPa isotropic compression

Conventional compression CD triaxial test

Model parameters

κ (-)	0.012	Slope of unload-reload line on v vs ln(p') space
G' (kPa)	70000	Elastic shear modulus
N (-)	1.77	v on NCL at p' = 1kPa
M (-)	1.41	Slope of CSL in q vs p' plane
λ (-)	0.073	Slope of NCL

Consolidation stage

Isotropic consolidation from	**0**	**kPa**
Maximum isotropic load p'	100	kPa
v at max. isotropic load N-λln(p')	1.434	-
Pre-shear isotropic load (normal/over cons.)	100	kPa
v at pre-shear isotropic load	1.434	-

Drainage and loading conditions

During isotropic loading	**D**	
During shearing	**D**	
Slope (dq/dp) of total stress path	3	-
p' at eta = M	188.7	kPa

Overconsolidation consideration

Value of p' at first yield	100.0	kPa
Pre-yield change in p' (0 or +value)	0.0	kPa
Post-yield change in p' (+/-)	88.7	kPa
Abs change in p' from shearing onset to eta = M	88.7	kPa
Total number of steps	200	
No. of pre-yield p' steps	0	
No. of post-yield p' steps	200	
Pre-yield p' increments	#DIV/0!	kPa
Post-yield p' increments	0.44	kPa

Table B. 2 Predicted results for decomposed granite soil under normal compression conditions at 100 kPa isotropic pressure

17	18	19	20	21	22	23	24	25	26	27	28	29	30	31	32	33	34	35	36	37	38	39	40
Initial Values									Load Step		Final Values					Elastic Strain Changes		Plastic Strain Changes		Total Strain Changes			Change in v
Step No.	p' (kPa)	q (kPa)	eta (q/p')	p'_0 (kPa)	v	ε_p	ε_q	ε_a	dp' (kPa)	dq (kPa)	p' (kPa)	q (kPa)	eta (q/p')	p'_0 (kPa)	dp'_0 (kPa)	$d\varepsilon_p^e$	$d\varepsilon_q^e$	$d\varepsilon_p^p$	$d\varepsilon_q^p$	$d\varepsilon_p$	$d\varepsilon_q$	$d\varepsilon_a$	dv
1	100.0	0.0	0.00	100	1.434	0.000	0.000	0.000	0.44	1.33	100.4	1.3	0.0132	100.4523	0.452256903	3.69451E-05	6.33E-06	0.00019241	0	0.000229	6.33E-06	8.28E-05	-0.000328849
2	100.4	1.3	0.01	100.4523	1.433	0.000	0.000	0.000	0.44	1.33	100.9	2.7	0.0264	100.9221	0.469822486	3.67911E-05	6.33E-06	0.00019903	2.6517E-06	0.000236	8.99E-06	8.76E-05	-0.000338041
3	100.9	2.7	0.03	100.9221	1.433	0.000	0.000	0.000	0.44	1.33	101.3	4.0	0.0394	101.4092	0.48715748	3.66388E-05	6.33E-06	0.00020546	5.4522E-06	0.000242	1.18E-05	9.25E-05	-0.00034696
4	101.3	4.0	0.04	101.4092	1.433	0.001	0.000	0.000	0.44	1.33	101.8	5.3	0.0523	101.9135	0.504265905	3.6488E-05	6.33E-06	0.0002117	8.3936E-06	0.000248	1.47E-05	9.75E-05	-0.000355608
5	101.8	5.3	0.05	101.9135	1.432	0.001	0.000	0.000	0.44	1.33	102.2	6.7	0.0651	102.4347	0.521151691	3.63387E-05	6.33E-06	0.00021776	1.1469E-05	0.000254	1.78E-05	0.000103	-0.000363987
6	102.2	6.7	0.07	102.4347	1.432	0.001	0.000	0.000	0.44	1.33	102.7	8.0	0.0777	102.9725	0.537818686	3.6191E-05	6.33E-06	0.00022364	1.467E-05	0.00026	2.1E-05	0.000108	-0.000372101
7	102.7	8.0	0.08	102.9725	1.432	0.001	0.000	0.001	0.44	1.33	103.1	9.3	0.0903	103.5267	0.554270652	3.60447E-05	6.33E-06	0.00022934	1.7991E-05	0.000265	2.43E-05	0.000113	-0.000379951
8	103.1	9.3	0.09	103.5267	1.431	0.002	0.000	0.001	0.44	1.33	103.5	10.6	0.1028	104.0973	0.570511272	3.58999E-05	6.33E-06	0.00023485	2.1425E-05	0.000271	2.78E-05	0.000118	-0.000387541
9	103.5	10.6	0.10	104.0973	1.431	0.002	0.000	0.001	0.44	1.33	104.0	12.0	0.1151	104.6838	0.586544151	3.57565E-05	6.33E-06	0.0002402	2.4965E-05	0.000276	3.13E-05	0.000123	-0.000394875
10	104.0	12.0	0.12	104.6838	1.431	0.002	0.000	0.001	0.44	1.33	104.4	13.3	0.1274	105.2862	0.602372818	3.56145E-05	6.33E-06	0.00024536	2.8607E-05	0.000281	3.49E-05	0.000129	-0.000401955
11	104.4	13.3	0.13	105.2862	1.430	0.003	0.000	0.001	0.44	1.33	104.9	14.6	0.1395	105.9042	0.618000725	3.54739E-05	6.33E-06	0.00025036	3.2343E-05	0.000286	3.87E-05	0.000134	-0.000408786
12	104.9	14.6	0.14	105.9042	1.430	0.003	0.000	0.001	0.44	1.33	105.3	16.0	0.1516	106.5376	0.633431254	3.53347E-05	6.33E-06	0.00025519	3.617E-05	0.000291	4.25E-05	0.000139	-0.000415371
13	105.3	16.0	0.15	106.5376	1.429	0.003	0.000	0.001	0.44	1.33	105.8	17.3	0.1635	107.1863	0.648667714	3.51968E-05	6.33E-06	0.00025985	4.0081E-05	0.000295	4.64E-05	0.000145	-0.000421714
14	105.8	17.3	0.16	107.1863	1.429	0.003	0.000	0.001	0.44	1.33	106.2	18.6	0.1753	107.85	0.663713346	3.50602E-05	6.33E-06	0.00026434	4.4071E-05	0.000299	5.04E-05	0.00015	-0.000427819
15	106.2	18.6	0.18	107.85	1.428	0.004	0.000	0.002	0.44	1.33	106.7	20.0	0.1871	108.5286	0.678571324	3.49249E-05	6.33E-06	0.00026868	4.8137E-05	0.000304	5.45E-05	0.000156	-0.00043369
16	106.7	20.0	0.19	108.5286	1.428	0.004	0.000	0.002	0.44	1.33	107.1	21.3	0.1987	109.2218	0.693244754	3.47908E-05	6.33E-06	0.00027285	5.2273E-05	0.000308	5.86E-05	0.000161	-0.000439331
17	107.1	21.3	0.20	109.2218	1.428	0.004	0.000	0.002	0.44	1.33	107.5	22.6	0.2103	109.9295	0.707736682	3.4658E-05	6.33E-06	0.00027688	5.6475E-05	0.000312	6.28E-05	0.000167	-0.000444747
18	107.5	22.6	0.21	109.9295	1.427	0.005	0.001	0.002	0.44	1.33	108.0	23.9	0.2217	110.6516	0.722050088	3.45265E-05	6.33E-06	0.00028074	6.0739E-05	0.000315	6.71E-05	0.000172	-0.000449941
19	108.0	23.9	0.22	110.6516	1.427	0.005	0.001	0.002	0.44	1.33	108.4	25.3	0.2331	111.3878	0.736187892	3.43961E-05	6.33E-06	0.00028446	6.5062E-05	0.000319	7.14E-05	0.000178	-0.000454919
20	108.4	25.3	0.23	111.3878	1.426	0.005	0.001	0.002	0.44	1.33	108.9	26.6	0.2444	112.1379	0.750152955	3.4267E-05	6.33E-06	0.00028803	6.944E-05	0.000322	7.58E-05	0.000183	-0.000459685
180	179.4	238.1	1.33	338.3505	1.352	0.059	0.113	0.133	0.44	1.33	179.8	239.4	1.3316	340.1788	1.828272571	2.18832E-05	6.33E-06	0.00024376	0.00286417	0.000266	0.002871	0.002959	-0.000359203
181	179.8	239.4	1.33	340.1788	1.352	0.059	0.116	0.136	0.44	1.33	180.3	240.8	1.3357	342.0101	1.831334322	2.18352E-05	6.33E-06	0.00024292	0.00300923	0.000265	0.003016	0.003104	-0.000357908
182	180.3	240.8	1.34	342.0101	1.351	0.059	0.119	0.139	0.44	1.33	180.7	242.1	1.3398	343.8445	1.834373534	2.17874E-05	6.33E-06	0.00024208	0.00316951	0.000264	0.003176	0.003264	-0.000356619
183	180.7	242.1	1.34	343.8445	1.351	0.059	0.122	0.142	0.44	1.33	181.1	243.4	1.3438	345.6819	1.837390427	2.17398E-05	6.33E-06	0.00024125	0.00334754	0.000263	0.003354	0.003442	-0.000355337
184	181.1	243.4	1.34	345.6819	1.351	0.060	0.126	0.146	0.44	1.33	181.6	244.8	1.3479	347.5223	1.840385221	2.16924E-05	6.33E-06	0.00024042	0.00354646	0.000262	0.003553	0.00364	-0.000354061
185	181.6	244.8	1.35	347.5223	1.350	0.060	0.129	0.149	0.44	1.33	182.0	246.1	1.3519	349.3656	1.84335813	2.16453E-05	6.33E-06	0.0002396	0.00377018	0.000261	0.003777	0.003864	-0.000352792
186	182.0	246.1	1.35	349.3656	1.350	0.060	0.133	0.153	0.44	1.33	182.5	247.4	1.3559	351.2119	1.846309367	2.15983E-05	6.33E-06	0.00023878	0.00402367	0.00026	0.00403	0.004117	-0.000351529
187	182.5	247.4	1.36	351.2119	1.350	0.060	0.137	0.157	0.44	1.33	182.9	248.7	1.3599	353.0612	1.849239142	2.15516E-05	6.33E-06	0.00023796	0.0043133	0.00026	0.00432	0.004406	-0.000350272
188	182.9	248.7	1.36	353.0612	1.349	0.061	0.141	0.162	0.44	1.33	183.4	250.1	1.3639	354.9133	1.852147663	2.1505E-05	6.33E-06	0.00023715	0.00464742	0.000259	0.004654	0.00474	-0.000349022
189	183.4	250.1	1.36	354.9133	1.349	0.061	0.146	0.166	0.44	1.33	183.8	251.4	1.3678	356.7684	1.855035135	2.14587E-05	6.33E-06	0.00023634	0.00503716	0.000258	0.005043	0.005129	-0.000347779
190	183.8	251.4	1.37	356.7684	1.349	0.061	0.151	0.171	0.44	1.33	184.2	252.7	1.3717	358.6263	1.85790176	2.14126E-05	6.33E-06	0.00023554	0.00549768	0.000257	0.005504	0.00559	-0.000346541
191	184.2	252.7	1.37	358.6263	1.348	0.061	0.156	0.177	0.44	1.33	184.7	254.1	1.3756	360.487	1.860747739	2.13667E-05	6.33E-06	0.00023474	0.00605021	0.000256	0.006057	0.006142	-0.00034531
192	184.7	254.1	1.38	360.487	1.348	0.062	0.163	0.183	0.44	1.33	185.1	255.4	1.3795	362.3506	1.863573269	2.13209E-05	6.33E-06	0.00023394	0.00672544	0.000255	0.006732	0.006817	-0.000344086
193	185.1	255.4	1.38	362.3506	1.348	0.062	0.169	0.190	0.44	1.33	185.6	256.7	1.3834	364.217	1.866378546	2.12754E-05	6.33E-06	0.00023315	0.00756937	0.000254	0.007576	0.007661	-0.000342868
194	185.6	256.7	1.38	364.217	1.347	0.062	0.177	0.198	0.44	1.33	186.0	258.1	1.3873	366.0861	1.869163763	2.12301E-05	6.33E-06	0.00023236	0.00865431	0.000254	0.008661	0.008745	-0.000341656
195	186.0	258.1	1.39	366.0861	1.347	0.062	0.186	0.206	0.44	1.33	186.5	259.4	1.3911	367.958	1.87192911	2.1185E-05	6.33E-06	0.00023157	0.01010076	0.000253	0.010107	0.010191	-0.00034045
196	186.5	259.4	1.39	367.958	1.347	0.063	0.196	0.217	0.44	1.33	186.9	260.7	1.3949	369.8327	1.874674777	2.11401E-05	6.33E-06	0.00023079	0.01212563	0.000252	0.012132	0.012216	-0.000339251
197	186.9	260.7	1.39	369.8327	1.346	0.063	0.208	0.229	0.44	1.33	187.3	262.0	1.3987	371.7101	1.87740095	2.10954E-05	6.33E-06	0.00023001	0.01516275	0.000251	0.015169	0.015253	-0.000338058
198	187.3	262.0	1.40	371.7101	1.346	0.063	0.223	0.244	0.44	1.33	187.8	263.4	1.4025	373.5902	1.880107812	2.10509E-05	6.33E-06	0.00022924	0.02022437	0.00025	0.020231	0.020314	-0.000336871
199	187.8	263.4	1.40	373.5902	1.346	0.063	0.243	0.264	0.44	1.33	188.2	264.7	1.4063	375.473	1.882795546	2.10065E-05	6.33E-06	0.00022847	0.03034722	0.000249	0.030354	0.030437	-0.00033569
200	188.2	264.7	1.41	375.473	1.345	0.064	0.274	0.295	0.44	1.33	188.7	266.0	1.4100	377.3585	1.885464332	2.09624E-05	6.33E-06	0.0002277	0.06071506	0.000249	0.060721	0.060804	-0.00034516

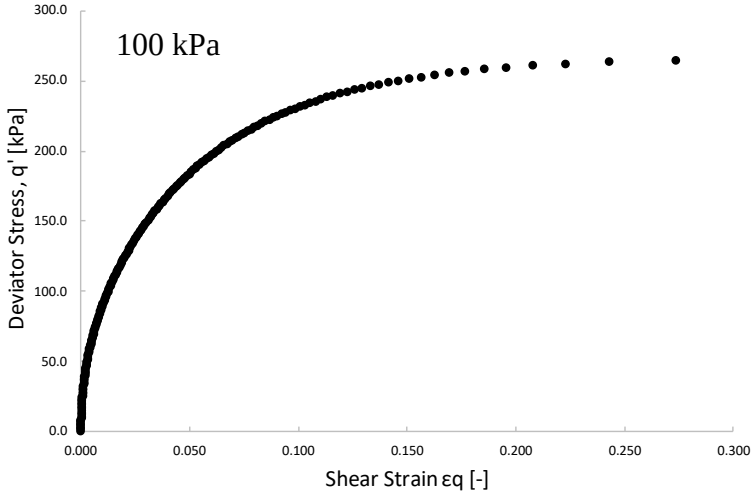

Figure B. 1 Drained critical state prediction in q': ε_q space for 100 kPa

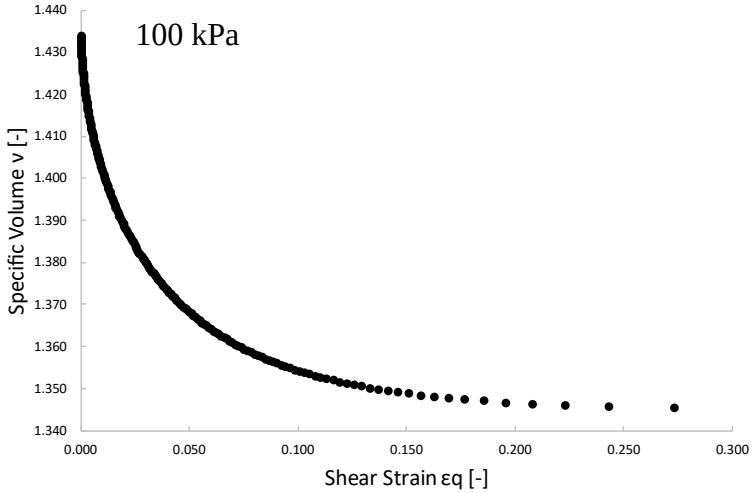

Figure B. 2 Drained critical state prediction in v: ε_q space for 100 kPa

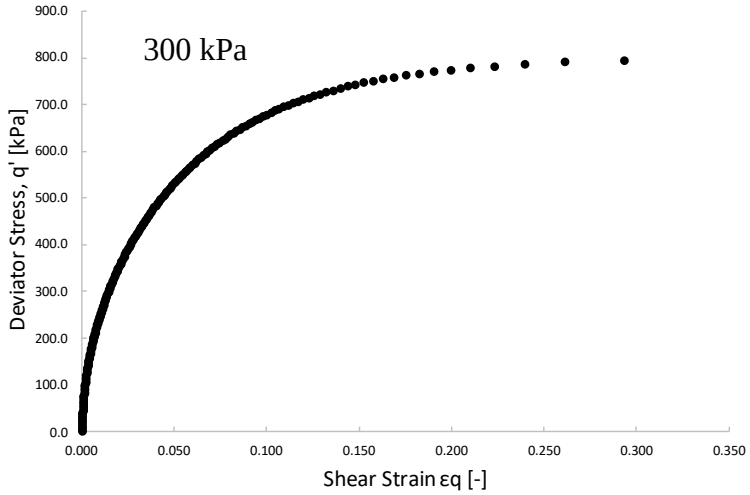

Figure B. 3 Drained critical state prediction in q': ε_q space for 300 kPa

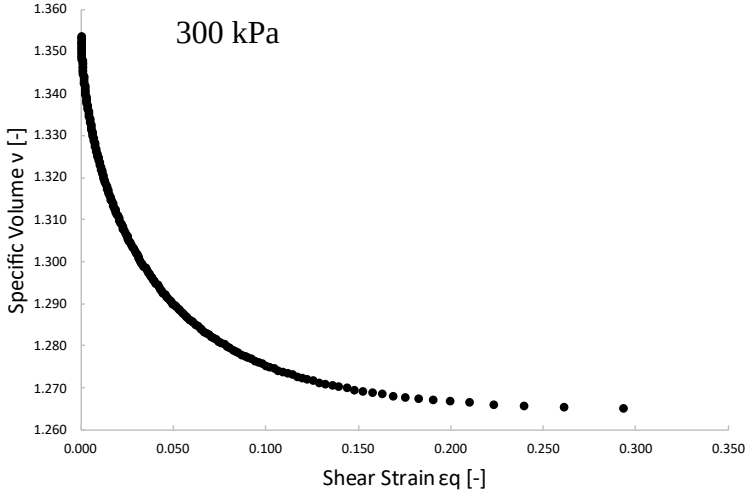

Figure B. 4 Drained critical state prediction in v: ε_q space for 300 kPa

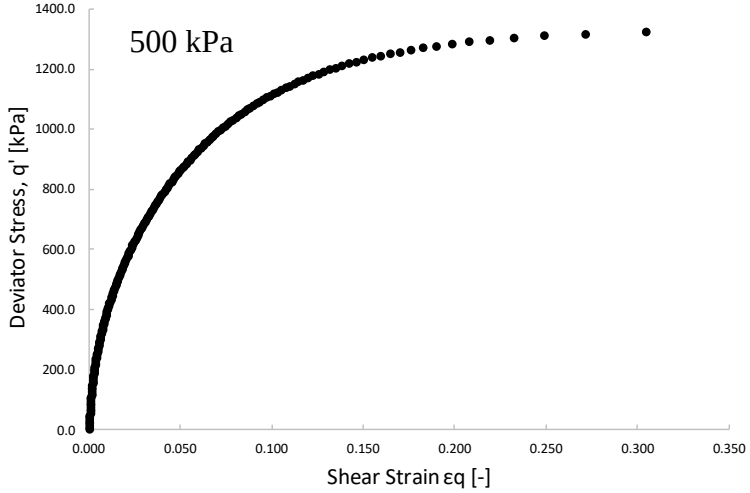

Figure B. 5 Drained critical state prediction in q': ε_q space for 500 kPa

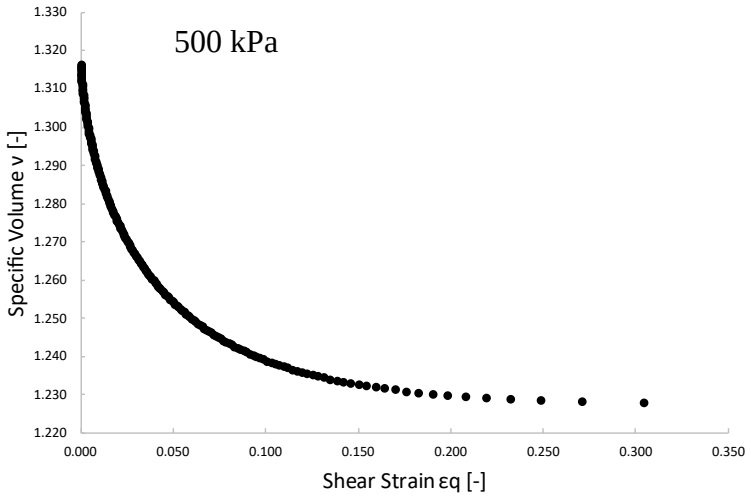

Figure B. 6 Drained critical state prediction in v: ε_q space for 500 kPa

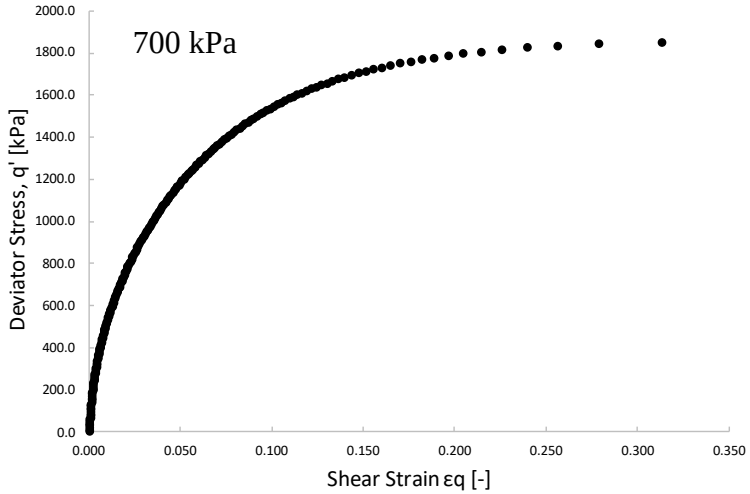

Figure B. 7 Drained critical state prediction in q': ε_q space for 700 kPa

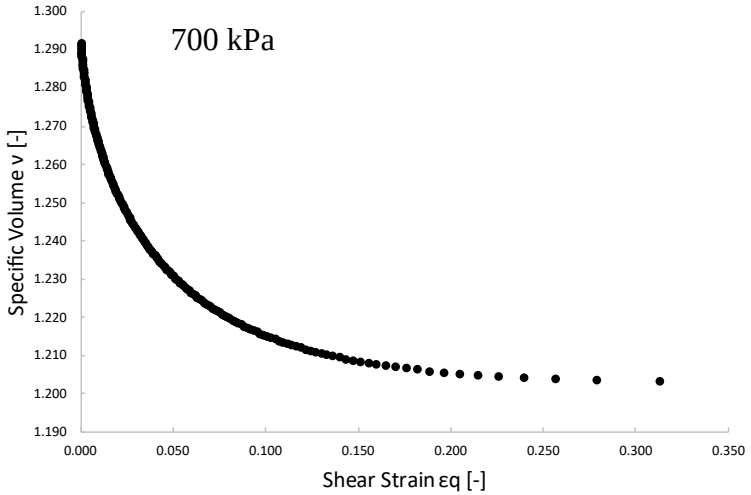

Figure B. 8 Drained critical state prediction in v: ε_q space for 700 kPa

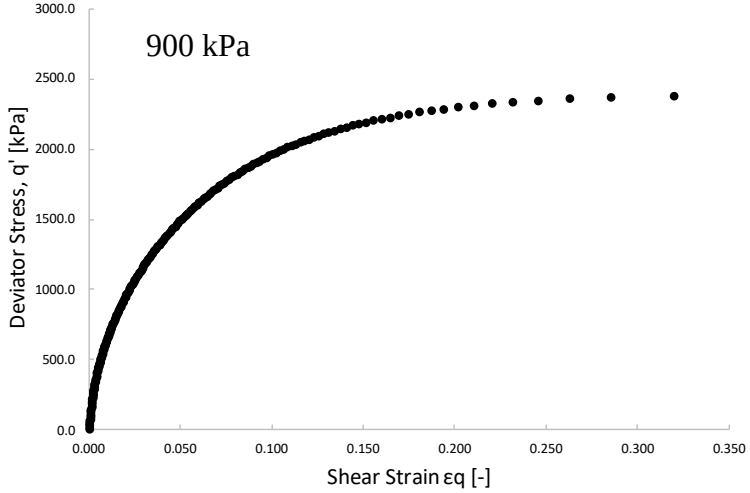

Figure B. 9 Drained critical state prediction in q': ε_q space for 900 kPa

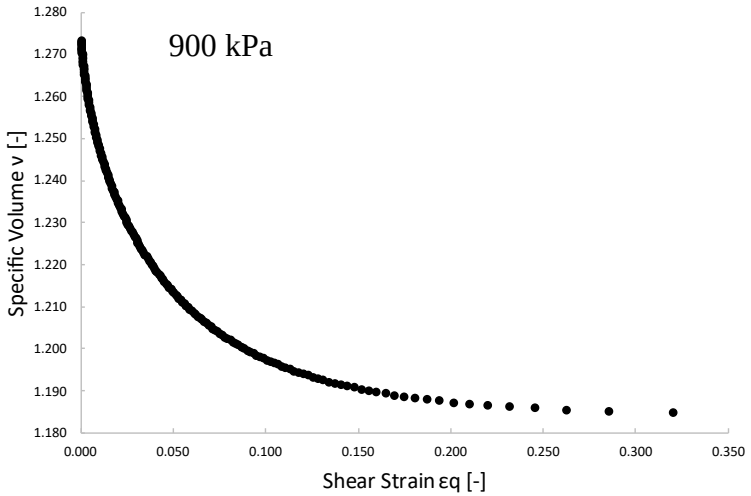

Figure B. 10 Drained critical state prediction in v: ε_q space for 900 kPa

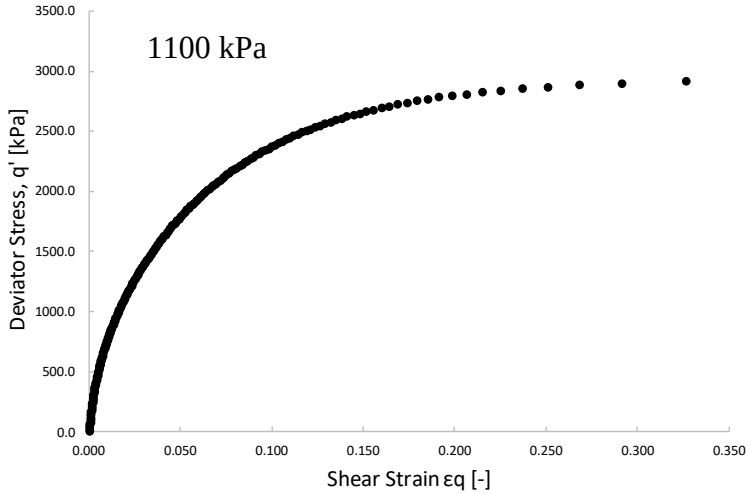

Figure B. 11 Drained critical state prediction in q': ε_q space for 1100 kPa

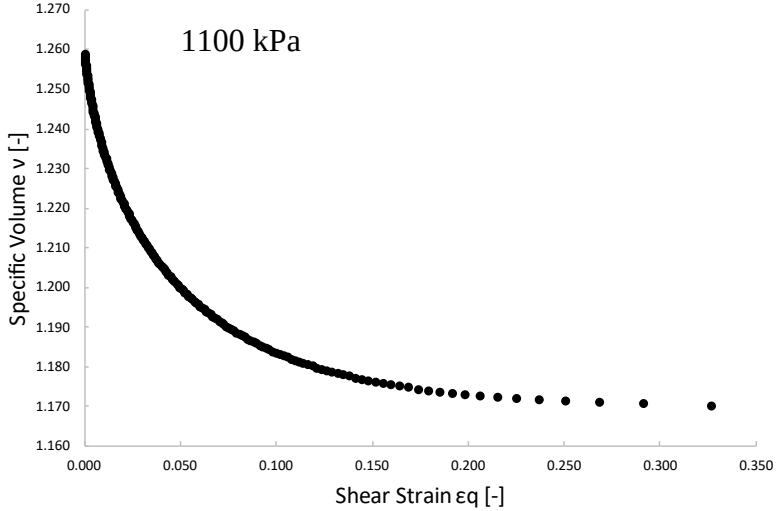

Figure B. 12 Drained critical state prediction in v: ε_q space for 1100 kPa

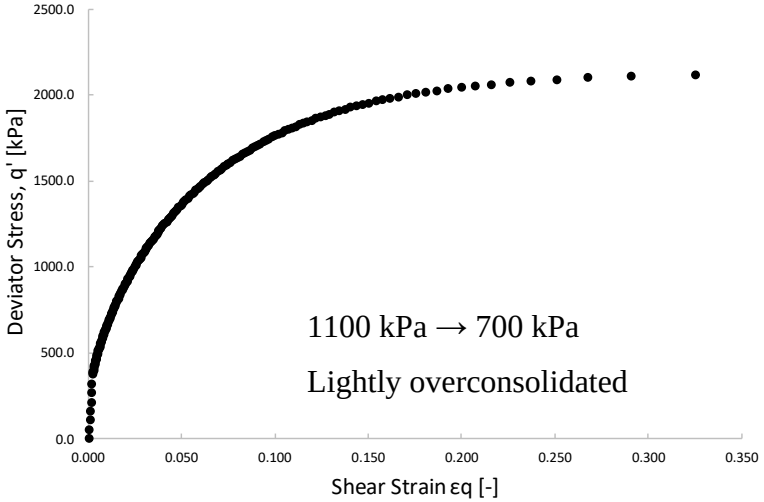

Figure B. 13 Drained critical state prediction in q': ε_q space for lightly overconsolidated test

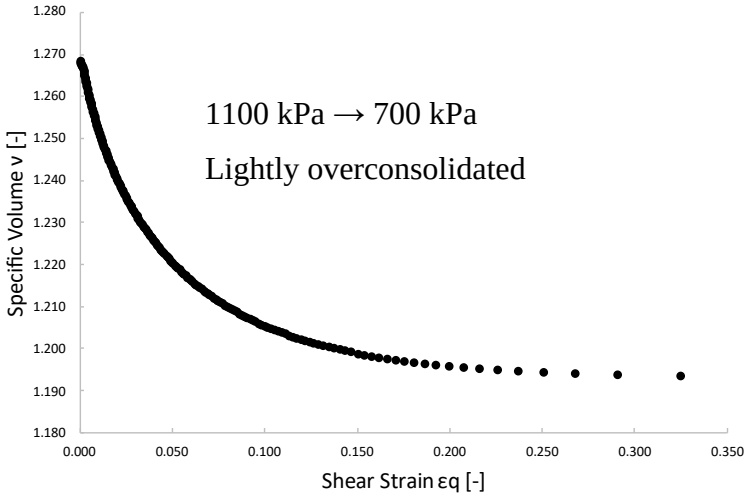

Figure B. 14 Drained critical state prediction in v: ε_q space for lightly overconsolidated test

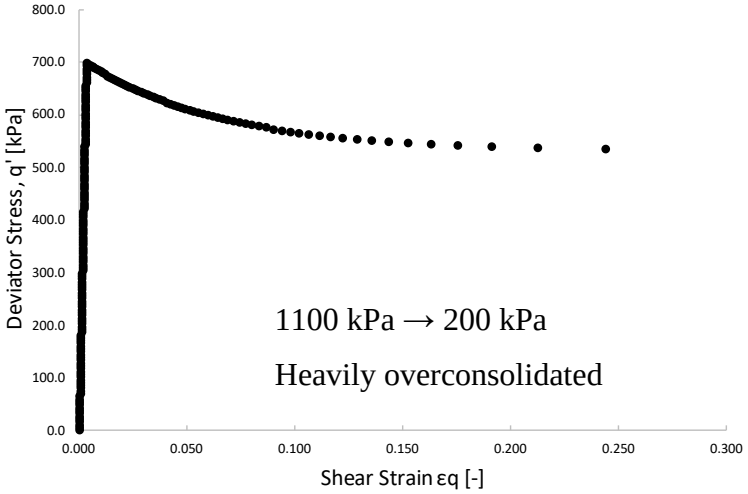

Figure B. 15 Drained critical state prediction in q': ε_q space for heavily overconsolidated test

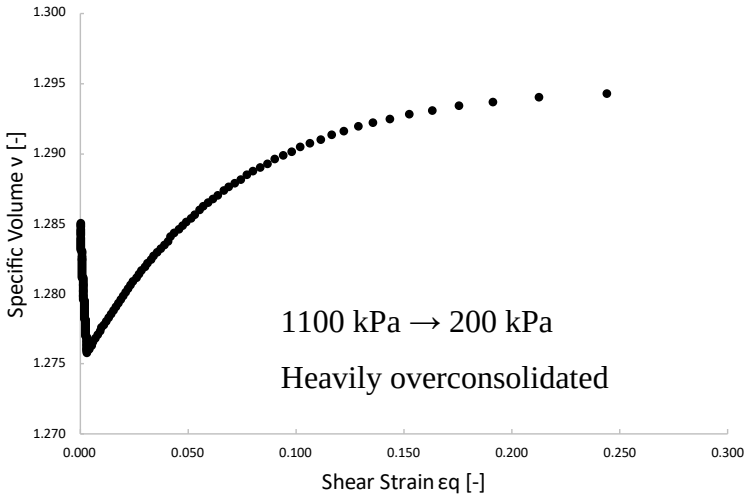

Figure B. 16 Drained critical state prediction in v: ε_q space for heavily overconsolidated test

APPENDIX C – TRIAXIAL TEST RESULTS

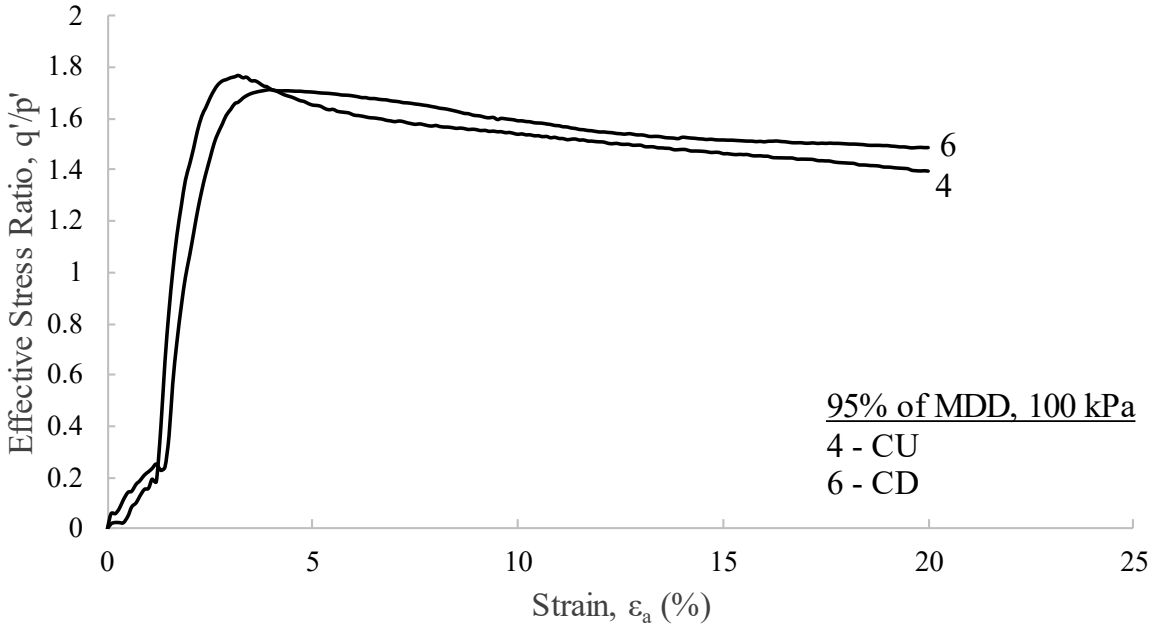

Figure C. 1 100 kPa Drained and undrained test of decomposed granite soil saturated samples in q'/p'': ε_a space

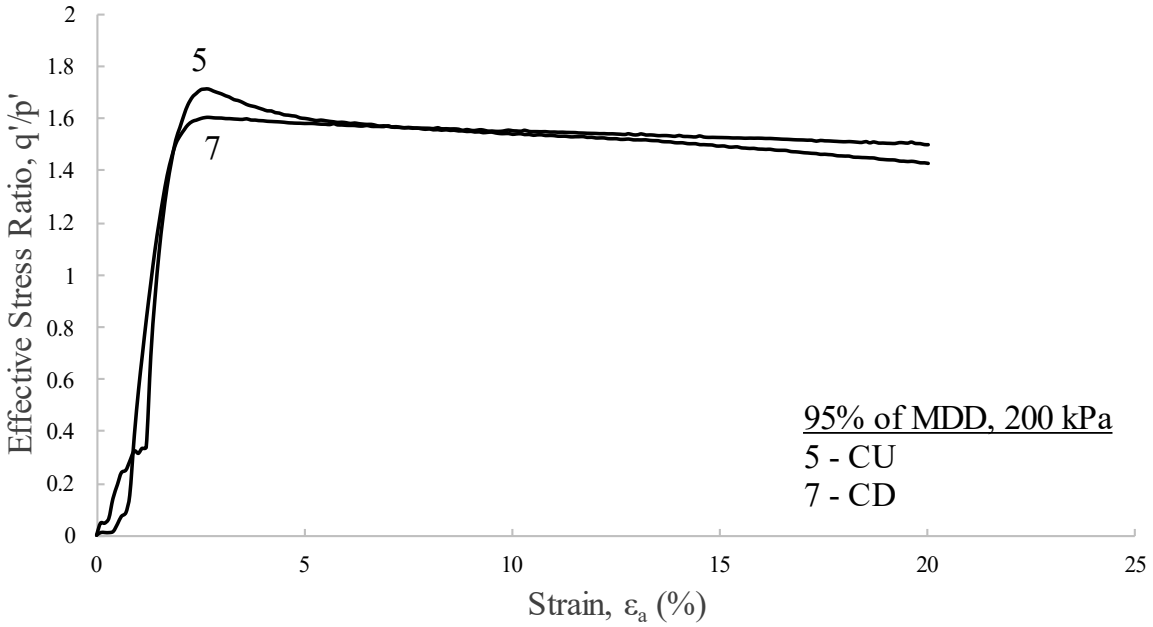

Figure C. 2 200 kPa Drained and undrained test of decomposed granite soil saturated samples in q'/p': ε_a space

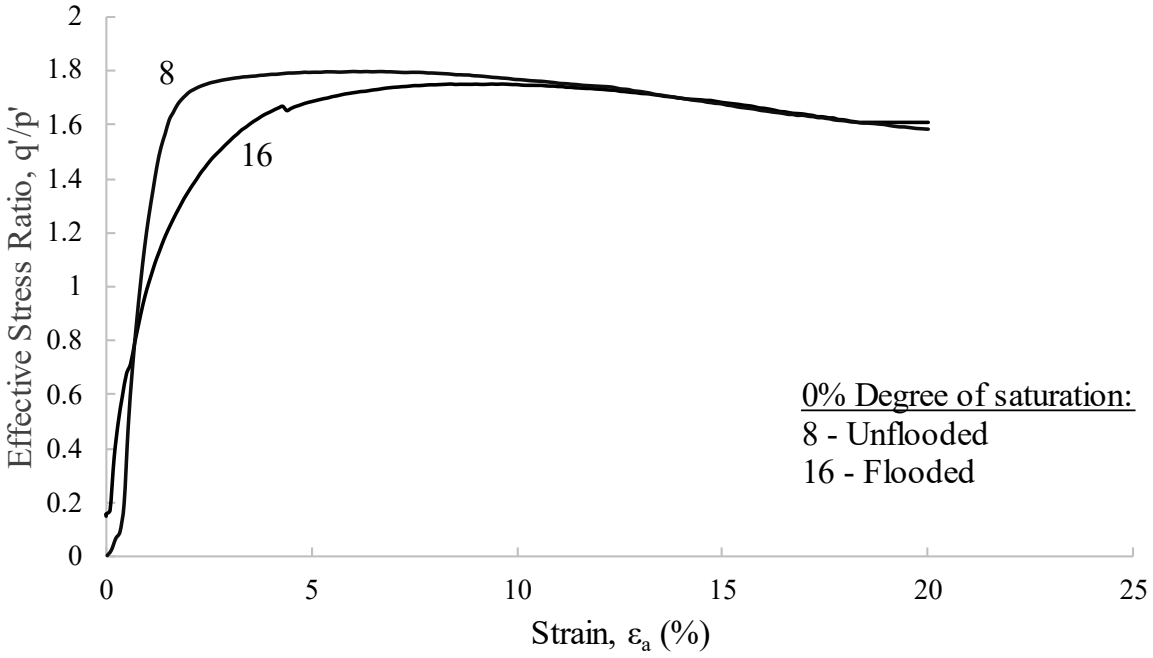

Figure C. 3 Behaviour of decomposed granite soil dry specimen 8 and 16 (flooded) in q'/p': ε_a space

APPENDIX D – PARTICLE BREAKAGE

CT scans of specimen CT 2

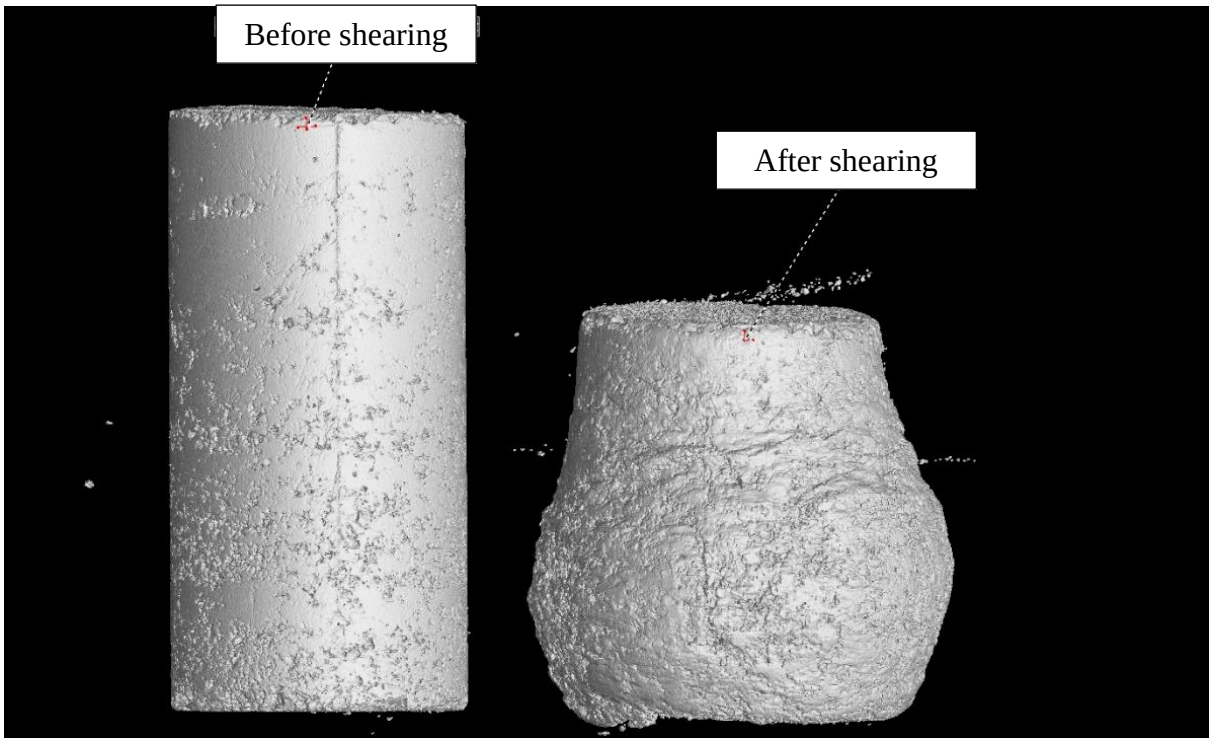

Figure D. 1 CT-scan front view of CT 2 before and after shearing

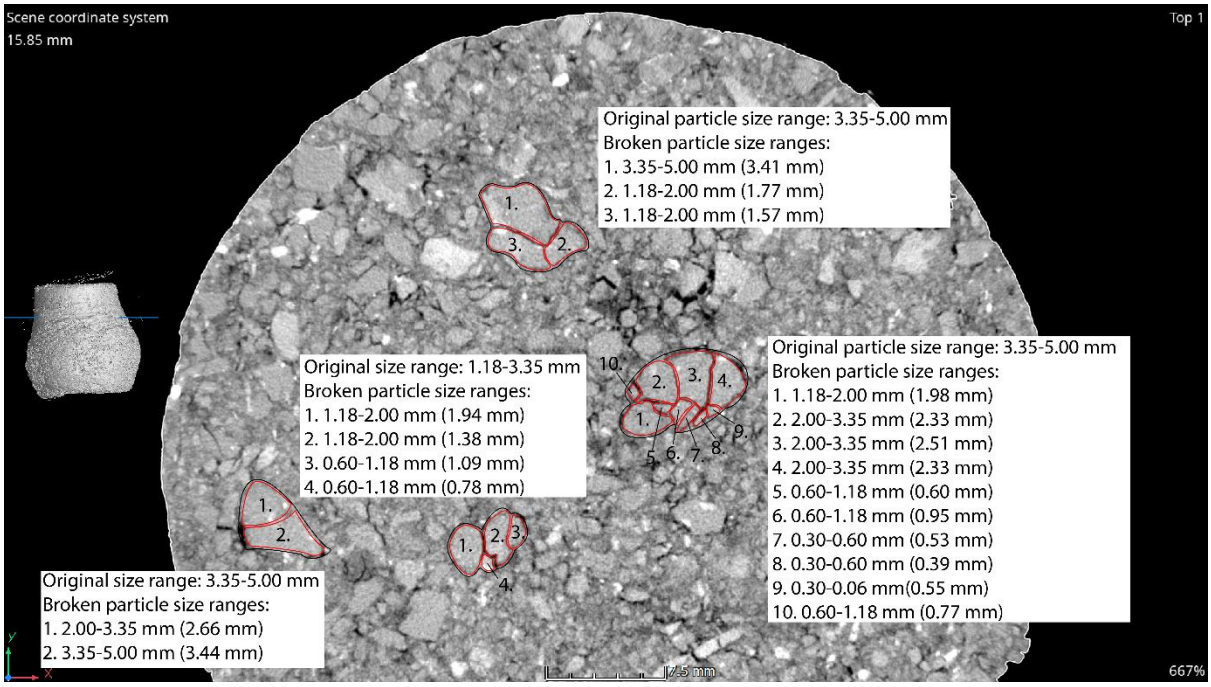

Figure D. 2 CT-scan top view of specimen CT 2 and its particle breakage – 1

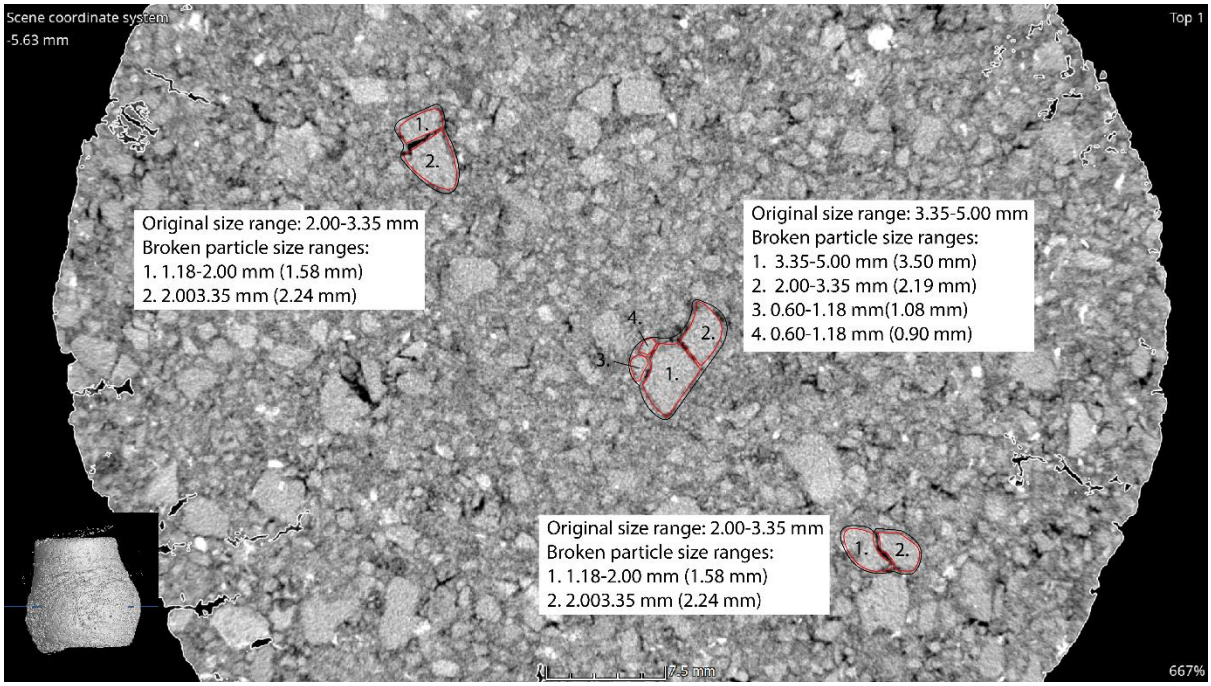

Figure D. 3CT-scan top view of specimen CT 2 and its particle breakage – 2

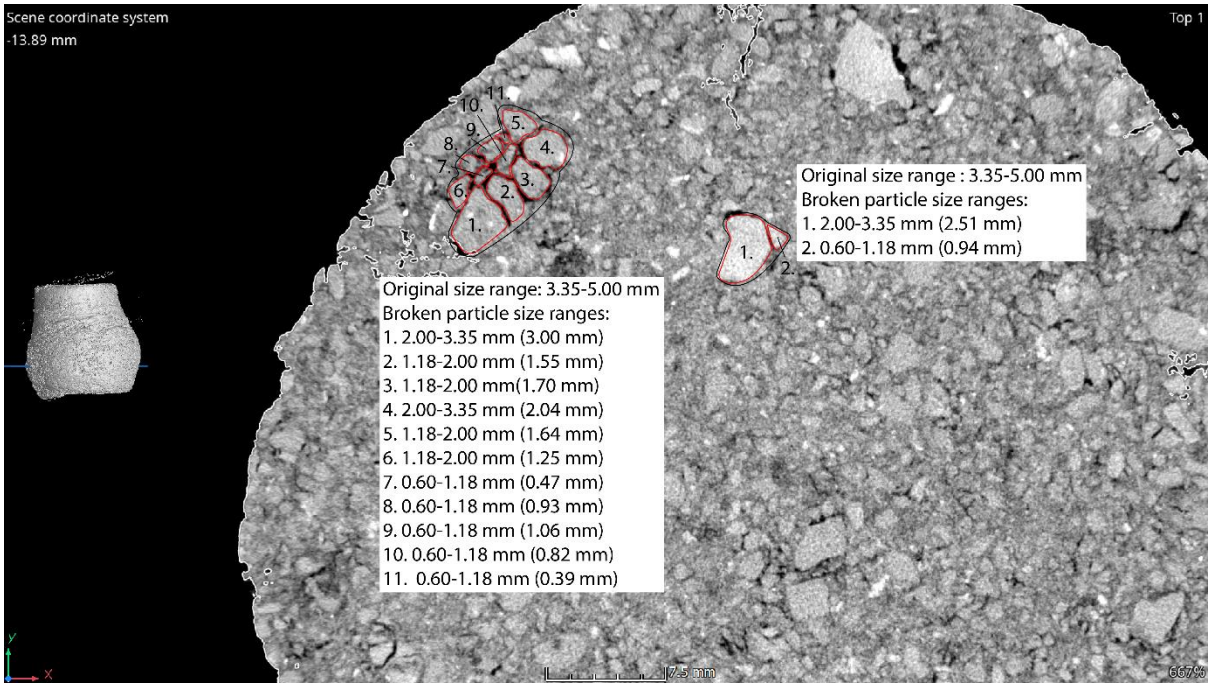

Figure D. 4 CT-scan top view of specimen CT 2 and its particle breakage – 3

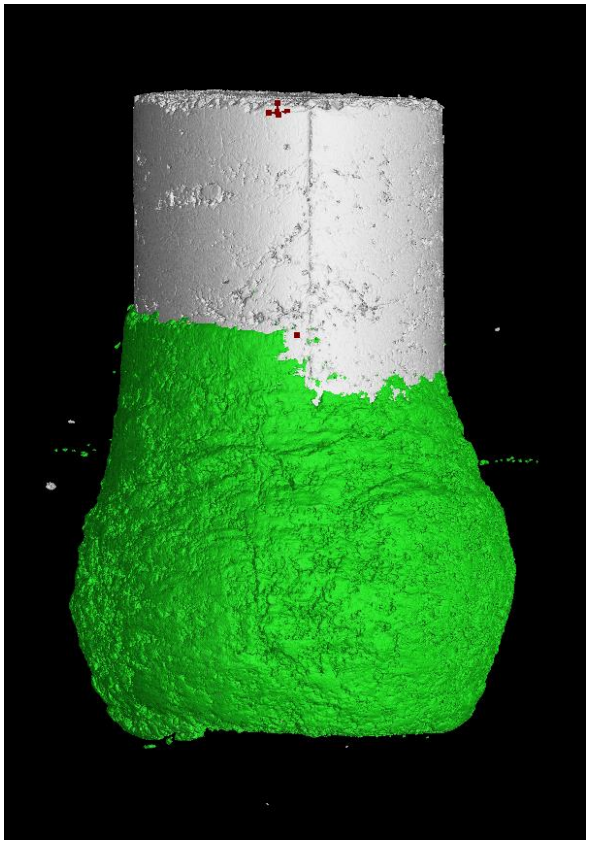

Figure D. 5 CT-scan front view of CT 2 overlying one another

CT scans of specimen CT 3

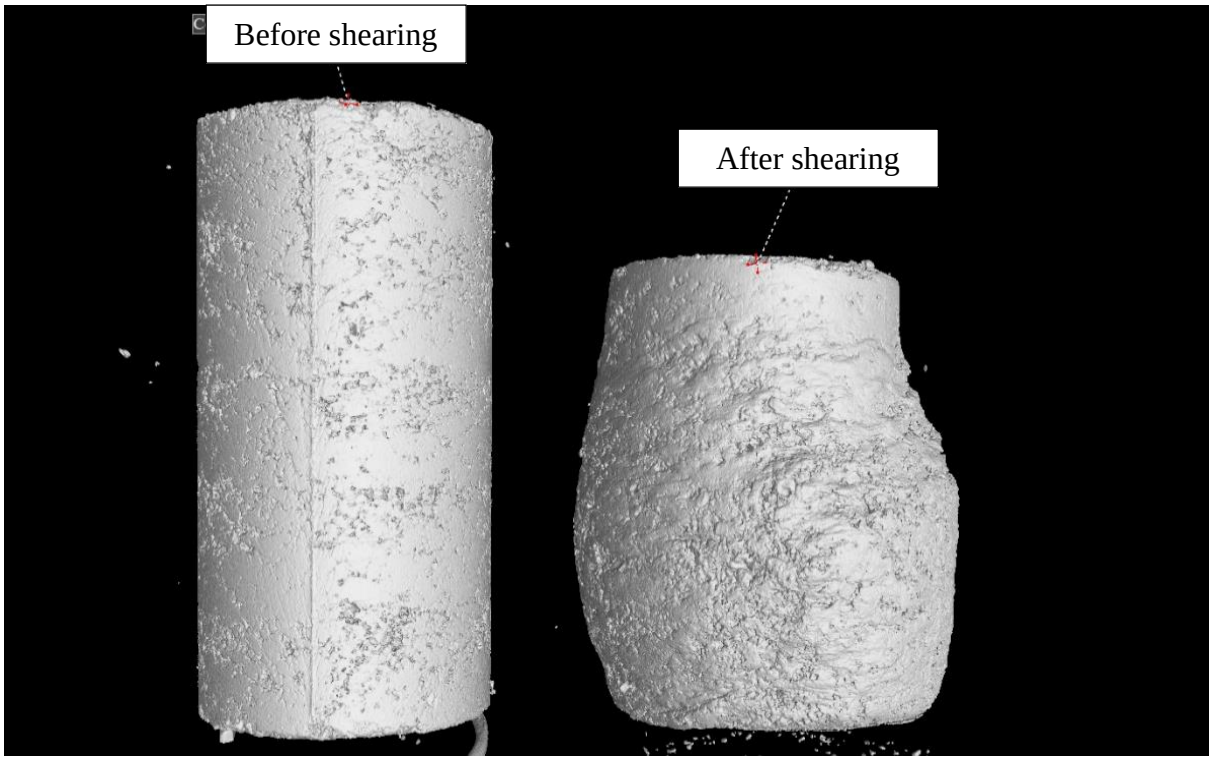

Figure D. 6 CT-scan front view of CT 3 before and after shearing

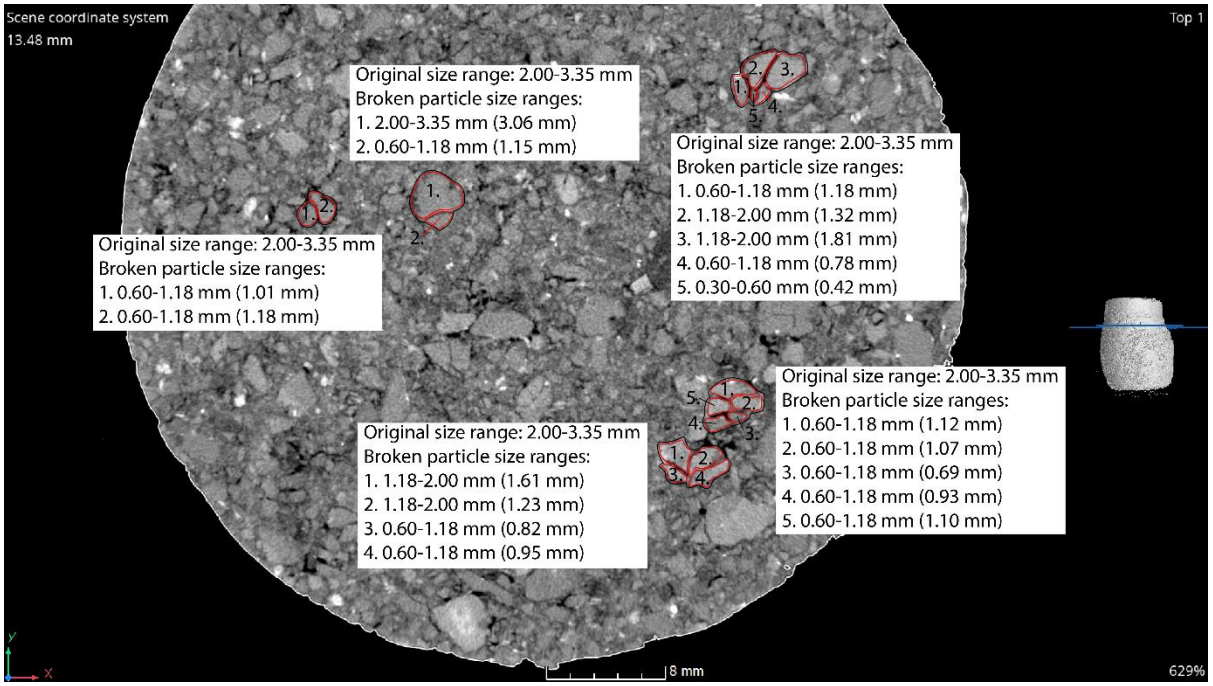

Figure D. 7 CT-scan top view of specimen CT 3 and its particle breakage – 1

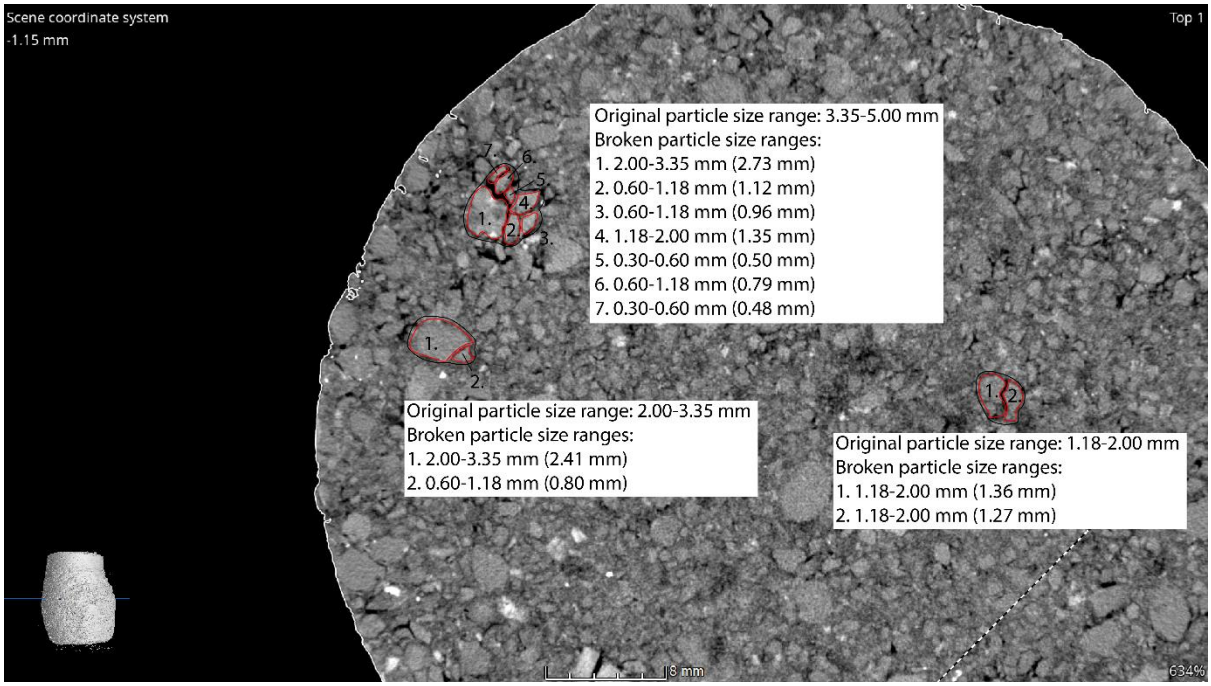

Figure D. 8CT-scan top view of specimen CT 3 and its particle breakage – 2

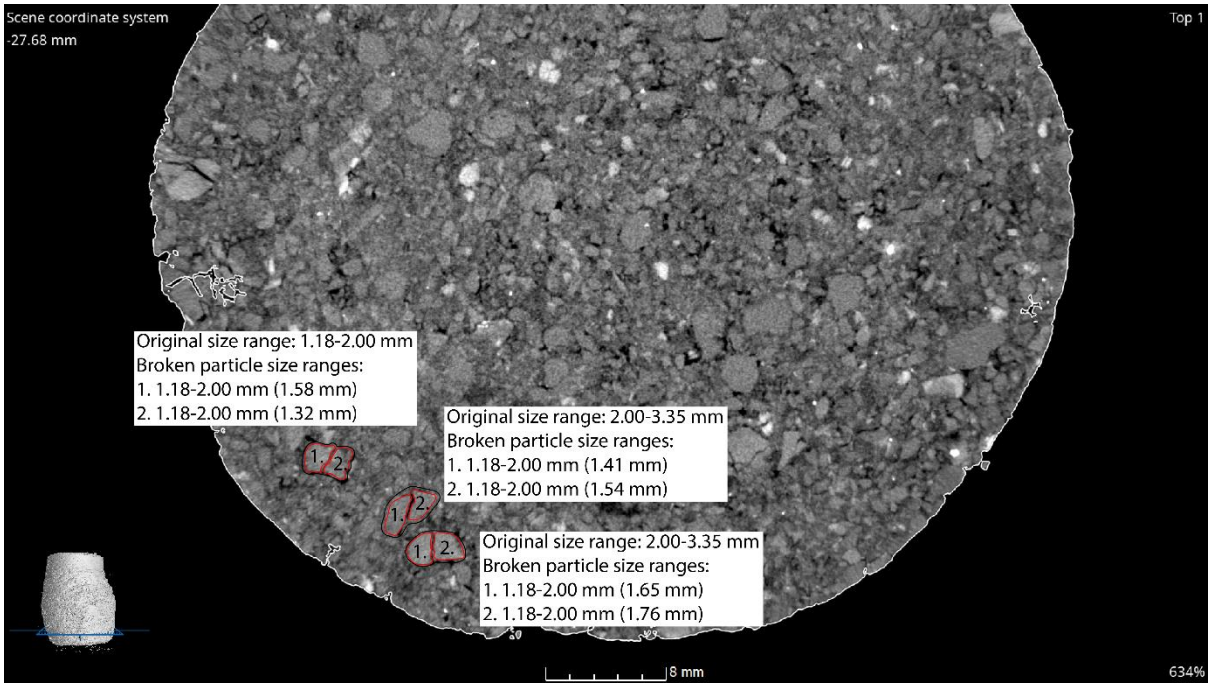

Figure D. 9 CT-scan top view of specimen CT 3 and its particle breakage – 3

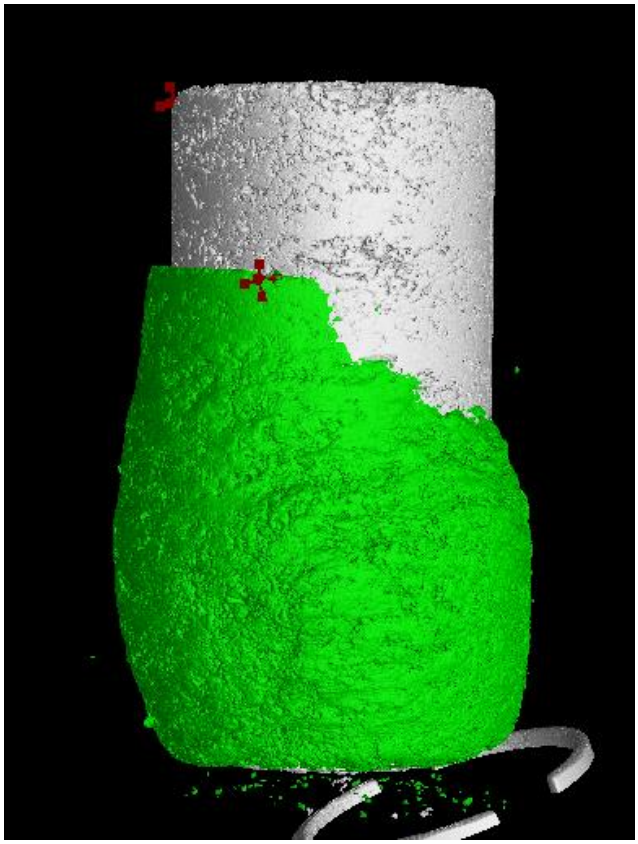

Figure D. 10 CT-scan front view of CT 3 overlying one another